INVESTIGATIONS INTO STRUCTURAL ELECTRICAL SUPERCONDUCTING AND OPTICAL PROPERTIES OF THIN TANTALUM FILMS

By

ROSA MARIA AGUADO BOMBIN

A thesis submitted to the UNIVERSITY OF ASTON IN BIRMINGHAM for the Degree of

DOCTOR OF PHILOSOPHY

THESIS
537.31262
BOM
190412
17 FEB 1976

September, 1975

DEPARTMENT OF PHYSICS.

SUMMARY

Thin films of tantalum of 99.996% purity were prepared by thermal evaporation using an electron gun in ultra high vacuum conditions.

The deposition conditions were varied in order to study their influence on the microstructural, electrical and optical properties.

Results are given of the effects of deposition rate and substrate temperature on the structure of films including grain sizes.

Three different crystalline structures were found:- pure f.c.c., pure b.c.c. and a mixture of f.c.c. and b.c.c. phases.

The effects of the various deposition parameters on electrical properties were noted; including normal resistivity (ρ), the variation of resistivity with temperature, the transition from the normal to the superconducting state and superconducting current densities.

Results given for over 80 films show that there is a good correlation between structural features and electrical properties. Not all films exhibited superconducting properties and reasons are given for those which did not.

The transition temperature from the normal to the superconducting state decreased from the bulk value of 4.48°K (for thick films) to a value of 1.4°K for a film 115Å thick.

Empirical relationships between critical temperature of films (T_{CF}) and resistivity ratio ρ_{300}/ρ_{10} are given covering the range of ratios 1.2 to 6 at which value the transition temperature corresponded to the value for bulk material. Other empirical equations give the relation between T_{CF} and ρ_{300} and T_{CF} and the temperature coefficient of resistivity.

An optical technique is described for the determination of the optical constants of tantalum with a superimposed oxide layer. The technique also gives the optical constants and thickness of the oxide layer, thus enabling the thickness of film responsible for conduction to be evaluated.

Correlation between film structure and optical properties have also

been found. Values of the optical constants n and k corresponding to the different crystalline phases are given.

Attempts have been made to explain the reduction of T_{CF} with reducing film thickness, either by assuming that modifications to the phonon spectrum occur through a reduction in the electron-phonon coupling constant λ or a variation of the density of states N(O) and/or an alteration of the square of the electron matrix element both of which affect λ and through λ the critical temperature.

ACKNOWLEDGMENTS

I should like to thank my supervisor, Dr. W. E. J. Neal, for his invaluable guidance and help throughout the course of this work.

Thanks are due to Professor S. E. Hunt, the head of the Physics Department, and many members of the academic staff, who gave advice and encouragement, particularly Dr. N. W. Grimes and Dr. R. W. Fane.

I wish to express my gratitute to the technical staff of the main workshop. I am particularly indebted to Messrs. F. Lane and H. Arrowsmith and also to Mr. G. Cochrane of the X-ray laboratory.

R. M. Aguado Bombin.

Birmingham, 1975.

TABLE OF CONTENTS

	Pages
SUMMARY	i
ACKNOWLEDGMENTS	iii
LIST OF FIGURES	viii
LIST OF TABLES	xi
CHAPTER 1	
Introduction	1
CHAPTER 2	
Essential Theory	
2.1 Film Formation	7
2.1.1 Preparation of thin films	8
2.2 Electrical Conductivity	8
2.3 Matthiessen's Rule	10
2.4 Film Resistivity	11
2.5 Superconductivity	13
2.5.1 Microscopic Theory	21
2.6 Transition Temperature	23
2.6.1 The Mac-Millan Equation	24
2.6.2 Critical Temperature in Thin Films	26
2.7 Critical Current Densities	27
2.8 Ellipsometry and Thin Film Optics	29
2.8.1 Theory of Compensator Method of Ellipsometry	33
CHAPTER 3	
Experimental Equipment	
3.1 Evaporation Unit	40
3.1.1 Vacuum System	41
3.1.2 Vacuum Chamber	41
3.1.3 Electron Beam Evaporator	45

Pages

3.1.4 Substrate Holder 45

3.2 Cryostat Assembly 51

3.2.1 Cryostat 51

3.2.2 Cryostat Sample Holder 54

3.2.3 Measuring Circuits 58

3.3 Ellipsometer 60

3.3.1 Form of Ellipsometer Used in the Visible Region. The Quarter Wave Plate. 63

3.4 X-Ray Equipment 63

CHAPTER 4

Experimental Procedure

4.1 Substrate Preparation 67

4.1.1 Electrical Contact Areas 67

4.2 Establishment of a Vacuum 68

4.3 Preparation of Films 68

4.4 Determination of Film Thickness 69

4.4.1 Optical Method 70

4.4.2 Electrical Method 73

4.5 Electrical Properties of Films 73

4.6 Optical Properties of Films 74

4.6.1 Determination of Reference Azimuths for the Ellipsometer 74

4.6.2 Determination of Ψ and Δ Using the Compensator Method 76

4.6.3 Determination of the Optical Constants 77

4.6.7 Determination of the Angle of Incidence 78

4.7 X-Ray Analysis 79

CHAPTER 5

Experimental Results

5.1 Deposition Conditions 80

5.2 Structural Data 83

Pages

5.2.1 Preferred Orientation 91

5.2.2 Lattice Constants 91

5.3 Electrical Properties 91

5.3.1 Resistivity 96

5.3.2 Temperature Coefficient of Resistivity 105

5.3.3 Resistivity Ratio and $d\rho/dT$ 105

5.4 Grain Size 108

5.5 Transition Temperatures 113

5.6 Measurements of Critical Current 121

5.7 Film Thickness 121

5.8 Ellipsometric Results 127

5.8.1 Optical Constants of Tantalum 127

5.8.2 Oxide Growth 131

5.8.3 Variation in the Optical Constants 133

CHAPTER 6

Interpretation and Discussion of Results

6.1 Film Growth 135

6.2 Film Structure 136

6.2.1 Tantalum Phases 137

6.2.2 Orientation 141

6.2.3 Lattice Parameters 143

6.2.4 Nature of f.c.c. Structure 144

6.2.5 Summary 147

6.3 Electrical Conduction 149

6.3.1 Matthiessen's Rule (Comparison of Present Results) 150

6.3.2 Impurities and Imperfections 151

6.3.3 Size Effects 155

6.3.4 Grain Boundaries Scattering 160

6.3.5 Influence of f.c.c. Structure 162

6.3.6 Summary 163

Pages

6.4 Grain Size 163

6.5 Superconductive Transition in Tantalum Thin Films 164

6.5.1 Critical Temperature and Resistivity Ratio 164

6.5.2 Influence of Phonon Spectrum in Transition Temperature 168

6.5.3 Application of Mac-Millan Equation to the Present Results 169

6.5.4 Empirical Consideration 179

6.5.4.1 Relationship between Tc and Resistivity 179

6.5.4.2 Relationship between Tc and Resistivity Ratio and Temperature Coefficient of Resistivity 180

6.5.5 Summary 184

6.6 Type II Superconductor 187

6.7 Critical Current Densities 189

6.8 Determination of Film Thickness 195

6.9 Ellipsometric Measurements 197

6.9.1 Oxide Layer 197

6.9.2 Ellipsometric Measurements of Structure 200

CHAPTER 7

Conclusions and Recommendations

7.1 Conclusions 201

7.2 Recommendations for Future Work 204

REFERENCES 207

LIST OF FIGURES

		Pages
1.	Magnetic induction B versus applied field He illustrating the Meissner effect.	15
2.	Behaviour of Type II superconductor in an external magnetic field.	20
3.	Behaviour of Type I superconductor in an external magnetic field	20
4.	Complex amplitudes of the successive beams reflected and transmitted by a single film.	31
5.	Application of ellipsometry to several layers.	34
6.	Basis of the compensator method of Ellipsometry.	35
7.	Experimental procedure for the compensator method.	37
8.	General view of the evaporation system.	42
9.	Arrangement of rough pumping element.	43
10.	Positioning of the water cooled shield around the e-gun evaporator.	46
11.	Overspray shield; position in the e-gun.	46
12.	Substrate holder; position inside the vacuum chamber.	48
13.	View of the substrate holder.	49
14.	Masks for the three positions.	50
15.	View of the cryostat and measuring assembly.	52
16.	Cryostat assembly.	53
17.	Cryostat sample holder.	55
18.	Details of the cryostat sample holder.	57
19.	Circuit used to investigate the electrical properties of films.	59
20.	Circuit used to reverse the current.	61
21.	Arrangement of the ellipsometer components.	62
22.	Ellipsometer with two angles of incidence.	64
23.	X-Ray Diffractometer.	65
24.	Thin film measuring microscope.	71
25.	Fringe formation.	72
26.	Field of view showing four orders of interference.	72

Pages

27. Typical diffraction pattern of a sample with pure b.c.c. structure 85

28. Diffraction pattern of a sample with 50 % of f.c.c. phase. 86

29. Diffraction pattern of a sample with 40 % of f.c.c. phase. 87

30. Diffraction pattern of a sample with 15 % of f.c.c. phase. 88

31. Diffraction pattern of a sample with 10 % of f.c.c. phase. 89

32. Percentage of f.c.c. phase versus deposition temperature. 90

33. Ration Intensities b.c.c. (200)-(211) lines versus deposition temperature. 92

34. Change in "d" parameter for f.c.c. phase versus deposition temperature 94

35. Resistance versus temperature Film Ta-67. 97

36. Resistance versus temperature Film Ta-34. 98

37. Resistance versus temperature Film Ta-45. 99

38. Resistance versus temperature Film Ta-71. 100

39. Resistance versus temperature Film Ta-27. 101

40. Resistance versus temperature Film Ta-47. 102

41. Resistivity versus thickness. 103

42. Percentage increase in resistivity versus % f.c.c. phase 104

43. TCR versus thickness. 106

44. ρ_{300}/ρ_{10} and $d\rho/dT$ versus thickness. 109

45. ρ_{300}/ρ_{10} versus deposition temperature. 110

46. $d\rho/dT$ versus deposition temperature. 111

47. % variation of ρ_{300}/ρ_{10} and $d\rho/dT$ versus percentage f.c.c. phase. 112

48. b.c.c. grain size versus deposition temperature. 115

49. f.c.c. grain size versus deposition temperature. 116

50. Critical temperature versus thickness. 117

51. Critical temperature versus resistivity at 300° K. 118

52. Critical temperature versus TCR. 119

Pages

53. Critical temperature versus ρ_{300}/ρ_{10} 120

54. Tc versus deposition temperature. 122

55. Critical current at 2.2° K versus thickness 123

56. Critical current versus temperature 124

57a. Reduction of Δ due to oxide growth for an angle of incidence of 64°. 128

57b. Reduction of Δ due to oxide growth for an angle of incidence 59.95°. 129

58. Variation of Ψ with respect to Δ. 130

59. Rate of growth of oxide layer. 132

60. Diffraction pattern of $Ta\ O_{0.9}$. 142

61. Comparison between Fuch-Sondheimer theory and present results. 158

62. Comparison between theoretical value of the ratio of the film to the bulk TCR and present results. 159

63. Comparison between Mayadas theory and present results. 161

64. Comparison between DeSorbo equation and present results. 166

65. Dependence of Tc on electron-phonon coupling constants. 171

66. Tantalum phonon density of states. 172

67. Tantalum $f(\omega)/\omega$ versus ω. 174

68. Variation of electron-phonon coupling constant versus cut-off frequency. 175

69. Dependence of Tc on cut-off frequency. 176

70. Grain size versus cut-off frequency. 177

71. Variation of Tc with resistivity ratio. 181

72. Variation of density of states N(o) with energy for transition metals. 186

73. Hysteresis effect in normal to superconductor transitions. 191

74. $Ic/(1 + T_R^2)^{1/3}$ versus $(1 - T_R^2)$. 193

75. Critical current versus $(1 - T_R^2) / (1 + T_R^2)^{1/2}$ 194

76. Plot of oxide layer versus log time. 199

LIST OF TABLES

Pages

1. Summary of deposition conditions for tantalum films. 81, 82
2. X-ray diffraction pattern of a pure f.c.c. - Ta film. 84
3. X-ray diffraction pattern for a typical thick b.c.c.- Ta film. 84
4. Effect of thickness and substrate temperature on lattice parameter of b.c.c. - Ta films. 93
5. Set of results from the electrical measurements on a tantalum film. 95
6. Variation of resistivity at 300° K with deposition temperature 107
7. Variation of TCR with percentage of f.c.c. - Ta phase. 107
8. b.c.c. grain size of films of differing thickness. 114
9. f.c.c. grain size of films of differing thickness. 114
10. Typical set of critical current measurements. 125
11. Variation of optical constants with structural properties. 134
12. Anomalous structures in thin films which transform with increasing thickness. 138
13. Comparison of structural properties of present thin films with other workers. 145
14. Change of resistivity ratio with thickness and deposition temperature. 153
15. Nitrogen concentration as a function of residual resistivity 153
16. Comparison of electrical properties of present thin films with other authors. 156
17. Experimental and calculated values of critical temperature an the corresponding resistivity. 183
18. Experimental and calculated values for Tc using the empirical relationships. 183
19. Comparison of Tc values for the present work with other workers. 188
20. Variation of critical current density with thickness. 196
21. Critical currents and critical current densities at 0° K. 196

Pages

22. Comparison of critical current measurement of this investigation with other authors. 198

23. Optical constants of Ta and TaO found in this work and by other authors. 198

CHAPTER 1.

Introduction

Kamerlingh Onnes liquified helium in 1908 and shortly afterwards began an investigation of the electrical conductivity of metals at the new low temperature below 4.2°K.

To reduce the resistance caused by impurities, he studied mercury of high purity and was surprised when he found no measurable resistance at this temperature. The resistance did not decrease smoothly to zero but dropped almost discontinuously to zero within a temperature range of 0.01°K at about 4°K.

By 1913 he concluded that mercury had passed into a new state which, on account of its remarkable electrical properties he called the superconductive state.

Although the fascinating phenomenon of superconductivity has been known for sixty years, it is largely through the concentrated experimental and theoretical work of the past two decades that a basic understanding of the effect has been reached.

Furthermore, thin film studies have opened many new and interesting areas of solid state research and have helped in the search for a better understanding of this field.

It is well known that superconducting properties are affected by microstructural defects. In order to understand the role of microstructural defects in superconductivity completely, it is desirable to have qualitative correlations between superconducting properties and structural properties.

One of the aims of this research is an attempt to obtain some correlations in the case of tantalum films. In particular, the microstructural properties which have been observed by X-ray are grain size, crystal structure and lattice parameters.

To accomplish this purpose, thin films of tantalum have been laid

down under different deposition conditions trying to correlate the microstructural properties with the deposition parameters and further on with the superconducting properties.

One difference found between the so-called "soft" and "hard" elemental superconductors is that whereas the former are not easily contaminated by gaseous impurities, the latter readily dissolves or reacts with large quantities of such impurities, particularly oxygen water vapor and nitrogen, this last gas in smaller proportions.

Thus, while the solubility of oxygen in lead and tin is quite small, the solubility of oxygen, in tantalum is of the order of several atomic per cent (at %) depending on temperature. Dissolved oxygen in tantalum changes many of its superconductive properties.

If thin films of tantalum are prepared in the presence of an appreciable partial pressure of oxygen or water vapor, they must be expected to contain gettered oxygen in appreciable amounts.

To reduce the oxygen partial pressure the gettering action, exhibited by a freshly exposed surface of tantalum, was used. This can be best accomplished by having present in the evaporation chamber a large surface (the chamber walls and metal shutters) on which the metal is constantly deposited prior to and during film preparation. This constantly renewed active surface is in competition with the surface of every film for the available oxygen in the system, reducing its partial pressure.

To further decrease the incorporation of oxygen or oxygen compounds on impingement on the growing film, the sticking coefficient must be lowered, or the lifetime of the impinged oxygen on the surface must be reduced and must be returned to the gas phase. This can be achieved by increasing the film temperature during preparation. Therefore, in order to reduce the gaseous impurity content of the tantalum thin films, which is one of the purposes of this work, an ultra-high vacuum system was used so that together with the gettering taking place in the system, this objective could be achieved.

Substrate temperature and deposition rate are another two parameters which have been found to affect the purity of the samples.

Different authors have reported in their works that electrical properties of thin films are affected by microstructural parameters and gaseous impurities, so we intend in this investigation to study the influence of these two mentioned factors - the mean free path which in turn will affect the electrical properties of the films, including the normal to superconductive transition.

To achieve this end the samples have been prepared at as low as possible a pressure and the other deposition conditions have been varied in order to obtain a correlation between the deposition conditions and mean free path through the structural properties and gaseous impurities.

Our investigation was undertaken in the expectation that the superconducting properties would provide, as well, a tool for studying the factors which affect thin film resistivity. To this end we have investigated the variation of the critical temperature with normal state resistivity for evaporated tantalum films.

The critical temperature of tantalum is very sensitive to small amounts of dissolved oxygen, only ultra-high vacuum techniques and high deposition rates can give films approaching the critical temperature of bulk material. By varying the substrate temperature during deposition, it has been shown that, if the temperature is lowered the transition temperature decreases.

However, Asada and Nose[1] reported transition temperatures which were too low to be solely accounted for by interstitial oxygen. It was suggested that the discrepancy could be due to the decrease in grain size of very thin films, although there was no confirmatory evidence to this effect.

In another context, Mac Millan[2] had derived an expression for the transition temperature of a superconductor in terms of Debye temperature, the electron-phonon coupling λ and the Coulomb coupling constant μ^*.

Leger and Klein[3] suggested that the enhanced transition temperature observed in thin aluminium films was due to a modification of the phonon spectrum which in turn affects the electron phonon coupling parameter. When the average phonon frequency, as determined from the experiments was substituted into the Mac Millan equation, the calculated transition temperature was found to be in good agreement with that observed experimentally.

In earlier work on thin niobium films prepared by evaporation in an ultra-high vacuum system, Salter[4] came to the following conclusions on the basis of his experiments:

1. Particle size was proportional to film thickness.
2. The temperature of transition from the normal to the super-conducting state, T_C, was a function of particle size.

The results showed a change in transition temperature from 9.2°K (as for bulk material) for thick films with a large particle size 210Å, to 3.2°K for a film 45Å thick with a particle size of 30Å.

This is in contrast to results found by other workers on materials such as aluminium, lead and tin which showed an enhancement of T_C as the particle size decreased. Tests in conjunction with this work have also verified the enhancement of the critical temperature of thin aluminium film as film thickness and particle size decrease.

Salter made an attempt to explain the results in terms of the Mac Millan equation in which the electron-phonon coupling λ was reduced by cutting out low frequency phonons in the phonon spectrum. A reduction in λ leads to a reduction in T_C. The amount of experimental evidence was not thought to be sufficient to reach absolute conclusions.

One of the objectives of the present work was to investigate some of the factors which affect the critical temperature of thin tantalum films prepared by evaporation and to compare the results with the results obtained previously with niobium, with particular reference to particle size. If this effect was as large as Salter had suggested, it should be

possible to isolate phonons responsible by obtaining changes in grain size in different crystallographic directions and observing the effect on T_C. Another possibility was to consider the effect of reduced electron mean free paths on the electron-phonon coupling. Therefore tantalum films of different thickness were prepared and consequently different grain sizes and mean free paths were obtained. Both parameters were measured: the first by X-ray diffraction and the second by measuring resistivity. Attempts were made to correlate the decrease in the transition temperature with the decrease in the values of grain size and mean free path.

In order to achieve all the mentioned objectives, apparatus was designed and built for the preparation and examination of thin tantalum films. As it was intended to examine different parameters independently, it was thought that it should be desirable to be able to lay down several samples under exactly the same deposition conditions except one which would be the independent factor, so a sample holder was designed which would carry eight substrates. The design was such that the temperature could be varied independently and films of differing thicknesses could be deposited in the same evaporation.

An ultra-high vacuum system and technique were employed to prepare pure films without interstitial impurities. In this way, any observed decrease in the transition temperature would be wholly attributable to the influence of the grain size and mean free path on the phonon spectrum.

To examine the films electrically and measure T_C, it was necessary to deposit the films in one system and examine them in a separate system.

Exposing the films to an atmospheric environment resulted in the growth of an oxide layer on the films. In the absence of information on oxide growth, it was considered advisable to examine the films electrically as soon as possible, so a sample holder, to be used in the cryostat, was designed, which was capable of holding four samples and the electrical parameters, and the transition temperature of four films could be measured

simultaneously.

To take values as frequently as possible when the temperature was being lowered, a wholly automatic system was designed and measurements could be taken at intervals of 1.5 seconds.

Resistive transitions were observed and the onset of resistivity was also observed at varying current densities.

Another objective of the present investigation was to study the optical constants of tantalum films, and an ellipsometer was used for such measurements. In order to reduce the time in sample changes and alignment, a sample holder to support four samples was designed and the optical constants of four samples could be determined in one run.

Initially it was hoped to make direct measurements of electron-phonon coupling constant λ by observation of optical properties in the infra-red where interband transitions take place.

The same ellipsometric technique was used to measure the growth of the tantalum oxide film.

Finally, in this work, we intend to correlate the different structures of the samples determined by different deposition conditions, with their optical constants n and k. The objective here being to assess the use of the ellipsometer in structural determination in thin films and imperfection in surface layers.

The experimental details of all the investigations mentioned above, the results and the interpretation and conclusions of the results, will be presented in the following chapters.

CHAPTER 2

Essential Theory

The different theories which are relevant for the interpretation of results in this investigation are described in this chapter.

2.1 Film Formation

Thin films are prepared by condensation which is determined by the interaction of atoms when they impinge on a surface or substrate from the vapor phase.

The impinging atom is attracted to the surface and as a result the atom loses its velocity component normal to the surface. The vapor atom which is then physically absorbed, is called the "adatom", the adsorbed atoms migrate over the surface during their lifetime to form pairs which, in turn, act as condensation centres for other atoms.

The characteristic sequential growth stages are 1) randomly distributed three-dimensional nuclei are first formed and rapidly approach a saturation density. These nuclei then grow to form observable islands 2) as islands increase their size by further deposition and come closer to each other, the larger ones appear to grow by coalescence of the smaller ones 3) when the islands distribution reaches a critical state, a rapid large-scale coalescence of the islands result in a connected network structure 4) the final stage of growth is a slow process of filling the empty channels.

The influence of the deposition parameters on film growth may be understood in terms of their effects on sticking coefficient, the nucleation density and the surface mobility of adatoms. Their effects are felt in some aspects of the physical structure of thin films as grain size, lattice constants, crystalline structure and orientated growth.

2.1.1 Preparation of thin films

Some difficulties arise in the preparation of films of high melting point materials such as tantalum.

Thermal evaporation techniques require heating the material to temperatures of the order of several thousand degrees kelvin, to achieve satisfactory evaporation rates. Such high temperatures in the evaporation chamber lead to increased outgassing rates and to a subsequent deterioration of the vacuum.

The gettering action of freshly deposited materials makes it important that the evaporation pressure and particularly the partial pressure of oxygen in the evaporation chamber should be as low as possible.

The method used in this investigation consisted of heating the tantalum material by means of electron beam bombardment, instead of supplying energy by filament or by induction heating.

A stream of electrons is accelerated through an electric field and focussed onto the evaporant surface. Upon impingement most of the particle kinetic energy is converted into heat, and temperatures exceeding $5000^{o}K$ may be obtained.

Since the energy is imparted by charged particles, it can be concentrated on the evaporating surface while other parts of the evaporant are maintained at lower temperature. Hence interactions between evaporant and support material are greatly reduced.

2,2, Electrical Conductivity

A theory of metallic electrical conductivity based on the average velocities of conduction electrons was developed by Drude.[5] This theory was modified by Lorentz[6] using the Boltzman transport equation and a simplified model for the collisions between the electrons and the atoms in the lattice.

Subsequently, Sommerfield[7] recalculated the conductivities along the lines of Lorentz's theory, but replaced classical statistics by Fermi-Dirac statistics.

Electrical conductivity of a metal in the free-electron gas theory of Drude-Lorentz-Sommerfield was given by

$$\sigma = \frac{n\, e^2 \tau}{m} \tag{2.1}$$

where n is the number of free electrons per unit volume

e is the electronic charge

m is the effective mass of the electron

τ is the relaxation time of electron-phonon interaction.

If the Fermi electron velocity is v_F then

$$\tau = \frac{\ell}{v_F} \tag{2.2}$$

where ℓ is the mean distance travelled between scattering collisions and is known as the mean free path.

Re-writing equation (2.1) to include the mean free path the resistivity is given by

$$\rho = \frac{m\, v_F}{n\, e^2 \ell} \tag{2.3}$$

This simple relation is only correct for an isotropic monovalent metal with a simple conduction band.

As a result of the wave nature of the electrons, they can pass through a perfect crystal without suffering any resistance. The actual cause of resistivity must therefore be sought in deviations from the periodicity of the potential in which the electrons move.

The generalized resistivity expression deduced from the free-electron model in the Quantum Mechanical Theory consisted of

resistivity arising from electron scattering by an ideal lattice and residual resistivity. The ideal resistance term was obtained from equation (2.3) and was found to be proportional to temperature ($T^{o}K$) at high temperatures and (T^5) at low temperatures.

The principally temperature dependent parameter in equation (2.3) is ℓ, the mean free path. At high temperatures ℓ is limited by lattice vibrations and therefore ℓ increases with decreasing temperature until close to the absolute zero of temperature it reaches an upper limit determined by impurities or specimen dimensions. This limiting value of the mean free path corresponds to the residual resistivity .

The dependence of the resistivity on the variation of temperature can therefore be explained in terms of the effect of temperature on the mean free path. The mean free path is also affected by impurities, lattice imperfections and the dimensions of the specimen, (the size effect).

2.3 Matthiessen's Rule

When a metal contains impurities, the field in the vicinity of the impurities is in general different from the periodicity of the potential and act as scattering centers for electrons. Thus electrons in an impure metal are scattered by impurity atoms as well as by the thermal vibrations of the atoms.

Denoting the relaxation times associated with each of these processes by τ_i and τ_{th} respectively, the resulting relaxation time is given by

$$\frac{1}{\tau} = \frac{1}{\tau_i} + \frac{1}{\tau_{th}} \qquad (2.4)$$

because the probabilities for scattering in this simple model are additive and they are proportional to the reciprocals of the relaxation times.

Since the resistivity is proportional to τ_F^{-1} , associated with electrons at the Fermi level, the impurity scattering leads to a constant term in Matthiessen's rule

$$\rho = \rho_i + \rho(T) \qquad (2.5)$$

where ρ_i is a constant which increases with increasing impurity content and $\rho(T)$ is the temperature-dependent part of the resistivity.

Actually τ_i will itself be slightly temperature dependent, but in general the temperature-independent part predominates strongly. For not too high impurity concentration $1/\tau_i$ is proportional to the impurity content and so is ρ_i .

2.4 Film Resistivity

Several authors have followed the original suggestion of Thomson[8] that the electrical resistivity of a thin film will increase when the electron mean free path (mfp) is restricted by the surface of the film.

Physical effects arising because of the geometrical limitations of the mfp are termed size effects.

The size effects theory was developed by Fuch[9] for a spherical Fermi surface and extended by Sondheimer,[10,11] to explain the fact that in thin films the resistivity is always higher than in bulk material and increases rapidly as the thickness decreases.

They postulated that ordinary scattering mechanisms in the bulk material are carry over to the film; in addition, external surfaces impose a boundary condition on the electron-distribution function which enhances the thickness.-independent bulk ρ_B to a thickness-dependent total resistivity ρ_F .

The result of Fuch-Sondheimer (F-S) theory for thin films is

$$\rho_F = \rho_B \left[1 - \frac{3}{2\gamma}(1-p) \int_1^{\infty} \left(\frac{1}{a^3} - \frac{1}{a^5} \right) \frac{1-e^{-\gamma a}}{1-pe^{-\gamma a}} \, da \right]^{-1} \quad (2.6)$$

where $\gamma = \frac{t}{\ell}$ is the ratio between film thickness t and intrinsic eletron mean free path ℓ.

p (a completely phenomenological parameter) is the probability that an electron will be specularly reflected upon scattering from a film surface and takes on values from 0 to 1.

The limiting values of equation (2.6) for thick and thin films yield respectively to

$$\rho_F / \rho_B = 1 + \frac{3}{8\gamma} (1-p) \qquad \gamma > 1 \quad (2.7)$$

and

$$\rho_F / \rho_B = \frac{4}{3} \frac{1}{\gamma(1+2p)} \frac{1}{\ln(1 \gamma)} \qquad \gamma \ll 1, \; p < 1 \quad (2.8)$$

where ρ_F is the film resistivity

ρ_B is the bulk resistivity which is thickness independent.

Mayadas et al[12] have shown that for evaporated polycrystalline Aluminium films the assumption that ρ_B and ℓ are constants with thickness is incorrect and, in fact, ρ_B decreases with increasing thickness.

They concluded that the decrease in ρ_B or increase in ℓ with thickness was due to the increasing grain size. The total or measured resistivity at any temperature must therefore depend on thickness, not only through the ordinary Fuch-Sondheimer size-effect theory but also because the dependence of ρ_B on grain size.

Usually this is the case, for although the scattering of

electrons by grain boundaries may be substantial, the grain size is normally much larger than the mean free path due to other scattering phenomena, so that the grain boundary contribution to the resistivity is small.

However, in the case of a thin film, the distance between grain-boundaries D, is generally smaller than ℓ and hence the grain boundary contribution can no longer be regarded as negligible.

The resultant resistivity is

$$\rho_F = \rho_B \left[1 - \frac{6}{\pi\gamma}(1-p) \int_0^{\pi/2} d\phi \times \right.$$

$$\times \int_1^{\infty} da \frac{\cos^2\phi}{H^2(a,\phi)} \left(\frac{1}{a^3} - \frac{1}{a^5}\right) \times$$

$$\left. \times \frac{1 - e^{-\gamma a H(a,\phi)}}{1 - p e^{-\gamma a H(a,\phi)}} \right]^{-1} \qquad (2.9)$$

where $H(a,\phi) = 1 + \alpha / \cos(1 - \frac{1}{a^2})^{1/2}$

$\gamma = t/\ell$ as in the case of F-S theory.

ℓ is the mean free path within a grain.

ρ_B is the resistivity which a single crystal film would possess if it were infinitely thick.

p is the same parameter used by F-S.

A plot of F-S and Mayadas equation is shown in Figures (61) and (63).

2.5 Superconductivity

The behaviour of electrical resistivity was investigated by Onnes[13] in 1911, after he had achieved the liquification of helium.

In measuring the resistance of a mercury sample as a function of temperature, he found that at about $4^{\circ}K$ the resistance falls abruptly to a value which Onnes could not measure. This extraordinary

phenomenon he called Superconductivity, and the temperature at which it appears, the critical temperature T_c .

From 1911 until Meissner's work in 1933, superconductivity was considered to be simply infinite conductivity and attempts were made to try to understand the lack of scattering.

Meissner had discovered that a superconductor excludes a magnetic field and that the state with the flux excluded is a thermodynamically stable state.

Meissner's experiment showed that superconductors are something more than materials which are perfectly conducting, they have an additional property that a merely resistanceless metal would not possess. A metal in the superconducting state exhibiting type I behaviour, would never allow a magnetic flux density to exist in its interior. (Figure(1) illustrates this by showing magnetic induction B versus applied field He for a perfect conductor and for a superconductor).

An early step towards a phenomenological theory of superconductivity was made by Gorter and Casimir[14] who showed that the thermodynamic properties of superconductors could be accounted for by assuming that their conduction electrons were divided into two fluids or phases.

The electrons in one phase were considered to retain their normal properties (n_n) but a proportion ($n_s / n_n + n_s$) was assumed to be condensed into a lower free energy phase in which it could carry current without Joule dissipation of heat. This proportion ($n_s / n_n + n_s$) was assumed to be unity at the absolute zero of temperature and zero at the critical temperature T_c

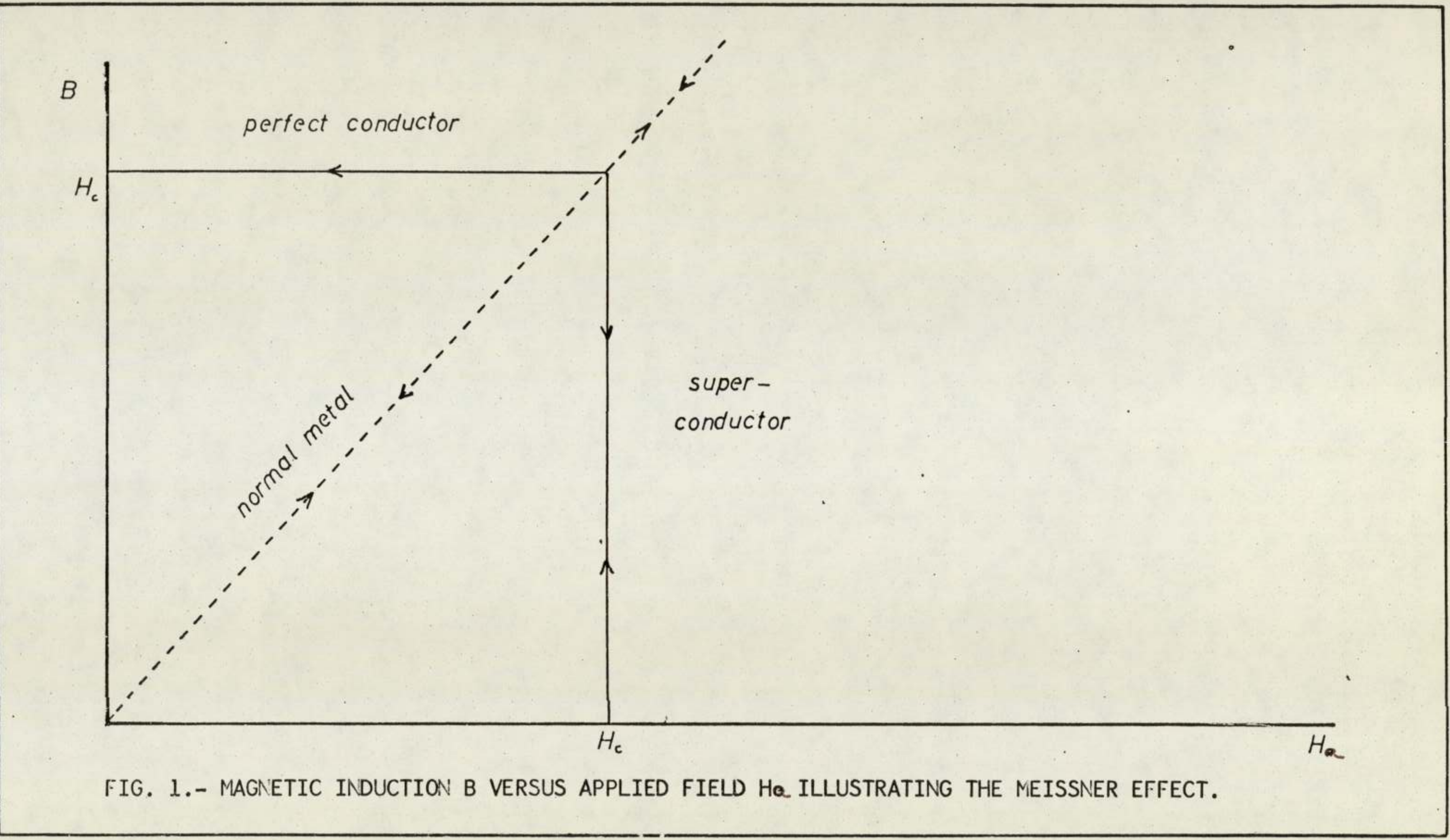

FIG. 1.- MAGNETIC INDUCTION B VERSUS APPLIED FIELD H_a ILLUSTRATING THE MEISSNER EFFECT.

In a perfect conductor, the equation of motion for an electron of mass m and charge e in the presence of an electric field E would be

$$m \dot{v} = e E \qquad (2.10)$$

with a current density of

$$J = nev \qquad (2.11)$$

where n is the number density of electrons, this leads to

$$E = (4\pi \lambda_L^2 / c^2) \dot{J} \qquad (2.12)$$

where

$$\lambda_L^2 = \frac{mc^2}{4\pi ne^2} . \qquad (2.13)$$

The parameter λ_L has the dimensions of length and for a density of electrons corresponding to one electron per atom it has a value of the order of 10^{-5}cm.

Applying Maxwell equations one finds that

$$\nabla^2 \dot{H} = \dot{H} / \lambda_L^2 \qquad (2.14)$$

For a semi-infinite slab extending in the x-direction from the plane x = o, the appropriate solution is

$$\dot{H}(x) = \dot{H}(0) \exp(-x/\lambda_L) \qquad (2.15)$$

Equation (2.15) confirms that in the interior of a perfect conductor the magnetic field cannot change in time from the value it had when the specimen became perfectly conducting.

To explain the Meissner effect E and H. London[15] proposed to add to Maxwell's equations the following two relations in order to

treat the electromagnetic properties of a superconductor

$$E = 4\pi\lambda_L^2/c^2 \dot{J} \tag{2.16}$$

and

$$(4\pi\lambda_L^2/c)\ \mathrm{curl}\, J + H = 0 \tag{2.17}$$

Applying Maxwell equations to equation (2.17) leads to

$$\nabla^2 H = H/\lambda_L^2 \tag{2.18}$$

Solution of this equation for any geometry now shows that H, and not only $\dot{H}$ decays exponentially upon penetrating into a superconducting specimen.

For the semi-infinite slab described above, the solution of (2.18) is

$$H(x) = H(0)\ \exp(-x/\lambda_L) \tag{2.19}$$

which now shows that for $x \gg \lambda_L$ $H(x) \approx 0$ in accordance with the Meissner effect.

The London equations (2.16) and (2.17) do not, in fact, yield the complete exclusion of a magnetic field from the interior of a superconductor. They predicted the penetration of a field such that it decays to $1/e$ of its surface value in a distance λ_L. This is called the London penetration length.

In the two fluid model, the particle and current densities $\rho = ne$ and J are given by the sum of superfluid (S) and normal (n) components,

$$\rho = \rho_s + \rho_n \tag{2.20}$$

$$J = \rho_s v_s + \rho_n v_n \tag{2.21}$$

Here v_s and v_n are fluid velocities.

The Ginzburg-Landau[16] (G-L) theory describes superfluid flow $\rho_s v_s$ in terms of an effective wave function with amplitude Ψ and phase χ

$$\psi(r) = |\psi(r)| e^{i\chi(r)} \tag{2.22}$$

The superfluid density ρ_s is assumed to be proportional to $|\psi(r)|^2$

For ρ_s = constant

$$m^* v_s = p_s - (e^*/c)\, A(r) \tag{2.23}$$

where $p_s = \hbar \,\text{grad}\, \chi(r)$ is the canonical momentum determined by the gradient of the phase. We now interpret p_s as the momentum per pair of electrons in the condensate state so that $m^* = 2m$ and $e^* = 2e$ i.e. effective mass and charge of carrier respectively.

It can be noted that phase plays the same sort of role for superfluid flow of electrons that voltage does for flow in normal metals. In normal metals the current density is proportional to the voltage gradient, and in the absence of current flow the voltage is everywhere the same. Correspondingly, when the superfluid flow vanishes and there is no magnetic field, the phase is the same everywhere.

The wave function does not describe a single particle or the centre of mass of a pair of particles, but rather the motion of the superfluid condensate as a whole.

In a very weak field $H \simeq 0$ the function ψ remains practically constant $\nabla\psi \simeq 0,\ \psi \simeq \psi_0$ and G-L Theory is equivalent to London's where k was the low field (London) limit and was given by

$$k = \frac{\sqrt{2}\, e^* H_c \lambda^2}{hc} \tag{2.24}$$

where e^* is the charge of the superelectron.

G-L predicted a negative interphase boundary energy when $\kappa > 1/\sqrt{2}$ and that a superconductor with a negative interphase boundary would remain superconducting up to a magnetic field

$$H_{c2} = \sqrt{2}\ \kappa\ H_c \tag{2.25}$$

without exhibiting the Meissner effect.

Abrikosov[17] called this Type II or hard superconductivity, Figure (2). The state below H_{c2} but above H_{c1} was called the mixed state. Superconductors which satisfy

$$\kappa < 1/\sqrt{2}$$

were termed Type I or soft superconductor, Figure (3). It is possible to produce films of the same material which exhibit type I or type II behaviour.

Pippard[18] introduced a phenomenological approach to superconductivity which like that of G-L, modifies the absolute rigidity of the superconducting order parameter or wave function which is implicit in the London model.

He suggested that the superconducting state could be characterized by a finite range of momentum coherence such that the order parameter gradually change over a distance ξ, the "coherence length".

The coherence length may be estimated from the Uncertainty Principle by

$$\xi \simeq \frac{\hbar}{\Delta p} \simeq \frac{h\, v_F}{K\, T_c} \tag{2.26}$$

Pippard estimated the value of ξ to be 10^{-4} cm from the available data on the field dependence of the penetration depth.

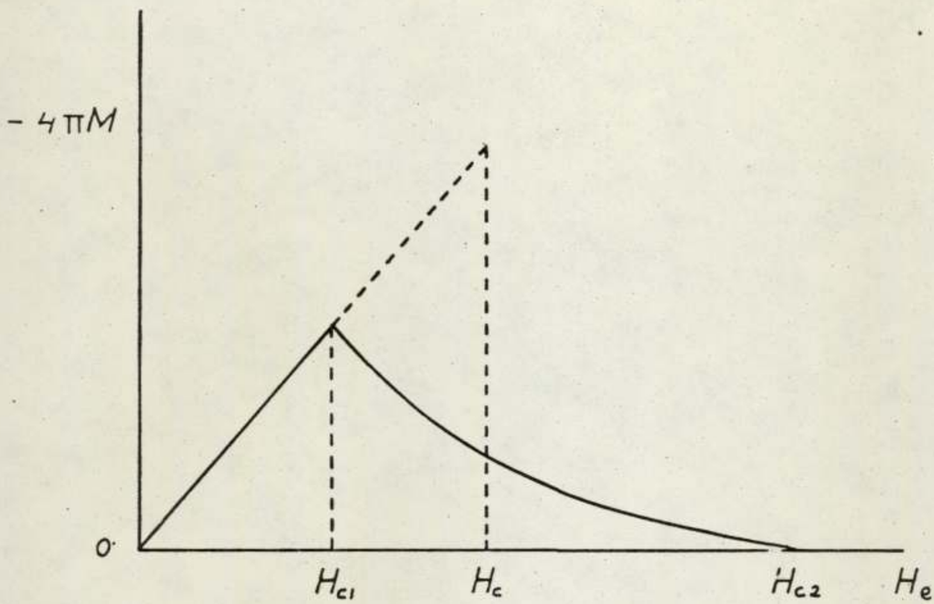

FIG. 2.- BEHAVIOUR OF TYPE II SUPERCONDUCTOR IN AN EXTERNAL MAGNETIC FIELD.

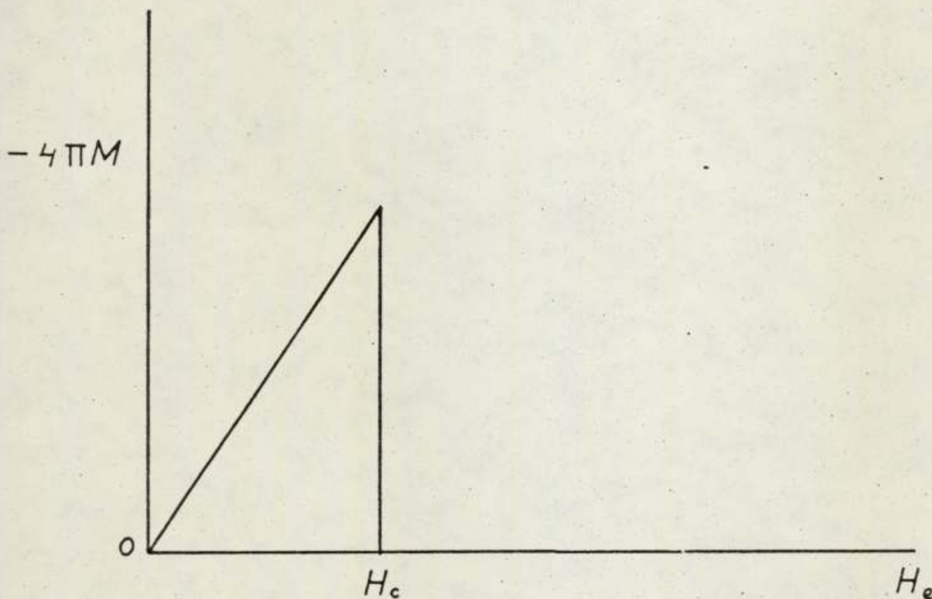

FIG. 3.- BEHAVIOUR OF TYPE I SUPERCONDUCTOR IN AN EXTERNAL MAGNETIC FIELD.

2.5.1 Microscopic Theory

The very small amount of energy involved in the normal superconducting transition (10^{-8} ev/atom) made the task of selecting the interaction responsible for a profound change in behaviour of conduction electrons accompanied by long-range order a difficult one.

The first clue to the correct interaction was provided by Frolich[19] who showed that phonon mediated interaction between electrons near the Fermi surface might be attractive.

Two electrons interact through virtual exchange of phonons (just as two nucleons inside a nucleus interact through exchange of mesons). For metals which are bad conductors in the normal state (these metals often exhibit superconductivity) this interaction may be strong enough to dominate repulsive Coulomb interaction leading to a net attractive interaction. (He also showed that the isotope effect of superconductors expressing isotopic mass dependence of the transition temperature would follow from such an interaction). The next important step was taken by Cooper[20] who showed that conduction electrons in metals could form a bound pair in the presence of an attractive interaction.

Two electrons in the bound pair, called the Cooper pair, have equal and opposite momenta and spin. Stability of the pair is ensured, no matter how weak the interaction is, by the presence of other electrons in a metal. This is in contrast with the case of two isolated electrons in the presence of attractive interaction. Any attractive interaction can bind a pair of electrons, if it is suffiently strong.

Cooper's work established that Frolich-type of interaction produces a profound correlation between electrons having equal and opposite momenta and energy of two electrons is lowered by

going over to the correlated pair state. Thus the Fermi sea is unstable against formation of Cooper pairs..

This prompted Bardeen, Cooper and Schrieffer[21] to assume that the superconducting ground state is one in which all electrons are paired among themselves.

The model proposed by BCS is a true many-body one. Existence in a metal of a large number of states having almost the same energy, rules out a conventional configuration-mixing type of calculation and nobody knew how to solve the model.

Here, BCS made a break-through. They made a remarkedly correct guess of the variational form of superconducting ground state function which was linear combination of normal metal configurations in which electron states were occupied in pairs.

Following self-consistent variational procedure, they correctly calculated the energy difference between normal and superconducting phases and showed that there was an energy gap in the electron density of states between normal and superconducting phases.

Physically, the BCS state is one in which Cooper pairs are scattered by phonon-interaction against each other such that momenta of the pairs are conserved. The net momentum of the pair is zero. Hence many pairs with individual momenta can be formed.

Resistanceless state is actually due to inhibition of random scattering of the pairs by the existence of an energy gap. BCS also extended their calculation to higher temperatures and showed that their theory could explain almost all of the experimental data collected on superconductors.

Further, the BCS function introduces in a natural way long-

range correlation between electrons of opposite spin which extends over distances of order 10^{-4} cm in real space. Since common value of the momentum is everywhere the same, there is also long-range correlation of average momentum similar to that suggested by London.

2.6 Transition Temperature

Matthias[22] had emphasized a number of interesting regularities in the appearance of superconductivity in the periodic system.

These regularities could be used as an empirical method for predicting whether a material would superconduct and at what temperature.

This method gives no indication of the mechanism responsible for superconductivity, whereas by a detailed study of the interactions which cause superconductivity it should be possible to predict the value of the transition temperature with some degree of accuracy.

The micrcscopic theory for superconductivity proposed for BCS[21] yields an energy gap of the right order of magnitude and reasonable values for other superconducting parameters, such as T_C, provided one fixes a certain parameter, V, which measures the average strength of the net interaction between electrons very close to the Fermi surface.

Both the screened Coulomb repulsion between the electrons, and the phonon-induced electron-electron interaction contribute to V. The criterion for superconductivity is that V be negative; i.e. the phonon-induced attractive interaction must predominate over the short-range Coulomb repulsion.

In the BCS theory,[21] the critical temperature, T_C, is given by

$$K T_c = 1{\cdot}14 \langle \hbar \omega \rangle_{AV} \exp \left\{ -1 / \left[N(0) V \right] \right\} \tag{2.27}$$

where $\langle \hbar \omega \rangle_{AV}$ is the average energy of the phonons which scatter electrons at the Fermi surface, and $N(0)$ is the-density in energy of electron states on that surface.

Thus a knowledge of V will enable us to calculate T_C.

2.6.1 The MacMillan Equation

MacMillan[2] derived an expression for determining the the transition temperature of a superconductor using the so-called "strong coupled" theory, as a function of the coupling constants for the electron-phonon and Coulomb interactions. It was assumed that the BCS theory of superconductivity was applicable and that given certain properties of the normal state of a metal it was possible to calculate the transition temperature.

Since the necessary properties were not sufficiently well known, the problem was approached from the reverse direction. For a large number of metals and alloys the transition temperature T_C, the Debye temperature θ and the electronic specific heat γ were well known and also for a few metals there were values of the phonon energies and the isotope shift of the transition temperature.

By making use of the theoretical formula for the transition temperature in conjunction with the known experimental data, empirical values for the electron-phonon coupling constant λ and the phonon enhancement of cyclotron mass and specific heat can be found. The measured isotope shifts can be used to find empirical values for the Coulomb coupling constant μ^*.

Solutions of the integral equations given by Ambegoakar and Tewordt [23] and Scalapino et al[24] for the normal and pairing self energies at the transition temperatures were computed by MacMillan following the procedure of Morel and Anderson.[25]

This let to the definition of a dimensionless electron-phonon coupling constant λ

$$\lambda = 2\int_0^{\omega_0} \alpha^2(\omega)\, F(\omega)\, \frac{d\omega}{\omega} \qquad (2.28)$$

where ω_0 is the maximum phonon frequency.

$\alpha^2(\omega)$ is an average of the electron-phonon interaction.

$F(\omega)$ is the phonon density of states.

The strong coupling expression analogous to equation(2.27) was found and given by Mac Millan as

$$\frac{T_c}{\omega_c} = exp\left[\frac{-(1+\lambda)}{\lambda-\mu^*-(\langle\omega\rangle/\omega_0)\lambda\mu^*}\right] \qquad (2.29)$$

where $\langle\omega\rangle$ is the average phonon frequency

μ^* is the Coulomb coupling constant of Morel and Anderson[25] given by

$$\mu^* = \frac{N(0)\ V_c}{1+N(0)\ V_c\ L_n\ \left(E_B/\omega_0\right)} \qquad (2.30)$$

V_C is the matrix element of the screened Coulomb interaction averaged over the Fermi surface.

E_B is the electronic bandwith.

The final formula for the transition temperature as determined by Mac Millan is given by

$$T_c = \frac{\theta}{1.45}\ exp\left[\frac{-1.04(1+\lambda)}{\lambda-\mu^*(1+0.62\lambda)}\right] \qquad (2.31)$$

Although Mac Millan used the Debye temperature θ for the characteristic phonon frequency, the maximum phonon frequency ω_0, or the average phonon frequency $\langle\omega\rangle$ could just as well have been used.

In weak coupled superconductors equation (2.29) reduces to the BCS result with $\lambda - \mu^*$ playing the role of $N(o)V$. In strong coupling the Coulomb interaction modifies the gap function in such a way that the phonon contribution is reduced from λ to $\lambda\left[1-(\langle\omega\rangle/\omega_0)\,\mu^*\right]$

2.6.2 Critical Temperatures in Thin Films

The conjectures of Ginzburg[26] that the surface region in thin films should be different from that in bulk materials and that observable effects in T_C would be found, have been proved experimentally to be correct.

The situation for transition metals such as tantalum (Ta) is very peculiar as far as changes in T_C are concerned.

First, T_C correlates extremely well with density of states in these materials and second, the correlation between T_C and density of states is consistent with the early point of view of Pines[27] where V_{PH} and V_C are expected to be largely independent of $N(0)$.

The properties of the transition metal films are extremely sensitive to gaseous impurities. De Sorbo[28] has studied the effect of gaseous impurities in the superconducting properties of transition metal films.

He determined how an increase in the percentage of oxygen concentration in the sample induced a decrease in the transition temperature.

According to De Sorbo the critical temperature of tantalum varies with oxygen concentration as

$$T_c = 4.48 - c\,\rho_{10} \qquad (2.32)$$

where c is a constant.

ρ_{10} is the resistivity at 10°K.

Rainden and Neugebauer[29] modified equation (2.32) by assuming that the increase in the room temperature resistivity was entirely due to the increase in the residual resistivity i.e. Matthiessen's rule was obeyed and $\rho_{300} - \rho_{10}$ = constant. Therefore the inverse resistance ratio also varies linearly

with oxygen concentration, hence

$$\frac{R_{10}}{R_{300} - R_{10}} = \frac{\rho_{10}}{\rho_{300} \ \rho_{10}} = (\text{constant}) \times (\text{oxygen concentration}) \qquad (2.33)$$

the resulting equation from combining (2.32) and (2.33) is

$$T_C = 4.48 - 0.77 \frac{R_{10}}{R_{300} \ R_{10}} \qquad (2.34)$$

A plot of equation (2.34) is shown in Figure (64).

2.7 Critical Current Densities

If the current carried by a superconductor film exceeds a critical value, a transition to the normal state is induced. For large specimens the critical current can be calculated from the critical magnetic field by making use of Silsbee's[30] criterion.

This states that in the absence of an applied magnetic field the critical current is that current which produces at the surface of the specimen a magnetic field equal to the critical field Hc.

This simple rule does not hold for specimens which have one or more dimensions comparable with the penetration depth (λ_L), the most obvious reason being that even if some sort of modified Silsbee's rule were to hold we should not know whether to insert the bulk critical field Hc or the actual critical field for small specimens.

Thus for a cylindrical wire of radius $a \gg \lambda$, the surface critical current density with no applied field can be obtained

$$2\pi a \lambda_L \frac{4\pi}{c} J_c = 2\pi a H_c \qquad (2.35)$$

or

$$J_c = \frac{c H_c}{4\pi \lambda_L} \qquad (2.36)$$

The spacial variation is given by

$$J(x) = J_c \exp\left(-x/\lambda_L\right) \qquad (2.37)$$

The limits of the integration are from the surface x = o to very deep inside the superconductor.

If Silsbee's rule were correct for thin films, the critical current density would be much larger than is experimentally observed.

The result for the critical current density as first obtained by London,[31] is

$$\frac{H_c^2}{8\pi} = \frac{1}{2} \frac{m}{n_s e^2} J_c^2 \qquad (2.37a)$$

The temperature dependence for the critical current density, for temperatures near the critical temperature, is obtained from the temperature dependence of the critical field and the penetration depth from BCS theory. These give

$$J_c = \frac{c H_0}{\sqrt{2}\,\pi \lambda(0)} (1 - T_R)^{3/2} \qquad (2.38)$$

where H_0 and $\lambda(0)$ are the critical field and the penetration depth, respectively, for bulk material at 0°K and $T_R = T/T_C$.

The Ginzburg-Landau theory gives the result for $t \ll \lambda_L$, T near T_c

$$J_c = \frac{2 c H_0 (1 - T_R)^{3/2}}{3\sqrt{3}\,\pi \lambda_L(0) (1 + \xi_0 \, l)^{1/2}} \qquad (2.39)$$

where the effect of scattering has been introduced. It is only through the mean free path that the film thickness affects the critical current which decreases slowly with decreasing film thickness.

The total critical current density is proportional to the thickness in the range $t \ll \lambda_L$ where the current density is uniform through the thickness. In the range $t \gg \lambda_L$, where the current is limited to near the surface, J_C is constant.

The London theory, applied to a flat, unshielded film, predicts

$$J_c = \frac{c}{2\pi} H_c \tanh \frac{d}{2\lambda_L} \quad . \qquad (2.40)$$

This equation has been derived with the assumption of uniform current across the width of the film.

2.8 Ellipsometry and Thin Film Optics.

In principle, the amplitude and phase of a beam of light reflected or transmitted by a thin film, or combination of films, may be determined by solving Maxwell's equations with the appropriate boundary conditions. The problem is considerably simplified by the use of Fresnel coefficients R and T, where R is the ratio of reflected to incident amplitudes and T is the ratio of transmitted to incident amplitudes.

For different boundaries between media the notation used here is adapted from that of Abele's[32] and used by Heavens.[33] A superscript + or - indicates the direction of propagation with respect to the normal to the film. The direction of the plane of polarization of any orientation is specified with respect to the plane of incidence.

The wave vectors are resolved into components parallel and perpendicular to the plane of incidence, and are denoted by a subscript (p) or (s) respectively. The media are numbered and the material identified by this number. If a medium is absorbing, the refractive index is a complex quantity $N = n - ik$, in which the imaginary part is related to the absorption of energy by the medium. For non-normal incidence, the angles of refraction become complex quantities.

The physical interpreation of this lies in the fact that the planes of equal phase are no longer parallel to the planes of equal amplitude.[34]

It may be shown that the Fresnel coefficients are given by

$$R_{12(p)} = \frac{E_{1p}^-}{E_{1p}^+} = \frac{N_1 \cos\phi_2 - N_2 \cos\phi_1'}{N_1 \cos\phi_1 + N_2 \cos\phi_1} \qquad (2.41)$$

$$R_{12}(s) = \frac{E_{1s}^-}{E_{1s}^+} = \frac{N_1 \cos\phi_1 - N_2 \cos\phi_2}{N_1 \cos\phi_1 + N_2 \cos\phi_2} \qquad (2.42)$$

for light travelling from medium 1 to medium 2 having an angle of incidence ϕ_1, and angle of refraction ϕ_2. Similar expressions exist for the transmitted (P) and (s) components.

The above equations may be applied to a single film, which is assumed to be homogeneous and isotropic and to have parallel plane boundaries as indicated in Figure (4). This represents a parallel beam of plane polarized light of unit amplitude and wavelength λ falling on an absorbing film of thickness t and complex refractive index N_2 , supported on an absorbing substrate of index N_3.

The complex amplitudes of the successive beams reflected and transmitted by the film are shown in Figure (4) in which δ_2 represents the amplitude and phase change in traversing the film once,

$$\delta_2 = \frac{2\pi}{\lambda} N_2 \, t \cos\phi_2 \qquad (2.43)$$

The reflected amplitude from the whole system is thus given by the infinite series:

$$R_{13} = R_{12} + T_{12} T_{12} R_{23} e^{-2i\delta_2} - T_{12} T_{12}' R_{12} \left[R_{13}\right]^2 e^{-4i\delta_2} + \text{-----}$$

which may be summed to give

$$R_{13} \simeq R_{12} + \frac{T_{12} T_{12}' R_{23} e^{-2i\delta_2}}{1 + R_{12} R_{23} e^{-2i\delta_2}} \qquad (2.44)$$

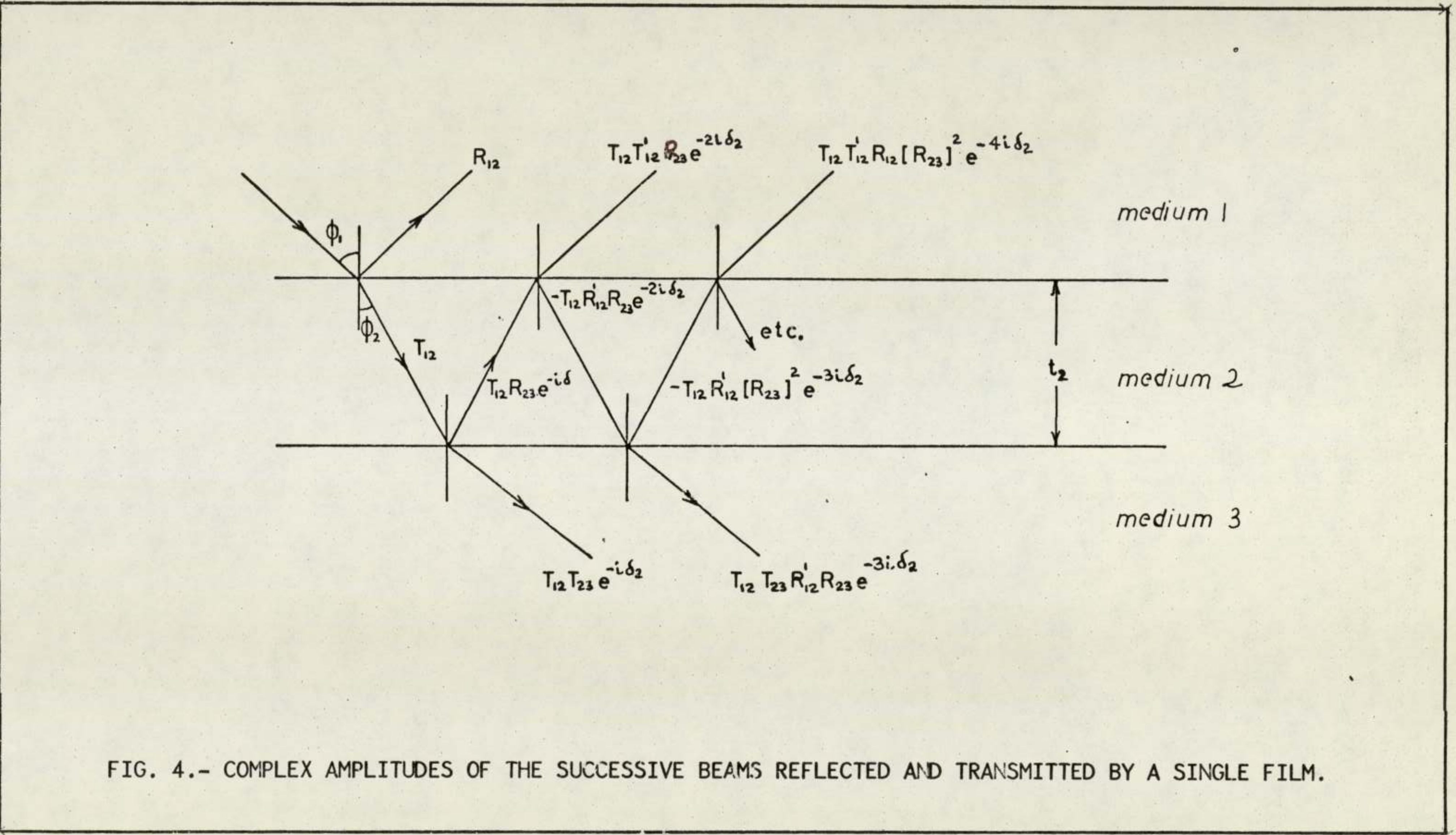

FIG. 4.- COMPLEX AMPLITUDES OF THE SUCCESSIVE BEAMS REFLECTED AND TRANSMITTED BY A SINGLE FILM.

It follows from the conservation of energy[34] that $T_{12}\ T_{12}' = 1 - \left[R_{12} \right]^2$ and substituting this into the previous expressions, the reflected amplitude becomes

$$R_{13} = \frac{R_{12} + R_{23}\ e^{-2i\delta_2}}{1 + R_{12}\ R_{23}\ e^{-2i\delta_2}} = \rho\, e^{i\Delta} \qquad (2.45)$$

where ρ is the amplitude ratio and Δ is the difference in phase of the reflected light compared to the incident light. Two identical expressions exist for the (p) and (s) components, although the numerical values are different.

The ratio of amplitude changes for the (p) and (s) components is given by

$$\frac{R_{13\,(p)}}{R_{13\,(s)}} = \frac{\rho_{(p)}\ e^{i\Delta_p}}{\rho_{(s)}\ e^{i\Delta_s}} = \frac{\rho_{(p)}}{\rho_{(s)}}\ e^{i(\Delta_p - \Delta_s)} \qquad (2.46)$$

For convenience, this ratio is usually expressed in the form

$$\frac{R_{13\,(p)}}{R_{13\,(s)}} = \operatorname{Tan}\Psi\ e^{i\Delta} \qquad (2.47)$$

As we shall show, the ellipsometer measures Tan Ψ, the relative amplitude reduction and Δ , the difference in phase change for the (p) and (s) components. The parameters Ψ and Δ are thus related, though the Fresnel coefficients, to the refractive index and thickness of the film, and the angle of incidence. The derivation of n and k for the film from the measured values of Ψ and Δ is extremely laborious, so that an electronic computer is essential. For an opaque,clean film surface, n and k are related to the instrument readings Ψ and Δ through equations (2.41), (2.42) and (2.47) and are given in a form suitable for computation by Ditchburn[35] as

$$n^2-k^2 = \frac{\sin^2\phi_1 \tan^2\phi_1 (\cos^2 2\Psi - \sin^2 2\Psi \sin^2\Delta) + \sin^2\phi_1}{(1+\sin^2\Psi \cos\Delta)^2} \quad (2.48)$$

$$2nk = \frac{\sin^2\phi_1 \tan^2\phi_1 \sin 4\Psi \sin\Delta}{(1+\sin^2\Psi \cos\Delta)^2} \quad (2.49)$$

The extension of the calculations to several layers is possible since a single film, bounded by two surfaces, has an effective reflection coefficient and phase change. Such a film may be replaced by a single surface having the same properties, as indicated in Figure (5).

In this way, it is possible to start at the supporting substrate and work upwards through each layer to the surface, as performed by Ronard,[36] or to start at the surface and work downwards towards the substrate, as proposed by Vasiček.[37] This last method has been used in the section on oxidation of tantalum films. For an oxidized surface, the angles Ψ and Δ are changed from the values for a clean surface. Providing that the optical constants of the oxide free surface are known, then any subsequent changes of the instrument angles Ψ and Δ can be used to determine the thickness of the oxide film formed.

If two angles of incidence are used, it is also possible to determine the optical constants of the oxide layer as will be demonstrated in Chapter 4.

2.8.1 Theory of Compensator Method of Ellipsometry.

The basis of the compensator method, as used in this work, is illustrated in Figure (6). Plane polarized light, produced by the polarizer P, is incident on the specimen with azimuth ψ i.e. its plane of polarization inclined at an angle ψ to the plane of incidence. Conventionally, inclinations are considered positive if anti-clockwise from the plane of incidence, looking towards the on-coming light. On reflection from the specimen

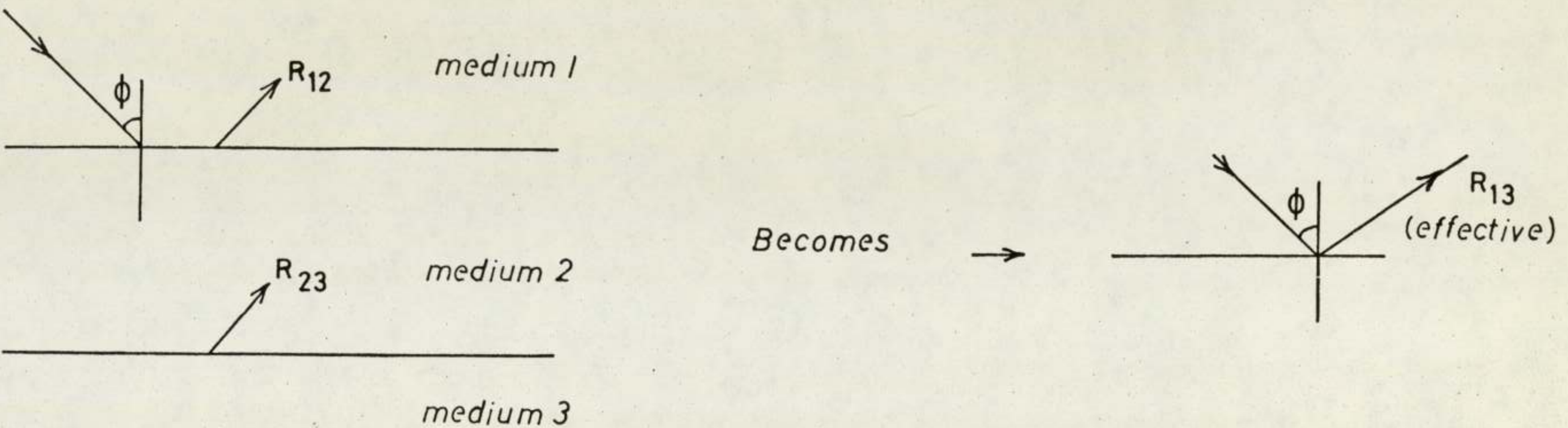

FIG. 5.- APPLICATION OF ELLIPSOMETRY TO SEVERAL LAYERS.

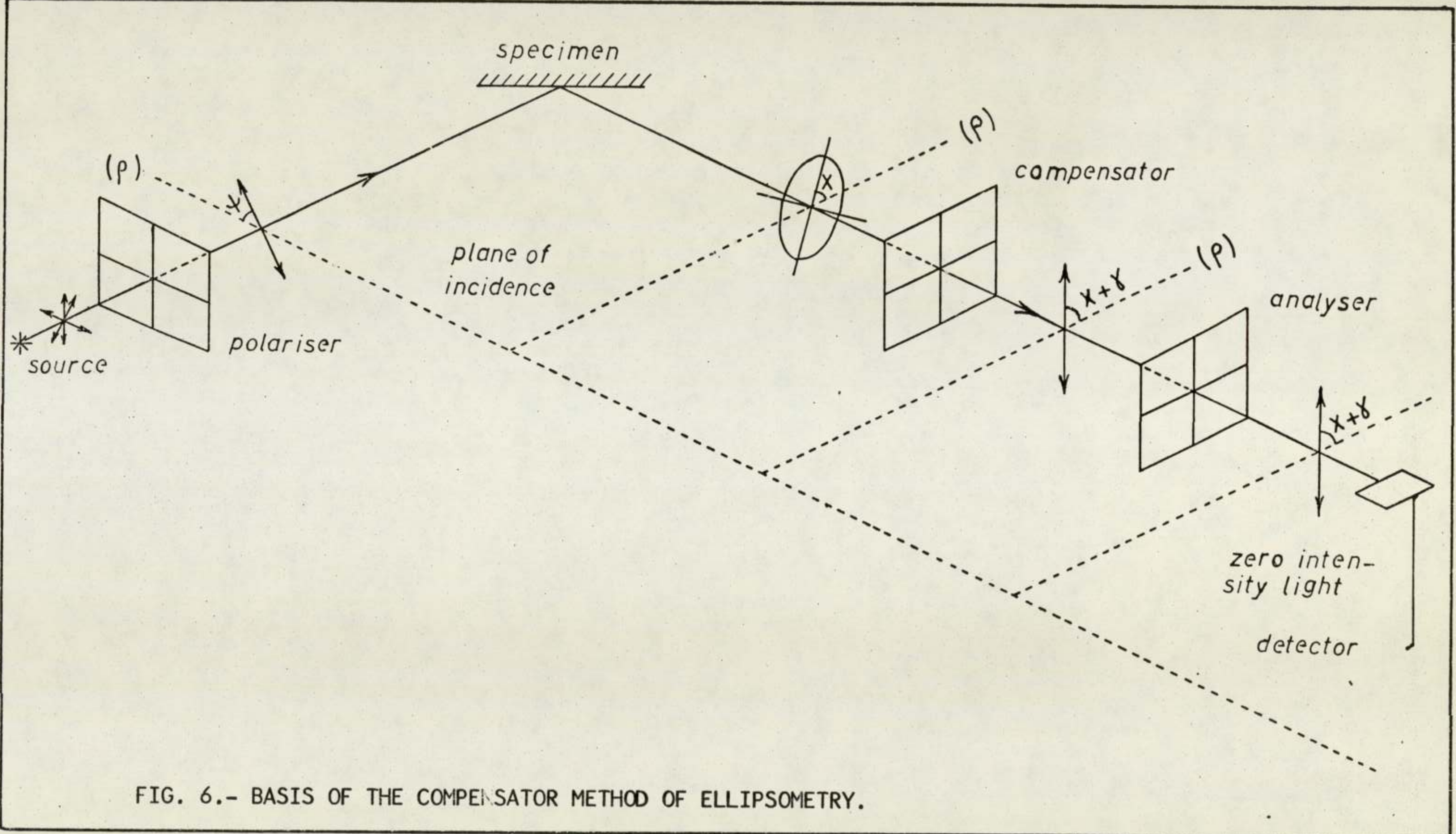

FIG. 6.- BASIS OF THE COMPENSATOR METHOD OF ELLIPSOMETRY.

the difference in amplitude reduction and the difference in phase change between the (p) and (s) components ensures that the reflected light is, in general, elliptically polarized i.e. the tip of the electric vector moves in an ellipse with azimuth of the major axis χ, and ellipticity (ratio of minor to major axes) γ. This elliptically polarized light then passes through the compensator, which consists of a bi-refringent sheet of mica.

If the fast axis of the compensator is arranged to be parallel to the major axis of the reflected ellipse, the vibrations along the major and minor axes of the ellipse (for which a phase difference of 90 degrees exists) are again brought into phase, and plane polarized light results. The azimuth of this "compensated" plane polarized light will be at an angle γ to the major axis of the ellipse. See Figure (7).

Finally, the light passes through the analysing polaroid A, which may be rotated until its transmission axis is perpendicular to the plane of polarization. In this condition and only in this condition, the light intensity received by the photomultiplier detector is zero.

The experimental procedure is considerably simplified if the compensator is first located with its fast axis at exactly 45 degrees to the plane of incidence. The polarizer and analyser are then adjusted for minimum light intensity received by the photomultiplier. The situation then corresponds to that shown in Figure (7). The azimuth of the reflected ellipse is always 45 degrees, or in other words, the amplitudes of the reflected (p) and (s) components are equal, i.e. $\bar{E}_p$ and $\bar{E}_s$ are equal.

The azimuth ψ of the polarizer is then equal to the

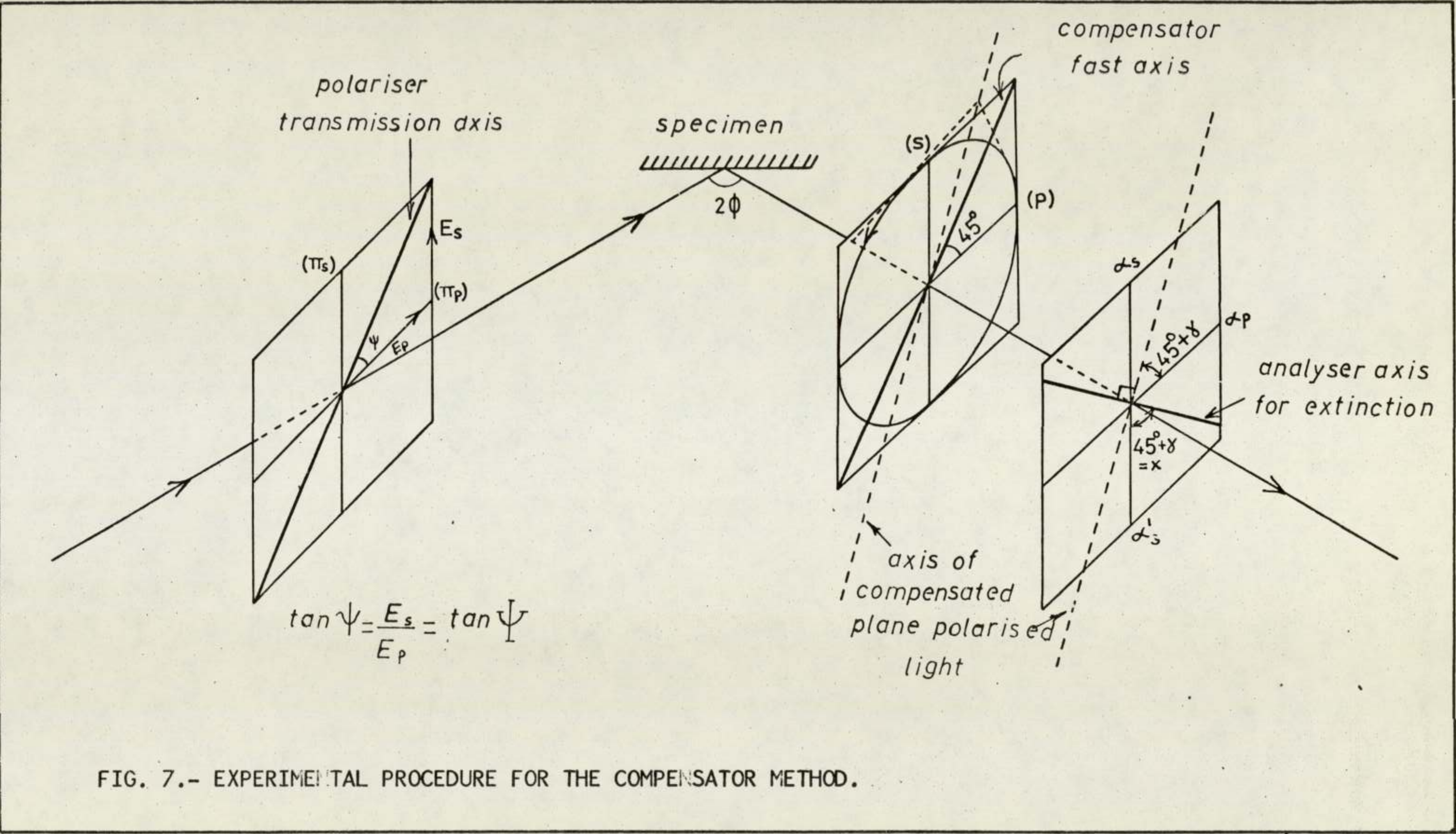

FIG. 7.- EXPERIMENTAL PROCEDURE FOR THE COMPENSATOR METHOD.

parameter Ψ mentioned previously, from figure (7).

$$\tan \psi = \frac{E_s^+}{E_p^+} \tag{2.50}$$

But

$$\tan \Psi = \frac{\rho_{(p)}}{\rho_{(s)}} = \frac{\left(\frac{E_p^-}{E_p^+}\right)}{\left(\frac{E_s^-}{E_s^+}\right)} = \frac{\left(\frac{E_p^-}{E_s^-}\right)}{\left(\frac{E_p^+}{E_s^+}\right)} \tag{2.51}$$

Since from above

$$\frac{E_p^-}{E_s^-} = 1 \cdot 00 \tag{2.52}$$

then

$$\tan \Psi = \frac{1}{\left(\frac{E_p^+}{E_s^+}\right)} = \frac{E_s^+}{E_p^+} \tag{2.53}$$

Hence from (2.50)

$$\tan \psi = \tan \Psi$$
$$\psi = \Psi \tag{2.54}$$

The ellipticity γ is related to the phase difference Δ between the (p) and (s) components. In general, it may be shown that

$$\tan \Delta = \frac{\tan 2\gamma}{\sin 2\chi}$$

Since, from above $\chi = 45^{\circ}$, $\sin 2\chi = 1.00$ and

$$\tan \Delta = \tan 2\gamma \ ; \ \Delta = 2\gamma \tag{2.55}$$

The ellipticity γ and hence the phase difference Δ is determined from the analyser aximuth, as shown in Figure (7).

The azimuth of the compensated light is $45^{o} + \gamma$, so that the azimuth of the analyser in its extinction position will be $45^{o} + \gamma$ with respect to α's, the perpendicular to the plane of incidence. It is this quantity, marked X on Figure (7) which is measured experimentally

Since $x = 45^{o} + \gamma = 45^{o} + \Delta/2$

then $\Delta = 2x - 90^{o}$ (2.56)

In general, pairs of polarizer and analyser azimuths for extinction occur which fall into four zones. MacCrakin[38] gives a detailed explanation of the effect, although it should be noted that in his paper, the names "polarizer" and "analyser" are interchanged with those in this work, because his experimental arrangement has the compensator placed before the reflection.

The total 32 pairs of polarizer and analyser positions for extinction can be understood in a methodical fashion by representing the state of polarization of light by means of the Poincare' sphere[39]

CHAPTER 3

Experimental Equipment

In order to achieve the objectives mentioned earlier it was necessary to design apparatus in which sets of films could be prepared under identical environmental conditions, but with some variation as indicated below:

a) With varying thickness

b) With the same thickness

c) At the same substrate temperature

d) At different substrate temperature

Subsequently the films were required to be transferred from the evaporation unit to a cryostat for the measurement of electrical properties over the temperature range $2^{o}K$ to $300^{o}K$.

In this connection equipment was developed for continuous monitoring of film resistance and film temperature.

Because of the inevitable delays in removing from a vacuum environment to the actual electrical testing, it was necessary to investigate oxidation properties of films exposed to atmospheric pressure by measuring a) oxidation rates and b) oxide thickness of reasonably stable films which had been exposed for prolonged periods.

In this chapter the items of equipment developed and used for the present work are given in some detail.

3.1 Evaporation Unit

The evaporation unit must satisfy certain conditions in order to obtain Tantalum films of sufficiently high purity so that reproducible superconducting characteristics are achieved. This includes : base vacuum of the order of 10^{-10} torr in the evaporation chamber, elevated deposition rate to avoid gaseous contamination of the films, high tantalum purity and also the possibility of keeping the substrates at

sufficiently high temperature in order to minimise the sticking coefficient of gas molecules during film deposition, also affecting particle size.

3.1.1 Vacuum System

The Vacuum System is shown in Figures (8) and (9). The U.H.V. in the experimental chamber was obtained by means of a 200 lit sec^{-1} ULTEK Sputter Ion Pump attached directly to the chamber.

The ion pump was surrounded by an oven containing two 500 watt heater elements controlled by a Variac, this together with another 4 heater elements, placed inside the four pipes which cross the ion pump from top to bottom and which are located in the four corners of the pump body, enable the pump to be baked and maintained at a temperature of 400°K while in operation.

For the rough pumping of the vacuum chamber a single stage rotary pump was used, together with three stainless steel purpose designed sorption pumps. To prevent backstreaming of rotary pump oil into the vacuum system, a liquid nitrogen trap containing ceramic discs was designed and interposed between the pump and the manifold.

3.1.2 Vacuum Chamber

The vacuum chamber was a stainless steel one constructed by FERRANTI LTD., it consisted of a cylinder, 25cm in diameter and 50cm long, fitted with a number of flanges. The five 6.5 inch diameter flanges were sealed by means of aluminium wire seals.[40]

The eleven remaining flanges were standard 2.75 inch diameter copper gasket flanges. The flange used to connect the vacuum chamber with the ion pump was sealed using a 6.75 inch diameter copper gasket. The 6,5 inch diameter flange in the

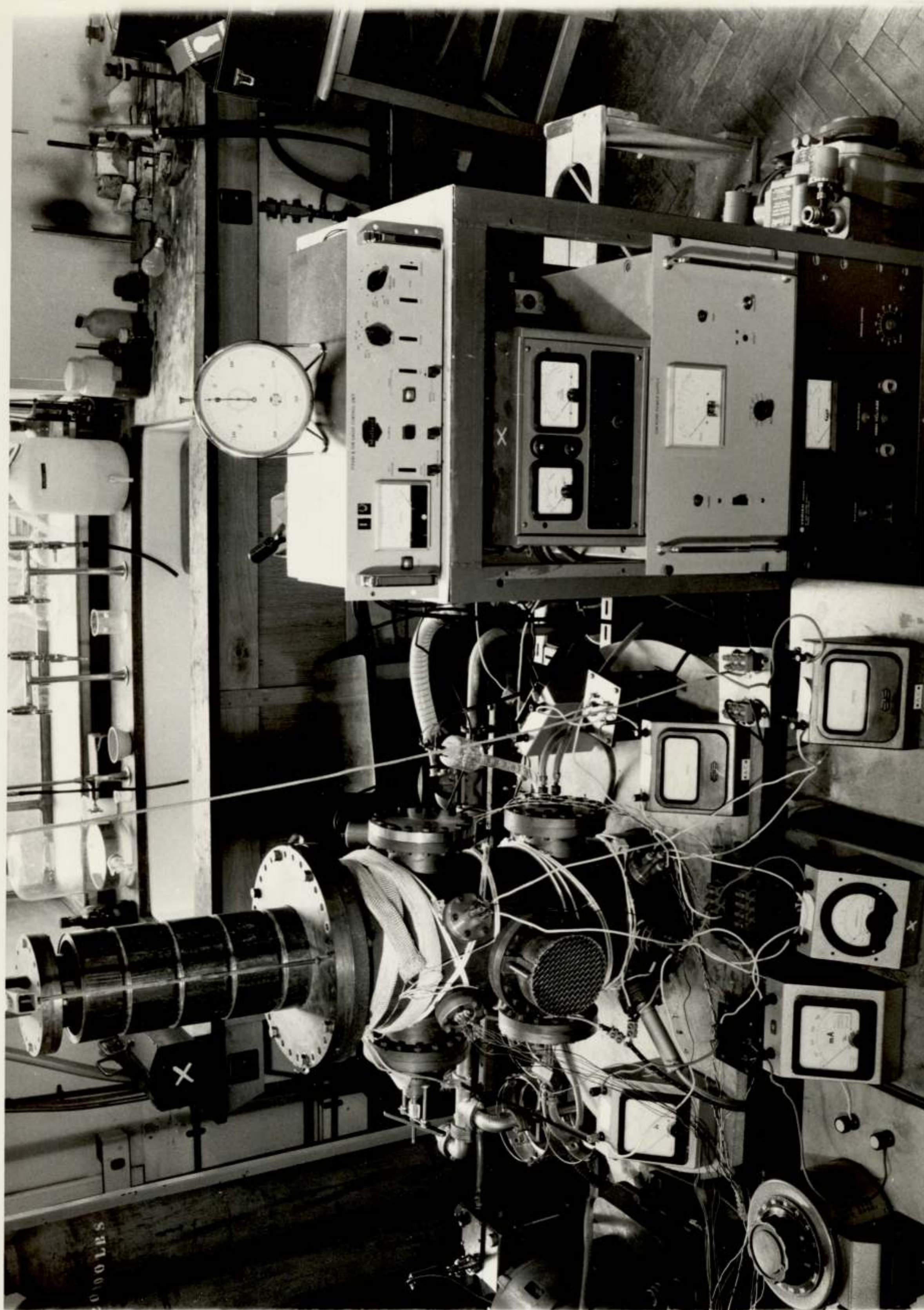

FIGURE 8 GENERAL VIEW OF THE EVAPORATION SYSTEM

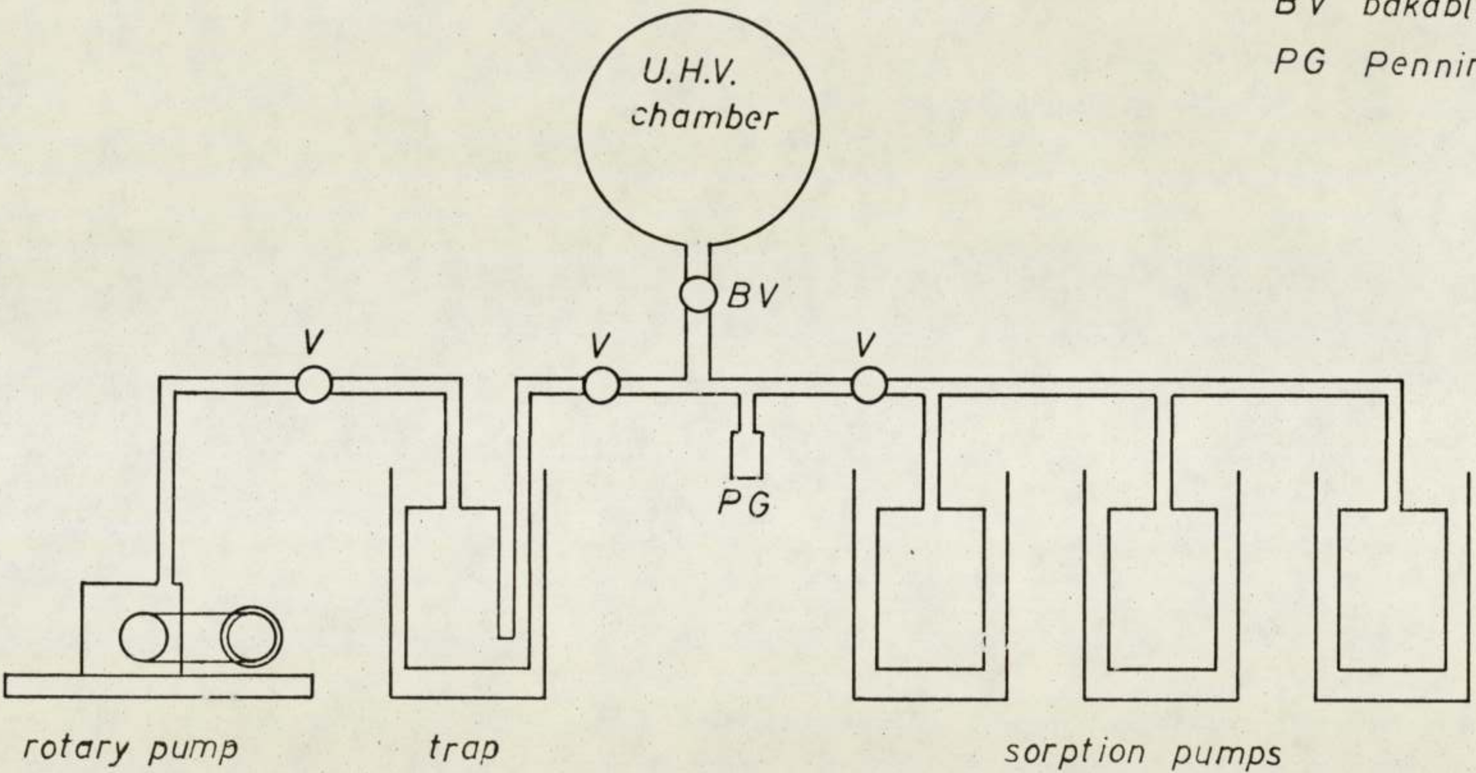

FIG. 9.- ARRANGEMENT OF ROUGH PUMPING ELEMENT.

middle of the front part of the chamber was fitted with an observation port so as to be able to view the sample holder, the shutter assembly and the tantalum sample in the crucible of the electron beam evaporator, the latter viewed indirectly via a stainless steel mirror positioned inside the vacuum chamber.

Two of the 2.75 inch flanges in the bottom of the chamber were used to carry electrical lead throughs for supplying power to the electron beam evaporator. Another four of the same type were fitted with 3-way lead throughs which carried all the electrical connections to the seven substrate heaters, and two of the remaining ones were equipped with 8-way lead throughs as to carry out the thermocouple wires.

One port 6.5 inch carried the electron gun evaporator in conjunction with cooling water for the crucible. It was found in preliminary tests on the vacuum system that radiation from the electron beam evaporator produced unacceptably high temperatures on the walls of the vacuum chamber. To overcome this a water cooled stainless steel shield was designed and fitted around the evaporator. Figure (10). The shield reduced the amount of radiant heat from the molten tantalum sample to the walls of the vacuum chamber and it also provided a cooled surface for the deposition of tantalum for gettering purposes.

One port 6.5 inch diameter was used for mounting a bellows type linear motion drive, which was designed to operate the shutter mechanism in the substrate holder. One of the two remaining 2.75 inch ports was used to locate an ion gauge for pressure measurements and the other a mass spectrometer head for partial pressure measurement.

3.1.3 Electron Beam Evaporator

The melting point and boiling point of tantalum are $3269^{\circ}K$ and $5698 \pm 100^{\circ}K$ respectively, and in order to obtain a reasonable evaporation rate, temperatures in excess of $5698^{\circ}K$ are required.

A VARIAN No.980.001 electron beam evaporator was mounted in the chamber so that the Tantalum sample in the crucible was about 20cm from the substrate position. The evaporator was supported by the stainless steel tubes which carried the cooling water for the crucible. Electrical connection between the evaporator and the lead throughs were made by uninsulated 12 SWG copper wire.

The electron beam current could be varied continuously from 0 to 500mA, giving up to 2000 watt beam power. The single crucible electron gun as supplied was found to give evaporation rates which were far too low for the stringent requirements. Even at maximum power the rate was only 50Å per minute. An overspray shield was developed in the present work in order to improve the deposition rate. The shield was cut from 0.05cm thick molybdenum sheet and attached as shown in Figure (11). The evaporation rate was increased by a factor of 5.

3.1.4 Substrate Holder

In view of the observations made at the beginning of this chapter a substrate holder was designed taking into consideration the geometrical configuration of the system as well as the importance of being able to keep certain deposition parameter constants in order to study the influence in the properties of the films of a particular one.

It was arranged so that eight different samples could be deposited simultaneously either at the same distance from the evaporation source (assuming it was a point source) or at

FIG. 10.- POSITIONING OF THE WATER COOLED SHIELD AROUND THE E-GUN EVAPORATOR.

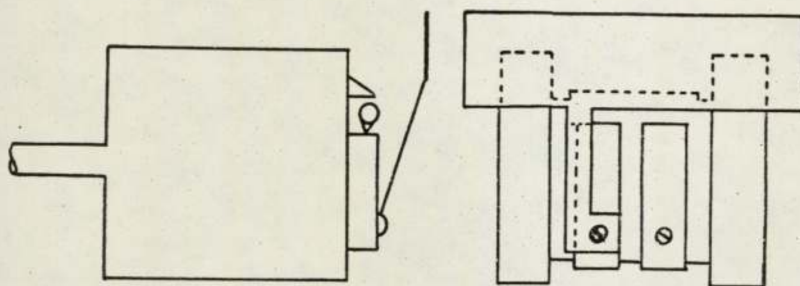

FIG. 11.- OVERSPRAY SHIELD; POSITION IN THE E-GUN.

different distances. The body of the holder was made of stainless steel and is shown in Figures (12) and (13), it consists of a plate 24cm long, 9cm wide and 0.075cm thick with an hexagonal hole in the middle. Attached to every side of the hexagon there is a mounting bracket, carrying the masks and the substrate which could be placed in three different positions and had been designed so that in each of the three different positions the centre of symmetry of the mask is always perpendicular to the radius of the sphere whose centre and radius are the evaporation source and the distance between the source and the substrates respectively.

For this purpose and from the geometrical arrangement, the relative position of the masks were calculated. The necessary condition was achieved by using three different masks having apertures of the same size but shifted towards the pole of the sphere as the distance between the substrate and the evaporation source decreases. (Figure 14).

Finally, an hexagonal piece, big enough to hold another two masks and substrates, joins the six mounting brackets together. The distance from the source to these last two samples is invariable, being able to change only the position of the remaining six described above.

The dimension of a single shutter required to shield the substrates from the source was more than half the chamber diameter. It was therefore necessary to convert a 2cm linear movement used to manipulate the shutter of the original design of the sample holder to a 90° rotation about a horizontal axis.

Seven separate nichrome heaters were also constructed (the two substrates on top of the sample holder share the same heater) each one being supplied independently by means of a Variac and a transformer and so the temperature of each

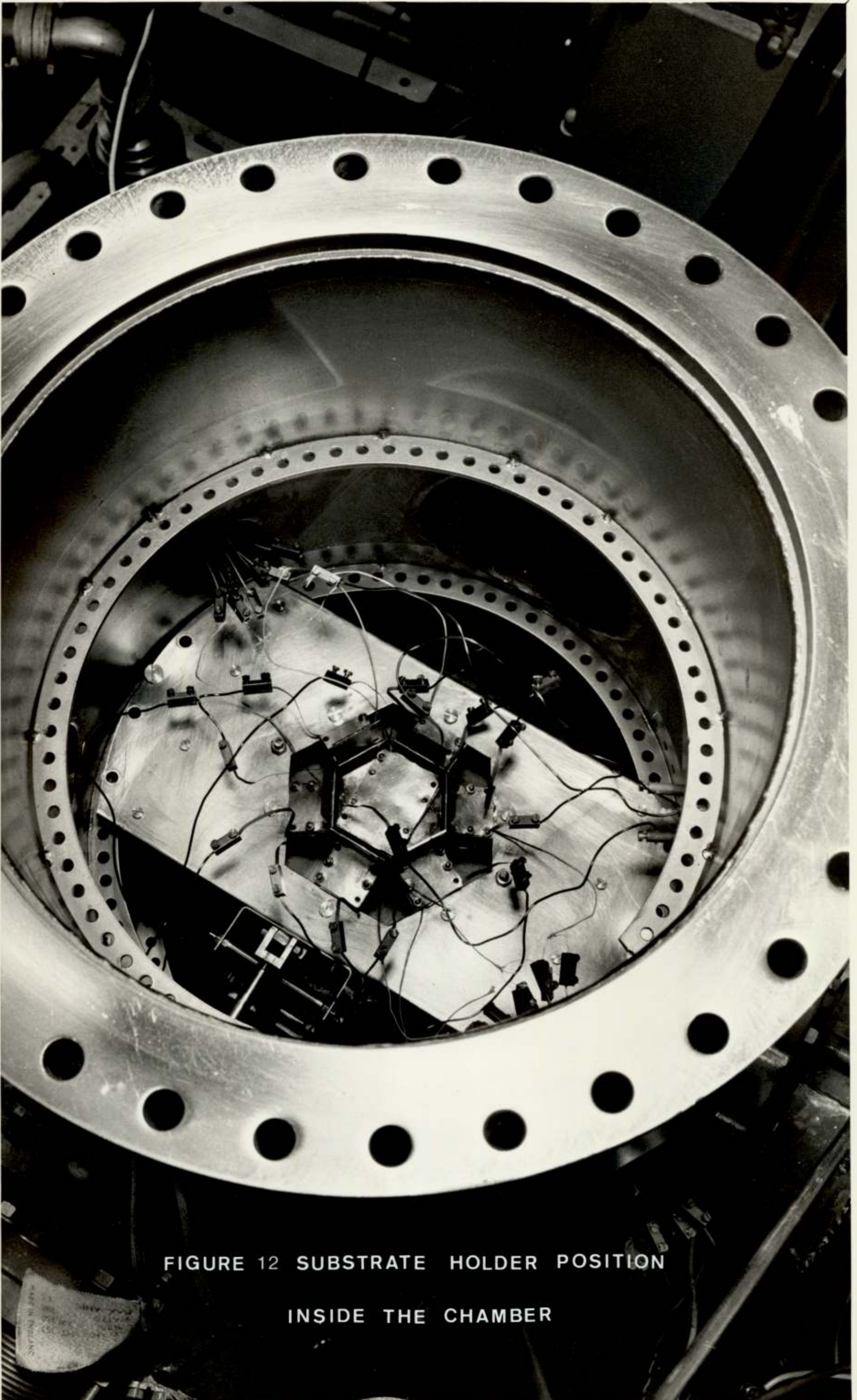

FIGURE 12 SUBSTRATE HOLDER POSITION INSIDE THE CHAMBER

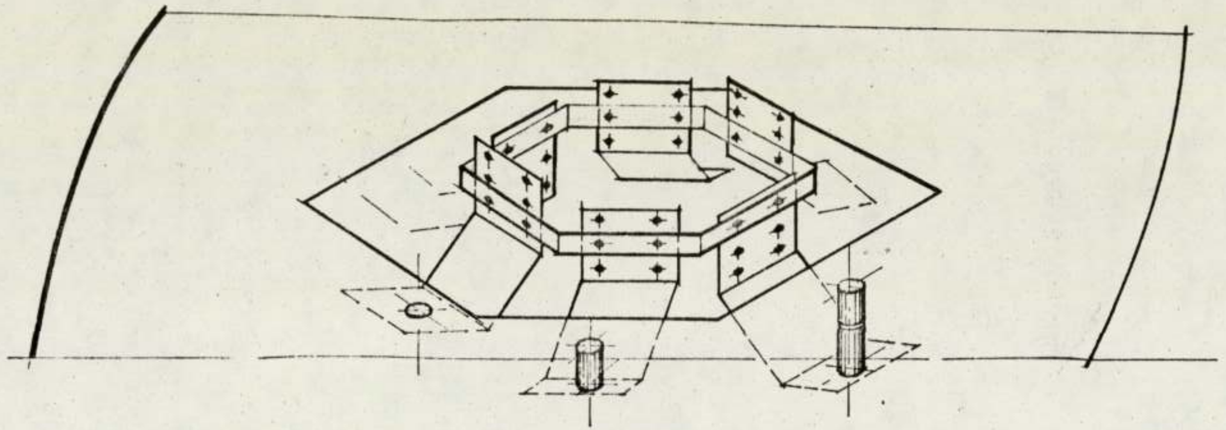

FIG. 13.- VIEW OF THE SUBSTRATE HOLDER.

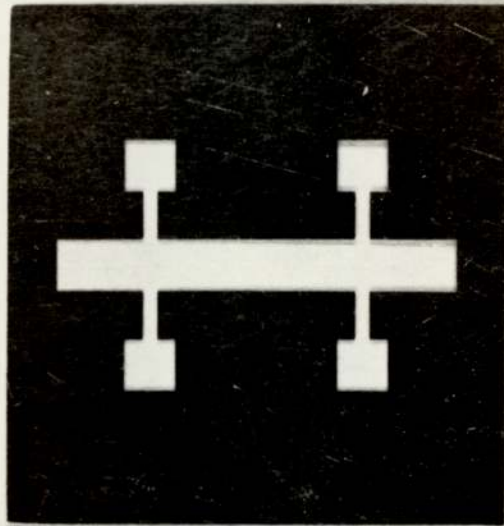

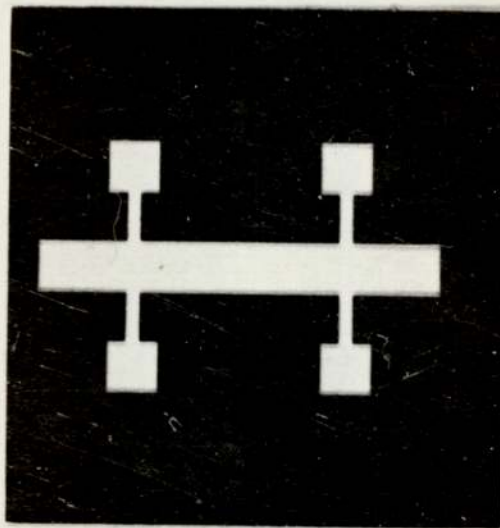

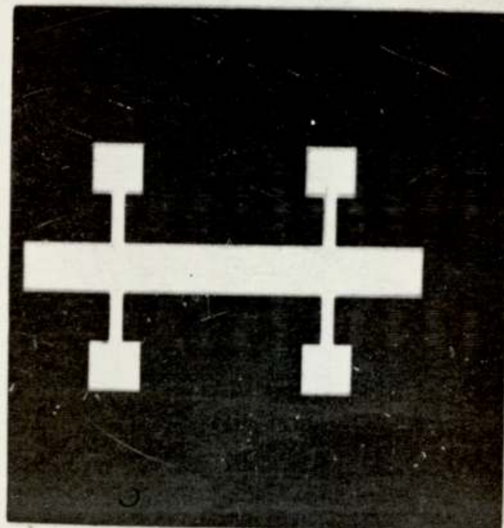

FIGURE 14 MASKS FOR THE THREE POSITIONS

substrate could be separately controlled.

The seven heaters were able to maintain substrates temperatures up to 773°K during the deposition of the films.

The temperatures of the samples were determined by eight copper/constantan thermocouples which were clamped onto each substrate.

It was necessary to remove the substrate holder after each sample preparation run.

3.2 Cryostat Assembly

Since the superconducting properties of the films were to be investigated, a helium cryostat was required to maintain the necessary low temperature for an extended period of time. The sample holder had to be attached to the cryostat so that good thermal contact existed between the liquid helium and the substrate.

3.2.1 Cryostat

The cryostat used in the investigation was a standard helium cryostat manufactured by the Oxford Instrument Company Figure (15). The liquid helium chamber had a usable volume of ≃ 5 litres. When fully operational the heat input to the helium chamber was $<$ 0.1 watt. Then the substrate could be maintained at liquid helium temperature for 10 to 15 hours.

A 250 lit sec^{-1} rotary pump was linked to the helium chamber for reducing the pressure over the liquid helium, in this way it was possible to cool the liquid helium to a temperature of about 1.5^{o}K. The assembly containing the substrate mounting was positioned in the cryostat by suspending it from a 2cm diameter stainless steel tube which also served for evacuating the assembly Figure (16).

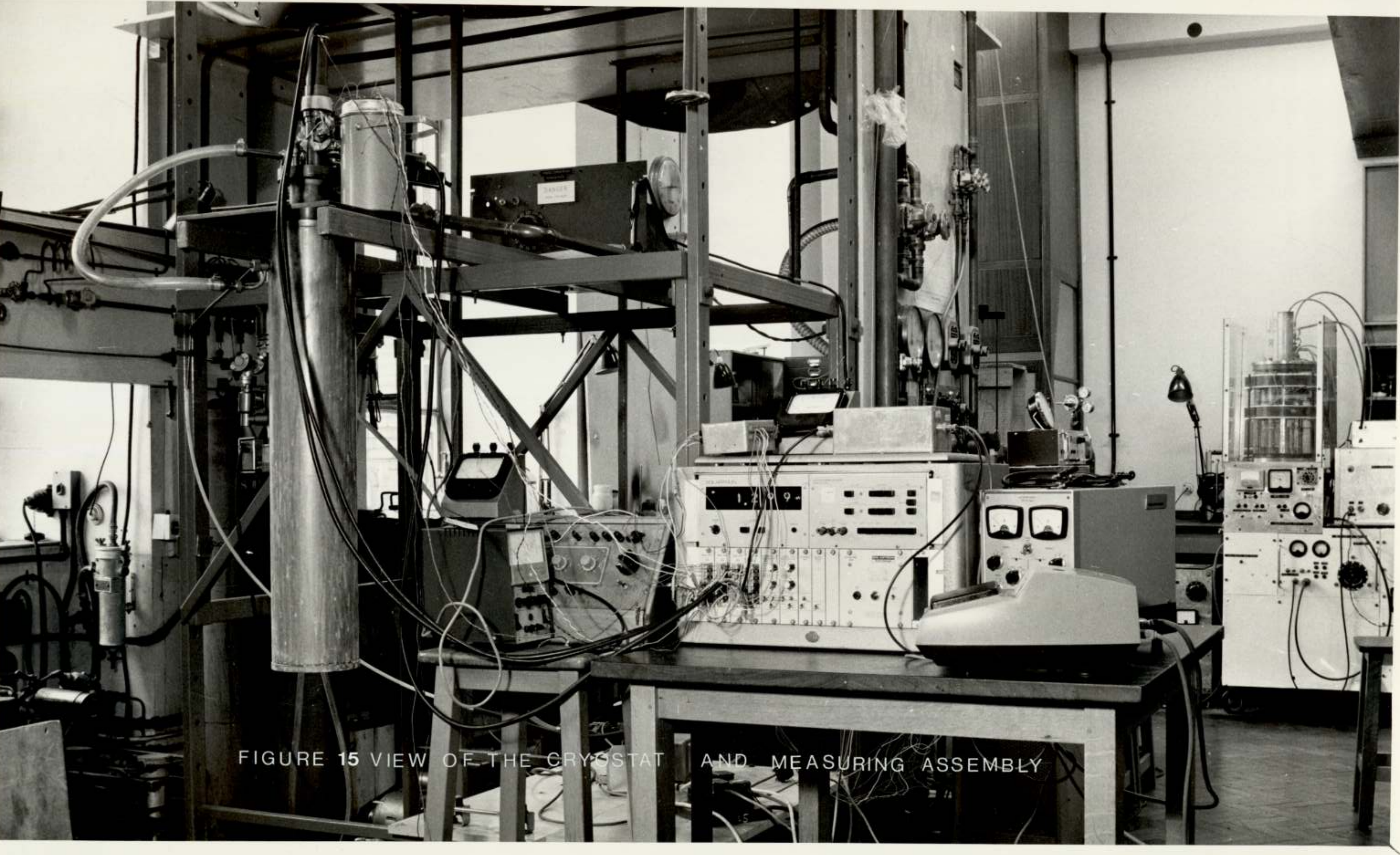

FIGURE 15 VIEW OF THE CRYOSTAT AND MEASURING ASSEMBLY

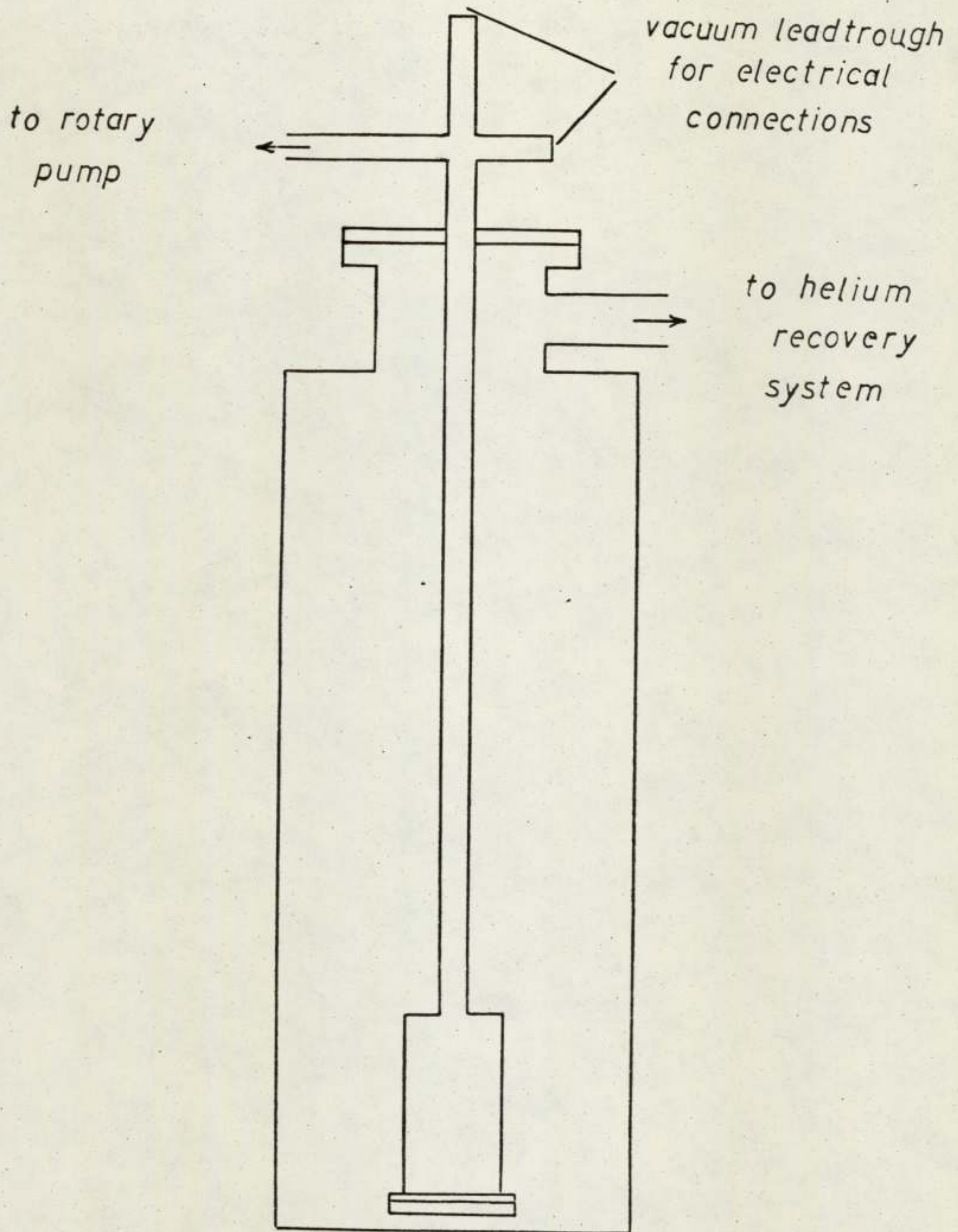

FIG. 16.- CRYOSTAT ASSEMBLY.

3.2.2 Cryostat Sample Holder

With the modified evaporator substrate holder it was possible to prepare eight samples simultaneously. In order to measure electrical properties of more than one sample at a time a new cryostat sample holder was designed.

The first intention was to eliminate difficulties from oxidation which would arise if films were measured at varying times after removal from the evaporation chamber.

The body of the substrate mounting was a copper cylinder 12cm long and 5.4cm in diameter. The base was a 0.3cm thick detachable brass flange sealed using an indium wire ring. Figure (17). The other end of the cylinder was an attached copper flange which also served as a mounting for the 0.3cm stainless steel tube that connects the assembly to the vacuum system.

The sample holder is shown in Figures (17) and (18). It consisted of a 1.25cm diameter and 3.25cm long brass rod soldered to the bottom flange. Around this rod was wound a 20 watt constantan heater to raise the film temperature from $1.5^{o}K$ to $300^{o}K$.

At the other end of the brass rod a rectangular copper block 2.5cm x 2.5cm x 4.5cm was attached, the four perpendicular faces were used as sample mountings.

The electrical contacts for each one of the four samples were made by using 6 copper strips cut from a copper sheet 0.102mm thick using two for the current and four for the voltage readings. All the strips were insulated in the back to prevent them from making contact with the copper block once they were mounted on top of it. Later they were soldered to two narrow strips of vero board, three to each one, and these

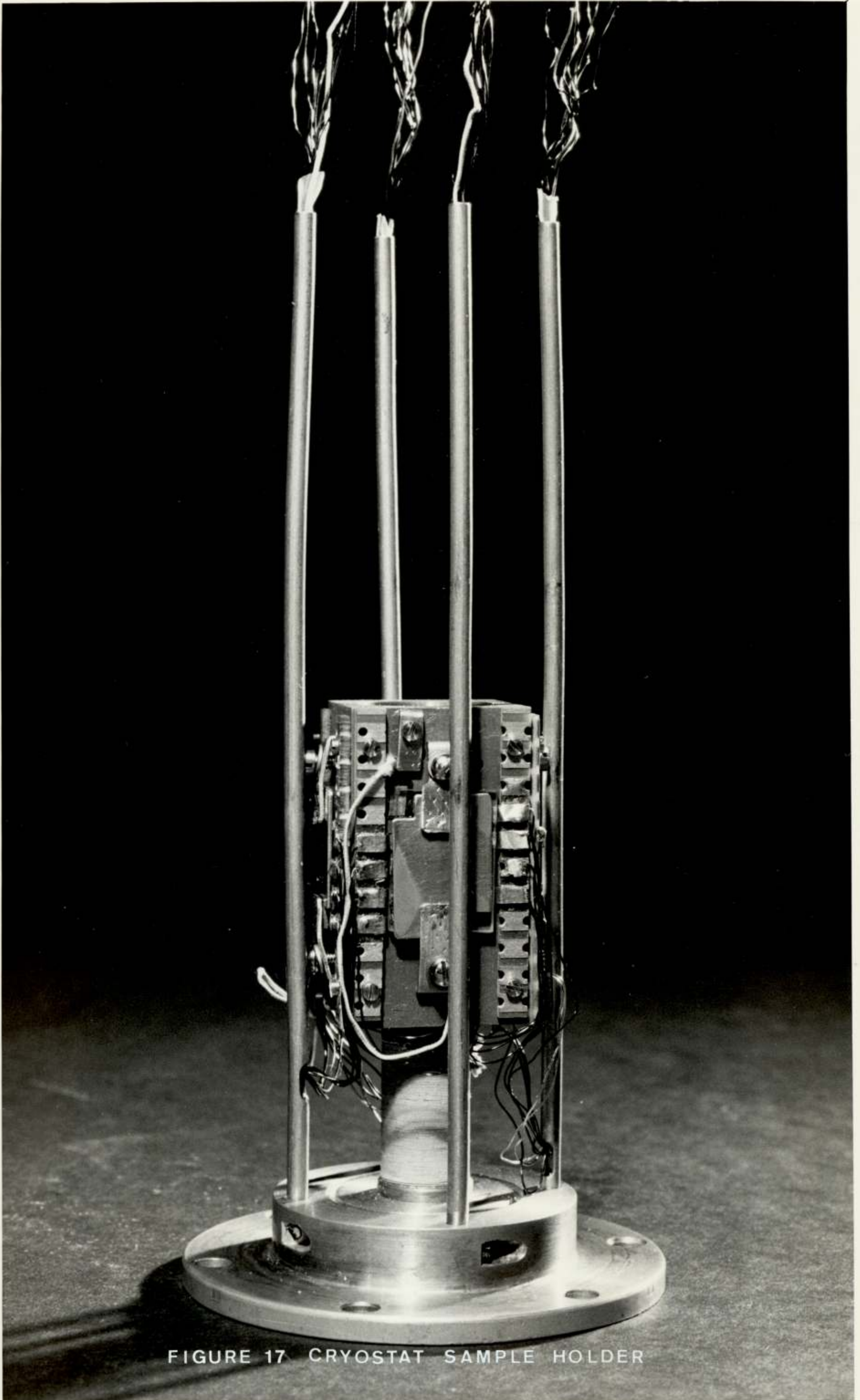

FIGURE 17 CRYOSTAT SAMPLE HOLDER

were screwed down on the sides of each mounting face.

Voltage and current leads were of 32 SWG copper enamelled wire, all leads were soldered to their respective copper contact. Six thermocouples were used to monitor the temperature of the substrates, two copper/constantan coupled on two opposite faces of the block, one at the top and the other at the bottom so that their readings would be averaged and four gold-iron/chromel placed one in every face of the block and underneath each substrate. The copper/constantan thermocouple was calibrated over the range 30°K to 500°K and the gold-iron/chromel thermocouple calibrated over the range 2°K to 80°K, and at spot temperatures up to 400°K to provide a check on the copper-constantan thermocouple. The substrates were mounted on each face of the block with the samples facing it down so that the actual electrical contacts were pressed in between the block and the substrate.

To prevent loosing contacts when cooling down quickly, the copper strips were compressed against the substrates by means of seven spring loaded ball-bearings inserted into the copper block which were retained by ring punching, two for the current, four for the voltages and one or two for the thermocouples. Figure (18).

To evenly distribute pressure a stainless steel plate was placed on top of the substrate and retained by two clamps.

The other three samples were mounted in exactly the same way using 30 spring-loaded ball-bearings inserted into the block. This technique was ultimately developed after experiencing a high percentage of contact failure. It has been in use continuously for over two years with 100% success.

To minimise the thermal input to the films, the four sets of leads from the samples were brought down along the edges of the block to the brass flange where four 1.5mm diameter

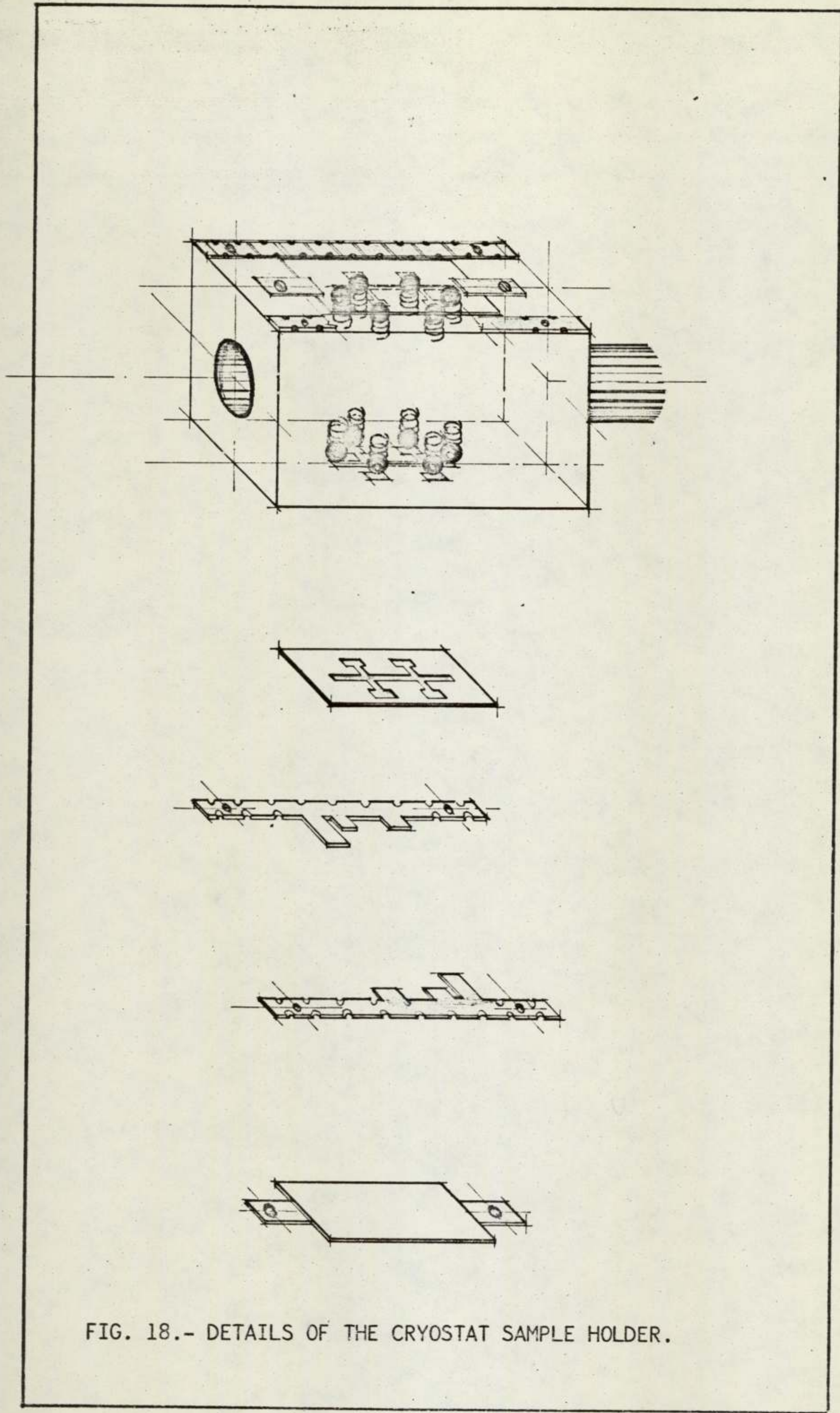

FIG. 18.- DETAILS OF THE CRYOSTAT SAMPLE HOLDER.

stainless steel tubes were pressed into it close to the walls of the copper cylinder to obtain better cooling.

Then four sets of electrical leads, every set corresponding to one sample insulated inside PTFE sleeving, were passed along the supporting tube and brought out to the measuring circuits via two vacuum leadthroughs. In order to prevent any stray emf in the thermocouples due to the use of normal leadthroughs they were brought out through a Perspex flange and then sealed using Araldite.

3.2.3 Measuring Circuits

The arrangement of the electrical circuits for the investigation of the electrical properties of the films is shown in Figure (19). The readings of the four samples were automatically taken and recorded to enable rapid changes in temperature and in resistance to be taken sufficiently accurately.

A Data Transfer Unit SOLARTRON DTU-3240 was used. The inputs to it, four pairs of current leads, eight pairs of voltage leads and six thermocouples, were connected to four Head Units-3214. The scanning of all the pairs was carried out by Relay Driver-3212 and controlled by the Controller-3211. The operation could be repetitive manual or directed by a Clock-3210. The time between the steps of the scan could be as low as one second.

The Interface 3205 fed the inputs to the Digital Voltmeter LM 1604 DC and brought the data back via one Output Driver 3220 to the data recording device which in the present work was an ADD MASTER-35 typeprinter.

The power to the samples was supplied by a stabilised D.C. supply; the current could be varied between 1μA to 1000μA. The current through each film was measured by reading

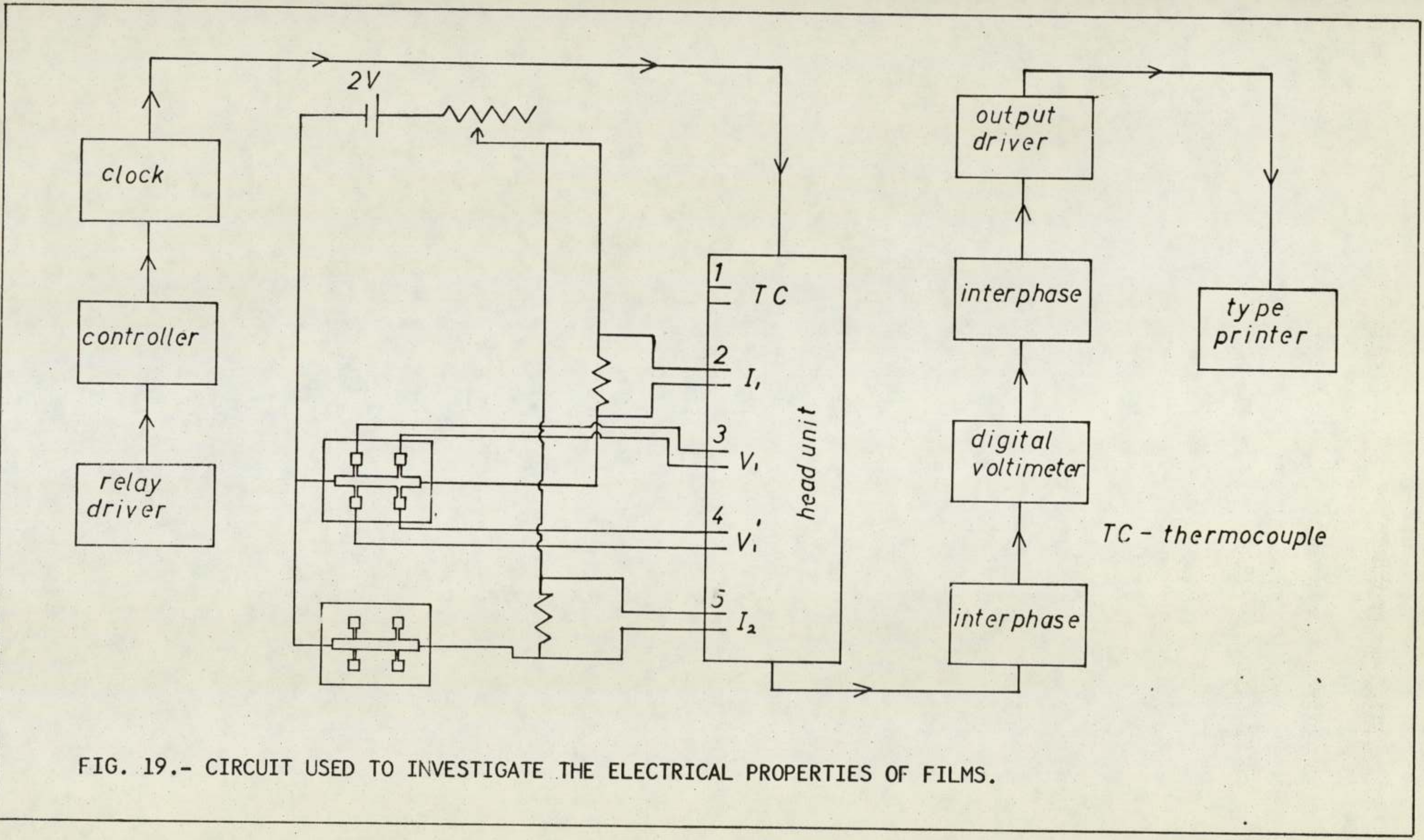

FIG. 19.- CIRCUIT USED TO INVESTIGATE THE ELECTRICAL PROPERTIES OF FILMS.

the potential developed across a resistance connected in series with the sample; VITROHM TYPE MM-2 resistance of T.C. = .00002 and accuracy ± .01% were used varying in value from 10KΩ to 1Ω, according to the current range.

The circuit in Figure (20) was constructed to reverse the current so that any standing voltages could be eliminated from the results. The circuit was connected to the last channel of the fourth Head Unit in the DTU and the current would be reversed every time a scanning through the four samples was completed.

3.3 Ellipsometer

The ellipsometer consisted of three triangular section optical benches bolted to fixed plates on the vacuum bench. The light source, a 150 watts projector lamp, provided adequate intensity in the visible and near infra-red regions. A condenser lens L1, in Figure (21) focuses the light on a pin-hole which is arranged to be at the focus of the lens L2. The wavelength of the parallel beam of light thus formed is chosen by means of a Balzer interference filter F, having a pass-band of about 2nm. The aperture A_2 restricted the beam so that the divergence was less than 0.005 radians. After falling on the specimen film the beam of light passed through the quarter wave plate and analyser before reaching the detector.

When the ellipsometric problem is to calculate the three unknown parameters, n, k and t (optical constants and thickness respectively) from two experimental values Ψ and Δ as explained in Chapter 2, the use of one angle of incidence is insufficient if a high resolution is to be obtained.

For this reason a new method was developed in the present work: the use of two different angles of incidence together with a range of wavelengths, thus providing for every wavelength two sets of

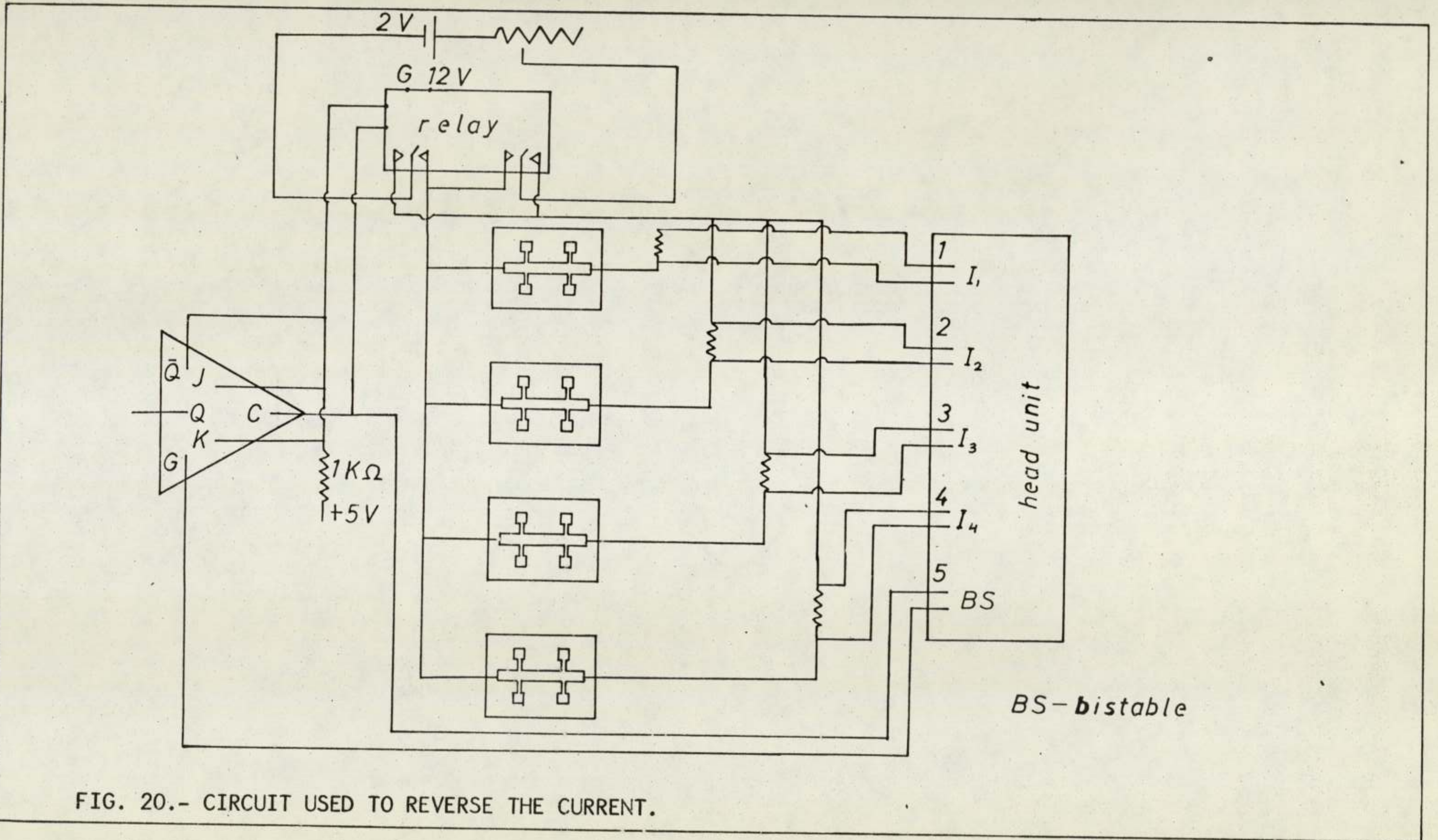

FIG. 20.- CIRCUIT USED TO REVERSE THE CURRENT.

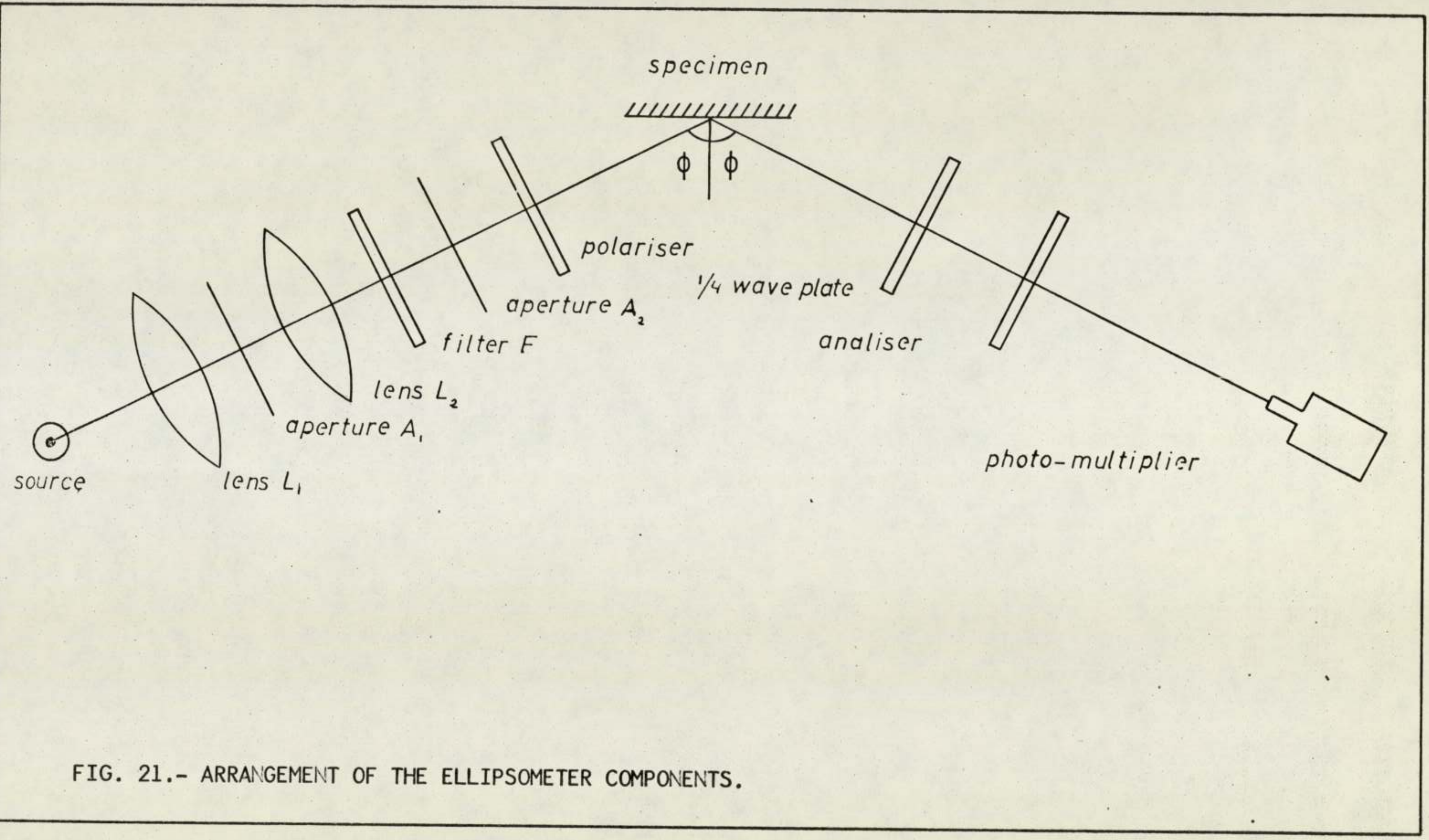

FIG. 21.- ARRANGEMENT OF THE ELLIPSOMETER COMPONENTS.

experimental values in order to obtain the three unknown parameters n, k and t.

The two angles of incidence used in this investigation were 64° and 59.95° as are shown in Figure (22).

The combination of polarizing filters and detectors used for the measurements over a range of wavelengths in the visible is different for the one used in the near infra-red.

3.3.1 Form of Ellipsometer used in the Visible Region

The Quarter Wave Plate

The method of compensation used is that due to Winterbottom.[41] The polarizer and analyser consist of HN22 polaroid in graduated circular vernier scales. These were supplied by the Precision Tool and Instrument Company, and are accurate to within ± 2 minutes of angle. The quarter wave plate is part of a Senarmont compensator and is made of mica sheet, also mounted in a circular scale. The error imparted to the analyser setting if a non-exact quarter wave plate was used has been discussed by Seward.[42] Calculations by O'Shea[43] showed that the quarter wave plate used was acceptable over the wavelength range 505nm to 565nm.

The detector used was a photomultiplier used in conjunction with a stabilised power supply. The current output was detected by a galvanometer having a sensitivity of 0.0113μA $m.m^{-1}$. Since the compensator method depends on the measurement of minimum light intensities, the detector does not have to be completely screened from the room lights, although it was found desirable to reduce the background to a minimum.

3.4 X-Ray Equipment

The apparatus used to obtain the X-ray diffraction patterns was a Philips PW 105 diffractometer, Figure (23), used in conjunction with

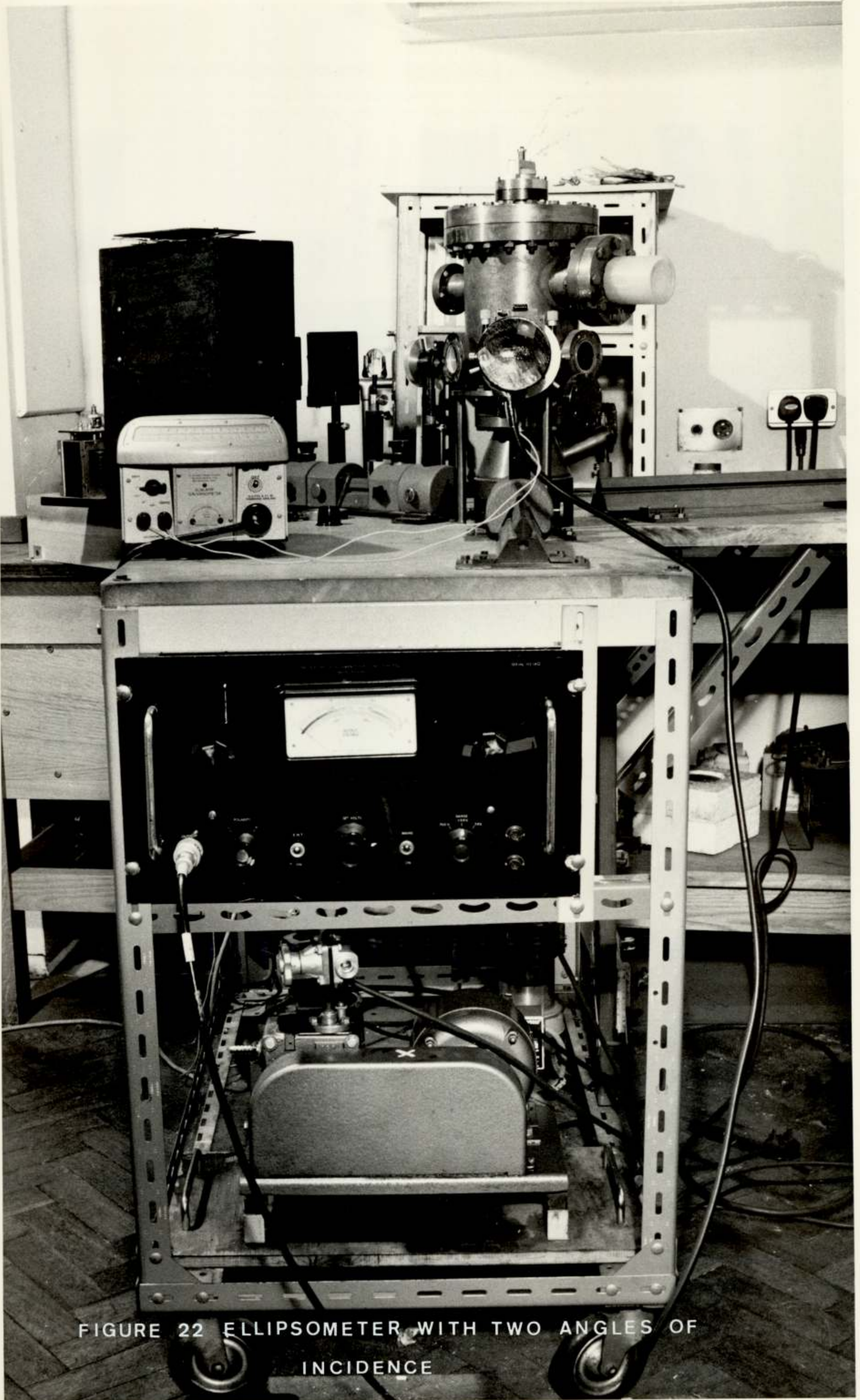

FIGURE 22 ELLIPSOMETER WITH TWO ANGLES OF INCIDENCE

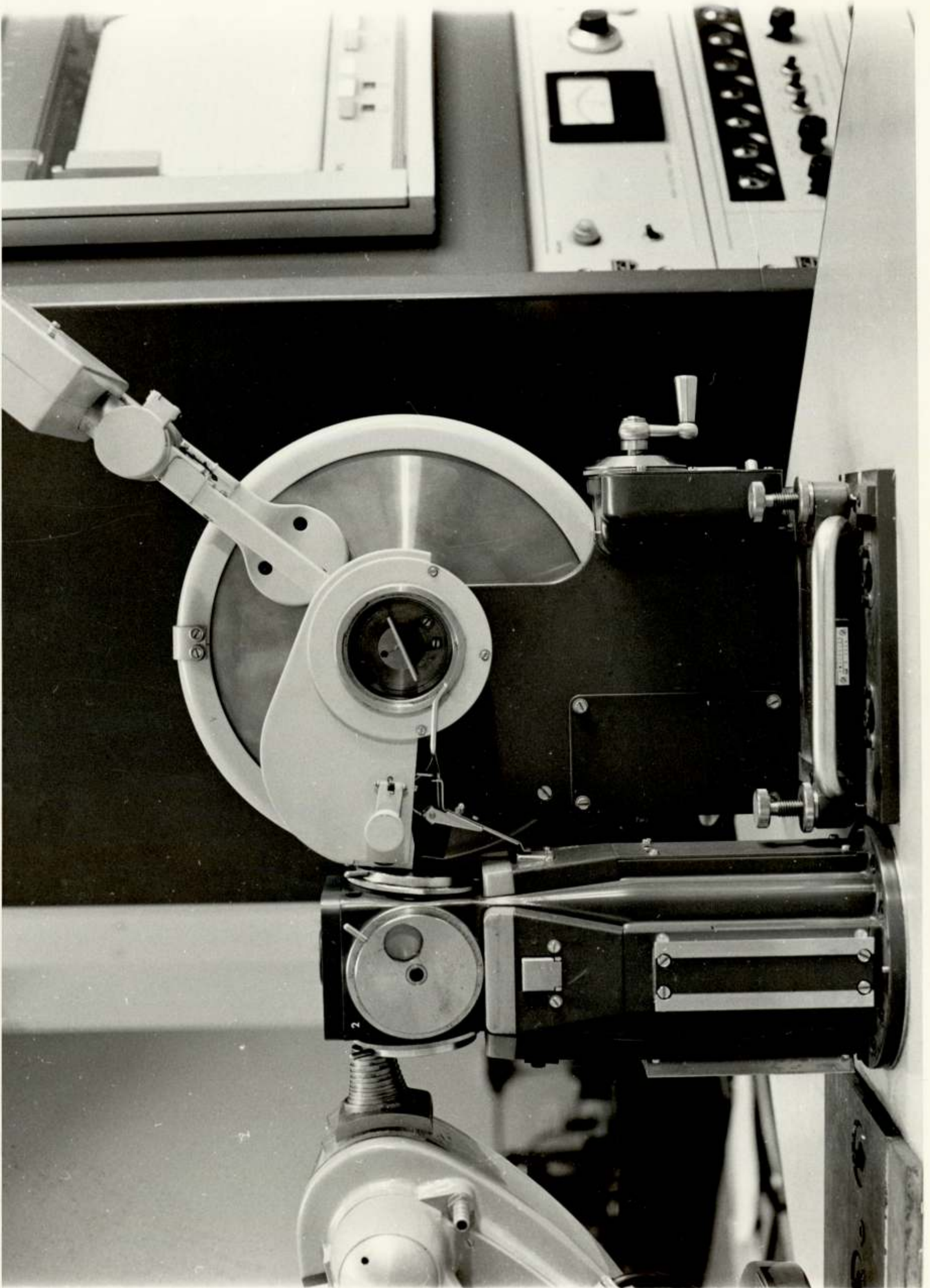

FIGURE 23 X-RAY DIFFRACTOMETER

a Philips 1010 X-ray generator. The radiations chosen for the analysis were Cu K_{α} and M_o k_{α} radiations which gave eight well spaced diffraction lines for b.c.c. Ta and two for f.c.c. Ta at angles ranging from 34° 2θ to 122° 2θ and from 15° 2θ to 48° 2θ respectively.

The facilities also available to use in conjunction with the diffractometer were:

i) automatic step scanning capabilities which allowed the collection of data across the line profiles to be performed.

ii) standard counting equipment including pulse height analyser.

iii) a printer and 8-hole punch tape outfit to register measured intensity values.

Using a standard specimen, the diffractometer setting was calibrated. The standard sample diffractometer peaks occur at precisely known values of 2θ; these were compared to the angles measured on the diffractometer goniometer over the whole range of interest in this study and it showed the diffractometer readings to be $0.02^{\circ}2\theta$ too high.

CHAPTER 4

Experimental Procedure

4.1 Substrate Preparation

The substrates for the films were cut from Tempax heat resisting glass slides with a temperature limit of 823°K.

The dimensions of all substrates were 2cm x 1.5cm. Those used in ellipsometric experiments were 0.05cm thick and ground on the reverse side with grade 200 carborundum powder in order to stop stray reflections from the back of the substrate especially when thin tantalum films were being investigated.

Those used for electrical studies were 0.1cm thick to prevent cracking when clamped in the cryostat sample holder.

The substrates were cleaned using the following procedure prior to mounting in the evaporation unit:

After standing overnight in 5% detergent solution they were boiled for ten minutes, rinsed five times with double distilled water, followed each time by ultrasonic cleaning in double distilled water again and then boiled for five minutes in iso-propyl alcohol. As the substrates were removed they were held in the vapour of the boiling alcohol for a few seconds.

4.1.1 Electrical Contact Areas

In the early stages of this work a subsidiary evaporation unit was used for the deposition of aluminium contact areas over which the test film could be evaporated. The substrate was mounted with a suitably shaped mask in the evaporation unit and aluminium contact areas were deposited on the substrate from a heated tungsten wire helix at a pressure of $< 2 \times 10^{-6}$ torr.

It was found later that after the evaporation of the contacts and subsequent recleaning in the vapour of boiling

iso-propyl alcohol that some contamination from the evaporation unit remains adhered to the substrate. Many tantalum samples had to be discarded as a result and in later samples tantalum was evaporated to form contact areas and a conducting silver paint was used on top of the tantalum.

4.2 Establishment of a Vacuum

The pressure in the vacuum chamber was reduced to 10^{-4} torr by rotary and sorption pumps. At this pressure the ion pump could be switched on and the rough vacuum elements isolated from the chamber. The ion pump was capable of producing a vacuum in the chamber of $< 1 \times 10^{-7}$ torr. Baking the chamber at $200^{\circ}C$ and outgassing the substrates at temperatures up to $500^{\circ}C$ and allowing them to cool afterwards, the pressure would fall to $< 1 \times 10^{-9}$ torr. A further reduction in the pressure was achieved by outgassing the tantalum slug and utilising the gettering action of freshly deposited tantalum to produce a vacuum of $< 1 \times 10^{-10}$ torr, whilst still maintaining an elevated substrate temperature.

4.3 Preparation of films

High purity tantalum 99.996 % was used. It was supplied by Materials Research Company Ltd in slugs 3/8" diameter x 3/8" long and weighing about 10gr. After melting, the material assumed a hemispherical shape.

The initial outgassing of the tantalum raised the pressure in the chamber from $< 1 \times 10^{-9}$ torr to the maximum safe pressure for the tungsten filament of 1×10^{-5} torr. The pressure soon started to fall and the tantalum could be outgassed further. The power input necessary to melt the tantalum was 1000 watts and it was held just above the melting point for several hours. At this point there was some evaporation of tantalum and the gettering action of this fresh tantalum could bring the pressure down to $< 1 \times 10^{-8}$ torr.

Increasing the power input the evaporation rate would increase and initially raise the pressure, but as the gettering action increased the pressure fell to about 5 x 10^{-8} torr. Meanwhile the shutter was kept in place.

The electron beam evaporator was switched off and the chamber allowed to cool for a few hours and after that the pressure had fallen to < 1 x 10^{-10} torr. This pressure could be maintained indefinitely with no further evaporation of tantalum.

The rate of evaporation for sample preparation could be controlled by varying the electron beam current. With the maximum electron beam current of 525mA the highest evaporation rate achieved was 400Å/m on a substrate positioned 17cm from the evaporation source.

Using the multiple substrate holder and placing the lateral substrates in the three different positions, the following deposition rates could be achieved top centre (20cm) = 350Å/m, top side (20cm) = 330Å/m, medium side (18.5cm) = 375Å/m and low side (17cm) = 400Å/m.

Meanwhile, the temperature of the substrates were steadily increased and when the selected deposition temperatures had been achieved and the required evaporation rate reached the pressure in the chamber was allowed to stabilize at about 5 x 10^{-8} torr.

At this point the substrates were exposed to the evaporation source, and when the required thickness of films had been deposited the shutter was closed.

4.4 Determination of film thickness

Since the film thickness is an important parameter in the calculation of optical and electrical constants, film thicknesses were

estimated by several methods:

a) Optical method

b) Electrical resistivity

c) Quartz crystal thickness monitor

d) Changes of ellipsometric parameters Ψ and Δ.

4.4.1 Optical Method

The principal technique used was that of multiple beam interferometry.

After removal from the ultra-high vacuum system the thickness of the tantalum films was measured using a Thin Film Measuring Microscope in conjunction with a Constant Deviation Wavelength Spectrometer, both instruments were supplied by Hilger and Watts Ltd. Figure (24)

The method used for determining the thickness followed that suggested by Tolansky[44] using fringes of equal chromatic order. The specimen films were overlaid with an opaque layer of aluminium rather than silver in order to maintain a high reflectivity for prolonged periods of time.

The technique is illustrated in Figures (24) and (25) and the thickness 't' is given by:

$$t = n\Delta\lambda/2 \ .$$

where n is the fringe order and $\Delta\lambda$ the fringe displacement Figure (26).

As the thickness decreased the error in the determination increased. For films of 200Å the error was about ± 5%, at 150Å the error was about ± 10% and at thickness below 120Å the error would be ± 50%.

For very thin films a correction was applied estimating the film thickness from the evaporation rate of the tantalum and the time taken for the deposition of the film.

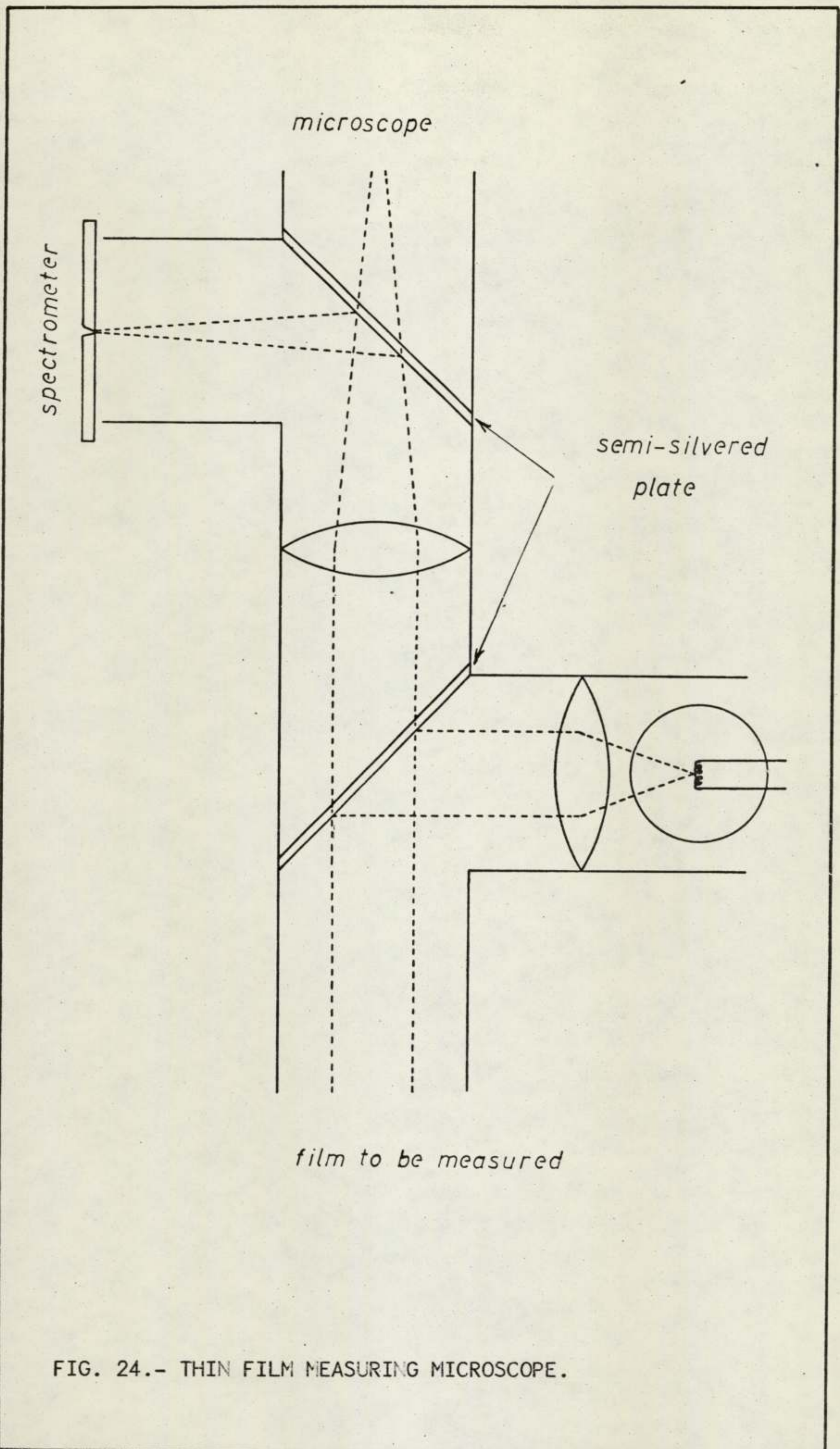

FIG. 24.- THIN FILM MEASURING MICROSCOPE.

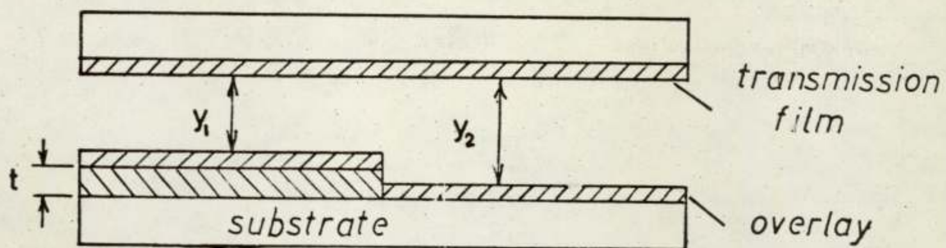

FIG. 25.- FRINGE FORMATION.

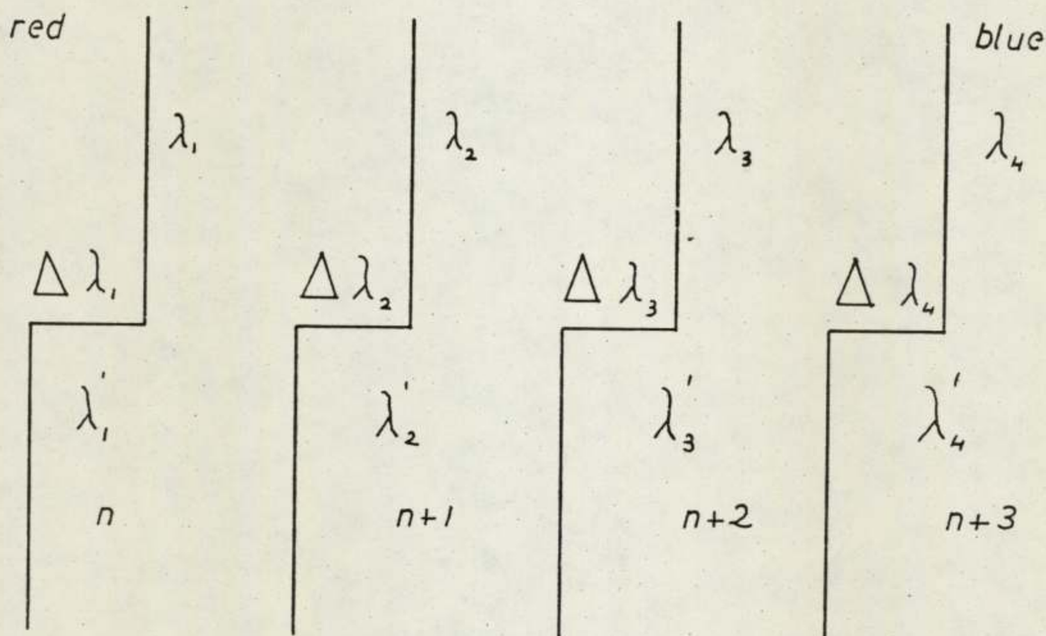

FIG. 26.- FIELD OF VIEW SHOWING FOUR ORDERS OF INTERFERENCE.

4.4.2 Electrical Method

The expression for the resistivity of thick films, equation (2.7) may be rewritten as

$$\rho = \rho_\infty + \frac{3\ \rho_\infty \ell_\infty}{8t} \tag{4.6}$$

If V_F is assumed to be temperature independent it follows from equation (2.3) that the term $\ell_\infty \rho_\infty$ is also independent of temperature, hence differentiating equation (4.6) with respect to temperature leads to

$$\frac{d\rho}{dT} = \frac{d\rho_\infty(T)}{dT} \tag{4.7}$$

which is independent of film thickness. Hence for a film resistance R

$$\frac{dR}{dT} = \frac{d\rho_\infty}{dT} \times \frac{\text{film length}}{\text{width x thickness}} \tag{4.8}$$

Since $d\rho_\infty / dT$ is a constant of the material the film thickness can be estimated from measured values of dR/dT if the width and length are known.

4.5 Electrical Properties of Films

Films were deposited onto substrates at different temperatures ranging from 150°C to 500°C (the maximum temperature being limited by the use of glass substrates). After being prepared the samples were allowed to cool to room temperature before removal and then transferred to the cryostat assembly.

The normal resistive properties of the films were determined by passing a constant current and observing the voltage developed across the samples. Current densities at room temperature of the order of 10 to 100 Acm^{-2} were used. Once the films were mounted in the cryostat, readings were taken at 300°K. The temperature

coefficient of resistance was deterined over the range 300°K- 77°K.

Then liquid helium was introduced into the cryostat and the temperature of the films lowered. The superconducting critical temperature of the films was determined by slowly reducing the temperature, passing a suitable current through the specimen and observing at what temperature the resistive transition took place. The temperature was then raised by means of the heater coil positioned in the substrate mounting and the transition temperature measured again.

This procedure was repeated with various values of currents and the critical temperature checked several times.

The critical currents were determined at various temperatures before the temperature coefficient of resistance was observed over the range 10 to 300°K.

4.6 Optical Properties of Films

Because of the initial growth of oxide on the film it was essential that the shortest possible time should elapse between removal from the vacuum chamber and installation in the ellipsometer. In practice it was found that this interval could be as little as ten minutes which was considered to be satisfactory.

Initial readings to determine Ψ and Δ were taken at half hourly periods until the rate of change of the readings dropped sufficiently for hourly reading and then progressively longer intervals over a period of three weeks.

4.6.1 Determination of Reference Azimuths for the Ellipsometer

The readings on the divided circles of the polarizer and analyser that correspond to the transmission axes of the polaroids being parallel and perpendicular to the plane of incidence are known as the reference azimuths. In the two methods of ellipsometry undertaken the experimental azimuths

are expressed relative to the plane of incidence. Approximate values are quickly obtained by arranging for light from a lamp to be reflected at approximately 56 degrees from a glass plate placed flat on a bench, and to pass through the polaroid. Each polaroid in time is rotated until minimum light is visible through it, the transmission axis is then approximately vertical. With the Quarter Wave Plate (Q.W.P.) removed from the ellipsometer, and with the light being reflected from a metal surface, the following procedure is adopted for both types of polaroids.

The polarizer is rotated 90 degrees so that the transmission axis is horizontal, the analyser remains with its transmission axis perpendicular to the plane of incidence, with a small voltage applied to the photomultiplier a slight adjustment of the polarizer and then analyser serves to reduce the signal to a minimum. The process is repeated, with the voltage steadily increasing until with the full allowed value minimum light is detected. The exact polarizer azimuth for extinction is obtained by measuring the azimuths at equal intensities on each side of the minimum. The extinction position is the average of the two values. With the polarizer set at its extinction position the analyser extinction position is obtained by the same method. Polarizer and analyser azimuths now correspond to π_p and α_s respectively. Both polarizer and analyser are then rotated 90 degrees and the entire procedure repeated, these alternative positions correspond to azimuth π_s and α_p .

A reference position for the compensator (when used) is obtained by setting the polarizer and analyser to a pair of related reference positions and then rotating the compensator until a position of minimum transmitted light is obtained. The

exact compensator reference position is again obtained by measuring the positions giving equal intensities on either side of the minimum. The position corresponds to either the fast or slow axis of the compensator being parallel to the plane of incidence.

The whole procedure was repeated for both angles of incidence used.

4.6.2 Determination of Ψ and Δ using the Compensator Method.

The essential basis of the method is explained in section 2.8.1. The compensator is located at 45 degrees to a reference position. As before the polarizer and analyser are successively turned to give minimum light intensity, while gradually increasing the photomultiplier voltage. The polarizer extinction position, P_1 , is then found by bracketing the minimum position, with the polarizer then set at its extinction position. The analyser extinction position, A_1, is likewise found by bracketing. The setting procedure is repeated for a polarizer azimuth in another quadrant, but not 180 degrees away, giving readings P_2 and A_2 on polarizer and analyser respectively.

The total 32 pairs of analyser and polarizer positions for extinction were measured once and the two best "high" and "low" pairs selected so that the averaged results will then be acceptably close to the average if all possible measurements had been made. This enables oxide growth rates to be made more rapidly without loss in accuracy.

The two polarizer positions P_1 and P_2 are symmetrically placed about π_p . In general, the polarizer settings are symmetrically placed about the plane of incidence. $P_1 - \pi_p$ should equal $\pi_p - P_2$. In general, the average is taken

$$\frac{(P_1 - \pi_p) + (\pi_p - P_2)}{2} = \Psi \qquad (4.9)$$

Tan Ψ equals the relative amplitude reduction between the (p) and (s) components produced by reflection from the specimen.

The analyser positions A_1 and A_2 are always separated by approximately 90 degrees. $\alpha_s - A_1$ should equal $\alpha_p - A_2$. In general, the average is taken

$$\frac{(\alpha_s - A_1) + (\alpha_p - A_2)}{2} = x \qquad (4.10)$$

where the angle 2x - 90 degrees gives the relative phase retardation Δ between the (p) and (s) components.

4.6.3 Determination of the Optical Constants

When the parameters Ψ_{exp} and Δ_{exp} have been determined, either by the above method or by that described in the previous section, the experimental values are compared with theoretical ones and therefore the unknown parameters n, k and t calculated. The procedure is the following:

a) An initial guess of $(n_o - ik_o)$ is done using a computer programme which uses the approximate ellipsometric equations described by Faininger and Reverz.[45]

b) Determinations of ψ and Δ are made at both angles of incidence.

c) A mesh of points (n_f and k_f) is established with a reasonable interval around the trial point (n_o, k_o). The theoretical Ψ and Δ are then evaluated using the full equations described in Section 2 solved by other two computing programs (one of them for the case of an oxide layer) as a function of thickness, for each angle of incidence and for each individual choice of optical constants.

Then the tabulated values for a given angle of incidence are compared with the corresponding experimental ones

retaining those values of thickness for which a numerical correspondence is fulfilled. Thus for a given angle and for each choice of the constants n_f, k_f there will be a set of Ψ values defined by

$$\Psi_{exp} - \varepsilon \leq \Psi(t) \leq \Psi_{exp} + \varepsilon$$

and an independent set of Δ values defined by

$$\Delta_{exp} - \mu \leq \Delta_{exp}(t) \leq \Delta_{exp} + \mu$$

where ε and μ are the experimental errors and the ones used in the present work were:

$$\varepsilon = 0.05$$

$$\mu = 0.05$$

The intersection of these two sets gives the values of thickness that ensure a simultaneous coincidence between the two theoretical quantities and the corresponding measurements for the angle specified.

In general there will be a definite spread of the constants n_f, k_f corresponding to this solution : the ambiguity is lifted if the operation is repeated using the second angle of incidence. The whole operation is repeated for the range of wavelengths used in this work.

A final check can be made by using the values of thickness obtained with the Thin Film Measuring Microscope. This technique was suitable for Ta films up to a thickness of 1000Å.

4.6.4 Determination of angle of incidence

The angle of incidence is determined by removing the detector and replacing it with a small telescope. Four saddles, each holding a sharp pointed spike were positioned on the ellipsometer benches. The saddles were adjusted so that their points were all in line with the illuminated pin hole,

as seen through the telescope.

The distance between the points were measured and the angle of incidence, ϕ, calculated by simple trigonometry to within 0.05°.

4.7 X-ray Analysis

Finally, the films were transferred to the x-ray diffractometer where the microstructural properties were observed. The microstructural properties observed were grain size, crystal structure and lattice parameters.

In this work it was not necessary to remove films from the glass substrates. The radiation used was k_{α}-Cu and when the thickness allowed it k_{α}-Mo was also employed in order to provide a check in both the grain size and lattice parameters.

The method of determining the grain size was the line broadening of x-ray diffraction patterns. Assuming that the grains are perfect and randomly orientated, the integral breadth of a diffraction line, B (integrated intensity/maximum intensity) is given by the Schemer formulae[(46)] as

$$B = \lambda / L.d.\cos\theta o$$

where

λ = wavelength of the x-rays

L = average particle size, dimensions in unit of d

d = interplanar spacing of $(hk\ell)$ in Å

θo = Bragg angle

The integral breadth is defined as

$$B = \int \frac{I(x)\ dx}{I_{max}}$$

CHAPTER 5

Experimental Results

In this chapter the experimental results of over eighty tantalum samples prepared during this programme of work are presented:

5.1 Deposition Conditions

Details of conditions for the growth of tantalum films on glass substrates in ultra-high vacuum are given in table (1). Substrate temperatures were varied between the limits of $423^{\circ}K$ to $773^{\circ}K$ while the rate of deposition changed from 40Å/m to 480Å/m. The deposition rates listed were calculated either by dividing film thickness by evaporation time or in some cases directly using a quartz oscillator monitor. Film thicknesses were measured in addition by multiple beam interferometry after removal from the evaporator. The pressure measured during evaporation interpreted as a residual pressure must always represent an upper limit for the partial pressure of any constituent gas.

A parameter characteristic of the film deposition process, deposition ratio, is given by

$$R_D = n_{Ta}/n_{Res}$$

which is the ratio of the flux of tantalum atoms at the substrate surface to the flux of residual gas molecules arriving there. n_{Ta} was measured and n_{Res} calculated from the partial pressure during deposition; the exact value of R_D is expected to be a higher one because the sticking coefficient for gases will be less than that for Tantalum atoms.

In some runs a quartz oscillator was used and the measured deposition rate was compared with the calculated one. This method in conjunction with the interferometer, used to measure thickness, gave values of film densities.

TABLE 1

SUMMARY OF DEPOSITION CONDITIONS FOR TANTALUM FILMS

Sample No.	Deposition Temperature (^{o}K)	Pressure ($X10^{-8}$torr	$R_o = nTa/nre$	Deposition Rate (Å/m)	Thickness (Å)
Ta-8	523	2	5	80	1567
Ta-17	553	"	12	195	2925
Ta-18	498	"	12.3	200	3000
Ta-19	573	"	13	213	3200
Ta-20	523	"	14	226	3400
Ta-21	548	"	13.3	217	6500
Ta-22	523	"	12.4	203	5100
Ta-23	573	"	15	250	7500
Ta-24	573	"	16	260	7750
Ta-25	598	1.5	9.5	116	2900
Ta-26	523	"	10.1	124	3100
Ta-27	548	"	11.1	136	3400
Ta-28	573	"	13	160	4000
Ta-29	473	"	10.5	128	3200
Ta-30	423	2	24.5	400	2000
Ta-31	523	"	20.8	340	1700
Ta-32	593	"	25.7	420	2100
Ta-33	423	"	29.4	480	2400
Ta-34	573	"	12.3	200	500
Ta-35	523	"	13.5	220	550
Ta-36	523	"	14.7	240	600
Ta-37	523	"	16	260	650
Ta-35A	423	"	13.5	220	550
Ta-36A	423	"	14	230	575
Ta-37A	423	"	15.3	250	625
Ta-42	523	"	5.5	90	5400
Ta-43	523	"	5.9	96	5750
Ta-44	523	"	8.8	143	8500
Ta-45	523	"	9.9	161	9650
Ta-46	523	"	8.4	137	8200
Ta-47	523	1.75	9.2	150	9000
Ta-48	773	"	6.6	107	3750
Ta-49	538	"	8.2	133	4650
Ta-50	548	"	7.4	120	4200

TABLE I (CONTD)

Ta-51	580	1.75	7.8	128	4500
Ta-52	598	"	6.7	110	3850
Ta-53	458	"	7.7	126	4425
Ta-54	608	"	7.2	117	4100
Ta-55	498	"	7.7	125	4325
Ta-56	598	1	38	310	310
Ta-57	523	"	39	320	320
Ta-58	523	"	41	335	335
Ta-59	523	"	46	375	375
Ta-60	523	"	35	285	285
Ta-61	523	"	30	245	245
Ta-62	523	"	37	305	305
Ta-63	523	"	33.6	315	315
Ta-64	748	2	19.6	320	160
Ta-65	493	"	17.2	280	140
Ta-66	648	"	23.3	380	190
Ta-67	683	"	18.4	300	150
Ta-68	523	"	16	260	130
Ta-69	453	"	15.3	250	125
Ta-70	573	"	14	230	115
Ta-71	573	"	21.4	350	1400
Ta-72	583	"	22.2	362	1450
Ta-73	473	"	20.6	337	1350
Ta-74	598	"	23	375	1500
Ta-75	523	"	24.5	400	1600
Ta-76	748	"	20.1	331	1325
Ta-77	648	"	21	345	1375
Ta-78	523	3	1.67	40	800
Ta-79	623	"	1.75	42	850
Ta-80	473	"	1.63	39	780
Ta-81	573	"	1.88	45	900
Ta-82	523	"	1.67	40	650

5.2 Structural Data

The structures of all samples can be divided into three general groups:

(1) f.c.c. - Ta (2) b.c.c. - Ta (3) a mixture of f.c.c. - Ta and b.c.c. - Ta.

(1) The f.c.c. - Ta phase was found in the very thin films ranging in thickness from 115Å to 190Å. The lines which appear in the diffraction pattern of the f.c.c. - Ta samples are shown in Table (2). The temperature of the substrates in this group of samples was varied from 423°K to 723°K, but no change in structure was observed due to deposition temperature.

(2) The b.c.c. - Ta structure occurred in films whose thickness varied from 245 to 9650Å. The lines appearing in the diffraction pattern of typical thick b.c.c. - Ta films are shown in Table (3).

All samples exhibiting pure b.c.c. phase show a certain preferred orientation in the [110] direction as indicated by the ratio of line intensities. Figure (27) shows a typical diffraction pattern of a sample with pure b.c.c. structure. Films which display only b.c.c. structure are found over the whole range of deposition rates, 40 - 400Å/m.

(3) The third structure, a mixture of b.c.c. and f.c.c. - Ta is the most common one, appearing indiscriminately with thickness. The proportion of f.c.c. structure changes from 1 to 50%. Figures (28, 29, 30, 31) show diffraction patterns of a series of samples with different proportions of f.c.c. phase.

When the proportion of f.c.c. structure is a small percentage there is an influence of the deposition temperature on the proportion of f.c.c. phase as shown in Figure (32) for a group of samples with the same thickness.

TABLE 2

X-RAY DIFFRACTION PATTERN OF A PURE f.c.c. - Ta FILM.

hkℓ	"d" observed Å	"a_o" calculated Å
111	2.581	4.496
200	2.248	4.497
220	1.594	4.497
222	1.301	4.496

Note No bulk values are available as the f.c.c. structure does not appear in bulk material.

TABLE 3

X-RAY DIFFRACTION PATTERN FOR A TYPICAL THICK b.c.c. - Ta FILM

hkℓ	"d" observed Å	"a_o" calculated Å	"a_o" bulk Å
110	2.3382	3.306	3.3058
200	1.652	3.305	"
211	1.349	3.305	"
220	1.1692	3.306	"
310	1.045	3.306	"
222	0.972	3.306	"

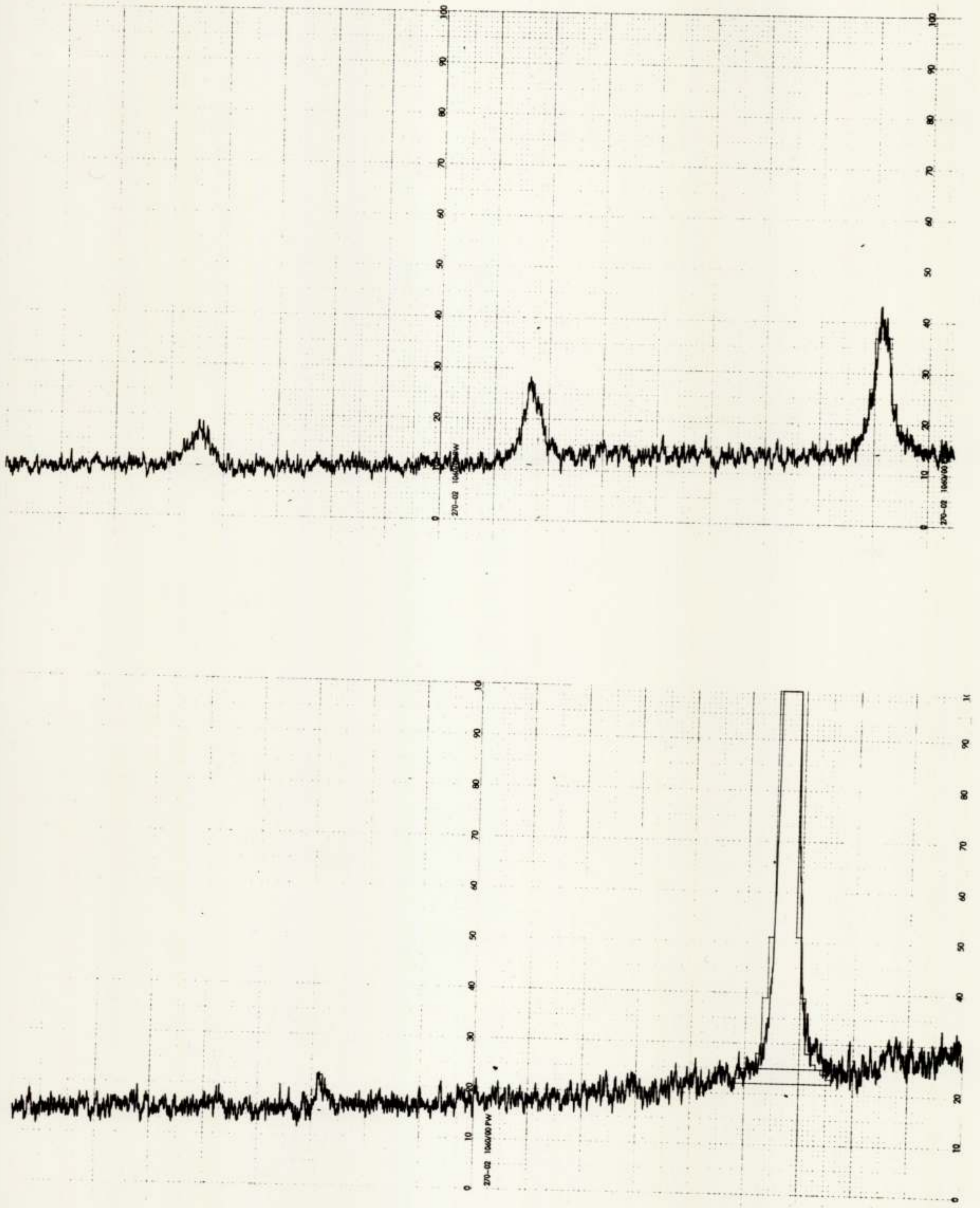

FIGURE 27 TYPICAL DIFFRACTION PATTERN OF A SAMPLE WITH PURE bcc STRUCTURE

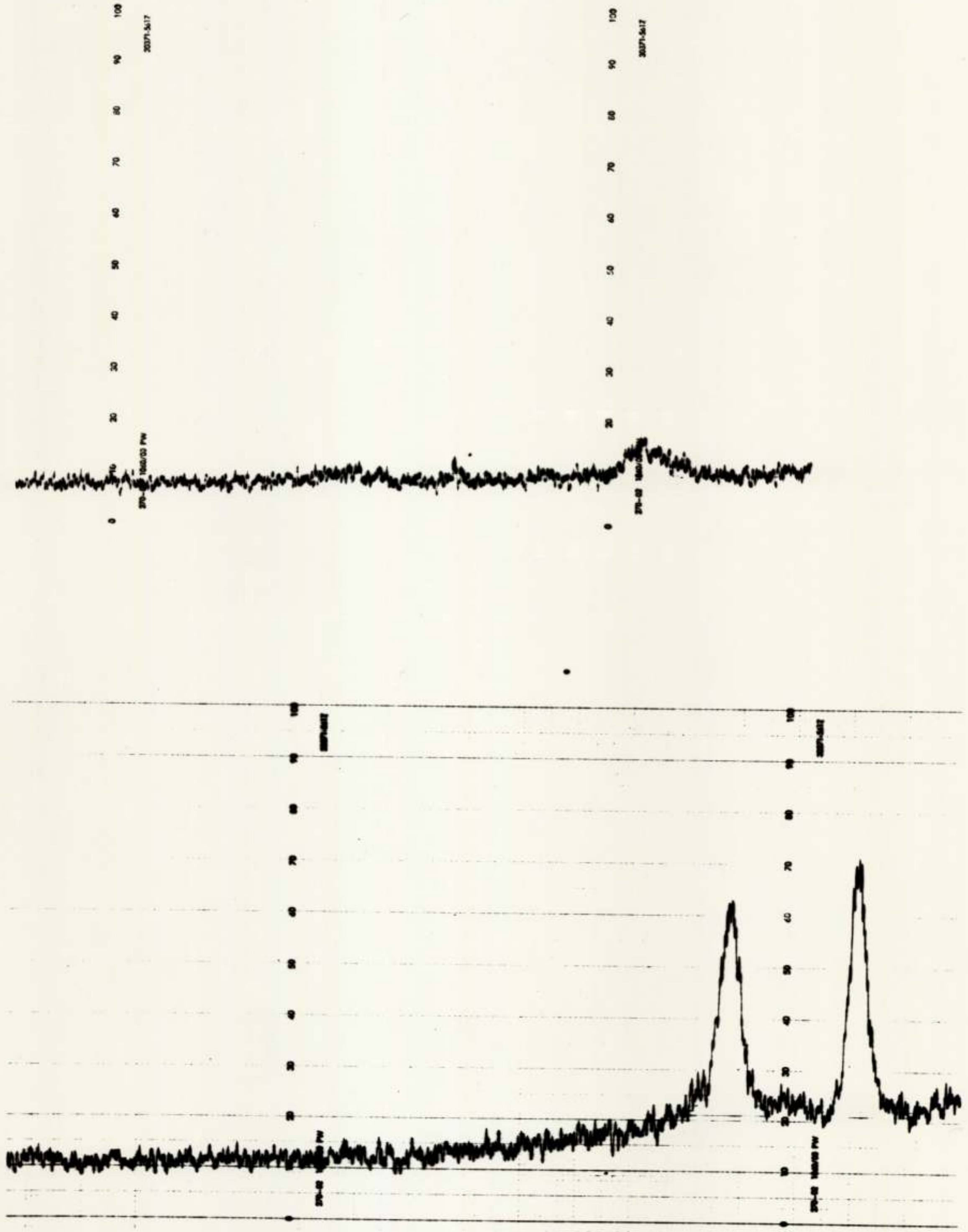

FIGURE 28 DIFFRACTION PATTERN OF A SAMPLE WITH 50% fcc PHASE

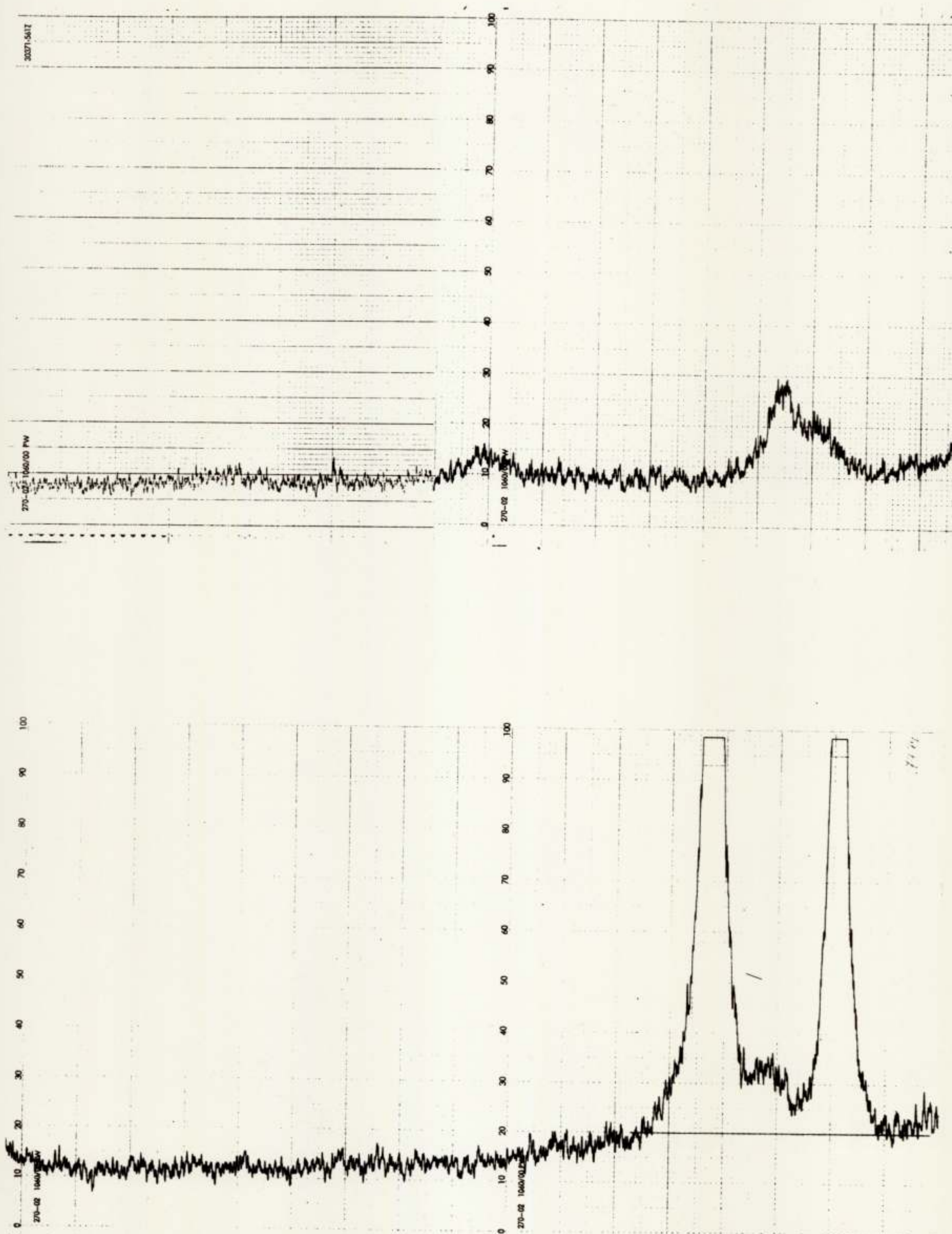

FIGURE **29** **DIFFRACTION PATTERN OF A SAMPLE**

WITH 40 % OF fcc PHASE

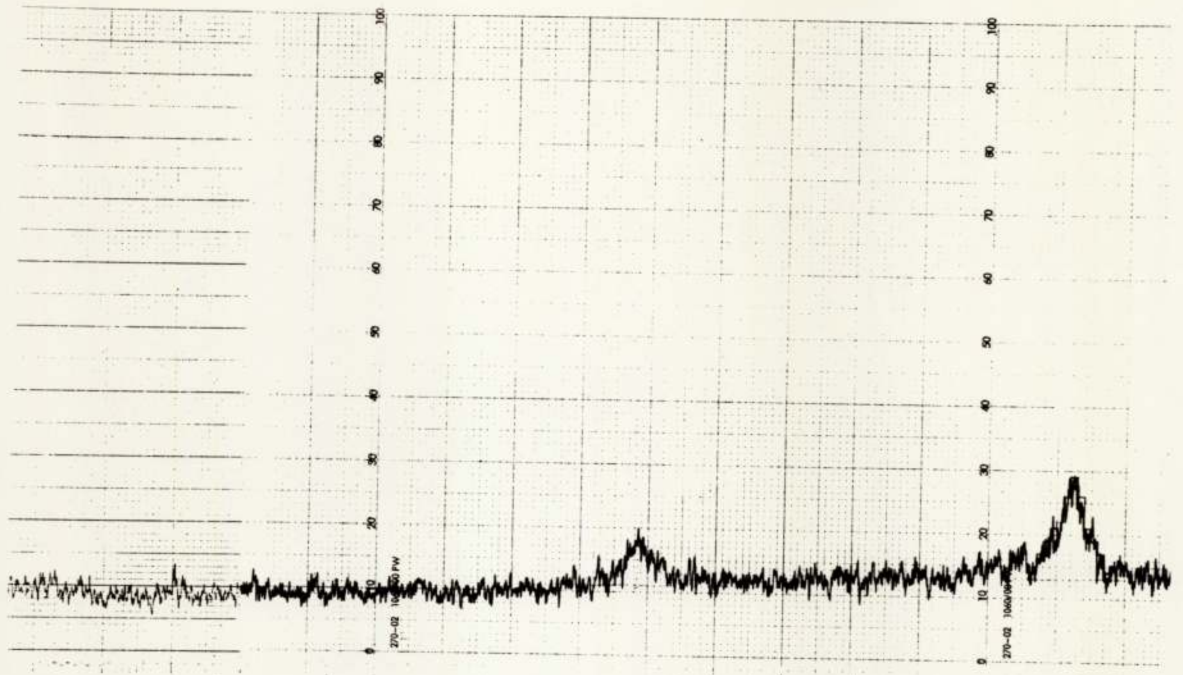

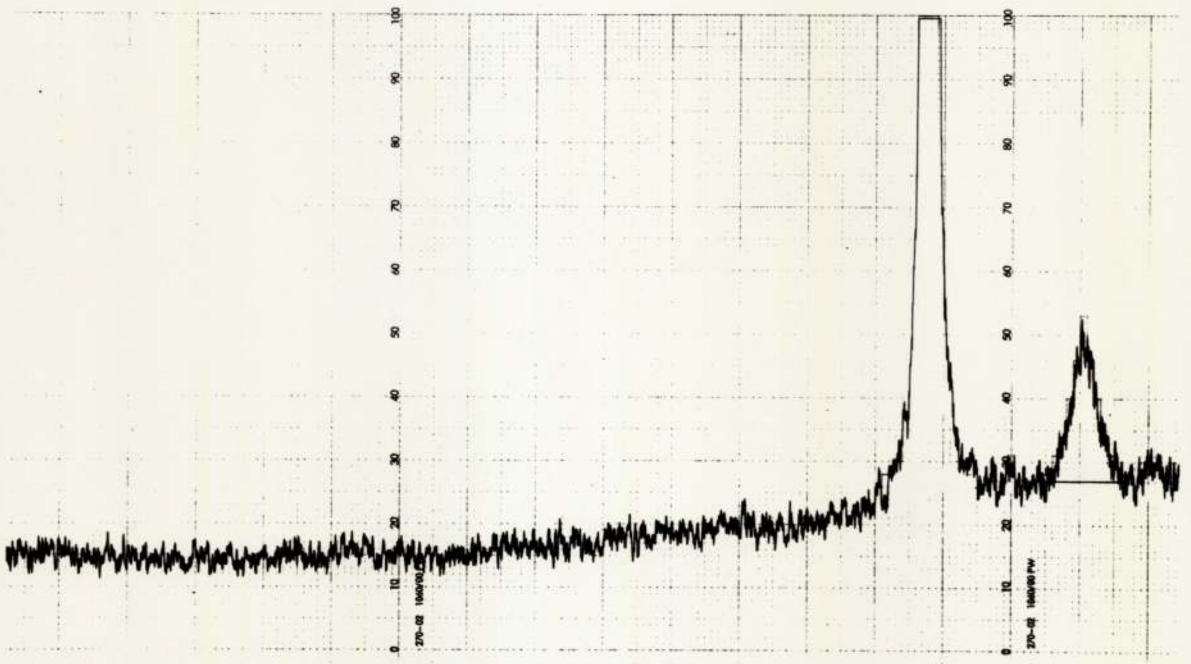

FIGURE 30 DIFFRACTION PATTERN OF A SAMPLE

WITH 15% OF fcc PHASE

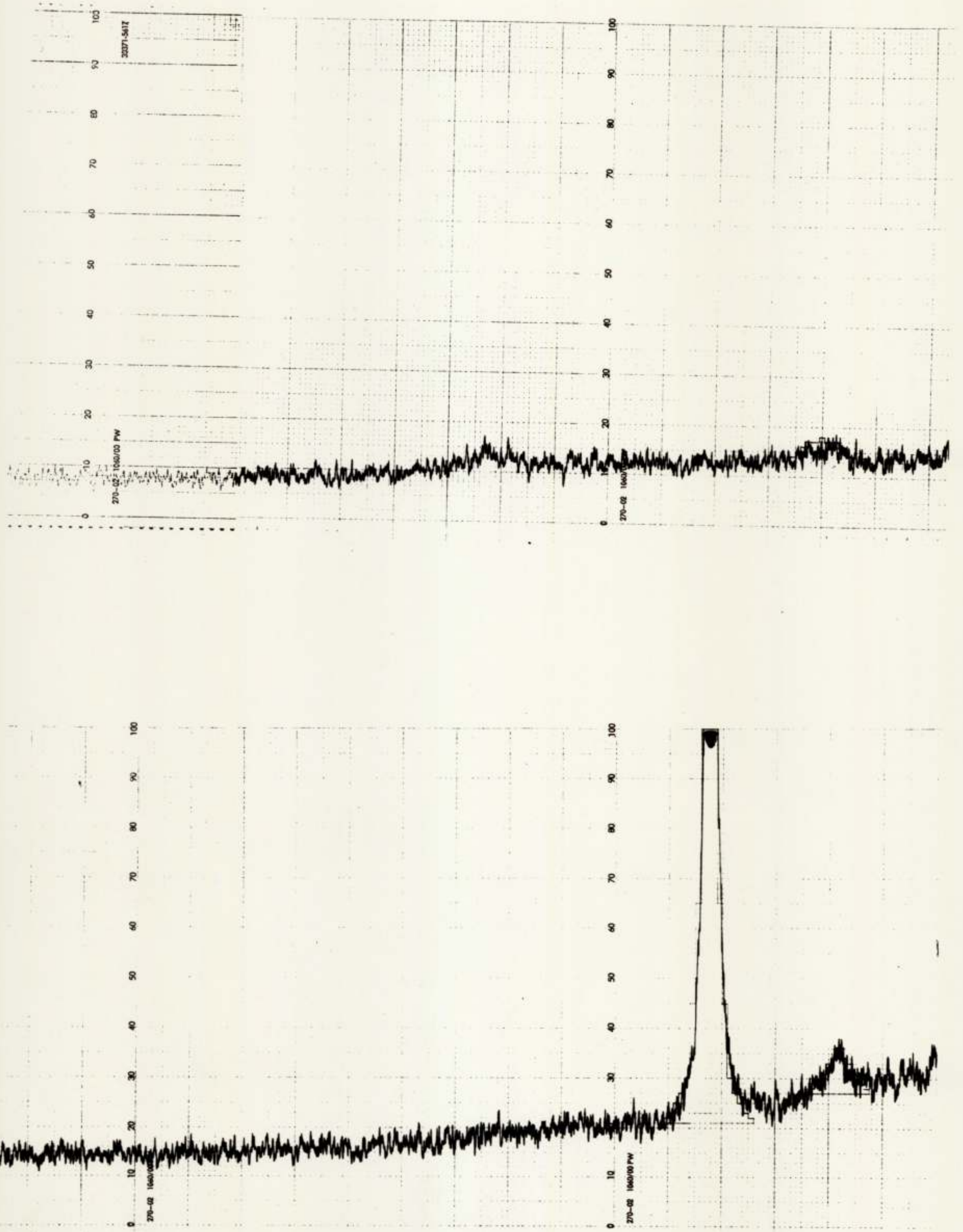

FIGURE 31 DIFFRACTION PATTERN OF A SAMPLE

WITH 10% OF fcc PHASE

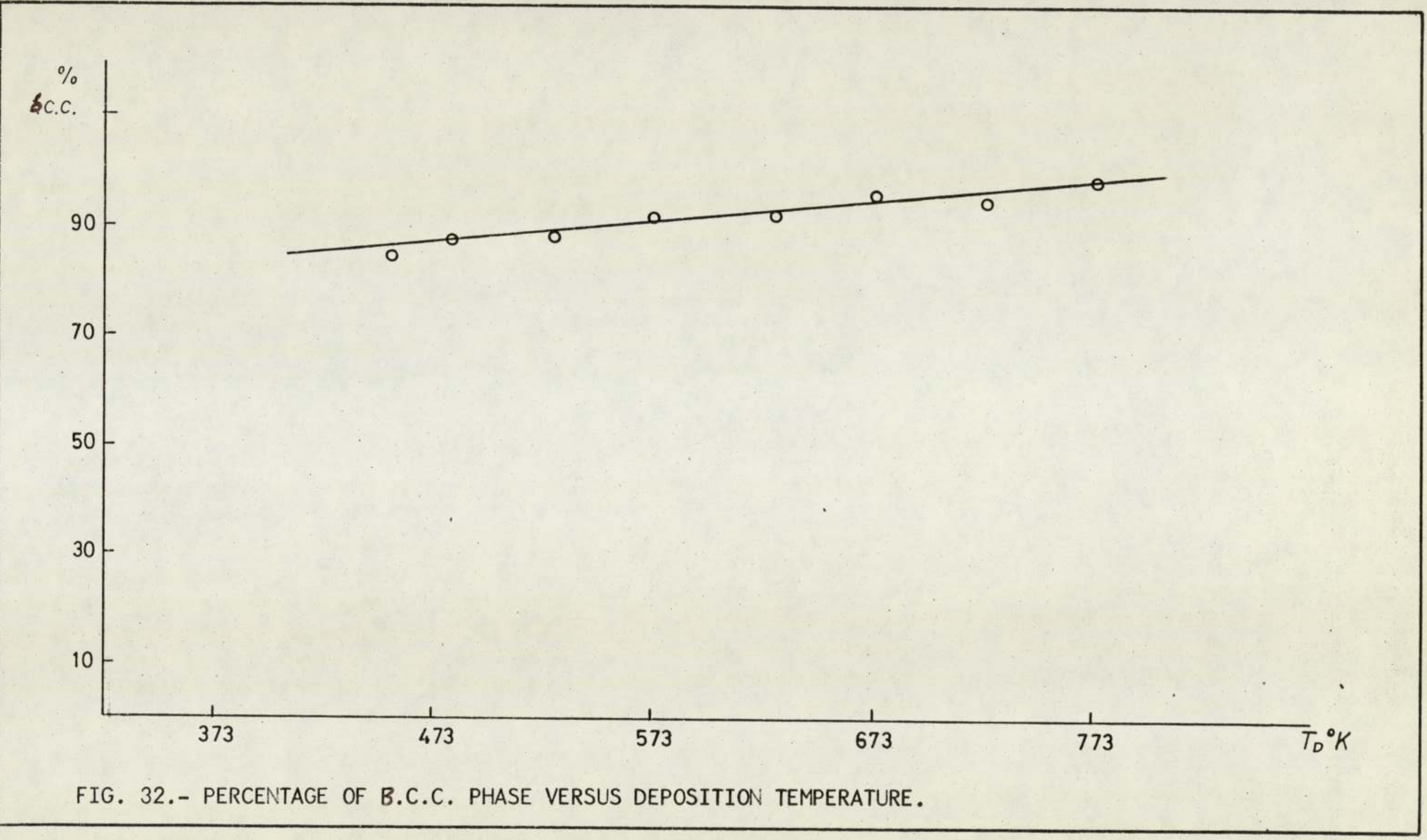

FIG. 32.- PERCENTAGE OF B.C.C. PHASE VERSUS DEPOSITION TEMPERATURE.

5.2.1 Preferred Orientation

The b.c.c. - Ta phase in the third group of samples display, as it does in the second group, a degree of preferred orientation in the [110] direction which is affected by the deposition temperature. Figure (33) shows the intensity ratio of the (220) and (211) lines, as a measure of the degree of orientation, versus deposition temperature.

5.2.2 Lattice Constants

The "d" spacing corresponding to b.c.c. and f.c.c. - Ta structures was calculated for all the samples prepared in this work. It was found that this parameter changes with thickness and deposition temperature. Table (4) shows how the "d" spacing parameter and the calculated lattice parameter a_o for b.c.c. - Ta phase vary with the thickness and deposition temperature while Figure (34) shows the same effect for f.c.c. - Ta.

It must be pointed out that sample Ta - 37A, deposited with a substrate temperature of 423°K, did not undergo any change in the "d" spacing when subsequently annealed at a temperature of 600°K.

5.3 Electrical Properties

The electrical properties were determined by passing a current through the film and observing the drop in potential across the sample. Measurements were taken while the temperature was varied from 300°K down to the temperature at which the sample became superconductive.

Table (5) shows a typical set of results from the electrical measurements on a tantalum film. A selection of 25 readings has been made from a typical run of over 60 readings.

From the measurements resistance, resistivity, TCR, $d\rho/dT$ and resistivity ratio ρ_{300}/ρ_{10} were determined. The film thicknesses used in

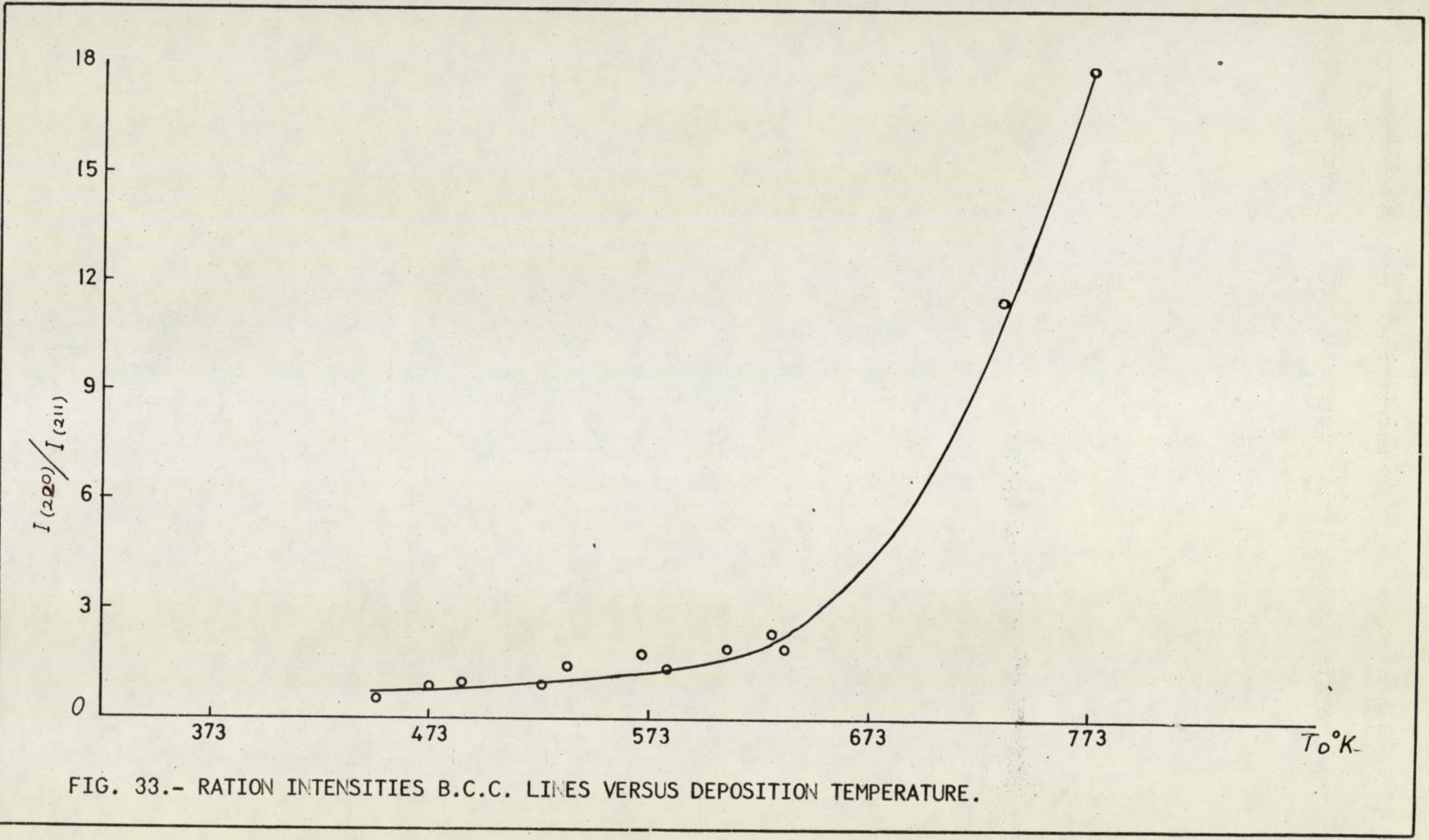

FIG. 33.- RATION INTENSITIES B.C.C. LINES VERSUS DEPOSITION TEMPERATURE.

TABLE 4

EFFECT OF THICKNESS AND SUBSTRATE TEMPERATURE ON LATTICE PARAMETER OF b.c.c. - Ta FILMS

Sample No.	Thickness (Å)	Observed "d" (Å)	Calculated "a_o" (Å)	Deposition Temp. (°K)
Ta-36A	575	2.386	3.374	423
Ta-37A	625	2.386	3.374	423
Ta-33	2400	2.368	3.348	423
Ta-61	245	2.362	3.34	533
Ta-35	550	2.356	3.332	523
Ta-26	3100	2.350	3.323	523
Ta-20	3400	2.344	3.315	523
Ta-49	4650	2.338	3.307	538
Ta-24	7750	2.332	3.299	573
Ta-52	3850	2.332	3.299	698
Ta-48	3750	2.332	3.299	773

a_o Bulk = 3.3058Å

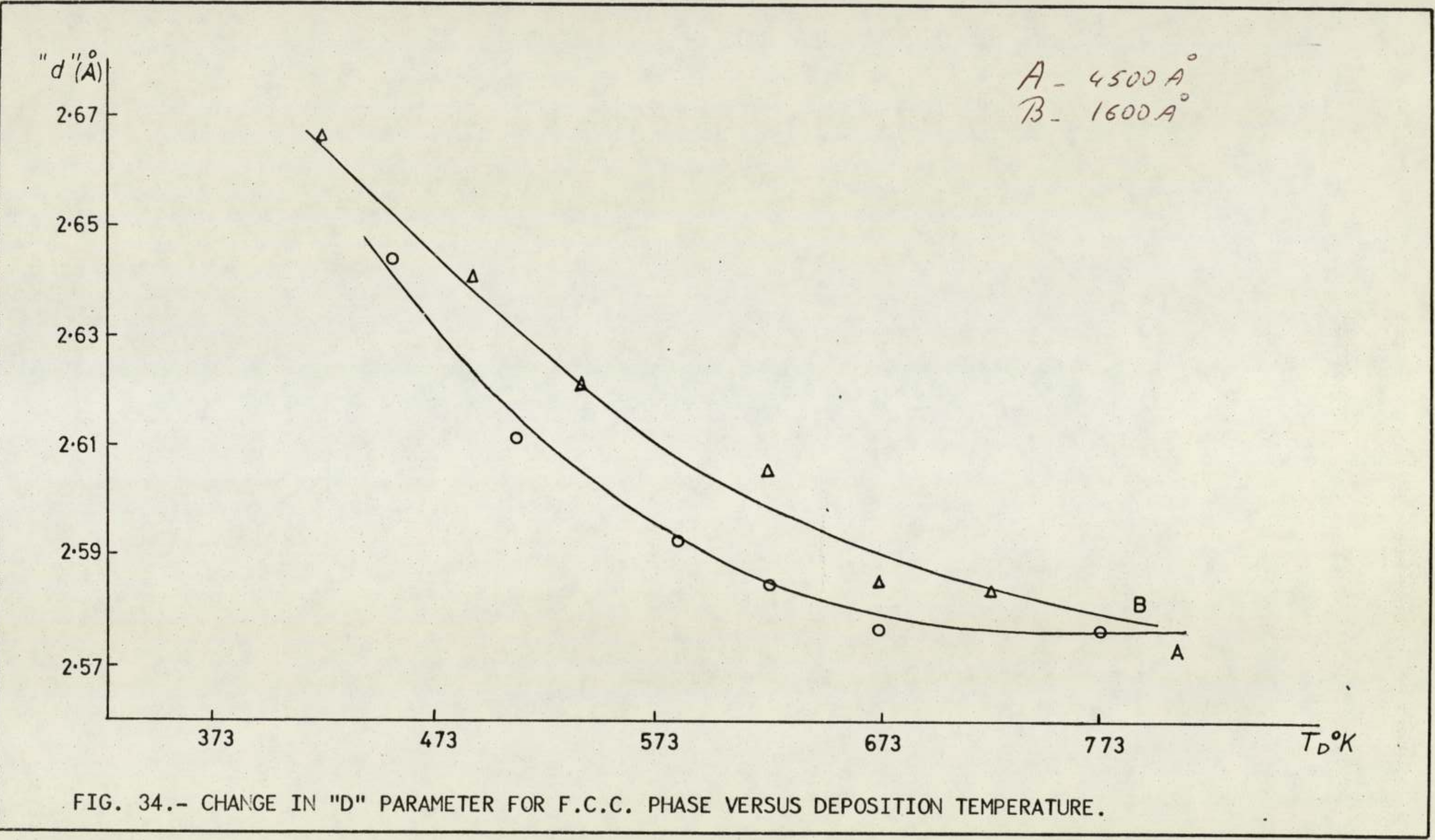

FIG. 34.- CHANGE IN "D" PARAMETER FOR F.C.C. PHASE VERSUS DEPOSITION TEMPERATURE.

TABLE 5

SET OF RESULTS FROM THE ELECTRICAL MEASUREMENTS ON A TANTALUM FILM OF THICKNESS 6000 Å

Current +ve mA	Current -ve mA	Resistance Ohms	An - Fe Chromel mV	Copper Const. mV	T^oK
11.015	11.013	1.290	4.169	6.552	300
11.015	11.013	1.263	4.051	6.309	294
10.971	10.967	1.230	3.772	5.757	280
10.974	10.971	1.161	3.218	4.739	253
10.982	10.980	1.052	2.441	3.425	215
10.964	10.961	0.924	1.799	2.403	182
10.953	10.951	0.824	1.387	1.789	160
11.015	11.011	0.720	0.850	1.042	130
11.024	11.021	0.670	0.596	0.710	115
11.031	11.028	0.581	0.255	0.293	94
11.034	11.032	0.547	0.069	0.082	82
11.038	11.035	0.528	0.000	0.000	77
11.046	11.044	0.465	-0.305	-0.304	56
11.084	11.082	0.430	-0.454	-0.436	45
11.074	11.072	0.385	-0.654	-0.588	30
11.055	11.052	0.377	-0.724	-0.622	25
11.080	11.077	0.370	-0.870	-	15
11.080	11.077	0.364	-0.974	-	8
11.078	11.075	0.353	-1.025	-	4.21
11.078	11.075	0.353	-1.026	-	4.14
11.078	11.074	0.353	-1.027	-	4.07
11.107	11.105	0.353	-1.028	-	4.00
11.115	11.113	0.353	-1.029	-	3.91
11.122	11.120	0.109	-1.030	-	3.83
11.122	11.120	0.000	-1.031	-	3.75

the calculations were the optical ones determined by interferometry.

5.3.1 Resistivity

The variation of resistivity with temperature for sample Ta-67 which exhibited pure f.c.c. structure and whose thickness is 150Å, is illustrated in Figure (35)

The behaviour of two films which are pure b.c.c. - Ta is shown in Figures (36) and (37). The first sample Ta-34 is 500Å thick and the second Ta-45 is 9650Å.

The same is presented in Figures (38, 39 and 40) for three samples which show a mixture of f.c.c. and b.c.c. structure; the first corresponds to film Ta-71, 1400Å thick, with a 10% proportion of f.c.c. phase; the second is sample Ta-27, 3400Å thick which has 42% of f.c.c. structure and the third corresponds to film Ta-47, 9000Å thick, with 25% of f.c.c. - Ta.

The variation of room temperature and residual resistivity with thickness is given in Figure (41) for films prepared under the same deposition conditions of pressure, deposition rate and deposition temperature. The samples containing more than 10% of f.c.c. - Ta phase have been omitted from Figure (41); the resistivity of films increases as the proportion of the f.c.c. phase increases. Figure (42) shows how the percentage increase in resistivity, over the value which would correspond to a pure b.c.c. - Ta film, of the same thickness and prepared under the same deposition conditions, varies with the percentage of f.c.c. - Ta phase present in the sample.

Another parameter which influences the resistivity of a film is the temperature at which the sample has been deposited. Table (6) gives the variation of room temperature resistivity with deposition temperature. The result corresponds to two sets of samples, the films in the first group are about 1450Å

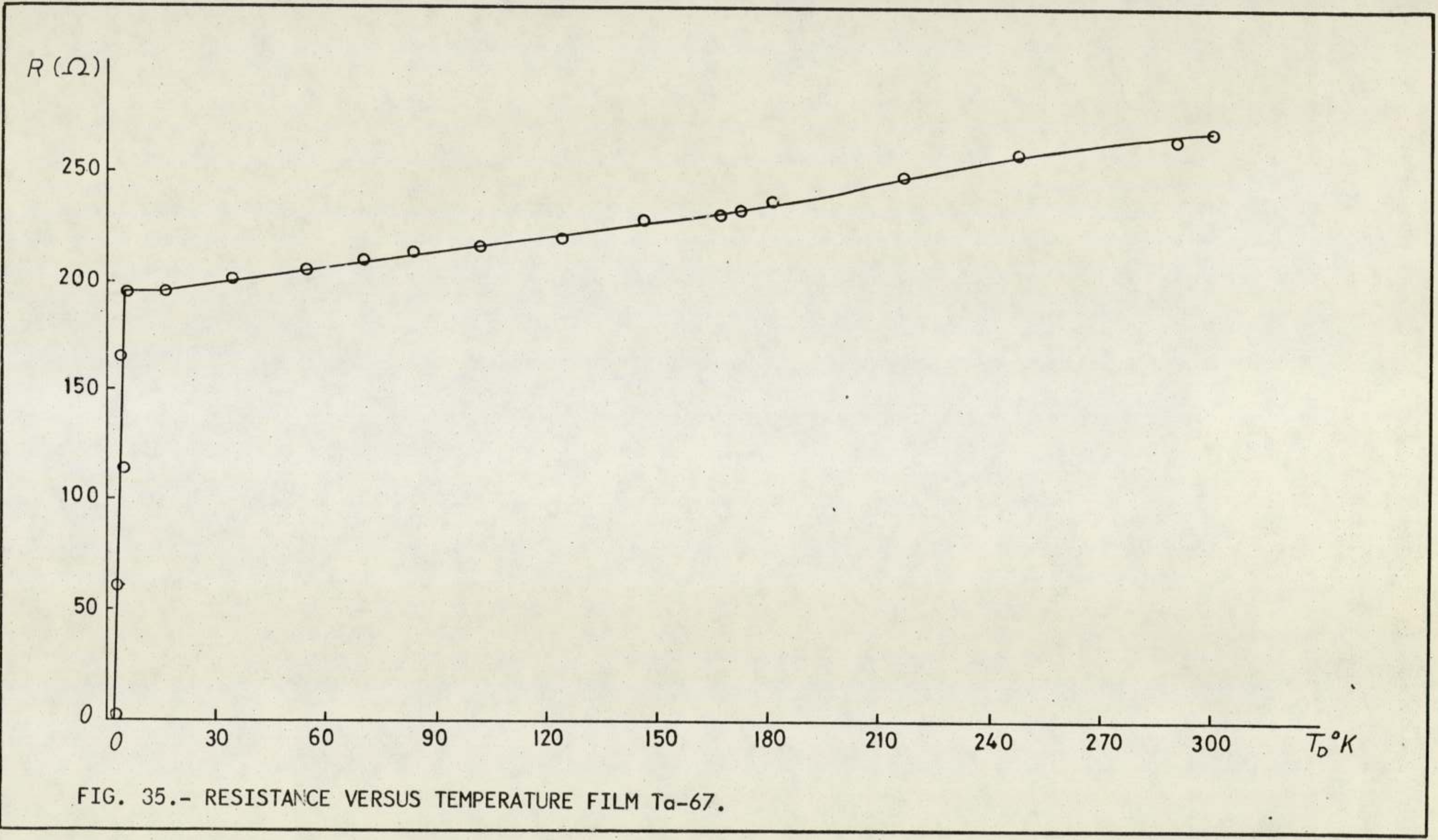

FIG. 35.- RESISTANCE VERSUS TEMPERATURE FILM Ta-67.

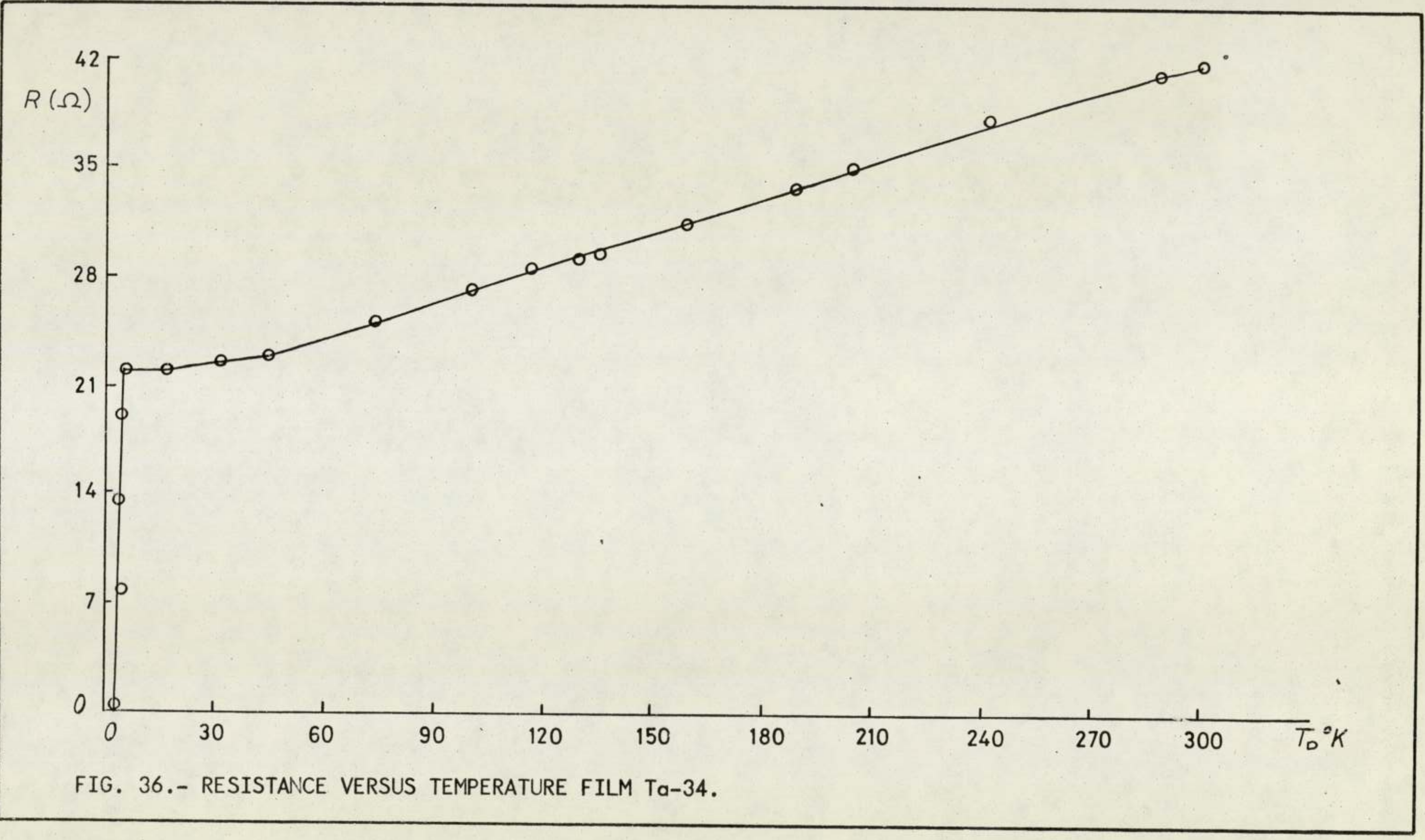

FIG. 36.- RESISTANCE VERSUS TEMPERATURE FILM Ta-34.

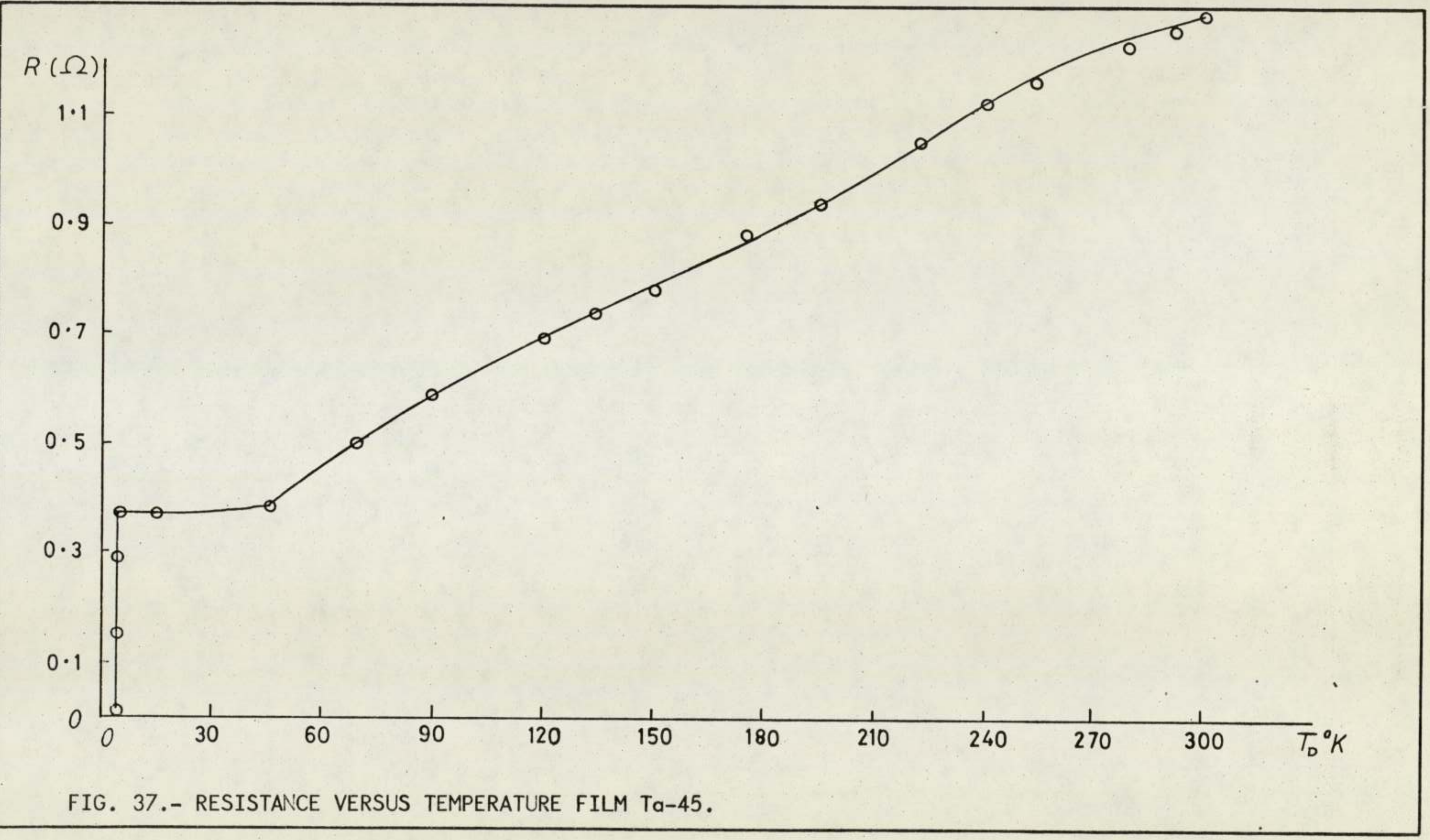

FIG. 37.- RESISTANCE VERSUS TEMPERATURE FILM Ta-45.

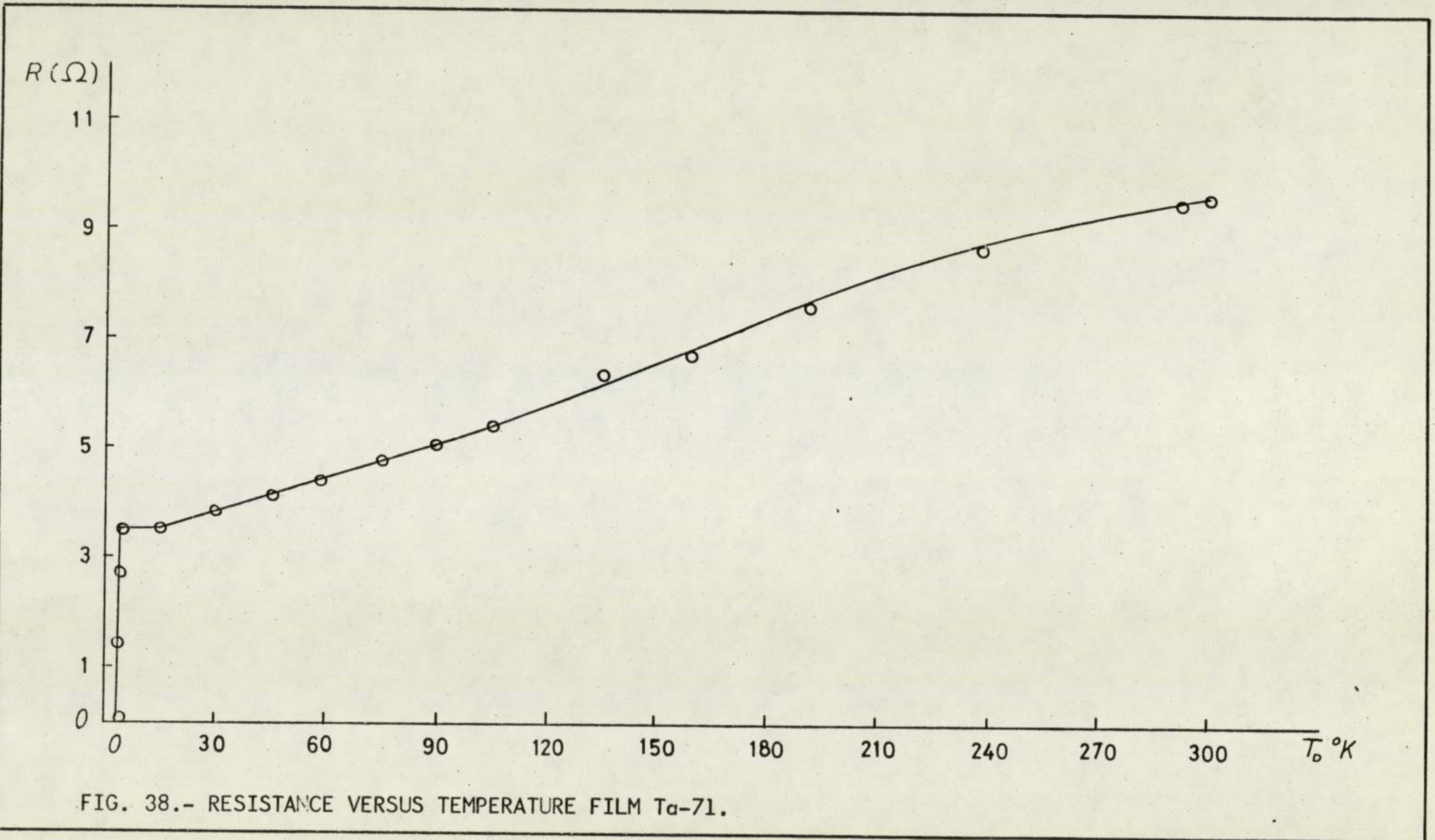

FIG. 38.- RESISTANCE VERSUS TEMPERATURE FILM Ta-71.

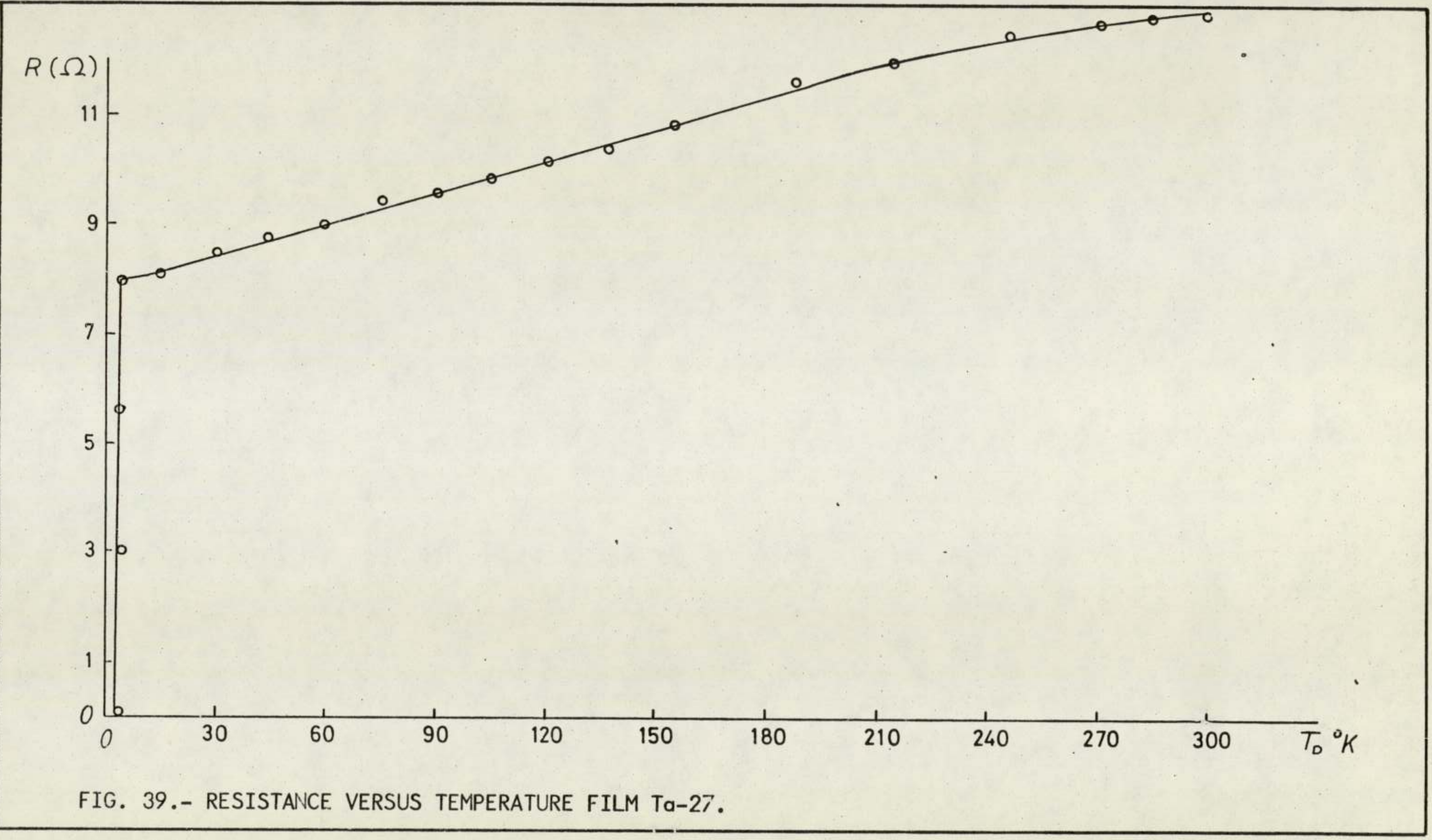

FIG. 39.- RESISTANCE VERSUS TEMPERATURE FILM Ta-27.

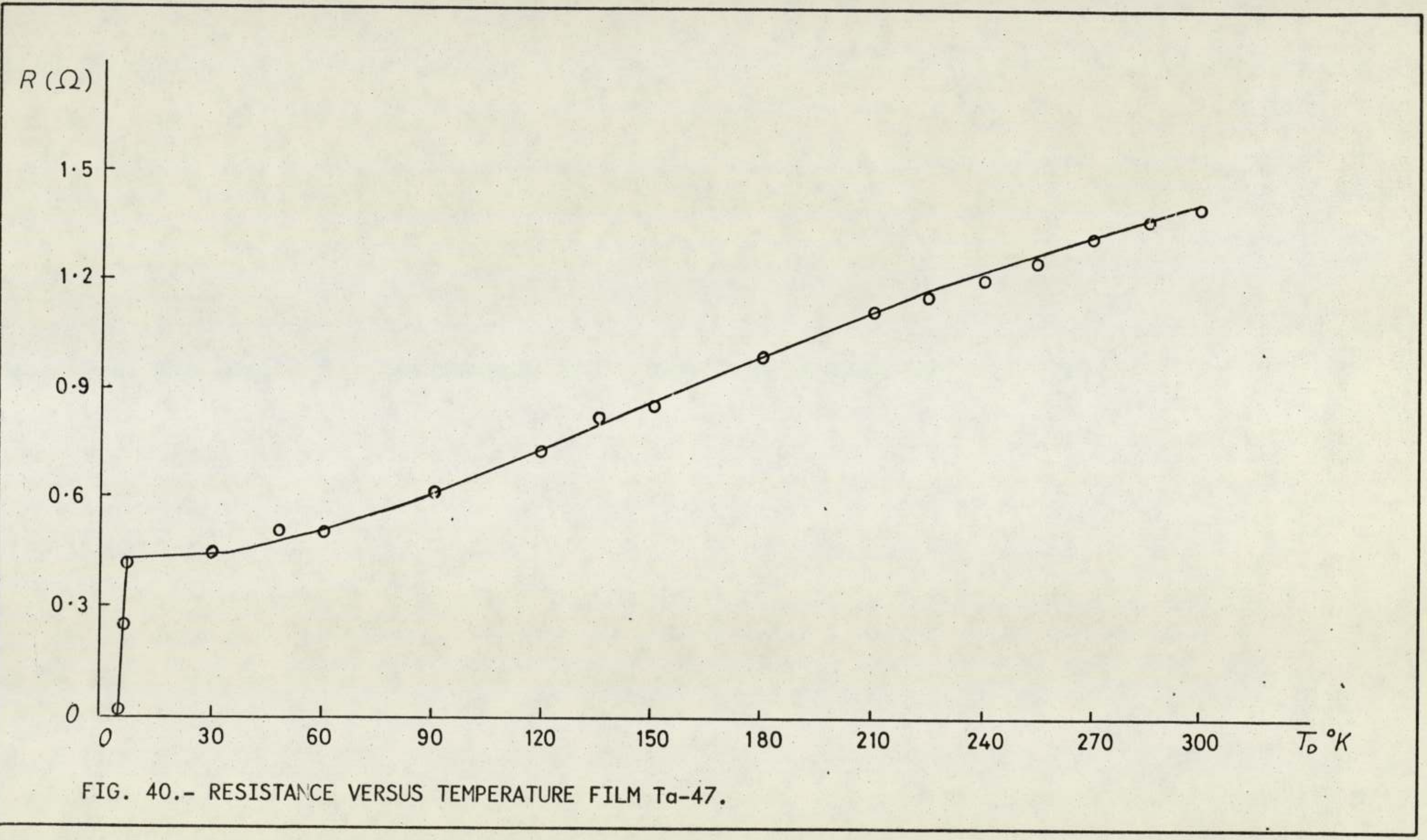

FIG. 40.- RESISTANCE VERSUS TEMPERATURE FILM Ta-47.

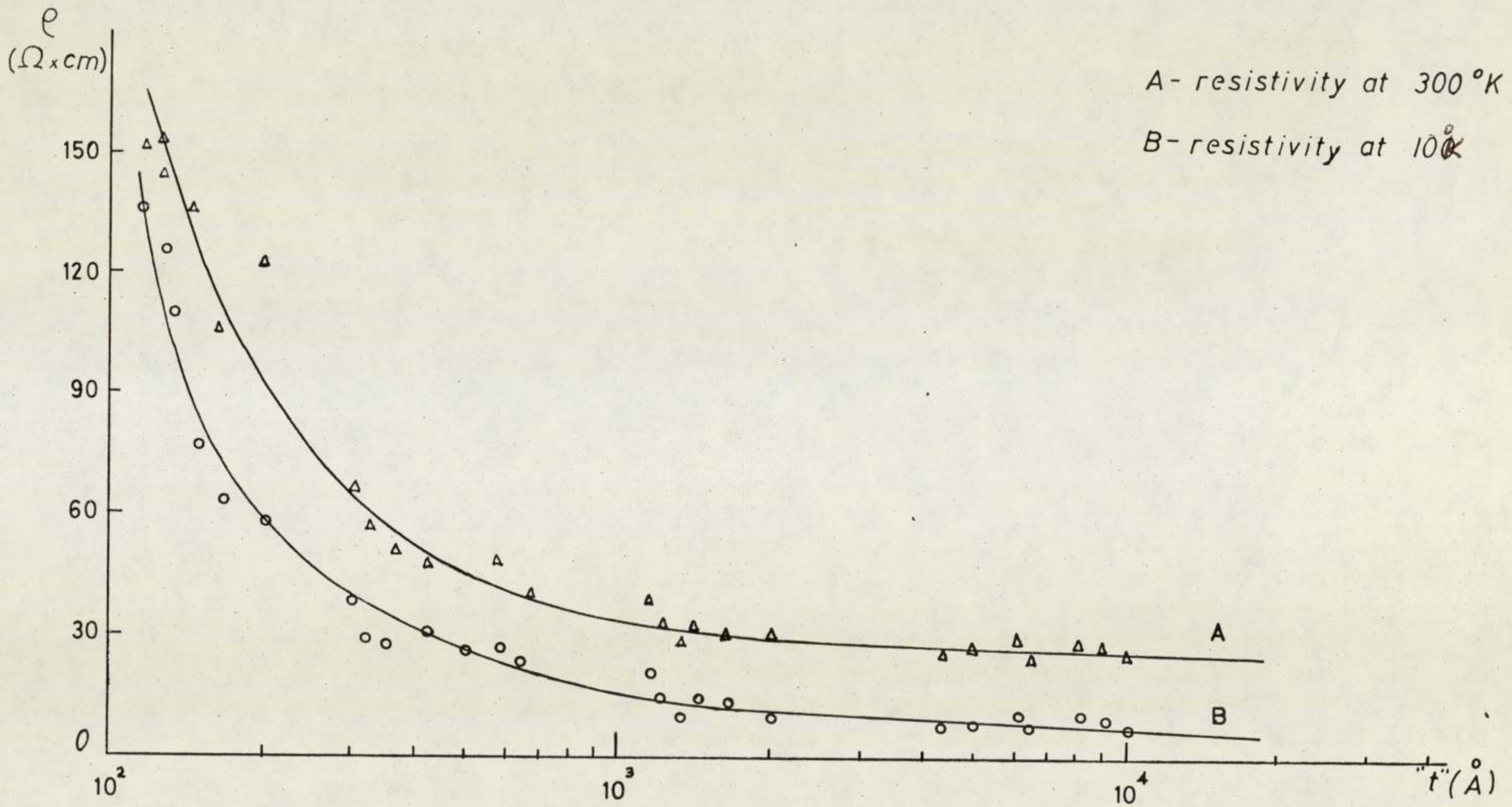

FIG. 41.- RESISTIVITY VERSUS THICKNESS.

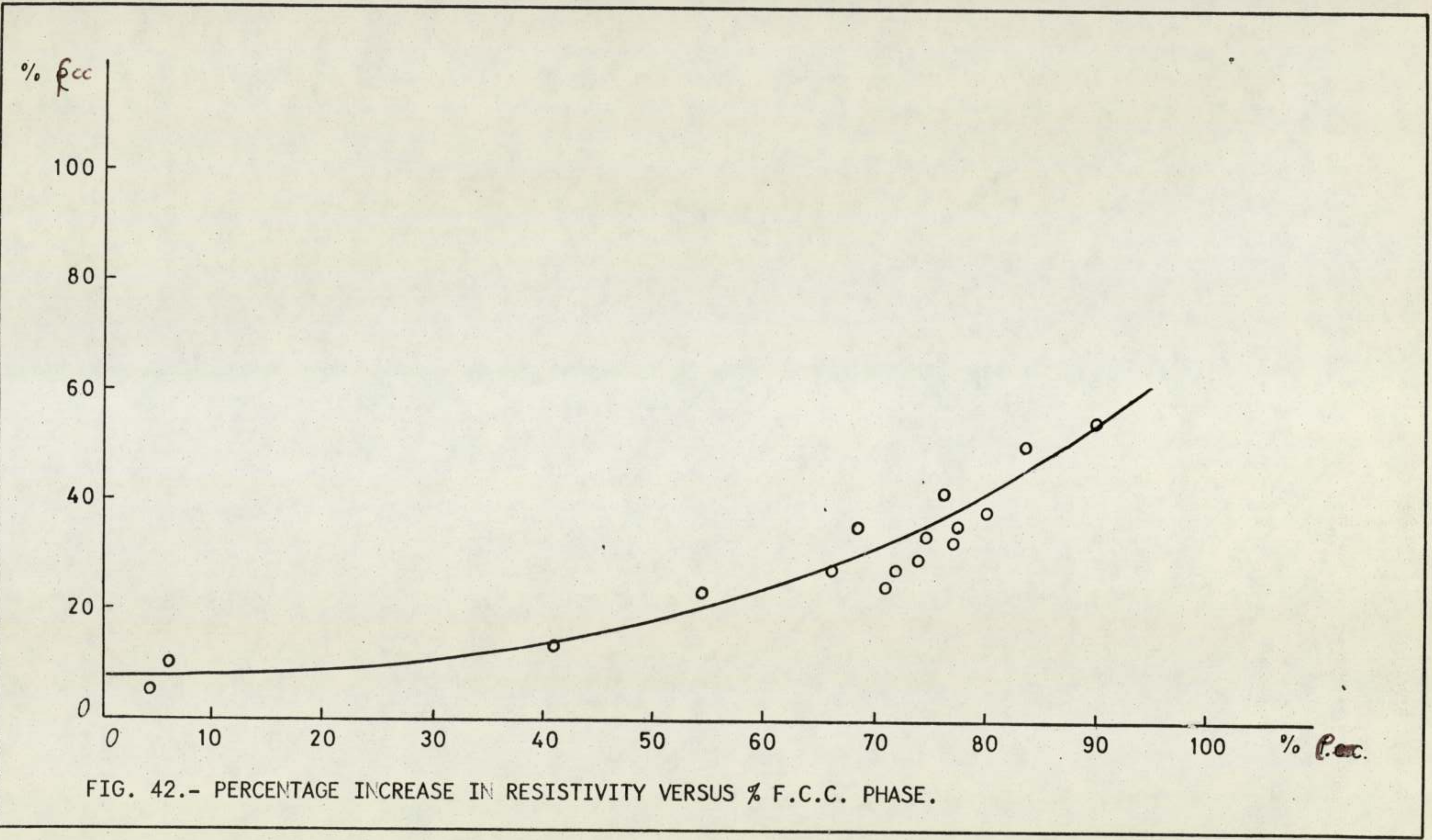

FIG. 42.- PERCENTAGE INCREASE IN RESISTIVITY VERSUS % F.C.C. PHASE.

thick while the samples in the second set are on average 4000Å thick. Each film in every set has been prepared under exactly the same conditions apart from the deposition temperature which was varied from 473 to 723°K.

The influence of deposition rate on resistivity was also investigated. It was found that when the deposition rate decreased from 250 to 40Å/m the values from the room temperature resistivity for samples of 650Å thickness increased from 40×10^{-6} to 250×10^{-6} Ω x cm.

5.3.2 Temperature coefficient of resistivity TCR

The TCR parameter is defined as

$$TCR = \frac{1}{R_1} \frac{(R_2 - R_1)}{(T_2 - T_1)}$$

where R_1 and R_2 are the film resistivity at T_1 (room temperature) and T_2 (77°K).

TCR's found for all the samples prepared in this work were all positive and ranged in value from 350 to 3000 p.p.m/°K. The variation of TCR with thickness for films prepared under the same conditions is shown in Figure (43). Samples with a percentage of f.c.c. - Ta phase higher than 10% have been omitted. The TCR decreases proportionally to the increase in percentage of f.c.c. phase. Table(7) shows the decrease of TCR, as compared with increase in resistivity, with increasing percentage of f.c.c. - Ta structure.

5.3.3 Resistivity Ratio and $d\rho/dT$

If we consider ρ_{300}/ρ_{10} and $d\rho/dT$ as a measure of film purity and film perfection, we would expect both parameters to vary with film thickness, deposition temperature and finally with percentage of f.c.c. - Ta phase present in the sample (if we consider the f.c.c. phase as an impurity in an otherwise

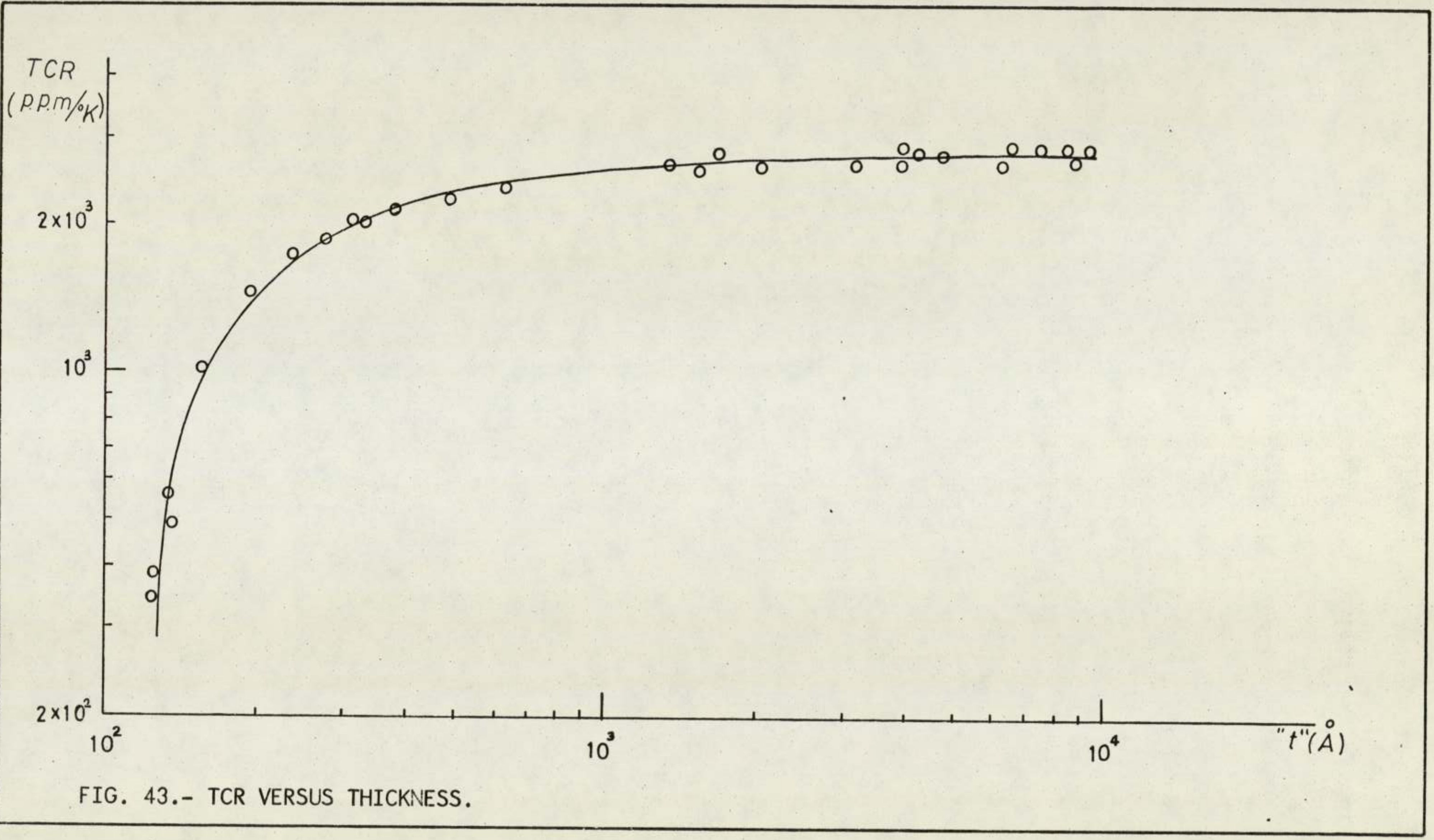

FIG. 43.- TCR VERSUS THICKNESS.

TABLE 6

VARIATION OF RESISTIVITY AT 300°K WITH DEPOSITION TEMPERATURE

To °K	473	523	573	623	673	723
ρ (μΩ.cm) 1450Å	40.8	37.7	34.2	26.8	25.1	22
ρ (μΩ.cm) 4000Å	34.5	19.7	17	15.3	14.5	13.1

TABLE 7

VARIATION OF TCR WITH PERCENTAGE OF f.c.c. - Ta PHASE

% f.c.c.	10	20	25	30	37	42	50
TCR p.p.m/°K	2280	2099	1467	1357	1245	1022	923

perfect b.c.c. Ta thin film) for films with less than 10% f.c.c. Figure (44) shows how ρ_{300}/ρ_{10} decreases when film thickness decreases and how $d\rho/dT$ remains practically constant over the whole range of thickness except for the very thin films for samples laid down under the same deposition conditions.

The variation of ρ_{300}/ρ_{10} and $d\rho/dT$ with deposition temperature for two different groups of samples is given in Figures (45 and 46). Every sample in each group had almost the same thickness.

Finally, the percentage variation of ρ_{300}/ρ_{10} and $d\rho/dT$ with the percentage of f.c.c. - Ta phase present in the samples is shown in Figure (47).

5.4 Grain Size

The grain size of all the samples was determined using the diffraction line broadening method described in section 4.7.

It was found when calculating the crystallite size of the b.c.c.-Ta phase, that using the (110) line it was difficult to find a correlation between film thicknes and grain size.

Later it was realised, that due to the fact that the Ta thin films prepared in this work all showed a certain degree of preferred orientation in the [110] direction, the use of the (110) line was misleading the results.

The broadening of the line was due not only to the size of the crystallite but to the preferred orientation in this particular direction.

With the use of the (211) line, it was found that the grain size of the b.c.c. - Ta phase changes with film thickness and Table (8) gives crystallite size for samples of differing thicknesses.

Grain size for the f.c.c. - Ta structure was calculated too.

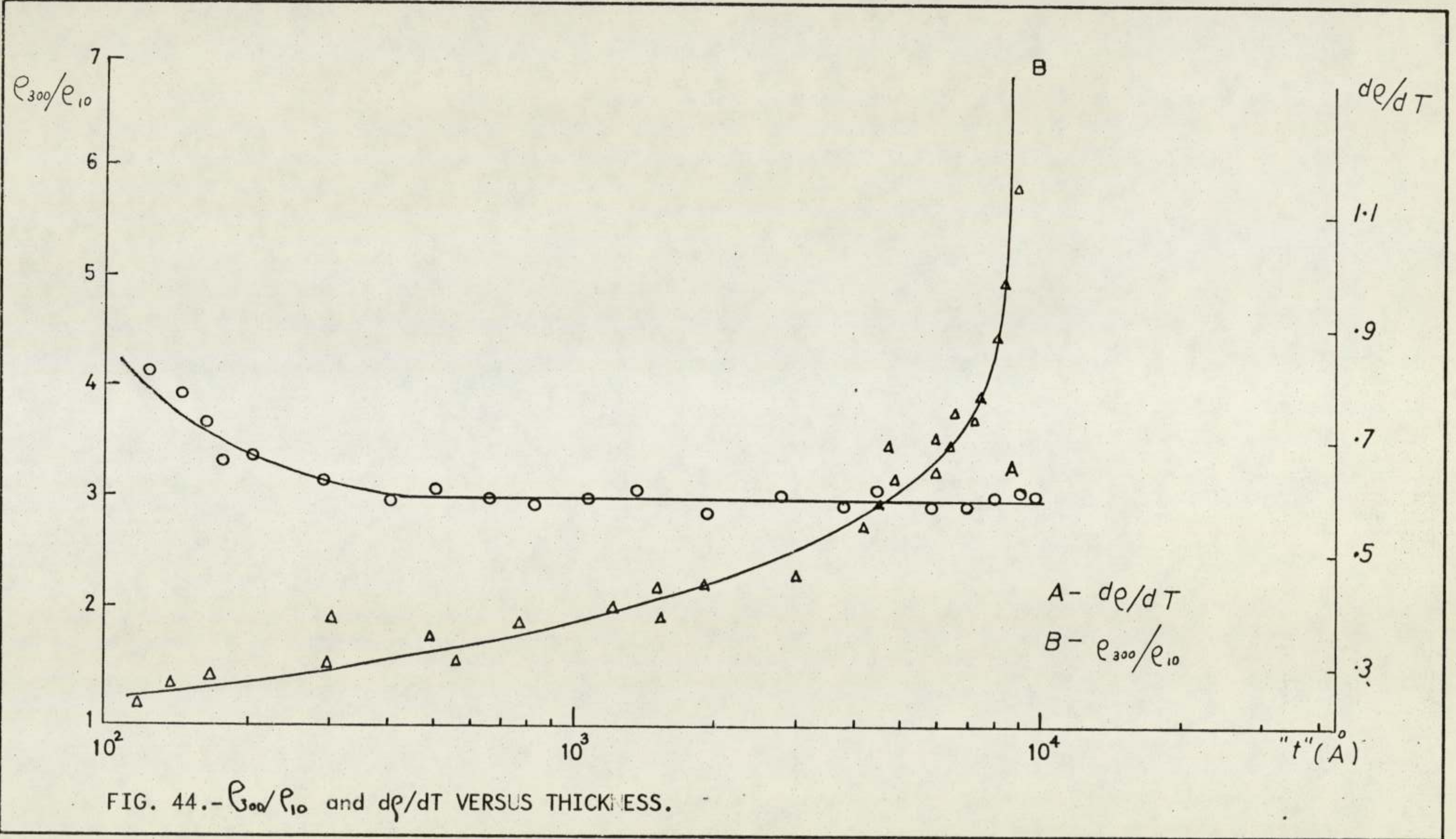

FIG. 44.- ρ_{300}/ρ_{10} and $d\rho/dT$ VERSUS THICKNESS.

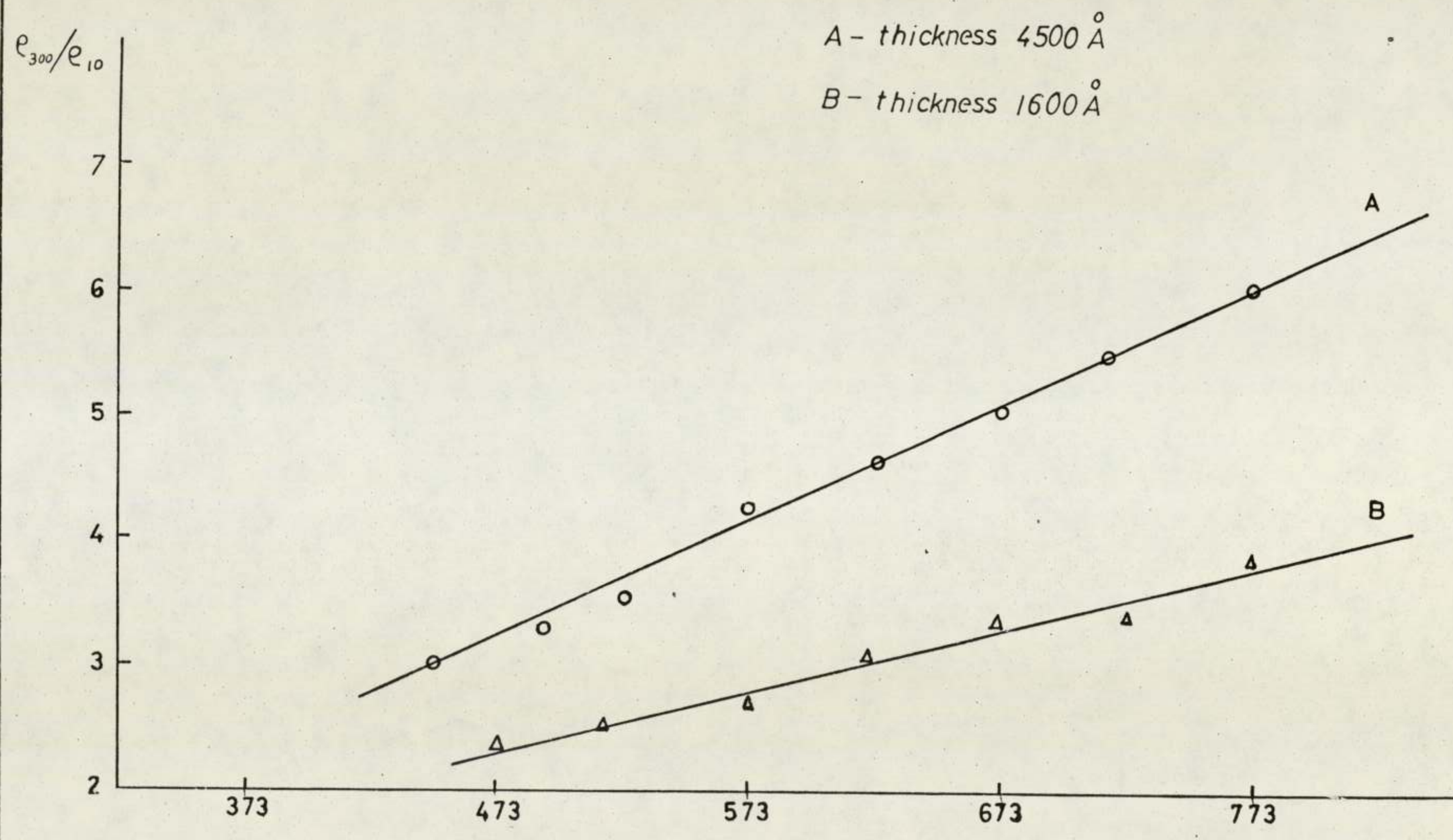

FIG. 45.- ρ_{300}/ρ_{10} VERSUS DEPOSITION TEMPERATURE.

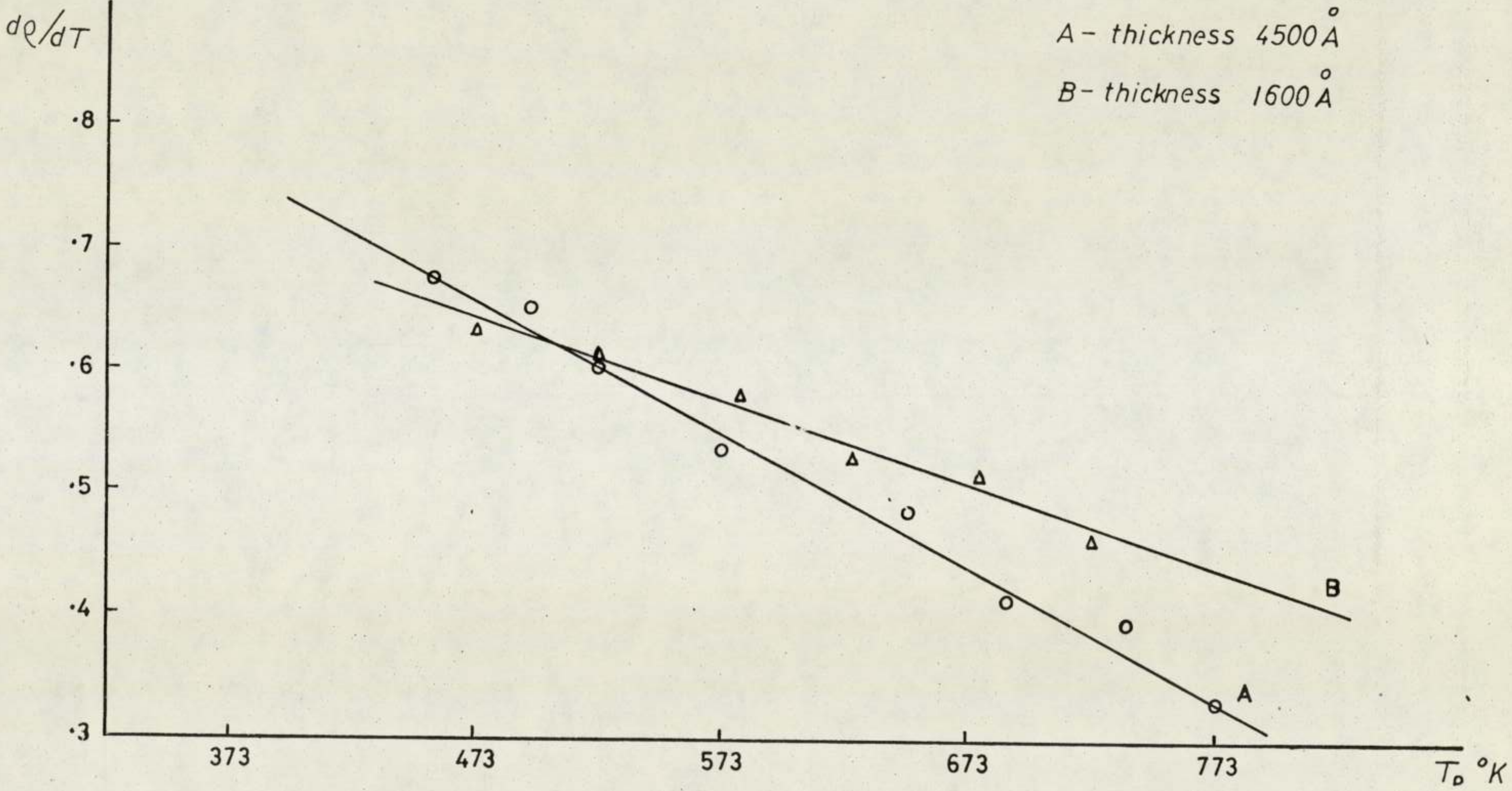

FIG. 46.- dρ/dT VERSUS DEPOSITION TEMPERATURE.

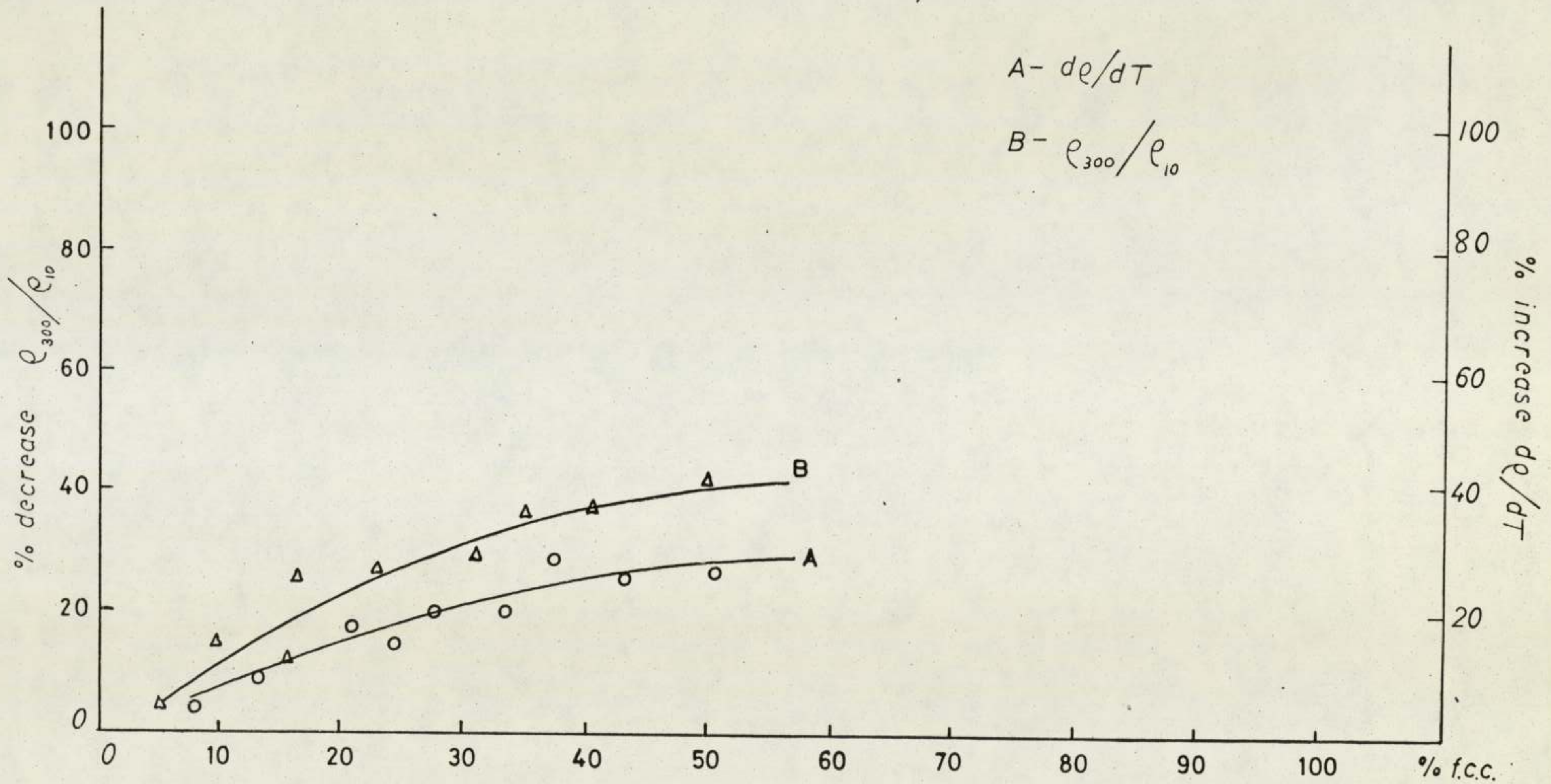

FIG. 47.- % VARIATION OF ρ_{300}/ρ_{10} AND $d\rho/dT$ VERSUS PERCENTAGE F.C.C. PHASE.

As with the b.c.c. phase the size of the grains was found to increase with thickness as can be seen in Table (9).

Another parameter to affect the crystallite size is the temperature of the substrate. Figure (48) shows how b.c.c. grain size changes with deposition temperature. Figure (49) gives the same effect for f.c.c. structure.

5.5 Transition Temperatures

All of the superconducting transitions were measured resistively. The transition temperature or critical temperature (T_C) defined as that temperature at which the resistance becomes zero.

It was found that T_C decreases with decreasing film thickness, Figure (50) is a plot of T_C versus thickness for films prepared at an average deposition temperature of $523^{\circ}K$, the other deposition conditions are also the same for all samples.

The variation of T_C with the electrical properties is shown in Figures (51), (52) and (53).

An increase in room temperature resistivity, which means an increase in residual resistivity is indicative of a decrease in the critical temperature Figure (51). A consequence of this is lower transition temperatures for lower temperature coefficient of resistance as is shown in Figure (52).

The variation of T_C with resistivity ratio is indicated in Figure (53). Films with increasing resistivity ratio show an increase in transition temperature.

All samples, with a proportion of f.c.c. - Ta structure higher than 10% have been excluded from the graphs relating to T_C with the electrical properties.

There is not a relationship between critical temperature and percentage of f.c.c. phase present in a film. For samples of the same thickness the different percentage of f.c.c. structure does not

TABLE 8

b.c.c. GRAIN SIZE OF FILMS OF DIFFERING THICKNESS

Thickness Å	Grain Size Å
245	50
550	69
650	78
1350	88
1600	107
2400	110
3400	112
4650	122
5750	127
6500	142
9650	176

TABLE 9

f.c.c. GRAIN SIZE OF FILMS OF DIFFERING THICKNESS

Thickness Å	Grain Size Å
115	30
1567	87
2100	129
3400	139
4200	155
4650	165
5750	183

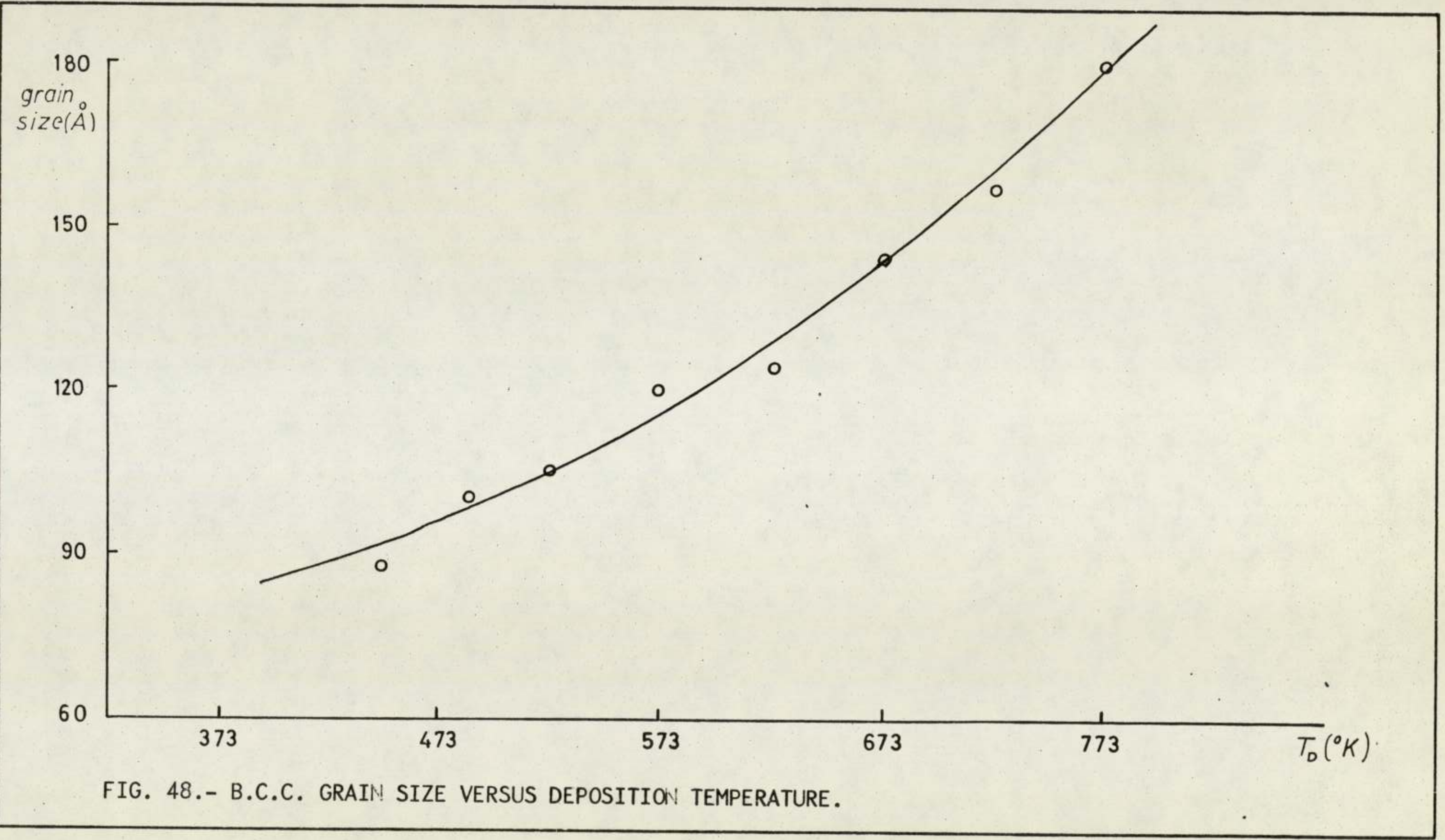

FIG. 48.- B.C.C. GRAIN SIZE VERSUS DEPOSITION TEMPERATURE.

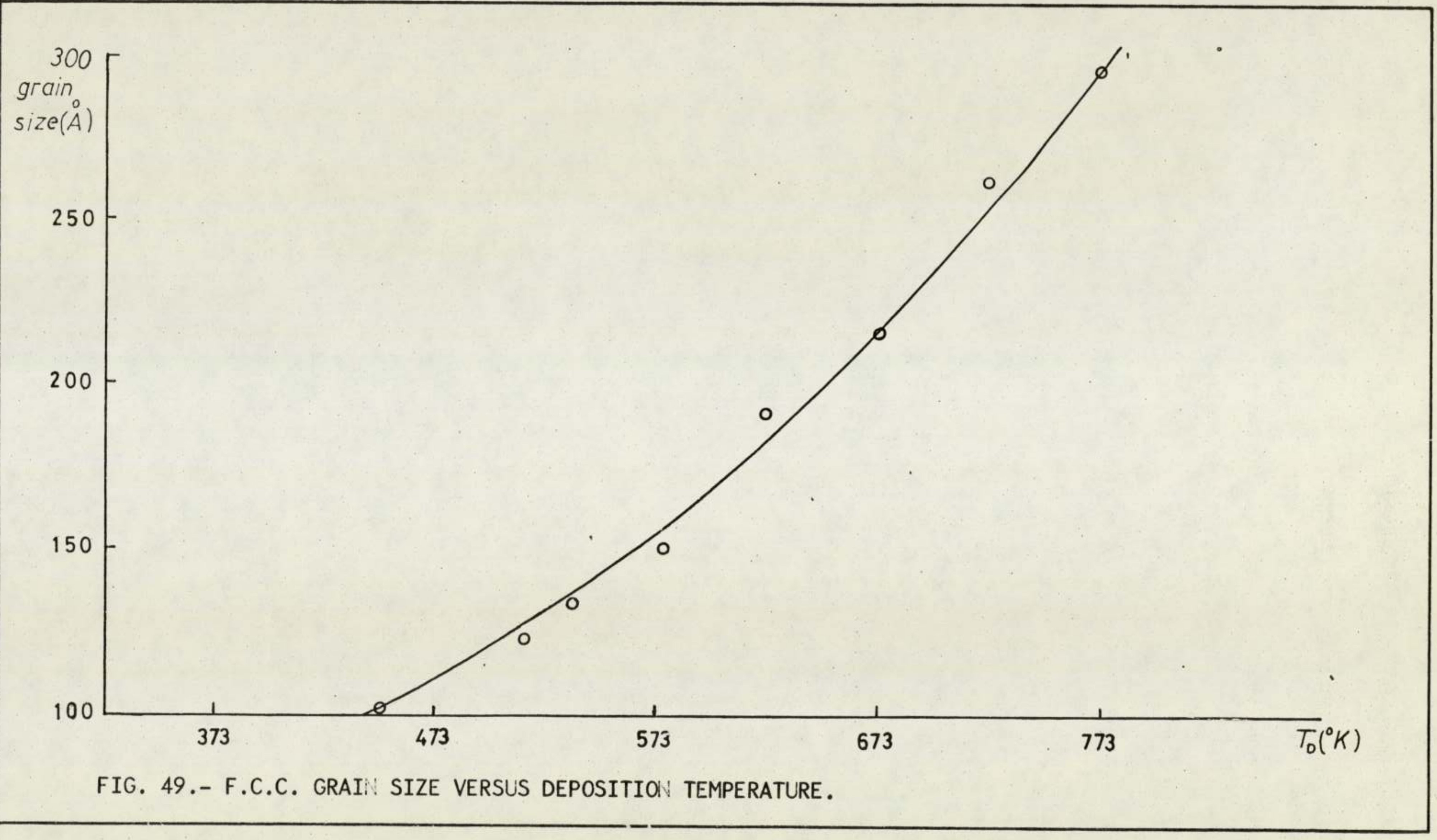

FIG. 49.- F.C.C. GRAIN SIZE VERSUS DEPOSITION TEMPERATURE.

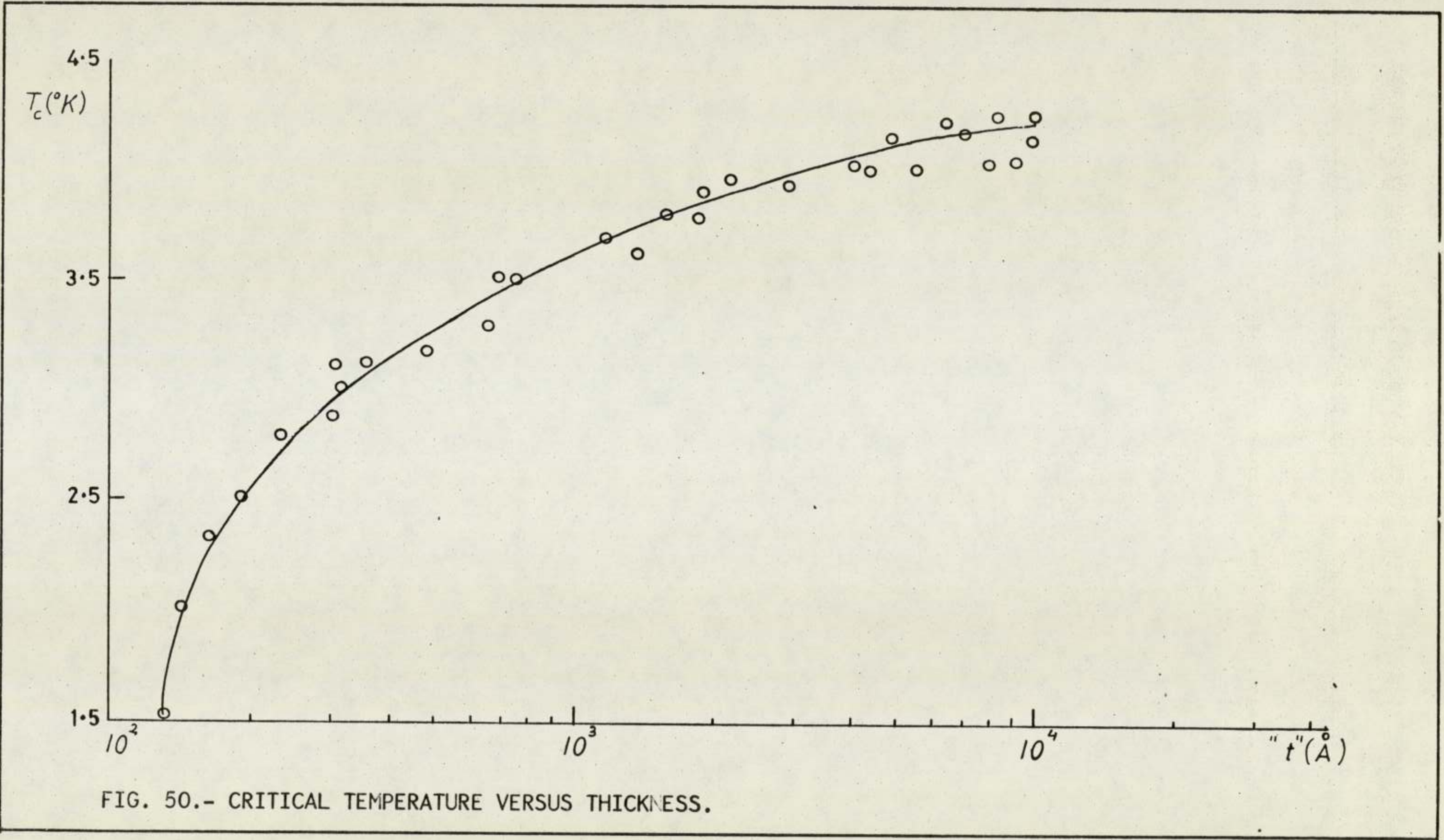

FIG. 50.- CRITICAL TEMPERATURE VERSUS THICKNESS.

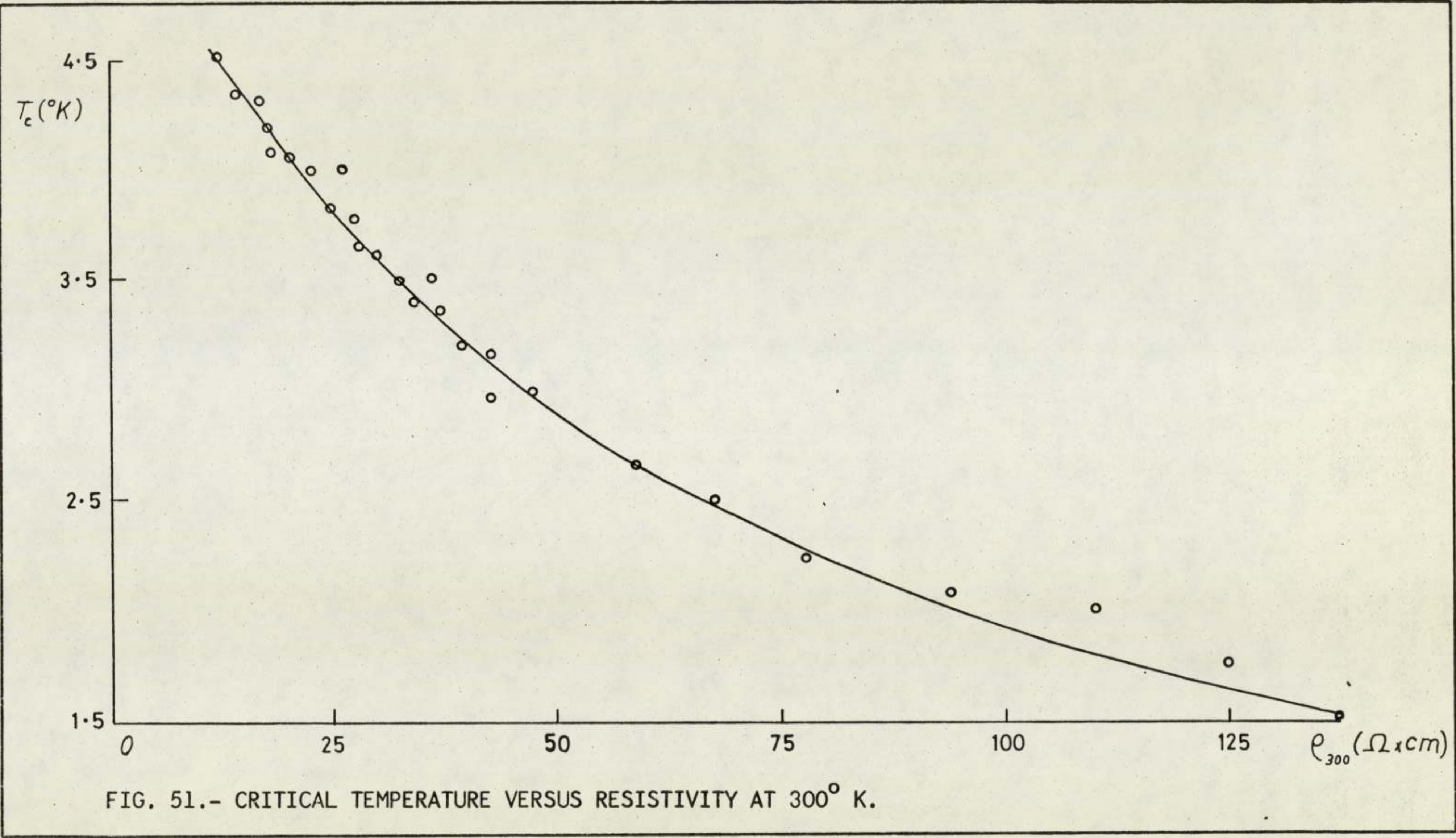

FIG. 51.- CRITICAL TEMPERATURE VERSUS RESISTIVITY AT 300° K.

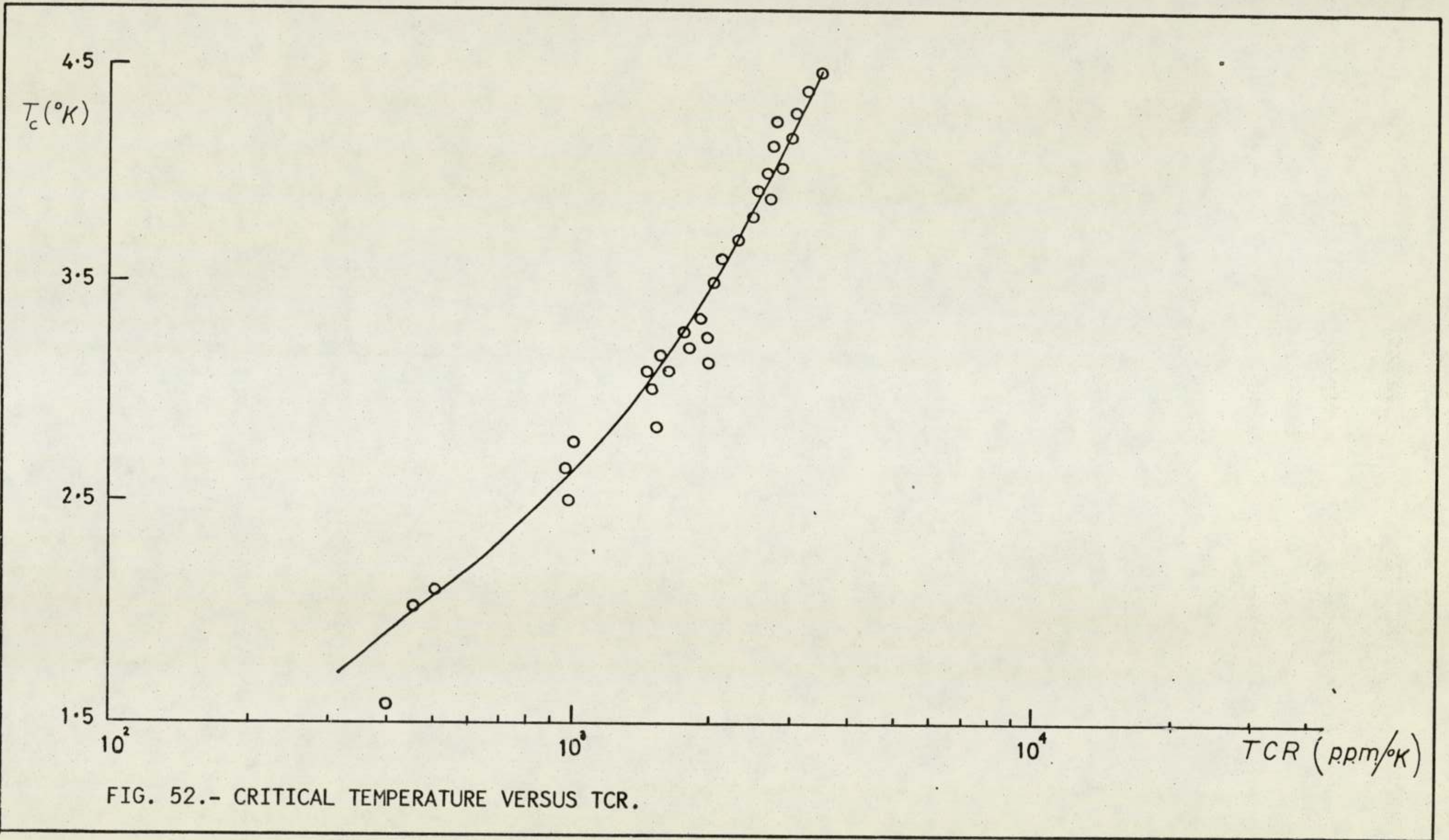

FIG. 52.- CRITICAL TEMPERATURE VERSUS TCR.

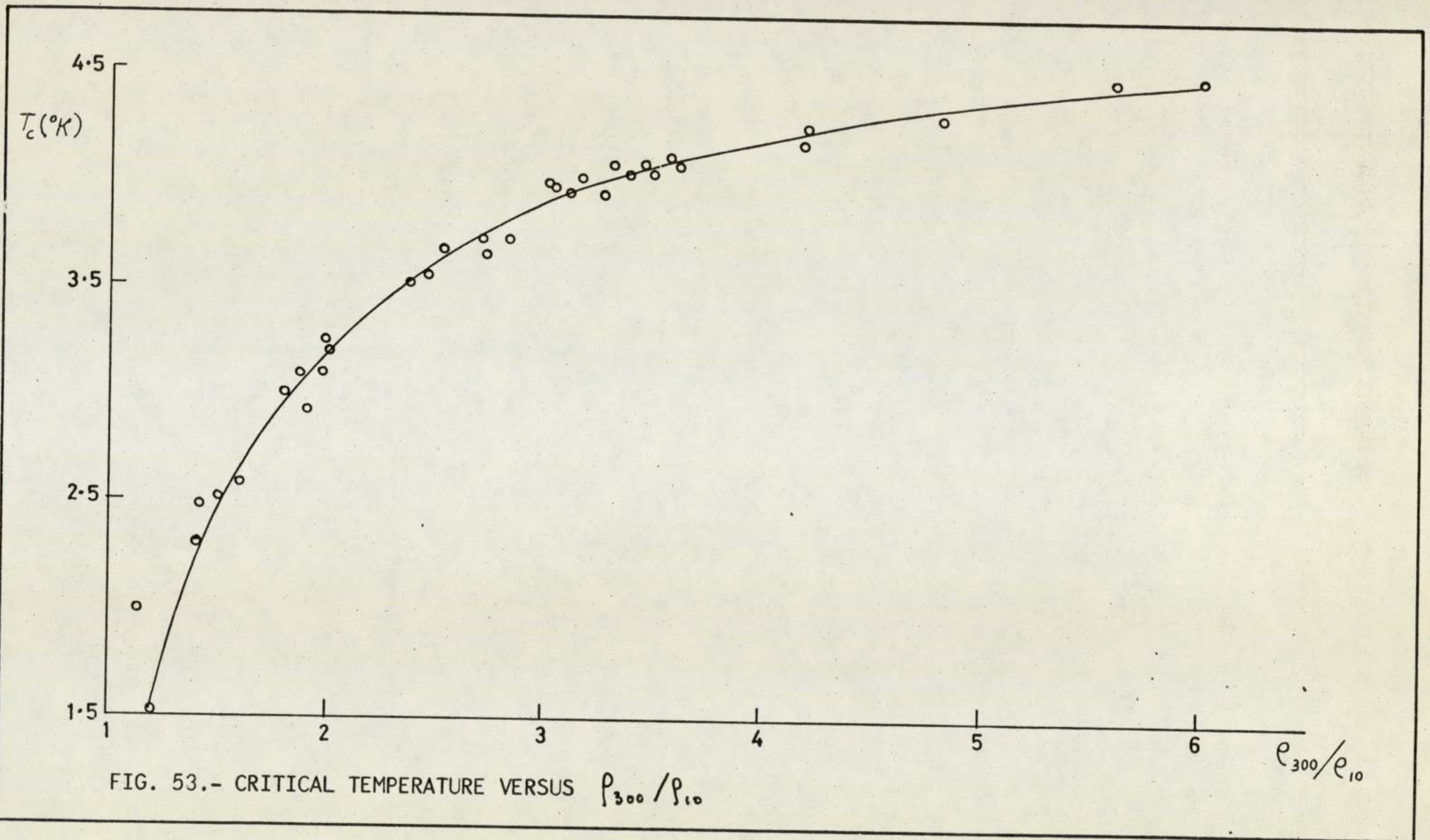

FIG. 53.- CRITICAL TEMPERATURE VERSUS ρ_{300}/ρ_{10}

affect the T_C.

Finally, the effect of substrate temperature on T_C was studied. Figure (54) illustrates how the critical temperature depends on deposition temperature. Each line in the graph corresponds to a different set of samples, prepared under the same conditions, the only difference between A, B and C being the deposition time.

In each case there is an increase in T_C with increased substrate temperature, in conformity with variations in other structural and electrical properties as shown in previous sections.

5.6 Measurement of Critical Current

The procedure followed for the determination of the critical current was the same for all films.

Once the sample was superconductive, and at a temperature as close as possible to the transition temperature, the current which passed through the film was increased until a resistive transition was observed. The procedure was repeated lowering the temperature steadily and taking measurements of the critical current at intervals of about $0.3^{\circ}K$.

As shown in Figure (55) the critical current decreases with the decreasing thickness of the film. Figure (56) indicates how the critical current increases with decreasing temperature for samples of different thickness.

The exact dependence of T_C on temperature will be discussed in the next Chapter.

Table (10) is a typical set of critical current measurements.

5.7 Film Thickness

The optical method used to measure film thickness was described in section 4.4.1. For very thin films of the order of 100Å the step observed in the fringes was very small, the error in determining the thickness of these films was large; ± 50%. Therefore it was considered

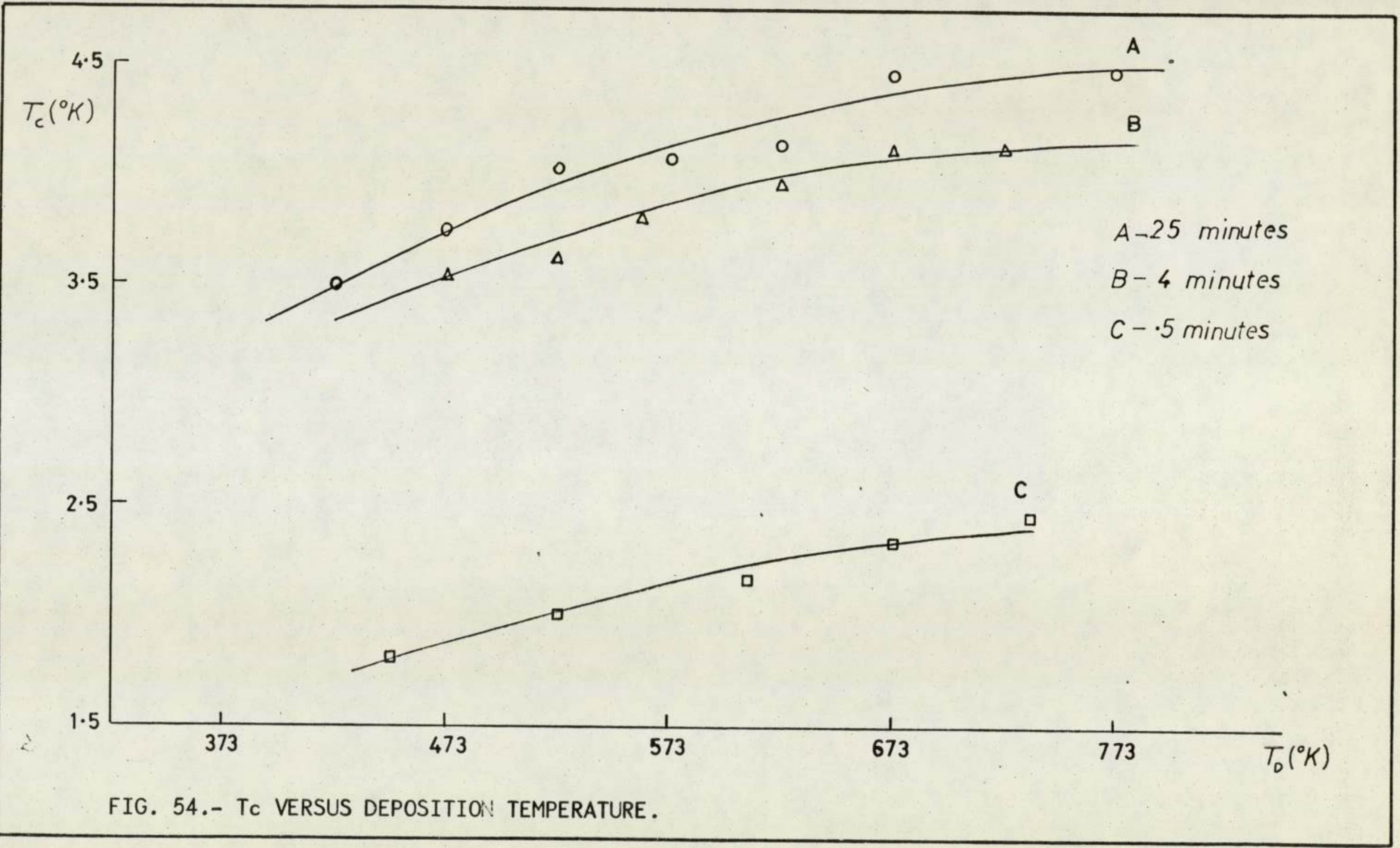

FIG. 54.- Tc VERSUS DEPOSITION TEMPERATURE.

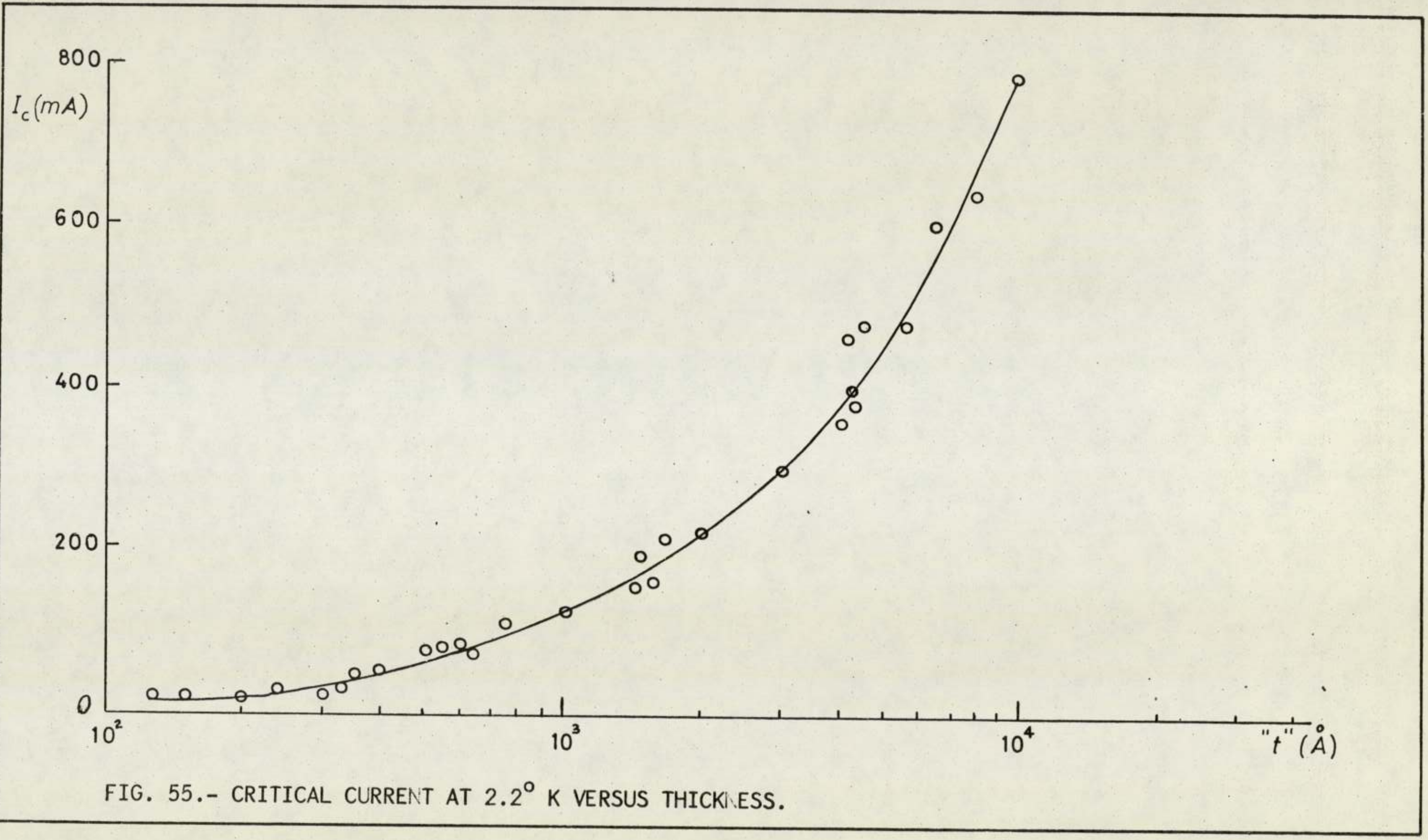

FIG. 55.- CRITICAL CURRENT AT 2.2° K VERSUS THICKNESS.

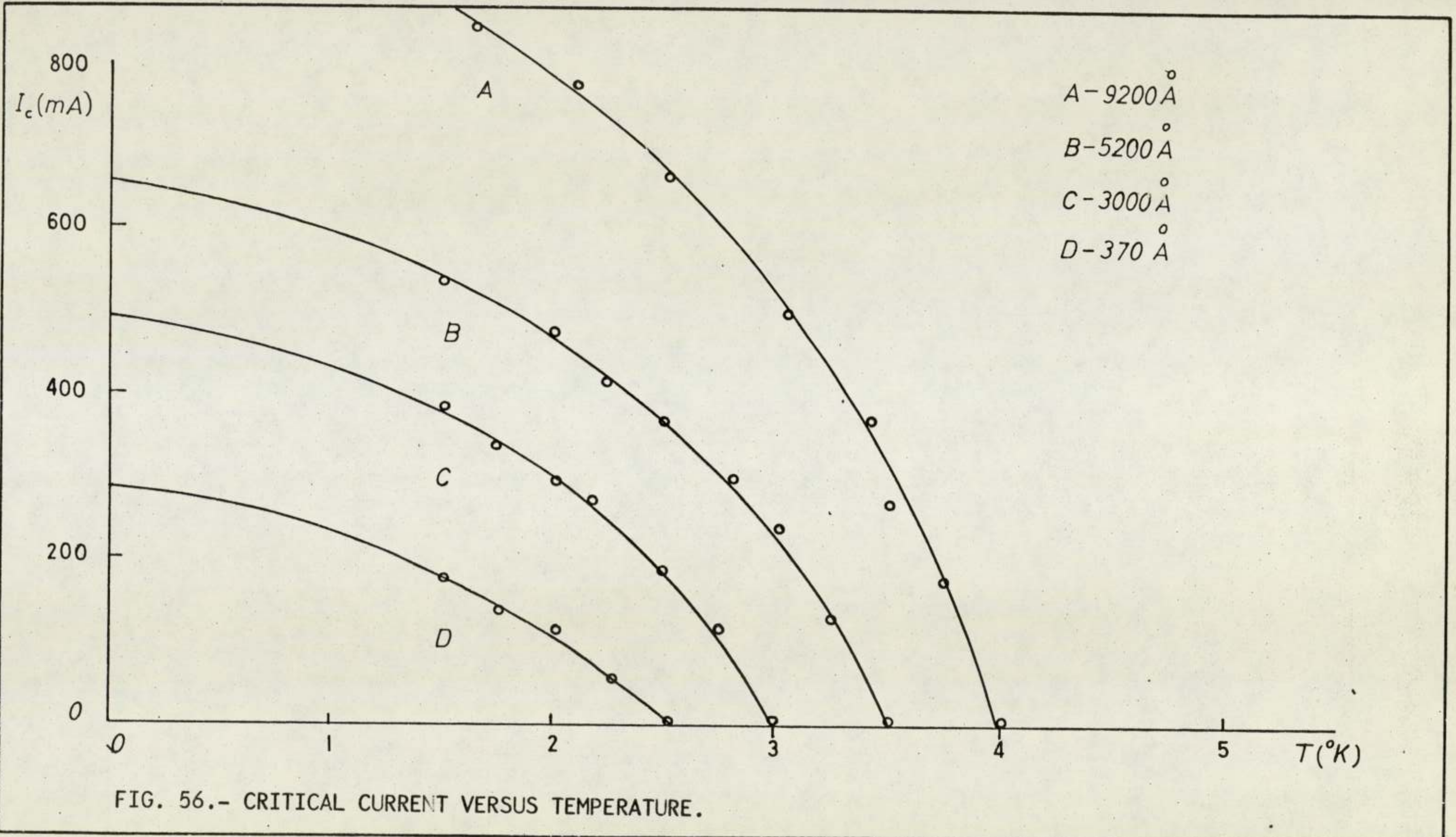

FIG. 56.- CRITICAL CURRENT VERSUS TEMPERATURE.

TABLE 10

TYPICAL SET OF CRITICAL CURRENT MEASUREMENTS

Film Thickness (4.200 Å)

Critical Current mA	An-Fe/Chromel mV	Temperature °K
20	-1.035	3.5
130	-1.037	3.3
180	-1.039	3.15
240	-1.041	3.00
300	-1.043	2.8
340	-1.046	2.55
390	-1.048	2.37
411	-1.051	2.18
473	-1.053	2.00
498	-1.055	1.83
510	-1.057	1.7
540	-1.060	1.5

more accurate to determine the thickness from the deposition rate and the deposition time.

An electrical method for the determination of film thickness was described in section 4.4.2 and was given by the equation

$$\frac{dR}{dT} = \frac{d\rho_\infty}{dT} x \frac{\text{film thickness}}{\text{width x thickness}}$$

Thus the thickness can be expressed as

$$t = \frac{d\rho_\infty}{dT} \cdot \left(\frac{dR}{dT}\right)^{-1} \frac{L}{w} \qquad (5.1)$$

The values for the variation of the resistivity of bulk material with respect to temperature $d\rho/dT$ were taken from Kaye and Laby.[46]

The length and width of the film were determined as .875cm and 0.2cm respectively from measurements of the evaporation mask using a travelling microscope.

The term $(dR/dT)^{-1}$ was calculated from the graphs of resistance versus temperature, if this term is used to evaluate film thickness as described in section 4.4.1, it leads to erroneous results since $d\rho/dT$ must comprise components other than due to lattice vibrations. From Figure (44) it is obvious that the technique is not suitable for thicknesses below 400Å.

It must be remembered that the interferometry method of determining film thickness measures total film thickness and makes no distinction between the conducting tantalum and non-conducting oxide layer. Using a quartz crystal oscillator, the mass per unit area of Ta deposited was calculated. This value in conjunction with the interferometric film thickness gives the density of the Ta thin film.

The experiment was carried out with samples of an average thickness of 550Å and the density found was 16.45 $gr.cm^{-3}$, which is lower than the bulk value of 16.6 $gr.cm^{-3}$ as would be expected for such thin film.

5.8 Ellipsometric Results

Oxide thickness and optical constants of Ta thin films were calculated from ellipsometric data.

To measure the oxide growth on films it is required by the technique that the substrate, in this case tantalum film, should preferably be opaque to the wavelength of light used so limiting the film thickness available for investigation.

The results presented here are obtained from two films, one of 1500Å and the other 3700Å as determined by interferometry.

Observations on the films were commenced about 10 minutes after removal from the vacuum chamber and continued over a period of thirty days.

The reduction in the value of Δ, due to the growth of the oxide layer, with respect to time, is illustrated in Figure (57a) for an angle of incidence of 64° and in Figure (57b) for an angle of incidence of 59.95°, both graphs show results for two samples of different thickness, at the same wavelength of 5487Å. By extrapolating the graphs of Figures (57a) and (57b), a value of Δ for an oxide free film can be determined and the corresponding value of Ψ estimated from Figure (58).

5.8.1 Optical constants of Tantalum

Prior to the determination of the oxide growth the optical constants of the samples at the three different wavelengths, were calculated using the values of Ψ_{exp} and Δ_{exp} found for the oxide free film.

To calculate the values of n and k the technique of using two different angles of incidence and three different wavelengths described in section 4.6.4, was used.

The calculated values for the optical constants of Ta were:

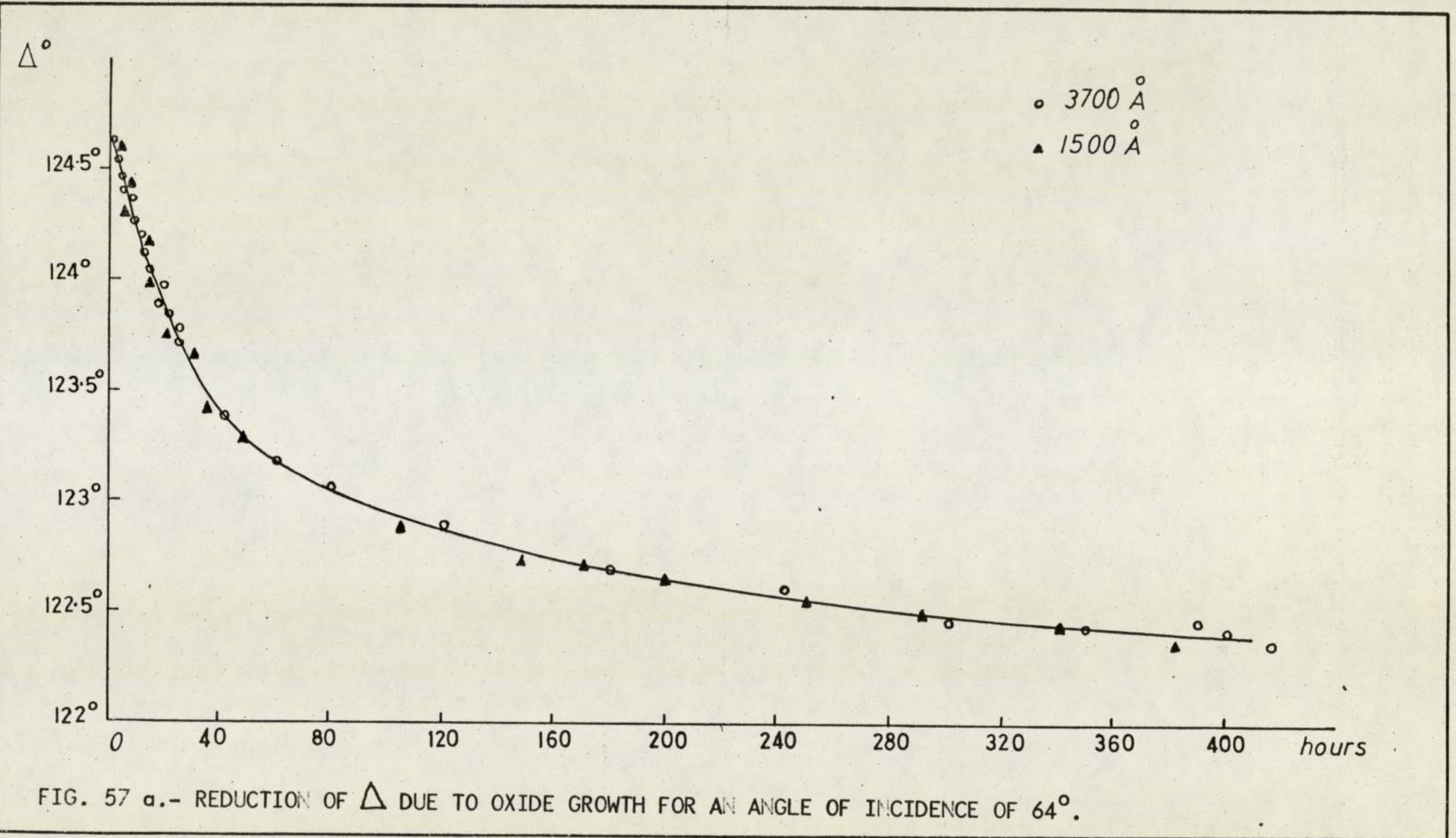

FIG. 57 a.- REDUCTION OF Δ DUE TO OXIDE GROWTH FOR AN ANGLE OF INCIDENCE OF 64°.

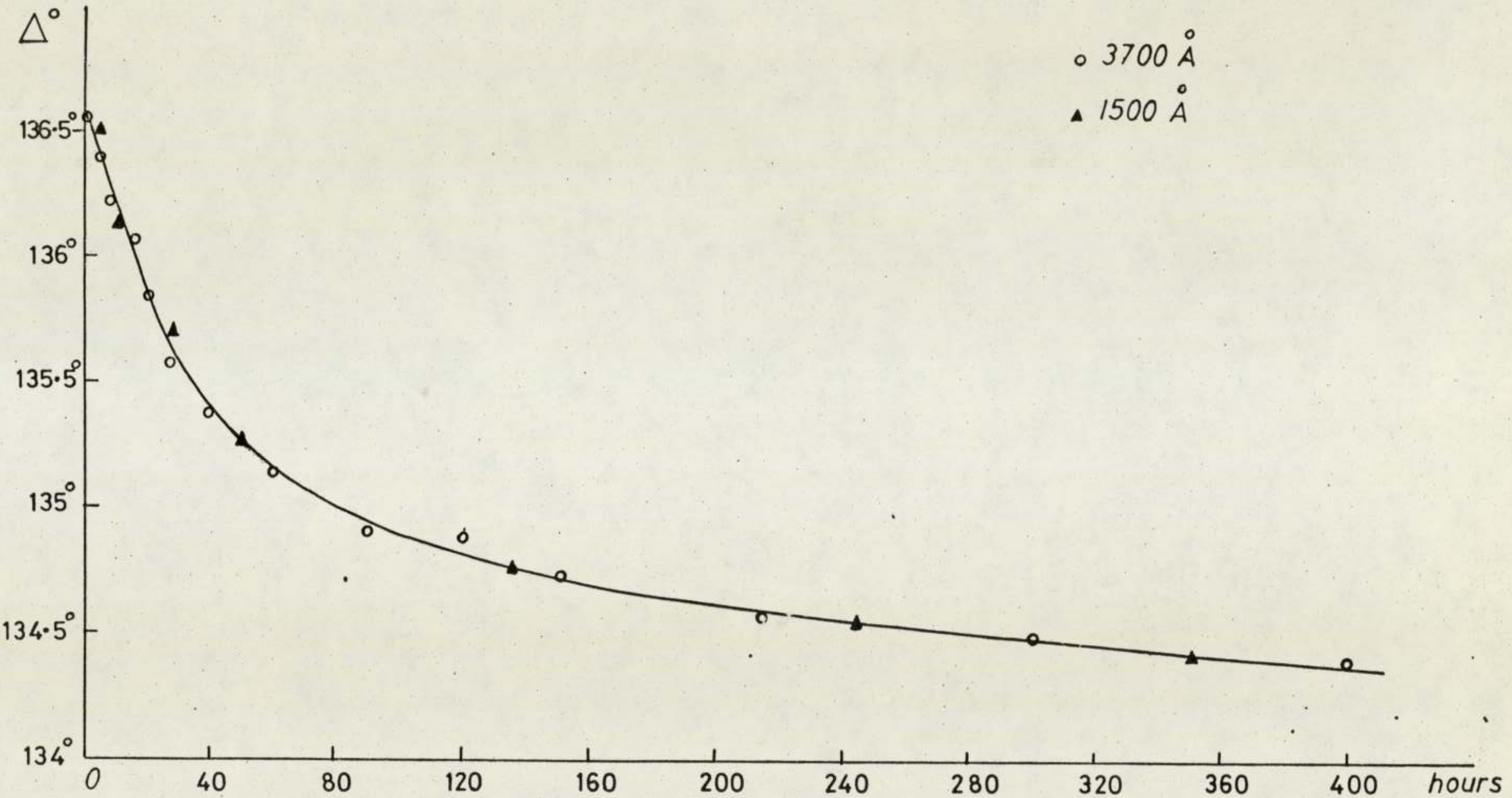

FIG. 57 b.- REDUCTION OF Δ DUE TO OXIDE GROWTH FOR AN ANGLE OF INCIDENCE 59.95°.

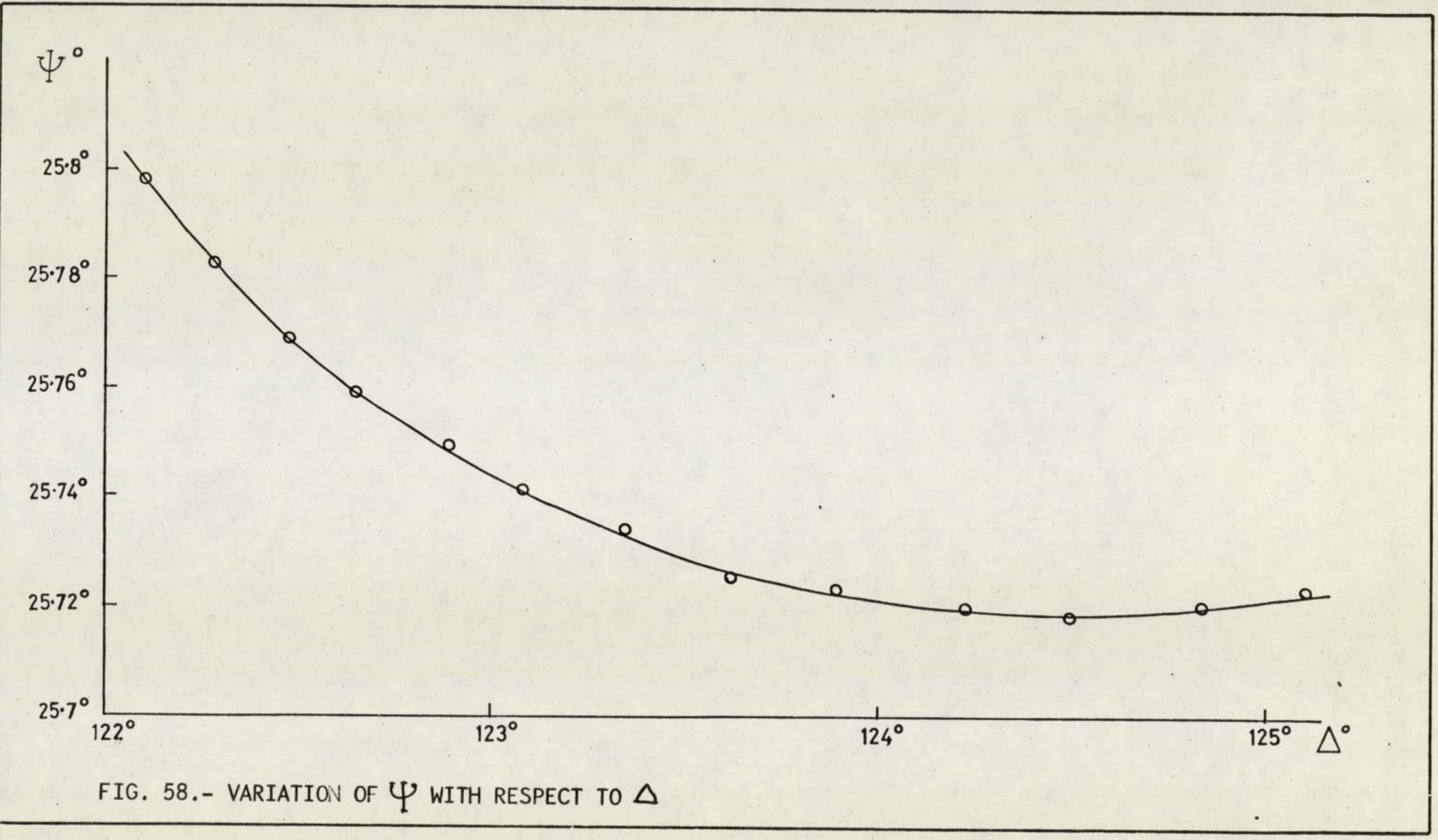

FIG. 58.- VARIATION OF Ψ WITH RESPECT TO Δ

λ = 4960Å n = 2.15 k = 2.07

λ = 5487Å n = 2.28 k = 1.89

λ = 6049Å n = 2.13 k = 1.79

5.8.2 Oxide growth

Using the calculated values for the optical constants of tantalum and the initial guess optical constants for tantalum oxide as determined by Young and Zobel[47] n = 2.22 and k = 0.00 for a wavelength of 5461Å, the optical constants of tantalum oxide and the variation of Δ and Ψ with respect to the oxide thickness were computed.

The exact Drude's equations used are described in section 2.8. The calculated values for the optical constants of tantalum oxide were:

λ = 4960Å n = 2.20 k = 0.00

λ = 5487Å n = 2.18 k = 0.00

λ = 6049Å n = 2.17 k = 0.00

The rate of growth of the oxide layer on the tantalum film would be determined, as shown in Figure (59) by combining the computed values for the variation of Δ and Ψ with respect to oxide thickness with Figure (57). From this it was established that after 420 hours the oxide layer was $\sim$ 10Å thick.

It was now possible to determine the actual tantalum conductive film thickness by subtracting the oxide thickness from the measured film thickness obtained by interferometry.

The ellipsometric measurements were used to check the values of the optical thickness obtained by interferometry, as was explained in section 4.6.4.

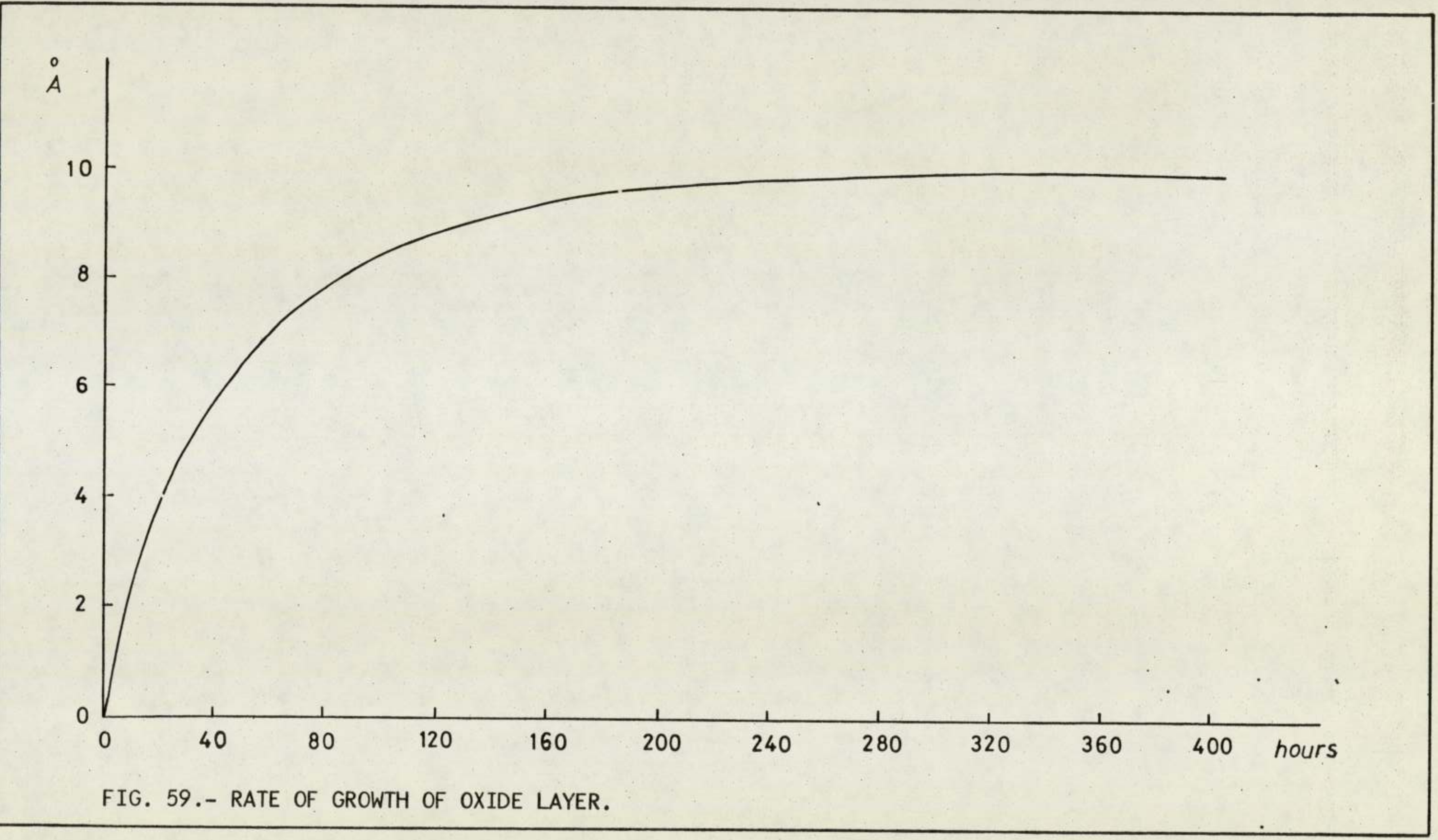

FIG. 59.- RATE OF GROWTH OF OXIDE LAYER.

5.8.3 Variations in the optical constants

By using the ellipsometer it was intended to see whether the different degrees of preferred orientation in the b.c.c. - Ta phase and the presence of f.c.c. - Ta structure would introduce significant changes in the optical constants of tantalum.

The results are shown in Table (11) for four samples. The first film Ta - 71A is pure b.c.c. - Ta, the second sample Ta - 48 shows the highest degree of preferred orientation in b.c.c. structure found in this work, the third film Ta - 55 presents a lower level of preferred orientation and the last sample Ta - 29 is the sample with the highest percentage of f.c.c. - Ta structure, about 50%, out of all the samples prepared in this investigation.

TABLE 11

VARIATION OF OPTICAL CONSTANTS WITH STRUCTURAL PROPERTIES

Ta - 71A	(Thickness 1400Å)	b.c.c. 100%
λ = 4960Å	n = 2.15	k = 2.07
λ = 5487Å	n = 2.28	k = 1.89
λ = 6049Å	n = 2.13	k = 1.79

Ta - 48	(Thickness 3750Å)	b.c.c. 95% f.c.c. 5%
λ = 4960Å	n = 2.32	k = 2.05
λ = 5487Å	n = 2.38	k = 1.90
λ = 6049Å	n = 2.14	k = 1.78

Ta - 55	(Thickness 4320Å)	b.c.c. 95% f.c.c. 5%
λ = 4960Å	n = 2.05	k = 2.08
λ = 5487Å	n = 2.14	k = 1.90
λ = 6049Å	n = 2.08	k = 1.80

Ta - 29	(Thickness 3200Å)	b.c.c. 50% f.c.c. 50%
λ = 4960Å	n = 1.93	k = 2.54
λ = 5487Å	n = 2.05	k = 2.39
λ = 6049Å	n = 1.95	k = 2.26

CHAPTER 6

Interpretation and Discussion of Results

An analysis of the results obtained from the study of tantalum thin films is presented in this chapter.

Comparisons are made between the different structures obtained in this work and the ones reported by other authors. In discussing and comparing results of various authors it is important to be aware of all deposition conditions. Reference to film thickness in itself is not sufficient. In many reports these conditions are omitted. It was felt necessary to proceed in this investigation by considering all deposition parameters.

From the electrical data obtained, an estimate is made of the applicability of the theories of size and grain boundaries effect to the samples prepared in this work, together with an analysis of the impurities and imperfections of the samples.

Experimental transition temperatures from the normal to superconductive states are compared with the theoretical values deduced from Mac-Millan and De Sorbo equations and a study is made of the possible influence of the phonon spectrum in the reduction observed in transition temperatures.

Superconducting critical current densities results are compared with those reported by other authors for films prepared under similar conditions.

6.1 Film Growth

In order to be able to compare films of different thicknesses, it is necessary for all films to be continuous electrically and thereby exhibit ohmic behaviour.

It was necessary to establish that films of the order of 100Å had achieved the final stage of growth since such films might be suspected to be discontinuous.

Depending on the growth stage, a film may be granular or insular, porous or continuous. Each stage has its characteristic electrical

properties.

Granular film conductivity is many orders of magnitude smaller than that of bulk material.

Hartman[48] suggested that transfer of electrons between particles takes place by tunnelling between their overlapped or "crossed" energy levels.

The Hartman model predicts ohmic behaviour and an exponential dependence on the reciprocal of temperature given by

$$\sigma \;\alpha\; \exp -\frac{E}{KT} \qquad (6.1)$$

where E = activation energy.

An exponential dependence of the conductivity of granular films on the inverse temperature has been reported by several workers. Neugebauer and Webb[49] studied films of Pt, Au and Ni but there has been no work done previously on evaporated or sputtered tantalum films.

Temperature coefficients of resistivity of both signs and of variable magnitudes have been reported in discontinuous metal films, while negative TCR have been found for porous films.

A plot of the variation of the conductivity versus the inverse temperature for the thinnest film in this work (110Å) showed that the film neither displayed the slope expected for a granular structure nor the negative TCR expected for a porous film.

This, together with the fact that all the films prepared in the present work had a positive TCR, supports the conclusion that all the films studied in this programme were continuous and had completed the final stage of the sequential growth.

6.2 Film Structure

According to K.L. Chopra[50] thin films of most materials assume crystal structure as the bulk material, however the structural order

invariably departs from that of the bulk.

Anomalous structures have been widely reported. Different mechanisms have been considered by many authors to explain the stability of anomalous phases.

Bublik and Pines[51] attributed the occurrence of anomalous thin film structures to Ni and Cr to the effect of surface forces. Hutchinson and Olsen[52] attributed the formation of an f.c.c. niobium film to oxygen from the substrate with the subsequent growth of the f.c.c. NbO. Miska and Gillet[53] did not offer an explanation for the stability of f.c.c. structure in Nb and Adamsky[54] considered that crystallographic order as well as the epitaxial temperature of films are affected by contamination and by surface condition of the substrate as well as the composition of the residual gas atmosphere.

Other observations have been made of anomalous thin film structures which transforms during growth, these are summarized in Table (12).

6.2.1 Tantalum Phases

1) Summary of other authors' work

Invariably the main structure found by all workers studying Tantalum thin films prepared by evaporation has been b.c.c.-Ta phase. Many of these workers have reported as well the presence of anomalous structures.

Chopra et al[55] contended that although the f.c.c. Ta was not predominant in thin films, nevertheless it was a stable phase, perhaps stabilized by a distribution of electrostatic charges. They reported a substrate temperature for phase change of 473 to 673°K.

Read and Altman[56] found b.c.c. - Ta and β - Ta structures in films prepared by evaporation and that β - Ta changes to b.c.c. - Ta at 1028 - 1048°K when heated in vacuum of <6x10^{-8} torr. Marcus and Quigley[57] reported f.c.c. - Ta prepared by

TABLE 12

ANOMALOUS STRUCTURES IN THIN FILMS WHICH TRANSFORM WITH INCREASING THICKNESS

Film/Substrate	Transformation
Aℓ/Pt	face centred → f.c.c.
V/various	complex cubic → b.c.c. > 50-60Å
Ni/various	f.c.c. → hcp > 50-70Å
V/various	f.c.c. → b.c.c. > 70-100Å
Fe/Cu	f.c.c. → b.c.c. > 80Å
Ta/various; Mo/C	f.c.c. → b.c.c. > 60Å
Nb/MgO	f.c.c. → b.c.c.
Mo, W, Re, Hf, Zn/ glass, mica, NaCl	f.c.c. → bulk > 1.2μ

evaporation with deposition rates varying from 12 to 500Å/min. f.c.c. appears in the very thin films and converts to b.c.c. as the thickness increases. Increasing deposition temperature also produces a change in structure, they reported a substrate temperature for phase conversion of 373 to 1073°K.

Schrey et al [58] have produced films up to 2μ thick using ion-beam sputtering. There was a critical substrate temperature for f.c.c. formation outside which the b.c.c. or an amorphous phase was produced.

The same group of workers also reported different tantalum structures produced by evaporation. They found f.c.c. phase for very thin films which changes to b.c.c. when the thickness increases up to 250Å. There is a change in the structure with temperature taking place at 1023°K. They also reported a mixing of f.c.c. and b.c.c. phases for films whose thickness is greater than 200Å at a substrate temperature of 600°K.

Denbigh and Marcus [59] found b.c.c. and f.c.c. - Ta by evaporation. f.c.c. shows (111), (220) and (311) lines, as the film thickness increases (111) and (200) lines die out to form a b.c.c. (110) line, (220) b.c.c. appears as (220) f.c.c. vanishes. f.c.c. appears in very thin tantalum films, b.c.c. first begins to appear in the 70-80Å range and above 250Å f.c.c. is not observed, the f.c.c. - b.c.c. transition is also temperature dependent. The same workers found a mixture of f.c.c. & b.c.c. - Ta structures for film thickness ranging from 100Å to 1000Å.

Lainer and Khohmyanskii, [60] Miska and Gillet [53] and Gerstenberg and Hall [61] also found f.c.c. structure in Tantalum thin films produced by evaporation, although the former team thought that the f.c.c. phase corresponded to TaO and the

latters did not give any reason to explain the anomalous structure.

Rairden and Neugebauer(29) and R.B.Marcus(62) prepared Ta thin films by evaporation, but only found b.c.c. structure.

Among the researchers who prepared Tantalum samples by sputtering the main structure found were b.c.c. and β - Ta. Belevskiy et al(63) found f.c.c. structure by sputtering but did not give any reason for the appearance of this anomalous phase.

This survey shows that even up to the time when these investigations commenced there were differences of opinion and a variety of results for the structures in tantalum films.

Table (13) gives a summary of the work of the different authors.

2) Present Work

The results of the present investigations, section 5.2, suggest that the pure f.c.c. - Ta phase found in very thin films, between 100 and 200Å thick, correspond to the same structure as reported by Denbigh and Marcus,(59) Schrey et al(58) and Chopra et al.(55)

In this work no other reason except increasing thickness has been found to affect the structure change from pure f.c.c. to pure b.c.c. phase.

No other authors have reported thickness change to be the unique factor in the f.c.c. → b.c.c. change and emphasizes the significance of controlling deposition parameters as has been attempted in this work.

The b.c.c. phase reported in this work corresponds to the bulk tantalum structure as can be seen for the values of the lattice parameters given in Table (4).

The existence of a mixture of f.c.c. and b.c.c. tantalum

phases found in about half the samples prepared in this investigation has never been reported before with the two characteristics of very high proportion of f.c.c. phase (up to 50%) and very thick samples (up to 3600Å) together.

The conditions under which both f.c.c. and b.c.c. - Ta phases coexist in tantalum films prepared by electron beam evaporation have been proved in this work not to depend on:

a) Pressure (certainly normally < 10^{-7} torr), different proportion of gaseous impurities does not affect the presence of f.c.c. phase.

   By accident on one occasion the vacuum chamber contained more oxygen than usual and the result we obtained is shown in Figure (60), it was what we consider $TaO_{0.9}$ for its similarity with the oxide of vanadium $Va\,O_{0.9}$

b) Deposition temperature, though it may affect the percentage of f.c.c. - phase present, opposite to Schrey et al[58] who needed a substrate temperature of 600°K to obtain a mixture of f.c.c. and b.c.c. structures.

c) Substrate treatment, neither chemical cleaning nor preheating, all substrates were treated in the same way.

d) Deposition rate, pure b.c.c. structures have been found in films prepared with deposition rates ranging from 40 to 400A°/min. Changes in deposition rate do not produce a mixture of f.c.c. and b.c.c. phases.

e) Thickness, the coexistence of b.c.c. and f.c.c. structures has been found in the whole range of thicknesses. Denbigh and Marcus[59] found a mixture of phases in samples 100 to 1000Å thick.

6.2.2 Orientation

Chopra et al[55] and Schrey et al[58] respectively show that

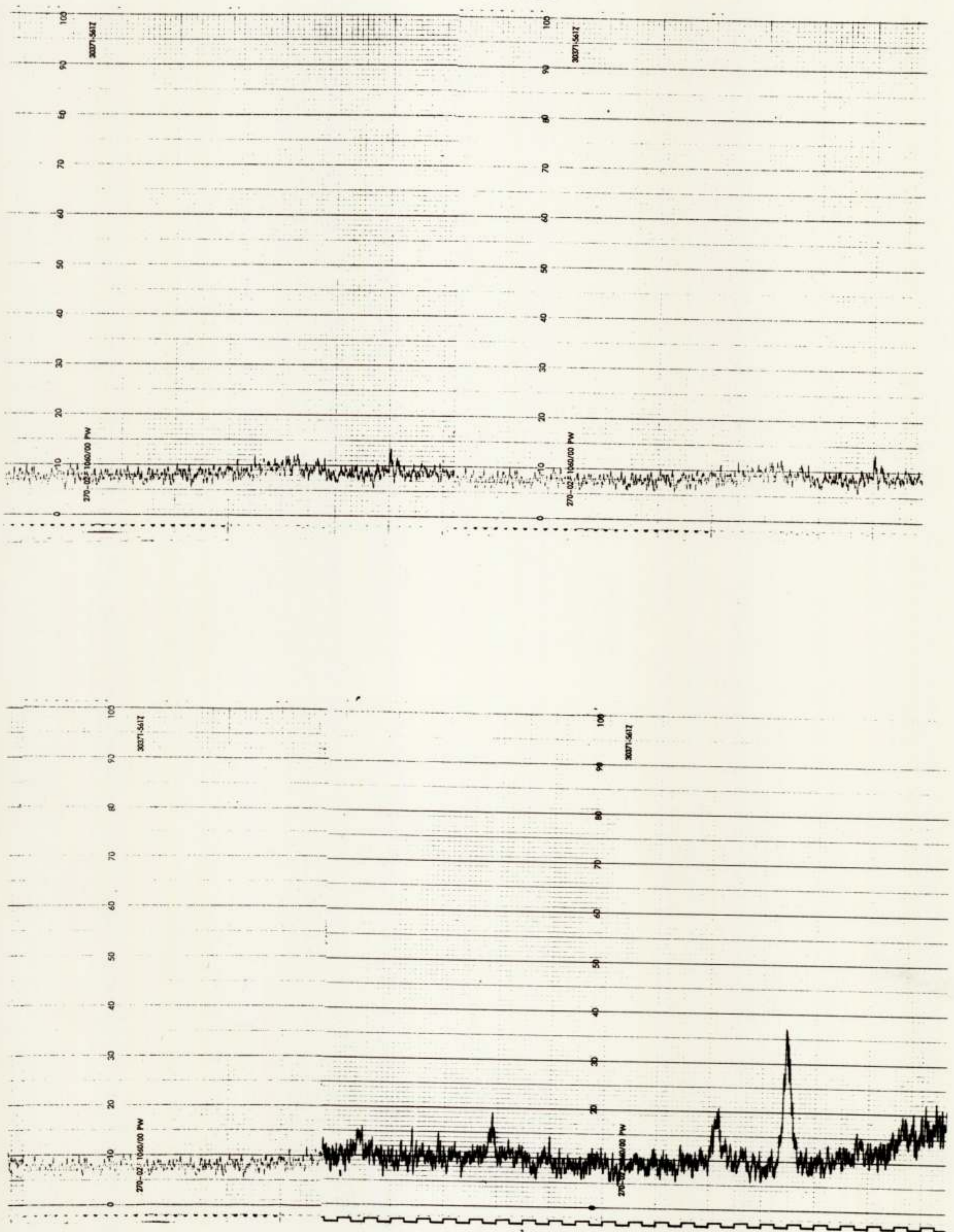

FIGURE 60 DIFFRACTION PATTERN OF Ta $O_{0.9}$

b.c.c. tantalum crystals are randomly orientated; at 673°K however, Chopra's films show epitaxial growth onto NaCℓ with the orientation Ta (100) //NaCℓ (100) whilst Denbigh and Marcus[65] reported Ta (001) //MgO (100) at similar temperatures.

R.B.Marcus[62] found as well epitaxial growth of b.c.c. samples prepared onto MgO substrates.

Westwood and Livermore[64] quoted a certain preferred orientation of b.c.c. - Ta prepared by sputtering. Read and Hensler[65] stated different degrees of orientation for their samples prepared by sputtering but give neither the conditions under which the samples have been prepared nor the reason for the different degrees of orientation.

Westwood[66] reported a strong preferred orientation in b.c.c. - Ta prepared by sputtering which increases with decreasing oxygen concentration.

The range of substrate temperature employed in the present work was intended to produce films of random orientation and of varying crystallite size. As can be seen in section 5.2.1. no films were completely random, all showed a certain degree of preferred orientation.

As far as the author is aware, there have been no reports in the literature about either preferred orientation in b.c.c.-Ta prepared by evaporation on glass substrate or that the degree of preferred orientation is a function of deposition temperature, as has been found in this investigation. The orientation results found by the different workers are included in Table (13).

6.2.3 Lattice Parameters

Rairden and Neugebauer[29] prepared Ta thin films by evaporation and found b.c.c. - Ta only in which the "d" spacing

changes with thickness and with deposition temperature: increasing with decreasing thickness and deposition temperature.

R. B. Marcus[62] described evaporated tantalum films with "a_o" parameter changing from 3.40 to 3.31Å as the thickness increases from 250 to 1200Å. The same is found by Denbigh and Marcus[59] and Marcus and Quigley.[57]

Read and Hensler[65] have measured an increase in "a_o" from 3.305 to 3.43Å for b.c.c. films with up to 20% oxygen content prepared by sputtering.

The changes in "d" spacing for both b.c.c. and f.c.c. tantalum structure with thickness and deposition temperature found in this work are in agreement with the above authors and is likely to be due, as pointed out by P. N. Baker[67] to the inclusion of some impurities in the films during the deposition process.

However, in the case of thick films the value of a_o (3.306 Å) is identical to the bulk material, Table (3) and is indicative of film perfection.

The lattice parameter "a_o" for the f.c.c. - Ta structure found by Denbigh and Marcus,[59] Chopra et al,[55] Miska and Gillet[53] and Lainer and Kholmyanskii[60] all agree within 1% (4.42Å, 4.39Å, 4.49Å, 4.47Å respectively). The value found in this work 4.49Å is in the same range.

The values of the lattice parameter for b.c.c. and f.c.c. tantalum phases as found by the different workers are shown in Table (13).

6.2.4 Nature of f.c.c. Structure

One question that arises when considering tantalum structure is whether the f.c.c. phase found is a pure metallic phase or not.

TABLE 13

COMPARISON OF STRUCTURAL PROPERTIES OF PRESENT THIN FILMS WITH OTHER WORKERS

Author	Method	Phase	Phase Stabilization	Orientation	Lattice parameter	Value of a_o parameter
Rairden & Neugebauer	E	bcc			increases with T_O and decreasing thickness	bcc - a_o = 3.31Å
Gerstenberg & Hall	S & E	fcc, bcc				
R.B.Marcus	E	bcc		epitaxial on gO	increases with decreasing thickness	bcc - a_o = 3.31Å
Denbigh & Marcus	E	fcc,bcc,fcc + bcc	fcc→bcc @ 973°K T_D	random & epitaxial on MgO	increases with decreasing (t) thickness	bcc - a_o = 3.40Å fcc - a_o = 4.41Å
Marcus & Quigley	E	fcc, bcc	fcc→bcc thickness & substrate impurities		increases with decreasing (t) thickness	bcc - a_o = 3.5Å fcc - a_o = 4.42Å
Lainer & Kholmyanskii	E	fcc, bcc	fcc attribute to TaO			fcc - a_o = 4.47Å
Miska & Guillet	E	bcc, fcc	fcc no reasons			
Schrey et al	S & E	fcc,bcc,fcc + bcc	fcc→bcc @ 573-673°K T_D and thickness	random		bcc - a_o = 3.33Å fcc - a_o = 4.48Å
Chopra et al	S & E	fcc,bcc,fcc + bcc	fcc→bcc with T_D	random & epitaxial on CℓNa		bcc - a_o = 3.30Å fcc - a_o = 4.39Å
Belevskiy et al	S	fcc, bcc				bcc - a_o = 3.42Å fcc - a_o = 4.48Å
M.H.Read	S	bcc, βTa		preferred orientation		bcc - a_o = 3.327Å
Fenistein & Gerstenberg	S	bcc, βTa		preferred orientation		
G. Das	S	bcc, βTa				bcc - a_o = 3.33Å
Read & Altam	E	bcc, fcc	βTa→bcc at 1028-1048°K			
Westwood & Livermore	S	bcc, βTa		preferred orientation		
Read & Hensler	S	bcc, βTa		preferred orientation	increases with proportion of O_2	
Westwood	S & E	bcc, βTa		preferred orientation		
Present Work	E	bcc,fcc,bcc+fcc	fcc→bcc thickness	preferred orientation	increases with T_D and decreasing thickness	bcc - a_o = 3.306Å fcc - a_o = 4.496Å

E = Evaporation
S = Sputtering
T_D = Deposition Temperature
t = thickness

The f.c.c. structure which appears in Ta is quite similar to TaC, TaO and TaN. Lainer and Khohnyanskii [60] reported Ta films which in the very thin samples show f.c.c. structure which he attributed to TaO and TaC, the deposition rate they worked with was 18Å/m, so the number of oxygen atoms falling on the substrate surface per unit time is greater than the number of metal atoms, and in their case one might accept that TaO would be present.

Marcus and Quigley [57] considered f.c.c. structure to be an impurity stabilized phase, as an order of magnitude estimate they considered an oxygen level of about 4 at % to be the impurity needed for stabilization of f.c.c. tantalum; they summarized the range of stoichiometry for bulk compounds of tantalum with nitrogen, oxygen, hydrogen and carbon.

In the work of Denbigh and Marcus [59] the f.c.c. modification appeared only as an intermediate layer, about 70Å thick, between the substrate and the normal b.c.c. phase and hence it was concluded to be a phase stabilized by oxygen diffusing from the substrate.

Schrey et al [58] showed the possibility of f.c.c. - Ta being TaN which would be structurally consistent, but the presence of 10% N needed to form TaN would be obvious in the diffraction intensities, the same they agreed applies to TaO and TaO_2.

Because of the observations of other workers and because higher proportions of f.c.c. phase have been reported in films prepared in this work, it was necessary to ascertain whether the f.c.c. phase was established.

It was certain that the f.c.c. - Ta phase found in this work is not one of the tantalum compounds mentioned above because of the high evaporation rate and low base pressure.

A comparison between the parameter $R_D = n_{Ta}/n_{res}$ reported in section 5.1 and the stoichiometric data given by Marcus and Quigley [57] shows that compounds requiring more than 30 at % impurities and which corresponds to the questionable compounds TaO, TaN and TaC are impossible on the grounds that more than 30% of O_2, N_2 or C_2 are required. Also TaC and b.c.c. - Ta have never been found to coexist in the same film. Therefore the f.c.c. structure co-existing with b.c.c. in these investigations must be a stable metallic phase of Tantalum.

In addition, Miller [68] has reported that the solubility for oxygen in bulk tantalum at 1173°K is 2.2% and it would certainly be lower at the deposition temperatures used in this investigation. This again emphasises the previous argument. The observation of a thickness dependent f.c.c. - b.c.c. transition in metals normally possessing a b.c.c. structure as is shown in Table (13) and suggest that such a condition may be a general phenomenon, not restricted to the presence of impurity atoms for stabilising the structure. Therefore, it is concluded that the f.c.c. - Ta phase found in this work is a stable metallic phase.

6.2.5 Summary

The behaviour of Ta as reported in the present investigation may be summarised as follows:

1) The films are initially deposited on the substrates as very small crystallites which can be as small as 30Å Table (9)

2) The structure of these crystallites is definitely f.c.c. Ta and not TaO, TaN or TaC.

3) As the film thickness increases, some of the crystallites increase in size, probably because of coalescence and transform to b.c.c, at this stage there is a mixture of f.c.c. and b.c.c.

crystals.

4) In general, as the film thickness increases further, the proportion of f.c.c. material decreases until, at a mean thickness of a few hundred Å the film is entirely b.c.c.

5) Under certain conditions, however, the complete transfer from f.c.c. into b.c.c. structure does not take place, but other different phenomenon occur.

From the present observations it would appear that there are three possible modes of growth when the two phases co-exist:

1) The growth of f.c.c. structure continues up to several hundred angstrom (in the present work up to 1600Å for a film 3200Å thick with 50% f.c.c. phase) changing further to b.c.c. structure.

2) After few hundred angstrom the b.c.c. phase starts to appear and both structures exist together through the whole sample forming a network of f.c.c. and b.c.c. grains.

3) After a few hundred Angstrom the b.c.c. phase starts to appear and both structures exist together but the concentration of f.c.c. phase decreases from the substrate to the surface.

Electrical observations of this work given in section 5.3 supports the second view. The f.c.c. phase behaves like an impurity in a pure b.c.c. - Ta phase, a mixture of f.c.c. and b.c.c. co-exists together and would from the point of view of conduction, behave like a system of conductors in series. Resistivity increases as the proportion of f.c.c. phase increases.

The fact that the same X-ray diffraction patterns have been obtained with the use of different X-ray radiations, Fe, Cu and Mo which have increasing penetration powers, sustains

the second mode of growth and rules out the third possibility.

Finally, the ellipsometric results for the optical constants of samples with varying proportions of f.c.c. section 5.8.3. give different values for the parameters n and k. This, together with the fact that the ellipsometric technique gives information of a portion of film of about 1500Å only is another proof of the validity of the second possibility about the constitution of samples with a mixture of f.c.c. and b.c.c. structures existing throughout the film.

The conditions which favour the presence of both structures at the same time cannot be clearly defined from this work but there is a possibility of an electrostatic effect taking place in the substrates which encourages the presence of f.c.c. structure and the co-existence of both phases.

It is possible that the substrate could collect charges because of the ion pump or the electron-gun, but this has not been positively established.

6.3 Electrical Conduction

The electrical conductivity of a metal is proportional to the mean free path (mfp) ℓ, which is defined by the relaxation time of electron-phonon interaction $\tau = \ell/V_F$ where V_F is the Fermi velocity.

According to equation 2

$$\ell = \left(\frac{3}{8\pi}\right)^{1/3} \frac{h}{\rho e^2 n^{2/3}} \tag{6.2}$$

where ρ = resistivity

n = number of conduction electrons per unit volume

which is related to the Fermi energy through the equation

$$n = \frac{8\pi}{3}\left(\frac{2mE_F}{h^2}\right)^{3/2} \tag{6.3}$$

Until recently there has been no calculations of E_F for tantalum other than from free electron theory.

In 1970 Mattheiss[69] arrived at a value of E_F = 0.697 Ryd from band structure calculation. This value was considered to be the most reliable to date and has been used in the present work to calculate $n = 1.33 \times 10^{23} cm^{-3}$.

This in turn gives a mfp of electrons in bulk tantalum at 300°K as

$$\ell = 37.3Å$$

corresponding to a resistivity at 300°K of $\rho = 13.1 \times 10^{-6}$ ohm.cm. as given by Kittel.[70]

In the present work the lowest resistivity value agrees with the bulk value. Therefore a mean free path of $\ell = 37.3Å$ is considered to be the highest value at room temperature applicable to the samples analysed in this investigation.

The residual mfp corresponding to the residual resistivity $\rho_r = 2.067 \times 10^{-6}$ ohm.cm, which is the lowest value found in this is $\ell_r = 236.5Å$ (i.e. at 10°K).

6.3.1 Matthiessen's Rule (Comparison of present results)

As mentioned earlier when discussing properties of thin films it is important to compare like with like. One measure of quality of a film can be obtained from resistivity measurements and this is one method by which comparisons can be made.

According to Matthiessen's rule, various frequency of scattering processes, and hence resistivity contributions, are additive provided that the lattice scattering remains predominant and the mean free path due to the scattering mechanisms are completely independent.

We can therefore write Matthiessen's rule as

$$\rho_F = \rho_L + \rho_r$$

or

$$\rho_F - \rho_r = \text{constant}$$

where

ρ_F = film resistivity

ρ_r = residual resistivity

Figure (41) shows that Matthiessen's rule holds for the present films whose thicknesses are greater than about 400Å.

Results reported by Gerstenberg and Hall,[61] Rairden and Neugebauer[29] and R.B.Marcus[62] for evaporated samples are in agreement with our results. Ta thin films prepared by evaporation satisfied Matthiessen's rule for thickness down to few hundred Å, in Marcus's samples, 450Å.

It can be seen in section 5.3 that the resistivity of the films prepared in this work changes with thickness, deposition temperature and deposition rate, increasing when these parameters decrease.

The fact that Matthiessen's rule is followed by most of the samples means that the high room temperature resistivity is entirely due to the increase in residual resistivity alone.

Any deviations from bulk values of the measured resistivity and consequently of the other electrical parameters could result from one of the following causes a) gaseous impurities b) structural defects c) lattice distortions d) limitation of mfp by film thickness e) limitation of mfp by grain boundaries and/or f) internal and external stresses which are temperature dependent.

6.3.2 Impurities and Imperfections

Gaseous impurities are incorporated in a film during preparation when gas molecules are adsorbed on the surface of the film during growth and are consequently buried by metal atoms arriving later. Thus the concentration of impurities incorporated depends on the partial pressure of the gas and evaporation rate.

In circumstances where tantalum is evaporated in other parts of the chamber, the gettering action reduces the pressure and the gaseous concentration decreases as the film thickness increases.

Gebhardt and Rothenbacher [71] showed that the room temperature resistivity of niobium films increases linearly with oxygen concentration. De Sorbo [28] found the same for the residual resistivity of Nb, the relationship being equivalent in both cases.

Due to the similarities between Ta and Nb, Matthiessen's rule is obeyed by both metals, $\rho_{300} - \rho_{10}$ = constant and we could assume, therefore, that the resistance ratio $(R_{300}-R_{10})/R_{10}$ also varies linearly with oxygen concentration and consequently with film thickness and deposition temperature.

Table (14) shows how the resistivity ratio $R_{10}/(R_{300}-R_{10})$ for the present films changes with thickness and substrate temperature, indicating that if the ratio increases with increasing O_2 concentration, the oxygen concentration for these films becomes lower as the thickness and deposition temperature increases, the latter reduces the sticking coefficient.

Gebhardt et al [72] have shown that the dependence of ρ_i on interstitial nitrogen concentration to be $d/\rho_i/d(\text{at \% N}) =$ $5.1\mu\Omega.\text{cm/at \%}$ for tantalum.

Using this information, nitrogen concentrations have been calculated for samples of different thicknesses and prepared at different deposition temperatures and are shown in Table (15). As in the case of oxygen, if there is nitrogen present the nitrogen concentration decreases with increasing thickness and substrate temperature.

The calculated values of N_2 concentration required to give the measured resistivities are much higher than concentrations

TABLE 14

CHANGE OF RESISTIVITY RATIO WITH THICKNESS AND DEPOSITION TEMPERATURE

Sample No.	Thickness	$R_{10}/R300-R_{10}$	Deposition Temp.
Ta-65	140Å	6.667	493°K
Ta-67	150Å	2.678	683°K
Ta-57	320Å	1.226	533°K
Ta-76	1325Å	.580	523°K
Ta-75	1600Å	.396	748°K
Ta-55	4325Å	.466	498°K
Ta-48	3750Å	.189	773°K

TABLE 15

NITROGEN CONCENTRATION AS A FUNCTION OF RESIDUAL RESISTIVITY

Sample No.	Thickness	Impurity Concentration	Deposition Temp.
Ta-63	315Å	7.4 at %	533°K
Ta-37	650Å	4.2 at %	523°K
Ta-73	1350Å	2.4 at %	473°K
Ta-75	1600Å	1.3 at %	748°K
Ta-53	4425Å	1.6 at %	418°K
Ta-52	3850Å	0.6 at %	698°K

appertaining to the partial pressures of nitrogen during evaporation of the present film, as can be seen from high R_D values in Table (1) as compared with lower values of other workers.

Although impurities have a profound effect on the resistivity, we must not ignore the fact that structural defects are frozen in during deposition of films; dislocations, stacking faults, interstitials and vacancies which is by far the most important one from the point of view of conductivity.

Contributions to resistivity from the latter effect can vary from 1 to 6μΩ.cm/ at %.

Neither gaseous impurities nor limitations of the mfp are temperature dependent and do not contribute to $d\rho/dT$ according to Matthiessen's rule. But the fact that $d\rho/dT$ increases for very thin films with high resistivity (i.e. less than 400Å), Figure (44), and decreases with increasing deposition temperature, Figure (46) indicates that variations of $d\rho/dT$ from bulk values, may be due to structural defects, lattice disorders and internal and external stresses which increase with decreasing thickness. Gerstenberg and Hall[61] reported the same effect in $d\rho/dT$ with Nb films. They suggested that this may be attributed to the purely geometrical effects due to cavities formed during deposition. This was also substantiated to some extent in the present work by the fact that measured film densities were less than bulk values, section 5.7.

The resistivity ratio ρ_{300}/ρ_{10} equivalent to $(R_{300}-R_{10})/R_{10}$ is included as a means of characterizing the perfection and purity of the sample, so it can be understood from Figures (45) and (46) that the quality of the samples improves with thickness and with deposition temperature.

This is in contradiction with Schrey et al[64] who prepared Ta thin films by R.f. sputtering and found that the resistivity

ratio only slightly improved with the thickness and became worse as the substrate temperature increased.

Rairden and Neugebauer[29] found that increasing the substrate temperature resulted in a striking increase in the resistance ratio in agreement with present results.

Taking into account the above considerations, Mattheissen's rule for thin films can be rewritten as

$$\rho_F = \rho_B + \rho_I + \rho_{SD} + \rho_{LD} \quad (6.4)$$

where

ρ_B = bulk resistivity

ρ_I = resistivity due to impurities

ρ_{SD} = resistivity due to structural defects

ρ_{LD} = resistivity due to lattice distortions

A comparison of the electrical properties of the films prepared in this work with the films prepared by other workers is shown in Table (16) which shows that the quality of films in the present work is much better than any previously reported by other authors. In particular, for thick films, bulk resistivity has been achieved as compared with the lowest value of 15.6μΩ.cm of Gerstenberg and Hall[61] and R. B. Marcus.[62]

6.3.3. Size Effects

As the thickness of the metal film is reduced to a value comparable to the mean free path, the film boundaries impose a limitation on the movement of the electrons and size effects take place. This could account partly for the deviation from bulk values of the measured electrical parameters.

The assumption made in the Fuch-Sondheimer[9,10] theory was that the scattering at the boundaries of some electrons will be entirely diffuse and a fraction p of the electrons will suffer

TABLE 16

COMPARISON OF ELECTRICAL PROPERTIES OF PRESENT THIN FILMS WITH OTHER AUTHORS

Authors	Deposition	ρ_{100}	ρ_i	$\rho_{300}-\rho_i$	ρ_{300}/ρ_i
Somak & Polito	S	28.2→186			
Gerstberg & Hall	(E) (S)	15.7→26.2 52.4	3.25→4.24	17	5.615
B. Marcus	E	15.6→178	2.4 →84.6	17.3→93	2.11→6.5
Westwood & Livermore	S	30			
Baker	S	150			
Present work	E	13.6-157	2.07-124	11.5-33	1.4 →6.6

S = Prepared by Sputtering

E = Prepared by Evaporation

specular scattering. The value of p is the same for the two surfaces and another term should be added to equation (6.4) for the Matthiessen's rule to take into consideration the size effects.

The Fuch-Sondheimer relation equation (2.6) takes account of this effect. Figure (61) is a plot of equation (2.6) for values of $p = 0$ and $p = 0.5$.

The mean free path for Ta has been calculated at the beginning of this section, at room temperature $\ell = 37.3\text{Å}$ and at $10^{\circ}K$ $\ell = 236.5\text{Å}$.

Therefore at room temperature all the samples prepared in this work satisfy $\gamma \gg 1$ and only the very thin films satisfy $\gamma < 1$ at $10^{\circ}K$, where $\gamma = t/\ell$.

Figure (61) shows, plots of F-S theoretical equation, and values of ρ_F/ρ_B versus t/ℓ for the very thin films of this work. ρ_F is the film resistivity, ρ_B is the resistivity of an infinitely thick sample, t is the film thickness and ℓ is the mean free path of electrons.

The disagreement between the F-S theory and the observed resistivity change shows that the influence of film thickness on electron mean free path is insufficient to explain the high values for the resistivity observed in this investigation.

If the temperature variation of the mean free path is the same as that for conductivity, the general expression for the Temperature coefficient of Resistivity (TCR) can be derived from the equation of F-S. Figure (62) shows the calculated values for $(TCR)_F$ / $(TCR)_B$ versus $\gamma = t/\ell$ derived from F-S Theory, where $(TCR)_F$ refers to the film and $(TCR)_B$ refers to bulk material. Curve C represents the experimental points corresponding to the range of thickness for films prepared in this

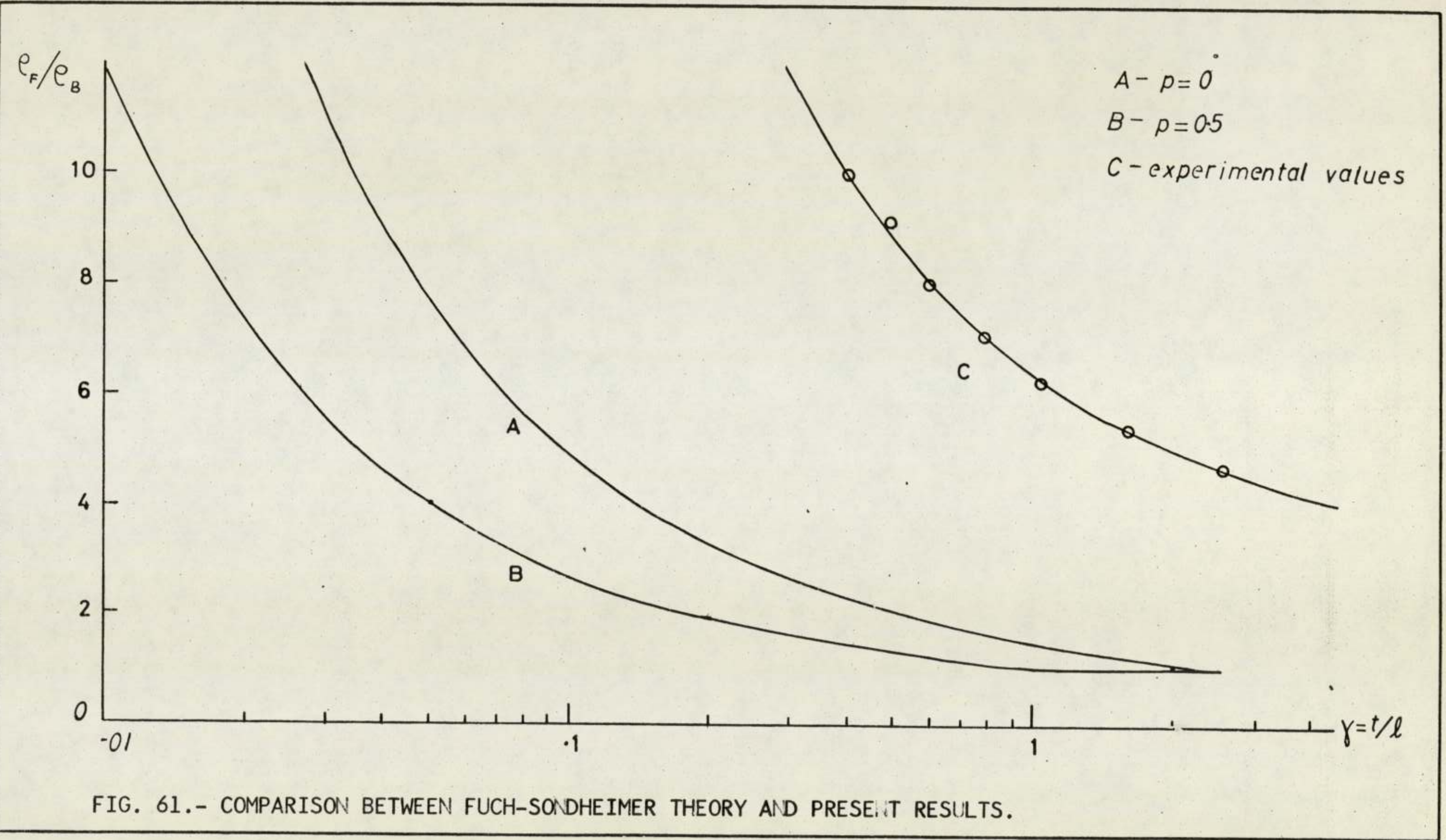

FIG. 61.- COMPARISON BETWEEN FUCH-SONDHEIMER THEORY AND PRESENT RESULTS.

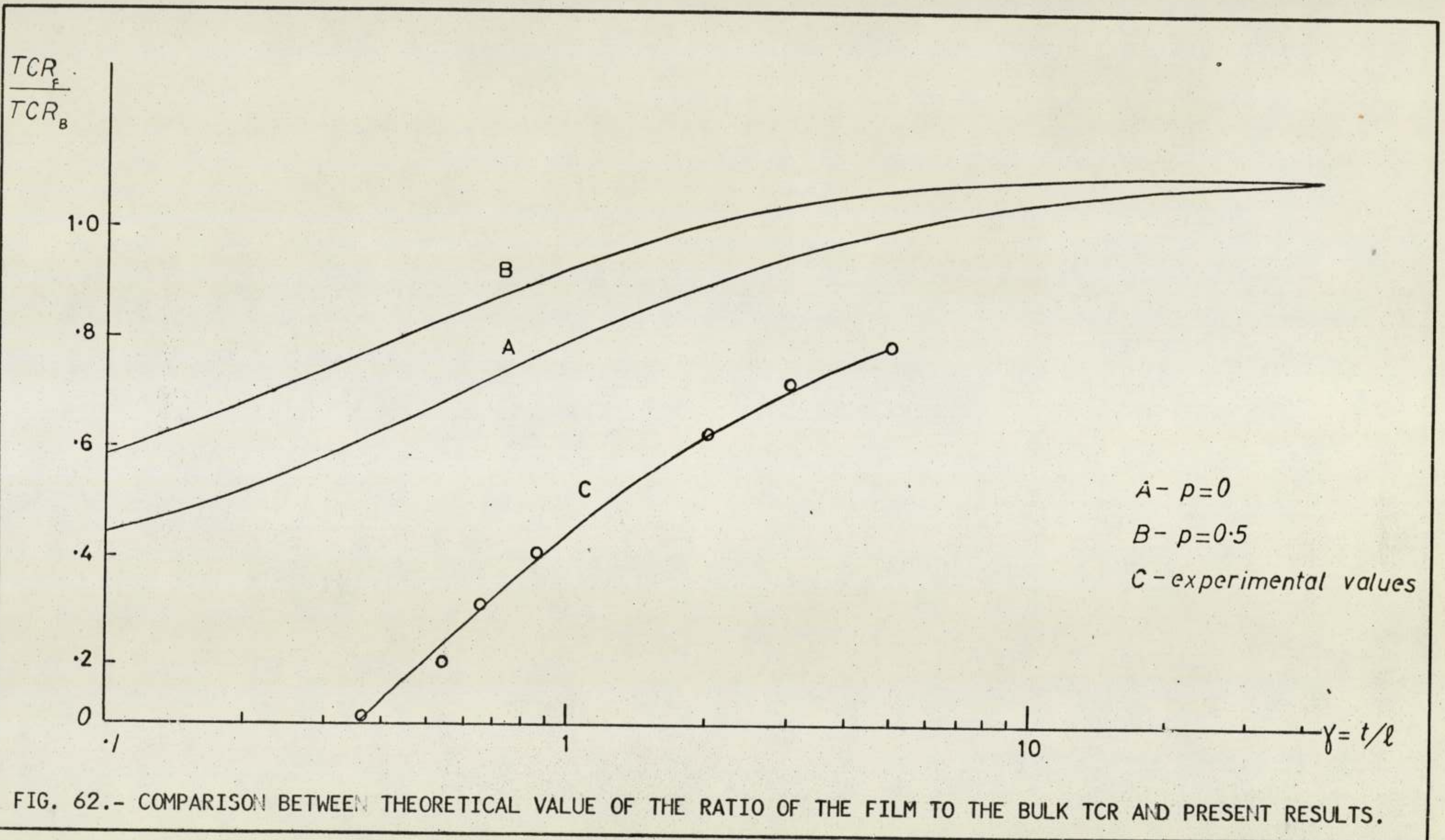

FIG. 62.- COMPARISON BETWEEN THEORETICAL VALUE OF THE RATIO OF THE FILM TO THE BULK TCR AND PRESENT RESULTS.

work and to which the theory can be applied.

Again the disagreement between the theory and experiment shows that the contribution of geometrical scattering to the decrease in α is minimal.

Size effects for Ta have been studied by other workers among them R.B. Marcus[69] who found that no substantial contribution to the electrical parameter would be ascribed to the size effects. We disagree with him in the assumption he made of $\ell = 200Å$ for tantalum at room temperature.

Desserre and Goulet[73] tried to apply size effects to the Ta thin films they prepared, but from our point of view they applied the wrong equation of the F-S theory. They assumed and applied equation (2.8) which leads them erroneously to a calculated value for the mean free path at $273^{o}K$ of 970Å (a factor of four better than copper) which is most improbable. This value was quoted in 1971 despite the fact that the band structure calculations for Ta were published in 1970.

6.3.4 Grain Boundaries Scattering

According to Mayadas'[12] theory the measured resistivity at any temperature (ρ_F) must depend on thickness not only through the ordinary Fuch size effect, but also because of the dependence on grain size. We would now add another term to Matthiessen's rule accounting for grain boundary scattering.

If in equation (2.9) deduced by Mayadas the parameter α, which includes the crystallite size D, is equal to zero then Mayadas and F-S theory become equivalent and equation (2.6) and (2.9) are identical.

Figure (63) is a representation of equation (2.9) for $p = 0$ and $p = 0.5$ for both curves α was held constant and equal to 1. ρ_F is the resistivity of the film, ρ_B is the resistivity of an infinitely thick polycrystalline film, t is the thickness of

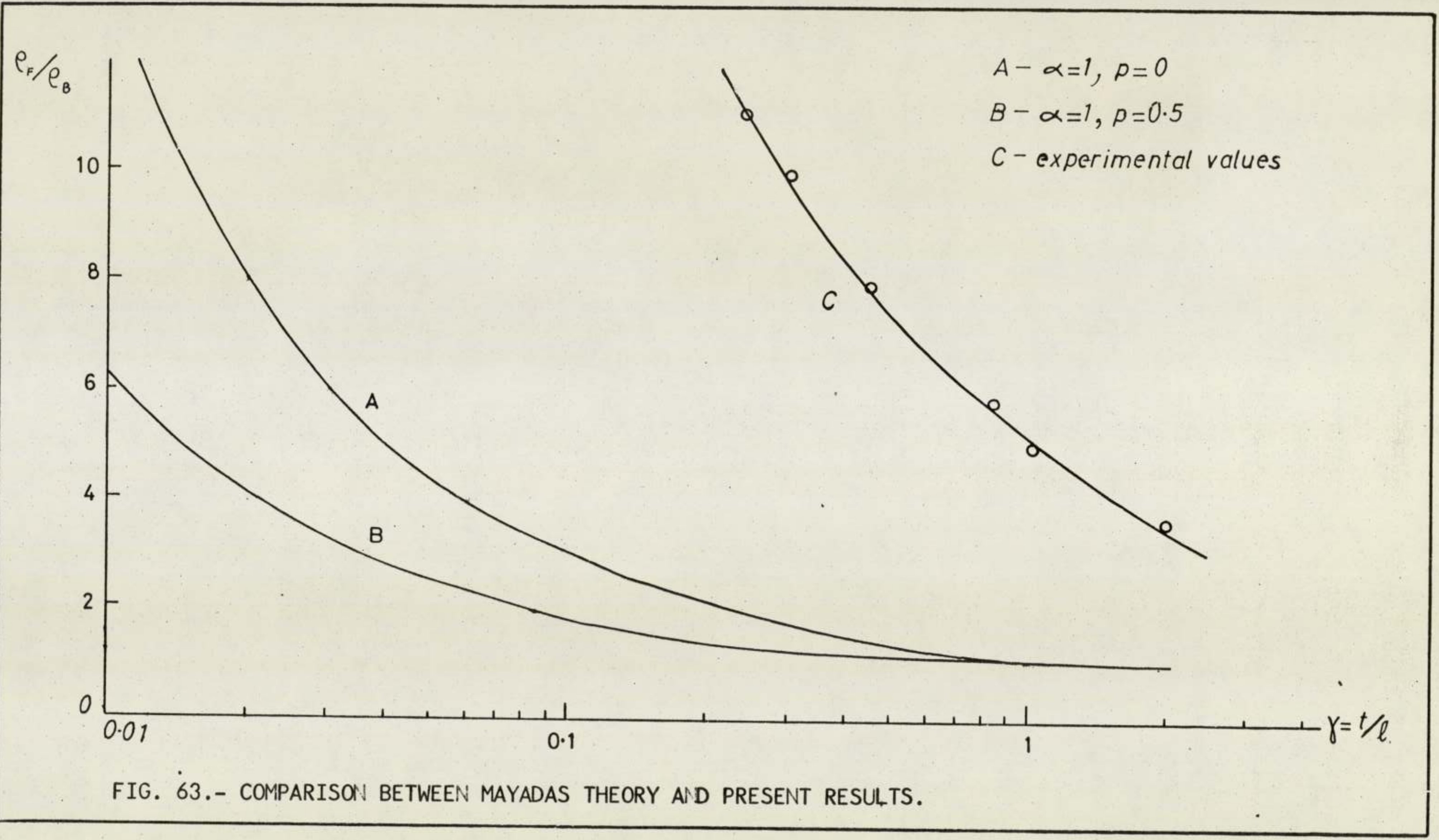

FIG. 63.- COMPARISON BETWEEN MAYADAS THEORY AND PRESENT RESULTS.

the sample and ℓ_o is the mean free path which is limited by grain size.

As has been said in section 5.4, the grain size found in the present films range from 50 to 176Å, therefore the mfp will be affected by the crystallite size only at low temperatures when the mfp is bigger than the size of the crystals.

We have plotted in Figure (63) together with Mayadas theoretical curves, the experimental one which corresponds to the sample of appropriate thickness to which the theory can be applied.

As in the case of F-S theory the disagreement with the theoretical curve is so large that the influence of the grain boundary scattering on the film resistivity is considered negligible for the present samples.

6.3.5 Influence of f.c.c. Structure

No account has been taken of the samples with more than 10% f.c.c. phase in the above considerations.

As was shown in section 5.3, all the electrical properties were affected by the presence of f.c.c. structure : resistivity increases, TCR decreases, ρ_{300}/ρ_{10} decreases and $d\rho/dT$ increases. All these changes became greater as the percentage of f.c.c. phase present in the film increases. Therefore we can assume that the presence of f.c.c. structure in an otherwise b.c.c. phase acts as an extra impurity in the way it affects the electrical properties. It is a special kind of impurity because it would be temperature dependent. Different reasons for this assumption are given in section 6.2.5. So in the samples with a higher proportion of f.c.c. there is another term to add to the Matthiessen's equation.

Westwood and Livermore[64] found the same effect was produced by β - Ta; an increase in resistivity and a decrease in TCR

when the percentage of β - Ta phase in the b.c.c. - Ta film increased.

6.3.6 Summary

The conclusions in this section can be summarized as follows:

1) Matthiessen's rule holds for the samples prepared in this work with film thickness greater than about 400Å.

2) Size effects and grain boundary scattering does not explain the high resistivities measured in the films.

3) Gaseous impurities, structural imperfections and lattice distortions are the causes of resistivity higher than bulk, but the quality of films reported here are better than other authors.

4) The quality of the samples improves with thickness and with increased deposition rate and deposition temperature.

5) The presence of f.c.c. phase in Ta films adds an extra term to Matthiessen's rule; i.e. it can be considered as a kind of impurity which is temperature dependent.

Finally, we can write the resistivity of a film as

$$\rho_F = \rho_B + \rho_I + \rho_{SD} + \rho_{LD} + \rho_{fcc} \qquad (6.5)$$

6.4 Grain Size

As is shown in Tables (8) and (9) the grain size for both b.c.c. and f.c.c. structures increases with increasing thickness in agreement with Gerstenberg and Hall[61] but in opposition to Lainer and Kholmyanskii[60] who did not find any influence of thickness on grain size. Another factor affecting the size of the grains is the deposition temperature and in agreement with Hauser and Theuseur[77] and Lainer and Kholmyanskii[60] an increase in T_D produces an increase in grain size as is shown in Figures (48) and (49).

6.5 Superconductive Transition in Tantalum Thin Films

The observed decrease in the values of the transition temperature of Tantalum films with film thickness has been reported by several authors.

There seem to be two main ways in which to explain the phenomenon; firstly, a decrease in Tc is correlated with a decrease in the resistivity ratio and explain using W. Desorbo[28] theory, and secondly, applying Mac Millans'[2] equation the change in Tc is related to the parameter λ, the electron phonon coupling constant. A decrease in λ would produce a decrease in Tc.

6.5.1 Critical Temperature and Resistivity Ratio

1) General Discussion

According to Desorbo[28] the addition of interstitial impurities decreases Tc while the resistivity is increased. The resistivity change brought about by interstitial solutes added to the film is larger than that brought about by similar additions of metallic solutes.

In interstitial solutions the decrease in Tc is accompanied by an increase in lattice parameter a_o.

The most important interstitial impurity is oxygen. Associating the increase in interstitial impurity concentration with an increase in resistivity (accompanied by a decrease in mfp and in ξ_o, the coherence length) Desorbo found for transition metals a linear relationship between resistivity ratio and transition temperature.

Seraphim et al[74] working with Ta thin films found that a decrease in Tc was related to an increase in the concentration of interstitial nitrogen according to the relation

$$dTc/d\ (at\ \%\ N) = -\ 0.46^{o}K/at\% \qquad (6.7)$$

Rairden and Neugebauer[29] applied DeSorbo's theory to their samples and quoted the relation between Tc and resistivity ratio for Tantalum as

$$Tc = 4.45 - 0.77 \frac{R_{10}}{R_{300}-R_{10}} \qquad (6.8)$$

To explain the discrepancies between the theoretical and experimental values they considered that structural defects such as vacancies and dislocations or impurities other than oxygen are contained in the films, thus lowering the mean free path and therefore the resistance ratio without greatly affecting Tc.

Using the same argument Budnick[75] concluded that for Ta, Tc is strongly dependent on the electron mean free path through the resistivity and varies approximately linear with resistivity ratio. Sulkowski and Mazur[76] reached the same conclusion.

Gerstenberg and Hall,[61] Marcus,[62] Sulkowski and Mazur[76] Hauser and Theuseur[77] and Lynton et al[78] all concluded that a decrease in resistivity ratio results in a decrease in transition temperature.

2) Present work

We have plotted in Figure (64) equation (6.8) of DeSorbo together with our experimental results.

The disagreement between the two graphs might possibly be due to the fact that the mean free path and so resistivity could be affected, not only by oxygen impurities but by some other gaseous impurities (nitrogen for example) together with structural defects and lattice distortions; this last factor producing an increase in the a_o parameter which in turn increases resistivity.

The fact that in this work Tc is found to increase with increasing deposition temperature is consistent with previous

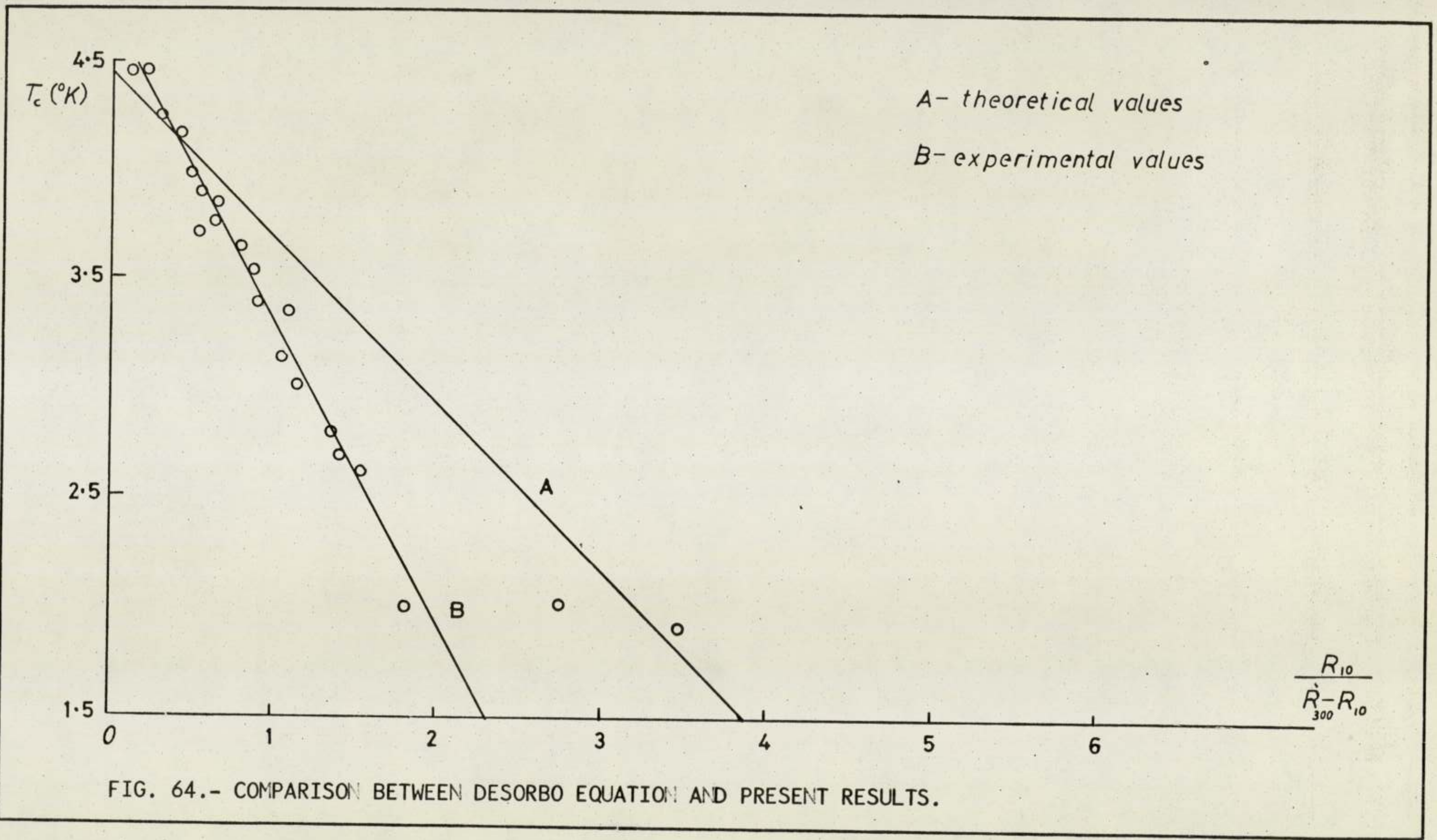

FIG. 64.- COMPARISON BETWEEN DESORBO EQUATION AND PRESENT RESULTS.

observations in that an increase in deposition temperature reduces the concentration of gaseous impurities, structural defects, stresses and the departure from the bulk lattice constant; all of which results in a shift of Tc towards the bulk value.

Schrey et al[58] found that as the substrate temperature increased Tc decreased, the disagreement with our findings may be due to the fact that their samples were prepared by sputtering which increases gaseous inclusions rather than by thermal evaporation at very low pressures.

Another factor in favour of these assertions is that a minimum substrate temperature of between 448 and 473°K was required to obtain superconducting Ta thin films. The non-superconducting samples prepared at lower substrate temperatures were accompanied by a departure from the bulk value of the lattice parameter a_o of 2.27%.

Also, films prepared with very low deposition rates of the order of 40Å/min had an increased a_o parameter and did not exhibit superconductivity.

Neugebaur and Ekwall[79] found the same relationship between Tc and lattice parameter a_o for Nb samples.

In agreement with Gerstenbergh and Hall[61] and R.B.Marcus[62] we found that ΔT, the temperature interval for the transition from normal to superconductor, was very sharp at high Tc but becomes broader as the resistivity increases and Tc decreases. The value changed from 0.01°K for a sample with Tc = 4.48°K to 0.95°K for a sample with Tc = 1.8°K.

In relation with the tantalum films which have a high proportion of f.c.c. structure, which we considered in section 5.3 as an impurity as far as resistivity was concerned, it was found that in spite of the fact that the presence of f.c.c.

structure raises resistivity and lowers resistivity ratio factors, both of which lead to the lowering of Tc, the transition temperatures of these samples are equivalent to the transition temperature of pure b.c.c. structure films of the same thickness.

Two possibilities can be suggested to explain this phenomenon, either (1) the transition temperature of f.c.c. structure is similar to that of b.c.c. phase or (2) that as was explained in section 6.2.5 the samples with a mixture of f.c.c. and b.c.c. structures are constituted by a network of b.c.c. and f.c.c. grains so if the b.c.c. phase present becomes superconductive at a higher temperature than the f.c.c. phase, the f.c.c. is short-circuited and what is measured is the Tc of b.c.c. structure. (It was not possible to get a thick film of 100% f.c.c. phase).

6.5.2 Influence of Phonon Spectrum in Transition Temperature

It has been found that in some materials the superconducting transition temperature Tc of the same metal prepared in the form of very thin films, or small grains is appreciably higher than that of the bulk material.

This enhancement was observed by Strongin et al[80] for aluminium and tin, Buckel and Hilsch[81] for tin and Abeles et al[82,83] for aluminium, and has also been observed in aluminium in connection with this work.

Leger and Klein[3] suggested that the enhancement was due to modification of the phonon spectrum. Rothwarf[84] proposed that for small grains or films the existence of a lower frequency phonon cut-off leads to a reduction in the pair breaking rate and to enhanced transition temperatures. The effect of small grain size on the phonon spectrum was discussed by Theil[85] as an extension of the work of Marshall and Wilenzick[86]. It was suggested that quantization of the phonon wave vector within

a small sample could be the cause.

For a cubical grain of size length do, the smallest wave number permissible is given by

$$q_o = \frac{\pi}{do} \quad (6.9)$$

In terms of phonon frequency, a cubical grain of side length d_o would cut-off all phonons having a frequency smaller than ω_c given by

$$\omega_c = c\frac{\pi}{d_o} \quad (6.10)$$

or the equivalent

$$\nu_c = \frac{c}{2\,d_o} \quad (6.11)$$

where C is the appropriate velcocity of sound in the material.

Using equation (6.10) to determine the cut-off frequency, Rothwarf[84] obtained a relationship between transition temperature and grain size that was in good agreement with the experimental results of Abeles et al[82] and Strongin et al[87] for aluminium and tin.

6.5.3 Application of Mac Millan Equation to the Present Results

L.T.L.Shin[88] and Meyers and Little[89] proved that the electron-phonon mechanism accounts for the whole of the coupling leading to superconductivity in tantalum. Therefore it was assumed that for the present work involving tantalum films, the Mac Millan relationship as given by equation (2.31) was applicable.

Following Mac Millan, the coulomb coupling constant μ^*, was considered constant and the transition temperature was considered to depend upon the electron-phonon coupling factor λ, given by

equation (2.28) as

$$\lambda = \int_0^{\omega_o} \alpha^2(\omega)\, F(\omega) \frac{d\omega}{\omega} \tag{6.12}$$

where $\alpha^2(\omega)$ is an average of the electron-phonon interation

$F(\omega)$ is the phonon density of states,

or its equivalent for

$$\lambda = \frac{N(0)\ \langle I^2 \rangle}{M \langle \omega^2 \rangle} \tag{6.13}$$

where $N(0)$ is the electron density of states $\langle I^2 \rangle$ is an average over the Fermi surface of the square of the electronic matrix element

M is the isotopic mass

$\langle \omega^2 \rangle$ is an average of the square of the phonon frequency

Figure (65) shows the dependence of the transition temperature on the electron-phonon coupling constant as given by equation (2.31). The value of the coulomb coupling constant μ^* was taken as 0.13 (being constant from transition metals) and the characteristic frequency was taken to be the Debye temperature $\theta = 258^{\circ}K$. As can be seen, to achieve the decrease of transition temperature observed experimentally, the electron-phonon coupling factor λ must also be reduced.

First we are going to consider equation (6.12) for the electron-phonon coupling factor λ. Values of the λ parameter may be calculated provided that the weighting function $\alpha^2(\omega)$ $F(\omega)$ can be determined. Mac Millan assumed that the function $\alpha^2(\omega)$ was constant over the phonon spectrum and $F(\omega)$ was taken to be the phonon density of states.

The neutron scattering experiment of Woods [90] provided the phonon density of states for Ta which is shown in Figure (66).

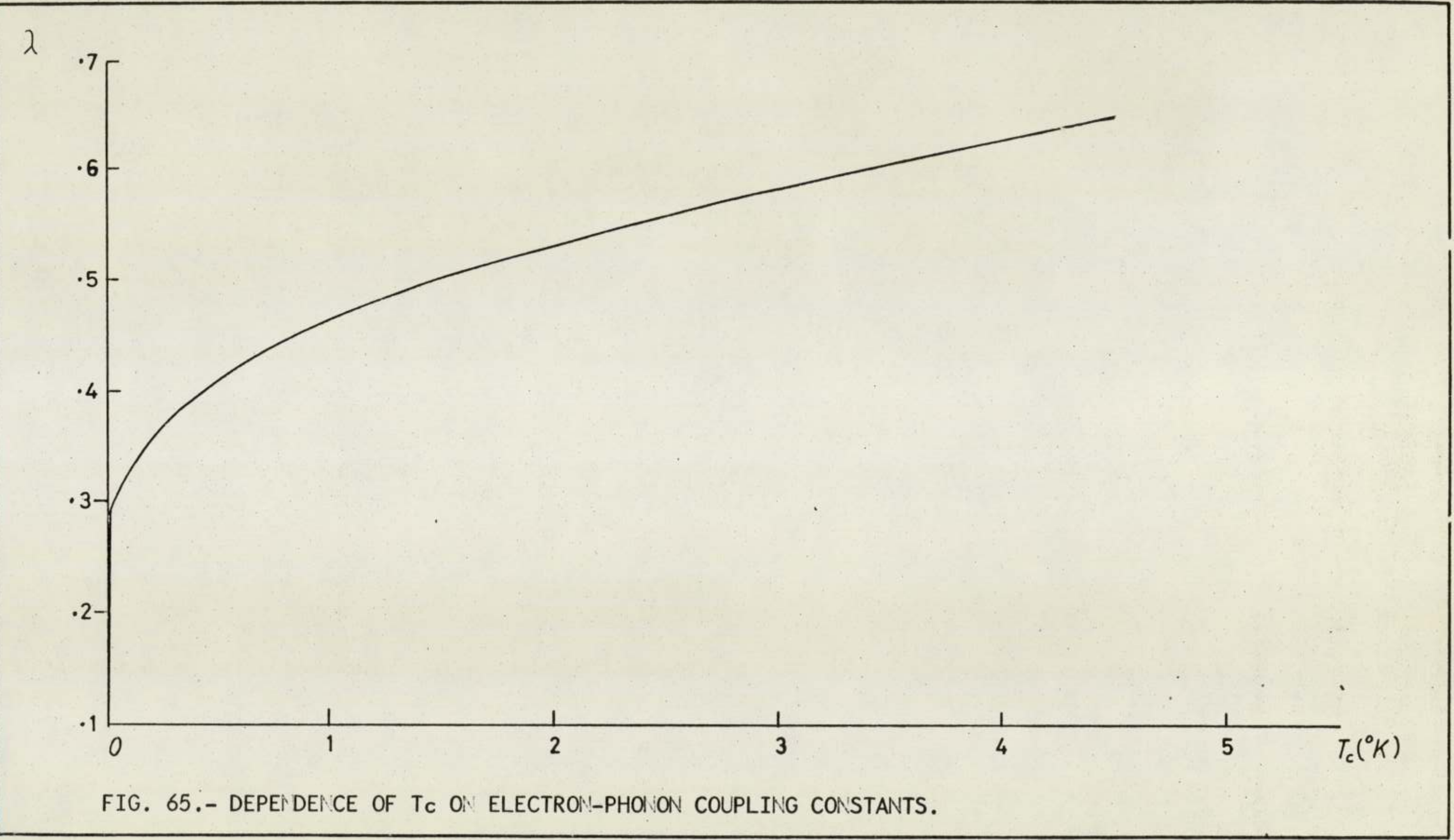

FIG. 65.- DEPENDENCE OF Tc ON ELECTRON-PHONON COUPLING CONSTANTS.

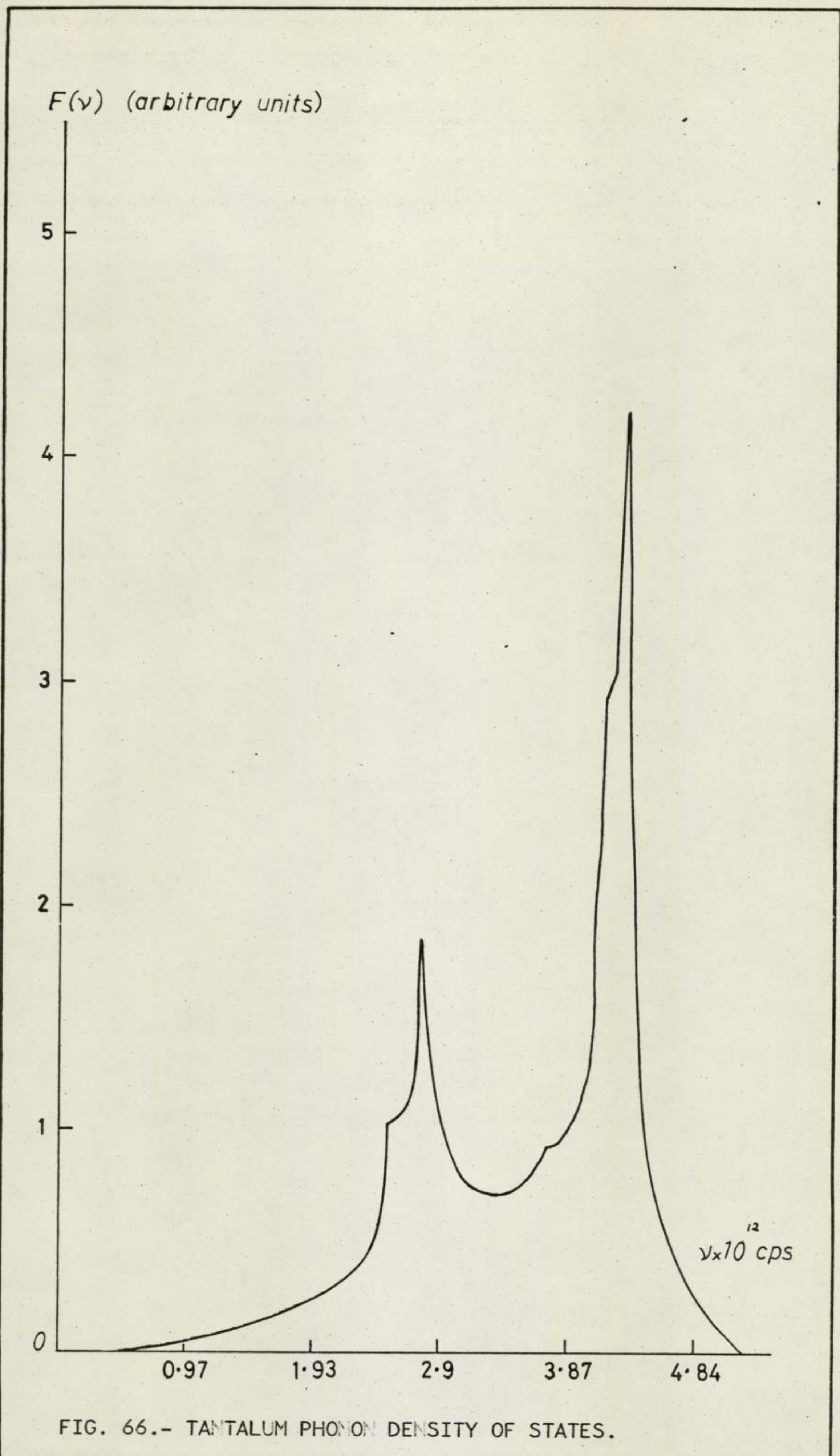

FIG. 66.- TANTALUM PHONON DENSITY OF STATES.

The plot of $F(\omega)/\omega$ versus ω determined from Woods' results, is shown in Figure (67).

To reduce the magnitude of λ the range of phonon frequencies over which the integration is to be performed must be reduced. The variation of the electron-phonon coupling with respect to the critical frequency is shown in Figure (68).

The dependence of the transition temperature on the phonon cut-off frequency Figure (69) was obtained by combining Mac Millan's equation with the variation of λ with respect to the critical frequency.

The dependence of cut-off frequency on grain size is shown in Figure (70), it has been calculated using equation (6.11). The average sound velocity for Ta has been taken as 2984.87 m/s using the values for the elastic constants given by Featherston and Neighbours[91]. Graph A has been calculated assuming a cubic grain of side length d_o while in Graph B the gain is a sphere of radius d_o .

A look at Figure (70) indicates that even for grain sizes as small as 30Å the highest phonon frequencies which are cut from the phonon spectrum are 0.527×10^{12} c/s and 0.72×10^{12} c/s for cubic and spherical grains respectively, which according to Figure (69) will reduce the Tc from the theoretical value obtained from Mac Millan's equation of 4.53^{o}K for bulk material to 4.3^{o}K and 4.1^{o}K respectively, insufficient in both cases to explain Tc's as low as 1.4^{o}K found in this work.

Another attempt to explain the reduced Tc's was made trying to calculate the cut-off frequency limited by the mean free path instead of by grain size, again the theoretical Tc's were too high in comparison with the experimental values found in that investigation.

Therefore, in spite of the suggestion by Salter[4] that a

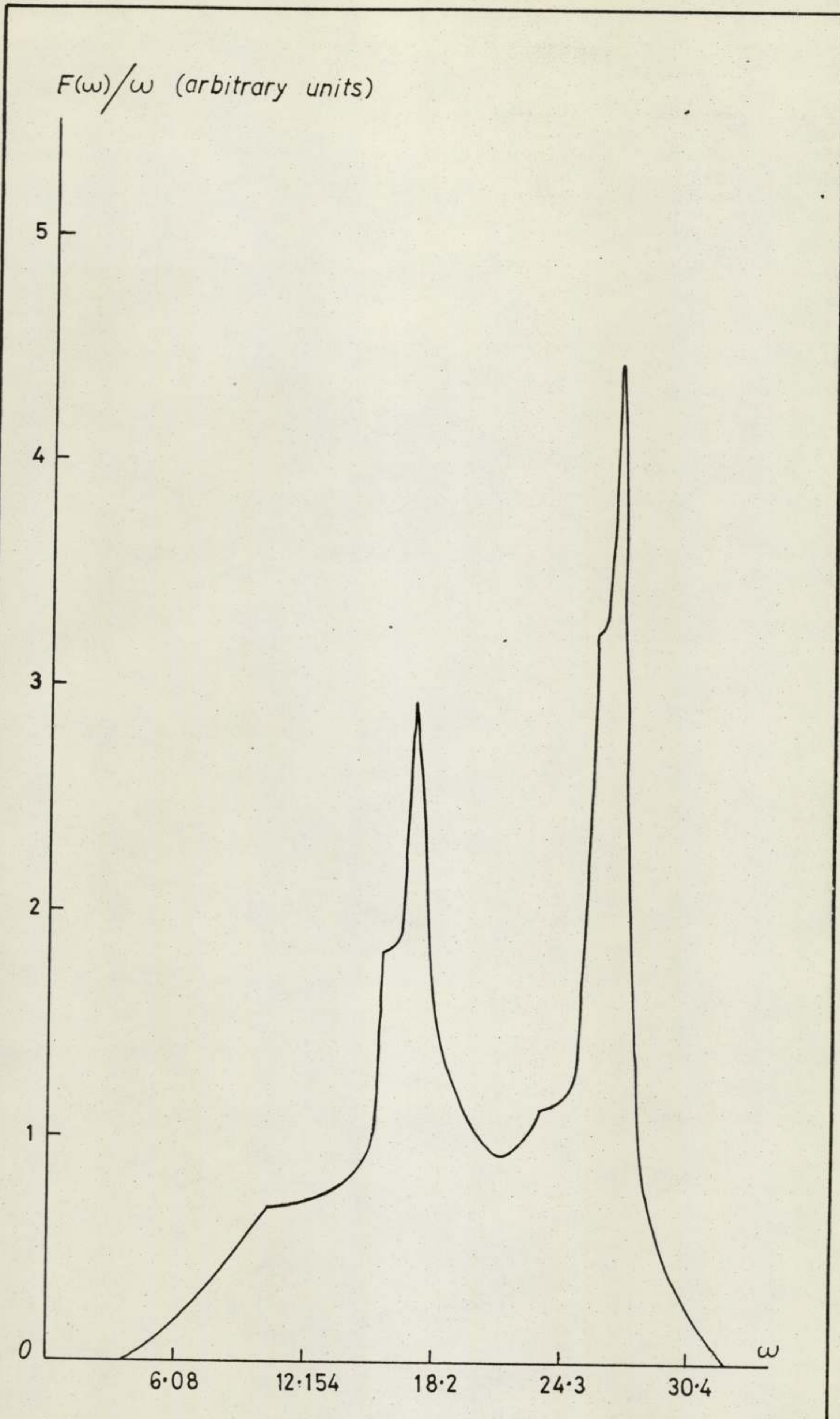

FIG. 67.- TANTALUM F $(\omega)/\omega$ VERSUS ω.

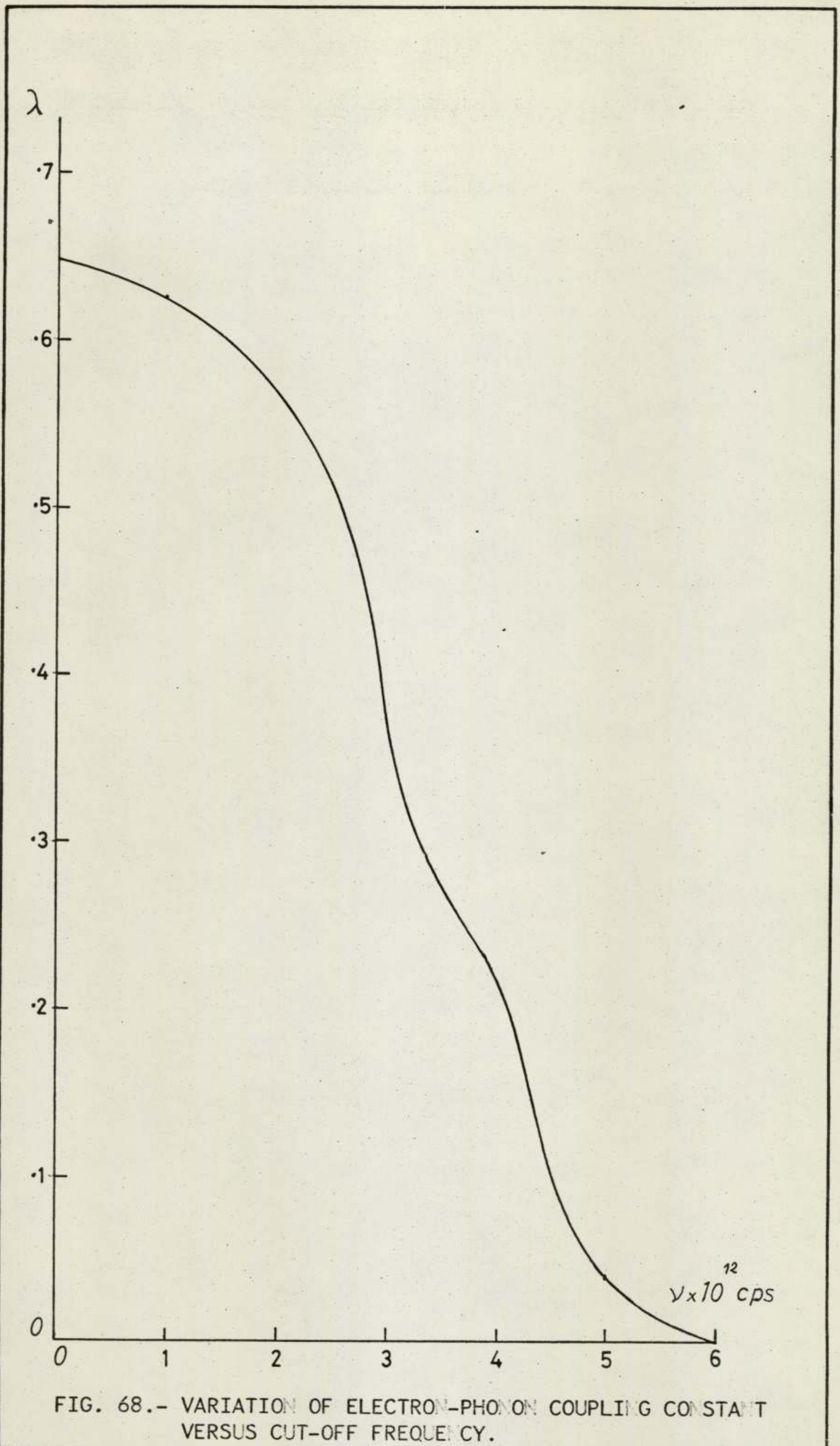

FIG. 68.- VARIATION OF ELECTRON-PHONON COUPLING CONSTANT VERSUS CUT-OFF FREQUENCY.

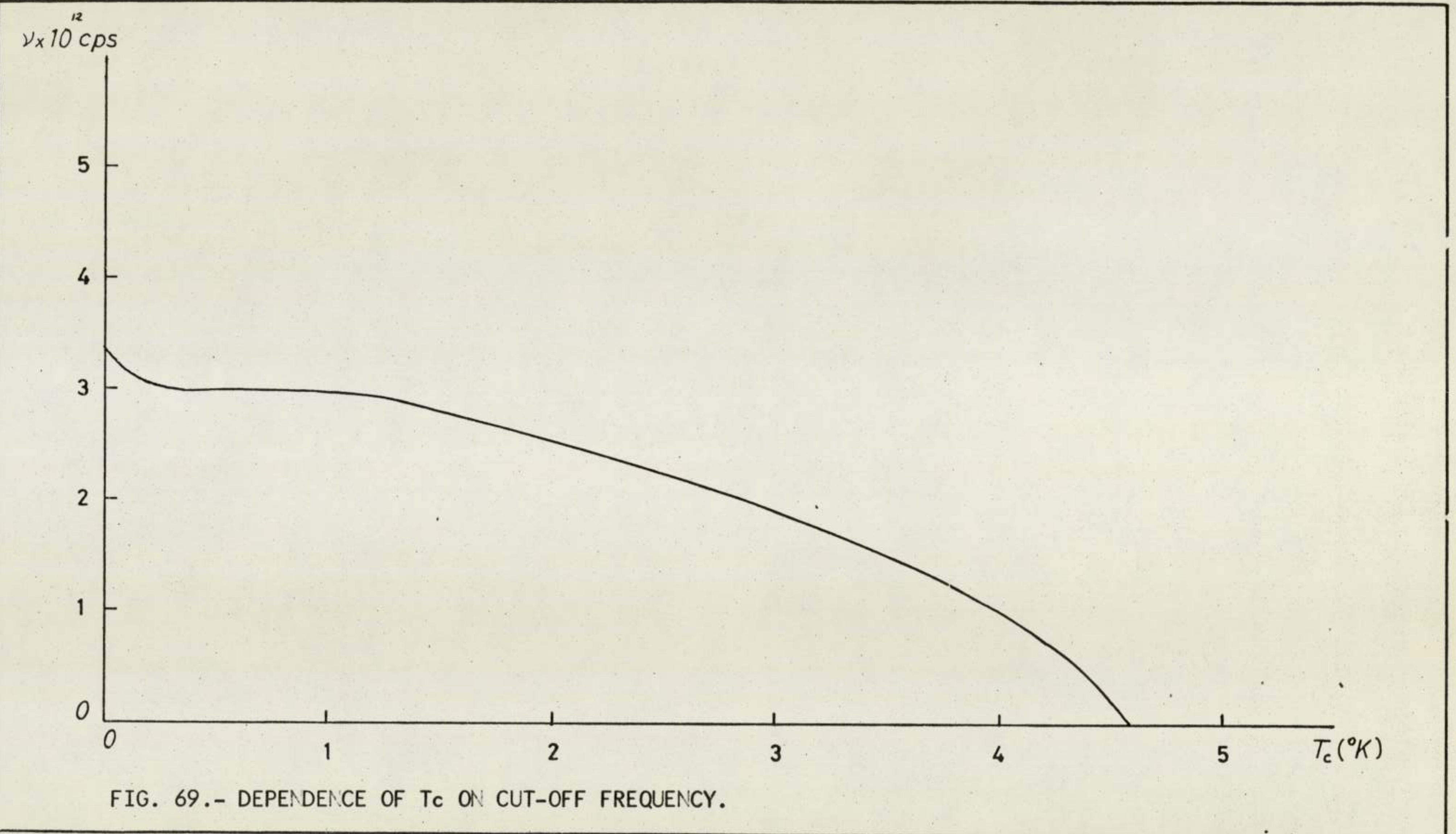

FIG. 69.- DEPENDENCE OF Tc ON CUT-OFF FREQUENCY.

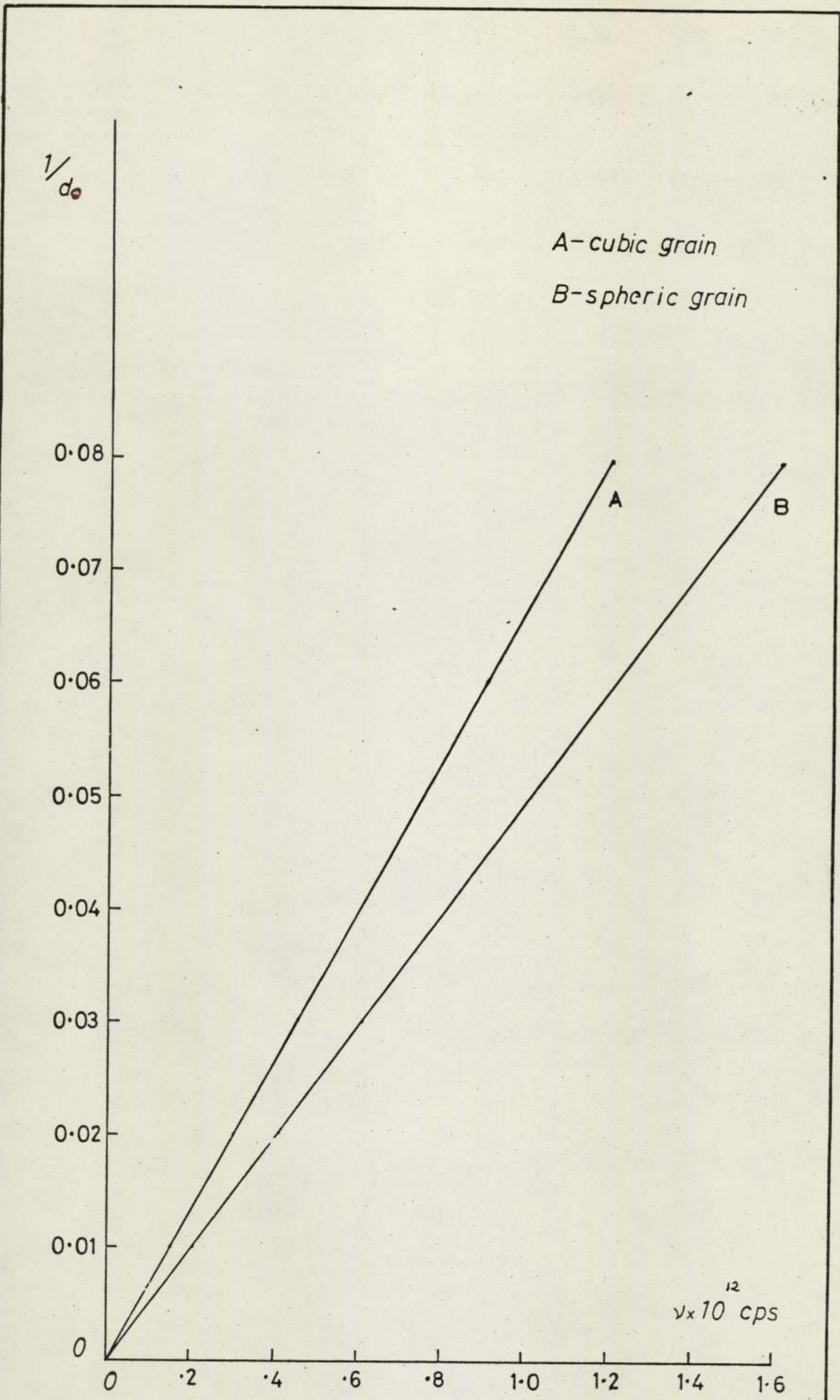

FIG. 70.- GRAIN SIZE VERSUS CUT-OFF FREQUENCY.

reduction in grain size followed by a reduction in the integration limits of equation (6.12), would account for the reduction in the transition temperatures he observed for Nb and in view of the similarity of the phonon spectrum of niobium and tantalum, we categorically reject such a possibility. One should also consider under what conditions, if any, it would be possible to obtain enhancement in Ta as has been observed in Aℓ and Sn. The exponent in the Mac Millan equation (2.31) giving an increase in Tc becomes positive when λ is less than 0.14 which, according to Figures (68) and (70), corresponds to a particle size completely unrealistic.

Next we are going to consider equation (6.13). For the reasons given above, any variation in $\langle\omega^2\rangle$ due to grain size is completely insignificant to explain the needed changes in λ which would explain the decrease in Tc observed for thin films of tantalum. Therefore, any change in the parameter λ must be explained in terms of changes taking place either in N(O) or in $\langle I^2\rangle$.

Lynton et al [78] suggested that for Tin a decrease in the density of states will bring about a decrease in Tc. Hanak et al [92] suggested that more attention should be given to the variation of N(O) and $\langle I^2\rangle$ with grain size in transition metals. Strongin [93] tried to explain the way in which the short mfp would affect the density of states. She suggested that an explanation for the reduced Tc values in transition metals should be found in terms of modified electronic properties.

In the context of the Mac Millan analysis it means that for Ta films either N(O) and/or $\langle I^2\rangle$ must decrease so that there is a decrease in λ which, in turn, lowers the critical temperature.

6.5.4 Empirical Considerations

Empirical relationships have been found between critical temperature and electrical properties which indicates that some form of microscopic defect which is sensed in the electrical properties may be one of the most significant factors affecting Tc. Values relating to the present work are given below:

6.5.4.1 Relationship between Tc and resistivity

Figure (51) gives the relation between Tc and ρ_{300}, an equation which gives the relationship between the two is as follows:

$$T_{CF} = K\, T_{CB}\, e^{-a\rho_{300}} \qquad (6.14)$$

where

T_{CF} is the critical temperature for the film

T_{CB} is the bulk critical temperature

K and a are constants

These constants can be identified as

$K = 1.15$ and $a = 0.01$

Table (17) gives the experimental and calculated values using the expression (6.14); between $2.3^{\circ}K$ and $4.5^{\circ}K$ the agreement is within 3% and below $2.3^{\circ}K$ within 10%.

The constant a has the dimension of conductivity, the corresponding resistivity would be $\rho_a = 90.9\ \mu\Omega\ cm^{-1}$.

As the samples prepared in this work satisfy Matthiessen's rule, according to which

$$\rho_{300} - \rho_{10} = \text{constant}$$

we can find as well a relationship between Tc and resistivity at $10^{\circ}K$.

$$T_{CF} = K\, T_{CB}\, e^{-a(\rho_{10} + b)} \qquad (6.15)$$

where b is a constant determined by Matthiessen's rule.

6.5.4.2 Relationship between Tc and resistivity ratio and Temperature coefficient of resistivity.

Figure (53) gives the relationship between Tc and ρ_{300}/ρ_{10}.

Suppose the critical temperature for thin films can be written as

$$T_{CF} = T_{CB}\left[1 - e^{-K'\,\rho_{300}/\rho_{10}}\right] \qquad (6.16)$$

where T_{CF} is the critical temperature for the film

T_{CB} is the bulk critical temperature

K' is a constant

Table (18) gives the measured and calculated values for Tc with K = 0.65, it can be seen that there is a good agreement near the bulk critical temperature down to about 3.4°K.

Rairden and Neugebauer[29] give a relationship for decreased Tc, if this is written in terms of resistivity ration we obtain

$$Tc = T_{CB}\ 0.77\ \frac{1}{\rho_{300}/\rho_{10}-1} \qquad (6.17)$$

Table (18) gives the appropriate values uwing this relationship. It can be seen that this expression holds for gaseous contamination i.e. for relatively high values of ρ_{300}/ρ_{10}. For low values of ρ_{300}/ρ_{10} the critical temperature according to Rairden and Neugebauer falls off rapidly.

The calculated values for Rairden and Neugebauer and for expression (6.16) are compared with the experimental values in Figure (71). It can be seen that the expression (6.16) gives values which are too high at low temperature, whilst giving better agreement than Rairden and Neugebauer at high temperatures.

If we assume that both resistivity and effects of particle size on phonon distribution are contributing then in general

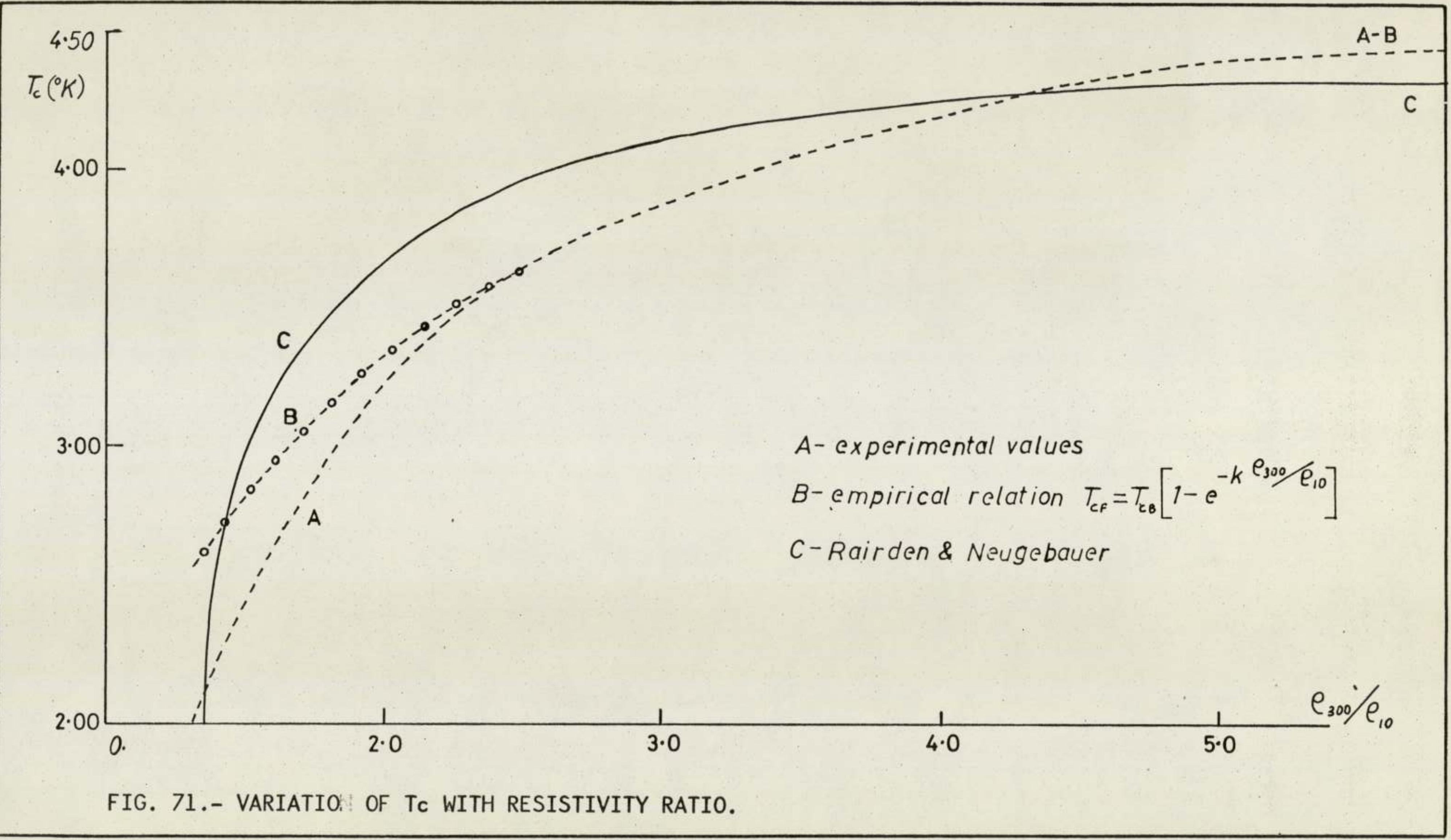

FIG. 71.- VARIATION OF Tc WITH RESISTIVITY RATIO.

the particle size effect (phonons) will be greater for low ρ_{300}/ρ_{10} ratios (i.e. for thinner films) since, in general, particle sizes for such films will be smaller.

If T_{C_M} = critical temperature as calculated by the Mac Millan relation

T_{CB} = critical temperature of bulk

T_{CF} = critical temperature of films

then

$$T_{CF} = T_{CB} \left[1 - e^{-K'\rho_{300}\,\rho_{10}}\right] - \left[T_{CB} - T_{CM}\right]$$

represents the combination of both effects

$$T_{CF} = T_{C_M} - T_{CB}\, e^{-K'\rho_{300}/\rho_{10}} \qquad (6.18)$$

This expression requires values of particle size corresponding to values of ρ_{300}/ρ_{10} in graph (53). Table (18) gives the calculated values for Tc according to Mac Millan equation and the values for T_{CF} according to equation (6.18).

The constant K' in expressions (6.16) and (6.18) of 0.65 is, in fact, equal to the value λ for bulk tantalum, although at this point in the argument no reason can be given for associating λ with K'.

Using the relationship (6.16) and applying it to Salter's results for Nb, similar effect was observed when the bulk value of critical temperature for Nb of 9.46^{o}K and K' value of 0.82 corresponding to the λ value of Niobium were used, the agreement was within 6%. Because of lack of information it was impossible to make connection for expression (6.18).

Another expression relating Tc and resistivity ratio was found

$$T_{CF} = T_{CB} \left[1 - 2\ e^{-\rho_{300}/\rho_{10}}\right] \qquad (6.19)$$

TABLE 17

EXPERIMENTAL AND CALCULATED VALUES OF CRITICAL TEMPERATURE AND THE CORRESPONDING RESISTIVITY

Tc (experimental)	ρ_{300}	Tc (calculated)
4.5	13.1	4.5
3.8	25	3.91
3.3	37.5	3.41
2.9	50	2.97
2.58	62.5	2.58
2.3	75	2.26
2.0	94	1.83
1.9	100	1.72

TABLE 18

EXPERIMENTAL AND CALCULATED VALUES FOR Tc USING THE EMPIRICAL RELATIONSHIPS

Tc(experimental) °K	ρ_{300}/ρ_{10}	Tc(6-16) °K	Tc(6-17) °K	Tc(Mac Millan) °K	Tc(6-18) °K	Tc(6-19) °K
4.45	6.0	4.41	4.33	4.5	4.41	4.47
4.3	4.5	4.26	4.26	4.5	4.26	4.4
4.2	3.4	4.1	4.16	4.48	4.09	4.2
3.75	2.75	3.74	4.04	4.48	3.72	3.92
3.5	2.3	3.49	3.89	4.48	3.47	3.6
3.25	2.05	3.31	3.75	4.45	3.26	3.34
3.00	1.8	3.11	3.52	4.42	3.03	3.02
2.75	1.65	2.96	3.30	4.38	2.84	2.77
2.5	1.5	2.83	2.94	4.35	2.68	2.53
2.25	1.4	2.69	2.56	4.3	2.49	2.28
2.0	1.3	2.57	1.82	4.2	2.51	2.05
1.5	1.2	2.43	.63	4.1	2.05	1.8

The calculated values for T_{CF} using this relationship are included in Table (18). The agreement is very good for the whole range of resistivity ratio (1).

This expression is simpler and more elegant in that it represents T_{CF} in terms of the bulk transition temperature and resistivity ratio only.

Finally, an attempt was made to correlate crital temperature and temperature coefficient of resistivity, the expression found was

$$T_{CF} = 2\,e^{-\alpha/K''T}$$

where T_{CF} has got the same significance as before and the value of the constant K" is 4.17×10^{-3}.

6.5.5 Summary

In view of our results and taking into account suggestions made by other authors, we may summarise the conclusions reached in the present analysis as follows:

The resistivity of tantalum thin films is very sensitive to various factors. Consequently, the mean free path on which the resistivity depends appears to be the crucial factor in reducing the critical temperature below bulk values. Samples with extremely high resistivity and low resistivity ratio did not become superconductors. The deposition parameters controlling non-superconductivity was deposition temperature, a minimum substrate temperature of between 448 and 473°K was required to obtain superconducting tantalum thin films.

DeSorbo theory accounts for the influence of the high resistivity of thin films, through gaseous impurities on the lowering of the critical temperature, but although it predicts the direction in the change of Tc, it fails to predict quantitative changes.

We said in section 6.4.1 that to explain the disagreement of present results with DeSorbo theory, we had to consider how the mfp will be affected, and so resistivity, not only by gases but also by structural imperfections, changes in crystal structure, stresses and grain size. Consequently, Tc will increase as mfp increases.

For a mean free path of the order of tens of Å and a Fermi velocity of about 10^8 cm/s, the relaxation time for a given state of about 10^{-15} s is estimated. Invoking the uncertainty principle ($\Delta E\ \Delta t \simeq \hbar$) the corresponding value of ΔE will be of $\Delta E \simeq 10^{-12}$ ergs or about 1eV which would easily break the bond of 10^{-4} eV corresponding to the energy gap. Figure (72) shows the variation of N(O) with energy for transition metals. It can be seen that the characteristic structure is of the order of about 0.2 eV. Hence the smearing of the order of 1 eV estimated above will drastically change the density of states structure.

If it is assumed that Tc correlates with N(O) then Tc will change with N(O). The fact that density (specific gravity) decreases with decreasing thickness as found in the present work, section 5.7 implies that the density of states N(O) decreases with decreasing thicknesses, therefore lowering the values for the electron-phonon coupling constant, according to the equation (6.13) and consequently producing a decrease in the transition temperature.

Another possible factor affecting Tc, as given by equation (6.13), is $\langle I^2 \rangle$ and if we assume that V_{PH} is not essentially constant but may change with changes in the lattice structure it will, in turn, affect Tc.

Therefore, it may be suggested that the changes in the phonon spectrum are not predominant and that any explanation

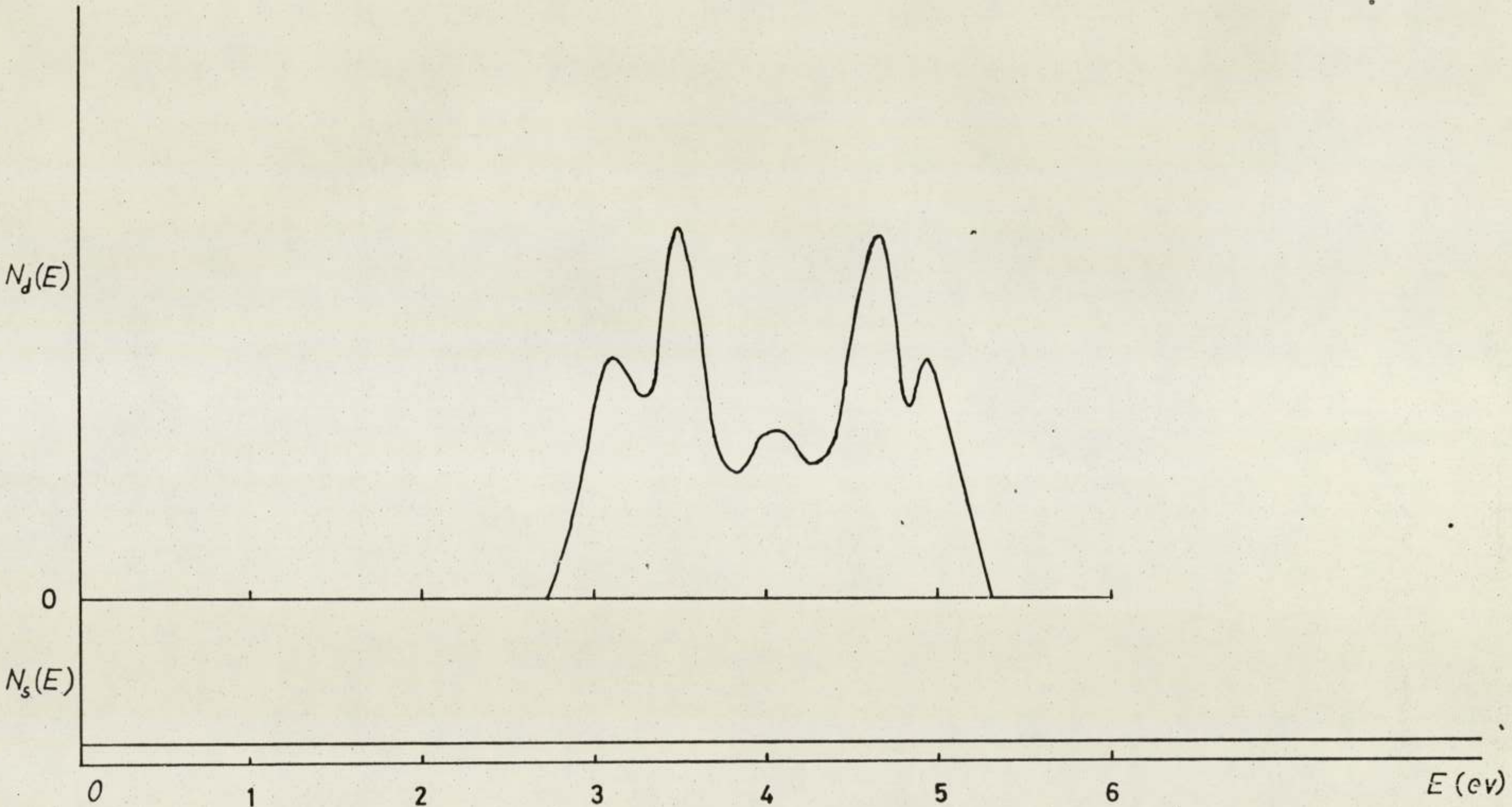

FIG. 72.- VARIATION OF DENSITY OF STATES N (o) WITH ENERGY FOR TRANSITION METALS.

as to the reason why Tc decreases in thin films must be explained in terms of any factor which can affect the sharp density of states N(O) and/or alter $<I^2>$, thus decreasing the value of the electron-phonon factor λ and subsequently by lowering Tc. If N(O) and $<I^2>$ are the important factors, one can suggest the required changes of these parameters to give the experimental changes in Tc. From Mac Millan equation and Figure (65) the percentage reduction in λ to reduce Tc from 4.5°K to 1.5°K is approximately 20%. Since λ is equal to N(O) $<I^2>$ equation (6.13) this will require a reduction of 20% in these factors either separately or combined.

Empirical relationships have been found which correlate Tc and the electrical properties of thin films; the error in the prediction is within 3% in most cases.

A comparison of the present results for the transition temperatures and the values found by other authors is shown in Table (19).

Testardi [94] briefly reports on a relation between resistivity ratio and Tc for Nb/Ge compounds. This was reported in March 1975 after the above conclusions had been reached. Testardi does not include any details or indicate whether a relationship has been found.

6.6 Type II Superconductors

Although the criterion for type classification of a superconductor is the same for both bulk and thin films, a thin film prepared from a Type I superconductor may behave as Type II, depending on the effective value of the electron mean free path.

For bulk Ta the values of the London [15] penetration depth λ_L and the Pippards [18] coherence length ξ_o defined in Chapter 2 are λ_L = 350Å and ξ_o = 780Å respectively as measured by Varhazis and Strongin [95] and k_o = 0.43 making Ta a Type I superconductor.

TABLE 19

COMPARISON OF TC VALUES FOR THE PRESENT WORK WITH OTHER WORKERS

Author	Tc	Comments
Gerstenberg & Hall	4.48°K 4.19°K	2500Å (thickness) 1100Å (thickness)
Schrey et al.	3.6°K	1800Å (thickness)
Hauser & Theuseur	4.25 to 3.16°K	
Schmidt et al.	4.48 to 1.48°K	
Present work	4.48°K to 1.4°K	Range of thickness 9650Å to 125Å (1).. 125Å

..(1) Thickness not method of identification.

Gorkov[97] pointed out that the microscopic values λ_L and ξ_o may not apply to thin films, because of their dependence on mean free path. He concluded that films should possibly be described (in the microscopic theory) from the same point of view as superconducting alloys.

Based on Gorkov's considerations Wipf[98] considered a new value for κ, which can be defined as

$$\kappa = \kappa_o + \kappa_L \tag{6.14}$$

where κ_L accounts for the impurity scattering term and plays the same role as the alloy term in Gorkov's theory. According to Gorkov-Goodman[96] the value of κ_L is

$$\kappa_L = 7.5 \times 10^3 \gamma^{\frac{1}{2}} \rho \tag{6.15}$$

where γ is the electronic specific heat

ρ is the low temperature residual resistivity.

For all the samples prepared in this work $\kappa_L > 0.277$ which is the value necessary to convert Ta from Type I to Type II superconductor.

Thus we concluded that all the tantalum thin films studied in this project were Type II superconductors.

Hauser and Theuseur[77] arrived at the same conclusion for the tantalum thin films they prepared.

6.7 Critical Current Densities

Two experimental difficulties exist in the measurement of the critical value of current density needed to suppress superconductivity in thin films. a) The details of the current distribution need to be known to determine accurately the critical current density. b) the warming of the film by Joule heating if small normal regions are present, for example, at electrical contacts, can be an acute problem since current densities approach 10^5A cm^{-2}.

By analogy with the distribution of electric charges over the

surface of a conductor of the same shape it can be seen that the current in a flat superconductor is far from uniform, being carried primarily by the film edges. Measured critical densities determined by dividing the critical current by the film cross section lead to values lower than calculated on the basis of the uniform current approximation and indicates non-uniform current distribution.

The problem of Joule heating may be overcome by ensuring good thermal contact between the films and the surrounding liquid helium, and by using current pulses rather than a steady current.

In the present work steady currents were used but the sample was immersed in liquid helium during the measurement of the critical currents.

If small normal regions are present the Joule heating due to the high current density would lead to an abrupt transition to the normal state at current densities lower than predicted theoretically. Such transitions are irreversible and exhibit hysteresis and this effect was observed in some of our samples as is shown in Figure (73)

If the current is distributed uniformly, the critical current density is given by Silsbee's rule and we obtain

$$J_c = \frac{c H_c}{4\pi \lambda} \left(\frac{\xi}{\xi_0} \right)^{1/2} \tag{6.16}$$

A more exact calculation by Bardeen[99] which takes into account the slight variation of the energy gap with current modifies this result by a multiplying factory $(2/3)^{3/2}$.

Equation (6.16) can be written as

$$\frac{J_c(T)}{J_c(0)} = (1 - T_R^2)^{3/2} (1 + T_R)^{1/2} \tag{6.17}$$

where

$$T_R \equiv T/Tc$$

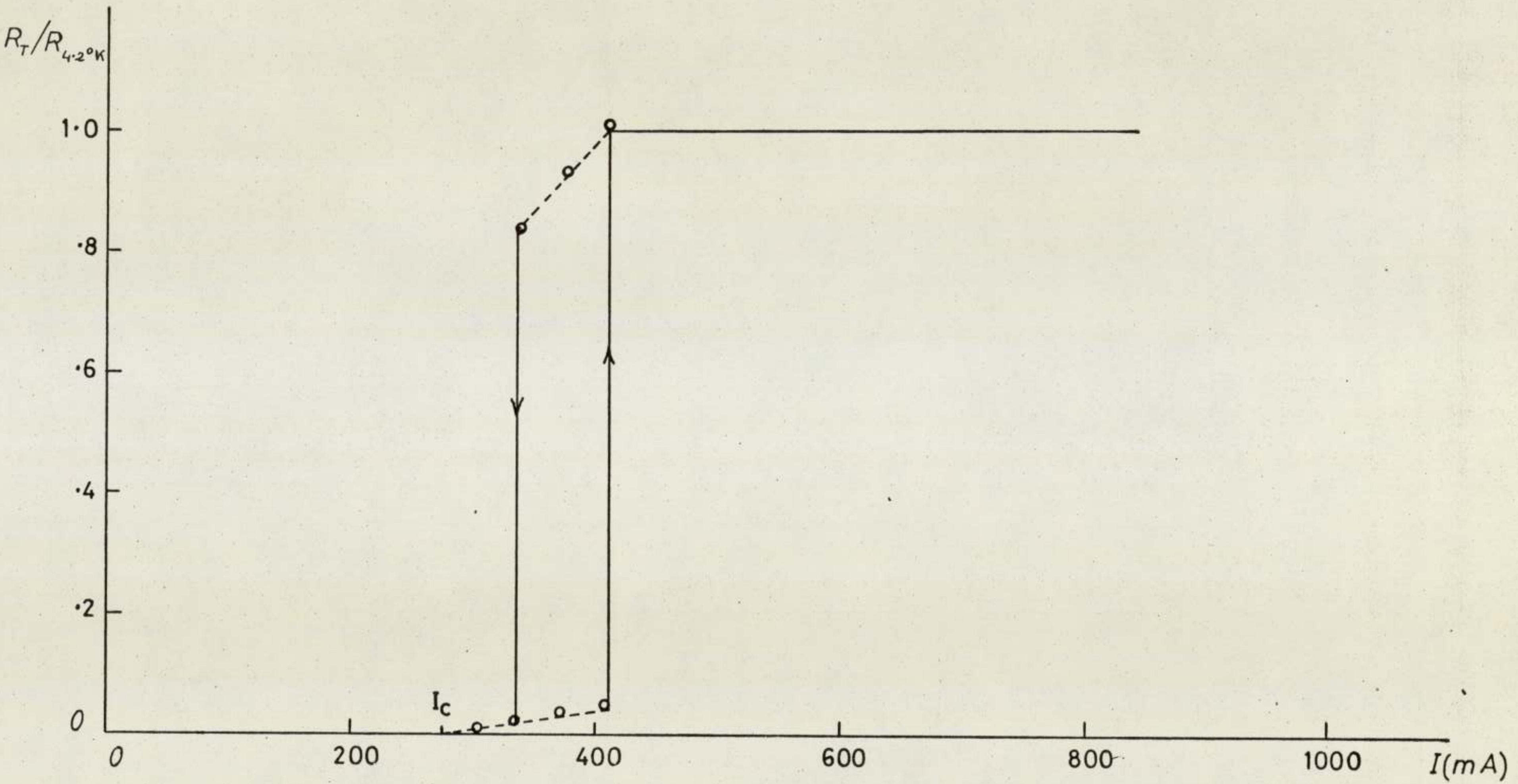

FIG. 73.- HYSTERESIS EFFECT IN NORMAL TO SUPERCONDUCTOR TRANSITIONS.

The dependence of Tc on film thickness does not appear explicitly but it enters through the mfp. An increase in critical current density with decreasing thickness was found in this work and is shown in Table (20).

By assuming a certain distribution along the width of the film, corrections for the non-uniform current distribution in planar films were made by Glover and Goffey.[100]

They deduced that the critical current Ic could be determined as

$$I_c(T_R) \propto \frac{(1-T_R^2)}{(1+T_R^2)^{1/2}} \qquad (6.18)$$

They obtain a good agreement of their data on Tin films with the theory.

Mydosh and Meissner[101] and Mercereau and Hunt[102] have observed a $(1 - T_R^2)^{3/2}$ dependence of critical current in tin films. London and Clark[103] observed a similar dependence in a 1050Å Nb film while Meiklejohn[104] obtained 2,3 instead of the three halves power for a 1000Å Ta film.

The results from the present work were plotted in Figure (74) in which $Ic/(1 + T_R^2)^{1/2}$ is plotted against $(1 - T_R^2)$, the slope of this curve is calculated as 1.2 which is small compared with Meiklejohn's value of 2.3 for tantalum but closer to the value of 1.5 predicted by Bardeen[99]. These results relate to 4 films of different thickness compared to one sample reported by Meiklejohn.[104]

Another graph is represented in Figure (75) in which the critical current is plot versus $(1 - T_R^2)/(1 + T_R^2)^{1/2}$, as can be seen the agreement is very good indicating the relevance of equation (6.18) for tantalum films.

By extrapolating the actual results obtained from the present work to a temperature of $0^{\circ}K$, we obtain the critical currents listed

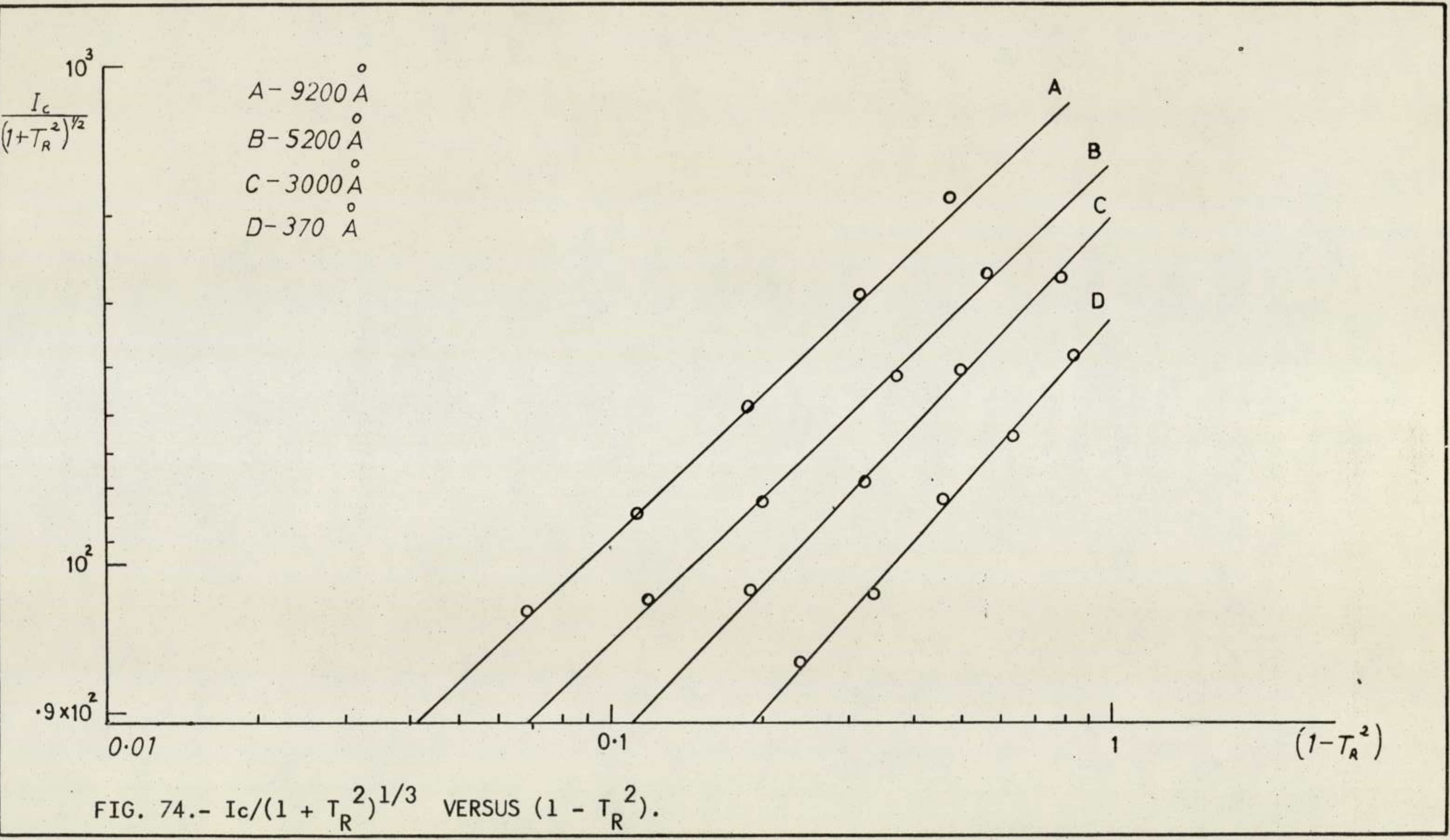

FIG. 74.- $Ic/(1 + T_R^2)^{1/3}$ VERSUS $(1 - T_R^2)$.

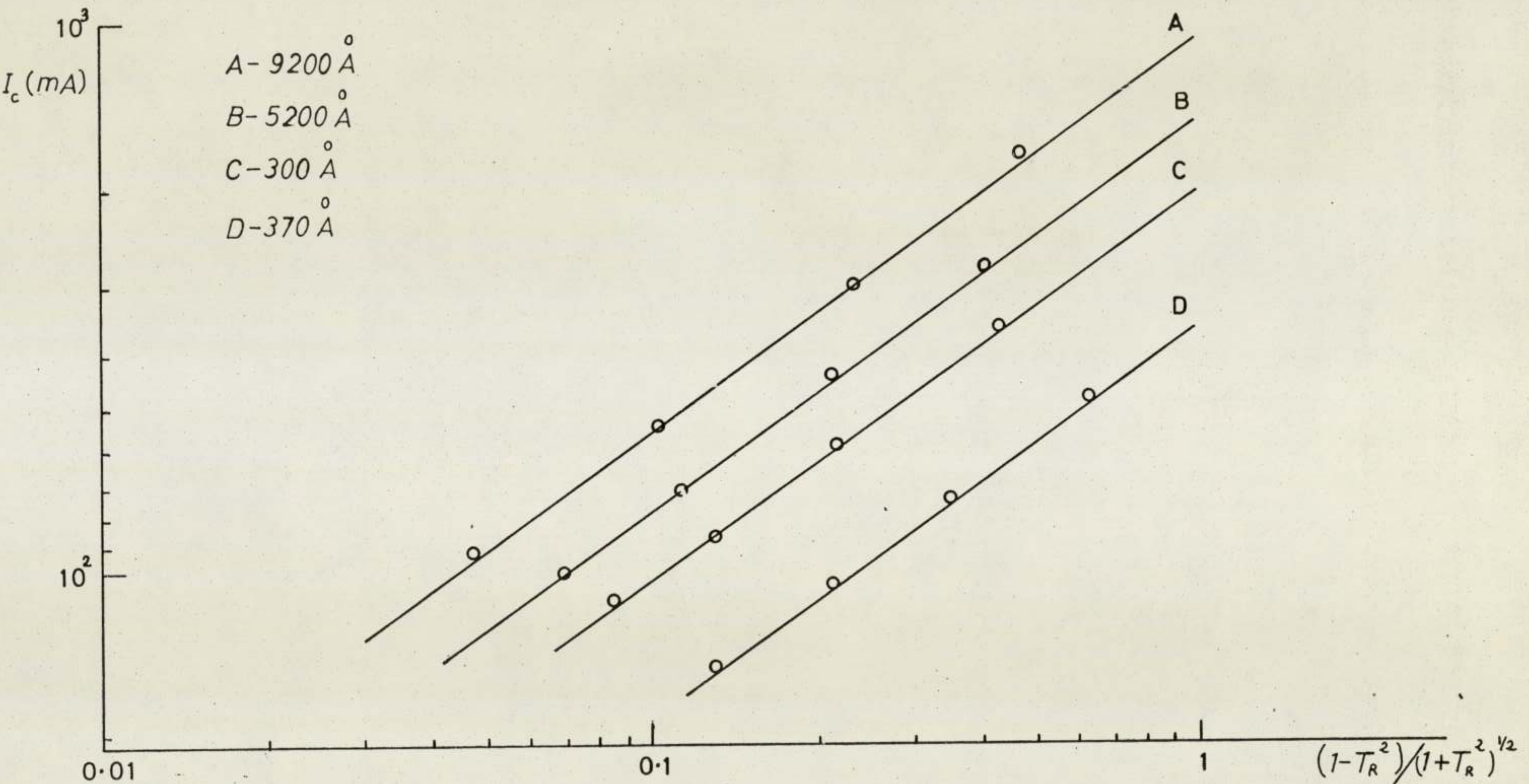

FIG. 75.- CRITICAL CURRENT VERSUS $(1 - T_R^2) / (1 + T_R^2)^{1/2}$.

in Table (21). The corresponding values of current densities are also shown, assuming a uniform current density.

It must be pointed out that these values of current density are merely intended as a guide to the order of magnitude which can be supported by a tantalum film deposited on a glass substrate.

In Table (22) the values reported by other workers on critical currents are compared with the measurements taken in the present investigation.

6.8 Determination of Film Thickness

The two main methods used in this work to measure the thickness of the samples have been described in section 4.4.

Although the calculated mean free path at $300^{\circ}K$ and $10^{\circ}K$ are $\ell = 37.3Å$ and $\ell = 236.5Å$ respectively, which means that most of the samples prepared in this work satisfied the condition that film thickness is greater than ℓ, the electrical method of measuring film thickness seems not very satisfactory.

The scattering from impurities, imperfections and stresses must be comparable to lattice scattering so that the thickness determined by the electrical method is unreliable because it is not relevent to use bulk b.c.c. values of $d\rho/dT$ in equation (5.1) for the calculation.

Another factor to make unsuitable the use of bulk $d\rho/dT$ is the presence of f.c.c. structure which is temperature dependent.

The fact that for samples prepared at substrates temperatures higher than $623^{\circ}K$, which have a higher degree of perfection, less impurities and stresses and smaller proportion of f.c.c. phase, the agreement between the optical and electrical method is much better than for the rest of the samples, supports the above conclusions.

Prutton[105] in his work showed how the average stress in thin films decreases with increasing deposition temperature.

TABLE 20

VARIATION OF CRITICAL CURRENT DENSITY WITH THICKNESS

Thickness	Critical Current Densities at 2.2° K
160Å	1.5×10^{-4} A/cm^2
500Å	1.35×10^{-4} A/cm^2
650Å	1.25×10^{-5} "
1325Å	1.2×10^{-4} "
3000Å	1.10^{-4} A/cm
5400Å	0.94×10^{-4} A/cm^2
9650Å	0.83×10^{-4} "

TABLE 21

CRITICAL CURRENTS AND CRITICAL CURRENT DENSITIES AT 0° K

Thickness	Critical Current $I_c(0)$	Critical current density $J_c(0)$
115Å	160 mA	1.4×10^5 Acm^{-2}
165Å	181 mA	1.1×10^5 Acm^{-2}
370Å	260 mA	7×10^4 Acm^{-2}
3000Å	440 mA	1.46×10^4 Acm^{-2}
5200Å	680 mA	1.32×10^4 Acm^{-2}
9200Å	1000 mA	1.09×10^4 Acm^{-2}

6.9 Ellipsometric Measurements

The determination of the optical constantans of bulk tantalum by ellipsometry has been done by several workers. Bulk measurements include oxide layers and surface difference due to polishing or etching in the preparation of smooth surfaces, both factors have been proved to affect the optical constants.

Table (23) shows the results obtained for some films in this work, together with the values measured by other authors on bulk materials.

It can be seen how our results agree with the value of Juenker[106] and Cornish and Young[107] but are smaller than the ones reported by Young and Zobel.[47]

The change in the values of n and k with wavelength has also been studied in the present work and as in the case of Juenker[106] the optical constant k decreases with increasing wavelength.

6.9.1 Oxide Layer

Vermilyea[108] has studied the oxidation of Tc at different temperatures, the agreement between his experimental and theoretical results deduced by Cabrera and Mott[109] theory is very good at high temperatures but starts to deviate from it at temperatures below 373°K.

The data for 323°K and 373°K gives linear thickness versus log time plots with equation

$$t = - 2.8 + 2.5 \text{ long } T$$

where t = oxide thickness

T = time

Our experimental results at 300°K can be described in the logarithmic scale linearly and the slope of the curve as is shown in Figure (76) is very close to the one found by Vermilyea[108] at 323°K.

TABLE 22

COMPARISON OF CRITICAL CURRENT MEASUREMENTS
OF THIS INVESTIGATION WITH OTHER AUTHORS

Author	Critical Current	Critical Current Density
Meiklejohn (at Tc ^{o}K)	1A (1000 Å)	No information
Sulkowski & Mazur	105 mA	No information
Hauser & Theuseur	No information	5×10^{3} A/cm ^{2} to 10^{5} A/cm
Present work (at 0°K)	160 mA to 1A (115Å to 9200Å)	1.09×10^{4} A/cm ^{2} to 1.4×10^{5} A/cm ^{2}

TABLE 23

OPTICAL CONSTANTS OF Ta AND TaO FOUND
IN THIS WORK AND BY OTHER AUTHORS

Author	n	k	Wavelength
Young & Zobel (Ta)	3.30	2.30	5461 Å
Young & Zobel (TaO)	2.22	0.00	5461 Å
Leslie & Knorr	2.3	2.6	6328 Å
Juenker & Le Blanc & Martin	2.4	1.97	5493 Å
Present work (Ta)	2.15	2.07	4960 Å
Present work (TaO)	2.18	0.00	5487 Å

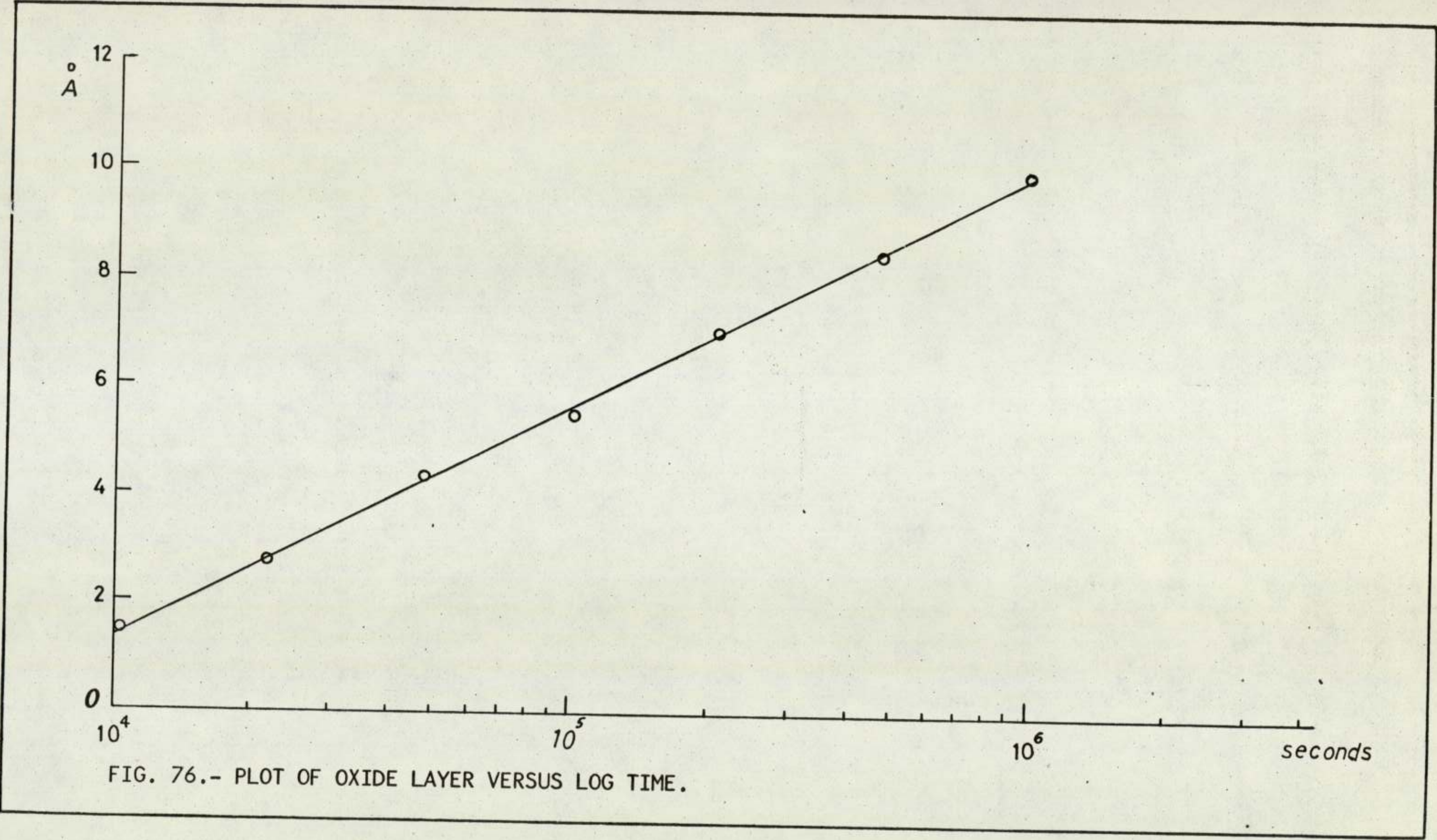

FIG. 76.- PLOT OF OXIDE LAYER VERSUS LOG TIME.

From the present observations it was concluded that the maximum oxide thickness on any film examined electrically could not exceed 2Å arising in the time delay in transferring from the preparation chamber to the cryostat. This means that there is less than a monolayer coverage of the surface. It can be seen from section (5.8.2) that even after several weeks there is only a 10Å layer which remains constant for a very prolonged period.

6.9.2 Ellipsometric Measurements of Structure

As was explained in section 5.8.3 the optical constants of four samples with different structural characteristics were studied in this investigation. From those results we can summarize the following findings:

a) One can get information relative to structure of surface layers up to a thickness of about 1500Å thick.

b) It is possible to say whether f.c.c. phase is present throughout the film or it is in a layer near the substrate.

If samples with different proportions of f.c.c. phase have got different values for n and k it means that f.c.c. structure is throughout the sample because samples are thicker than it is possible to determine thickness.

c) The limits observed are outside the limits of experimental error which means that the trends are significant.

CHAPTER 7

Conclusions and Recommendations

In this chapter, a summ ary of the conclusions reached and some possible extensions to the present work are presented.

7.1 Conclusions

All the samples prepared in this work have been proved to be electrically continuous.

Three main crystalline structures have been found in tantalum thin films, a) pure f.c.c. structure, b) pure b.c.c. structure and c) a mixture of f.c.c. and b.c.c. structures.

A study of the factors which favour the presence of different phases has been made. f.c.c. structure, which is shown to be a metallic phase appears in very thin films (up to 200Å thick) and as film thickness increases there is a conversion from f.c.c. to b.c.c. phase.

The existence of a mixture of b.c.c. and f.c.c. structures has been proved, in this investigation, to be independent of pressure, deposition temperature, substrate treatment, deposition rate and varying thickness so we conclude that the co-existence of both phases is due to some type of electrostatic effect taking place in the substrate.

Based on electrical, ellipsometric and X-ray measurements we deduced that the constitution of this mixture of phases is a network of b.c.c. and f.c.c. grains throughout the whole sample.

None of the samples prepared were randomly orientated, the degree of preferred orientation in the [110] direction, which the films showed is a function of the deposition temperature : increasing T_D produces an increase in the degree of preferred orientation.

Lattice parameter and "d" spacing are also affected by the deposition temperature; decreasing T_D causes an increase in the lattice parameter. Another factor which induces a change in the lattice constants

is the thickness of the sample decreasing thickness which leads to an increase in the values of the lattice parameter.

Matthiessen's rule is satisfied by all the samples prepared in this exercise except for the ultra thin films.

The resistivity, TCR and resistivity ratio of a series of pure films deposited under similar conditions of pressure, deposition rate and substrate temperature, were found to vary with thickness.

Resistivity increased from the bulk value of 13.1μΩ×cm for thick films to a value of 153 μΩ×cm for a film 115Å thick. TCR decreases with decreasing thickness from 2850 to 300p.p.m.°K. Resistivity ratio varies from 1.12 for a sample 115Å thick to 5.8 for a sample 9650Å thick.

Again substrate temperature affects the electrical properties of the films : increasing substrate temperature provokes a decrease in resistivity and an increase in TCR and resistivity ratio. Deposition rate operates in exactly the same way as substrate temperature.

An extra factor to take into account in samples which show a mixture of f.c.c. and b.c.c. phase is the proportion of f.c.c. structure present in the film. Increasing proportion of f.c.c. phase produces an increase in the values of resistivity and a decrease in TCR and resistivity ratio.

Size and grain boundaries effects have been applied in this work and it has been found that they are unable to explain the high resistivities and low TCR exhibited by the very thin films. Gaseous impurities, structural imperfections and lattice disorders are the main reason for these extreme values.

Grain size was found to increase with increasing thickness and substrate temperature.

The superconducting transition temperatures of thick tantalum films were found to be close to the bulk value of 4.48°K. As the film thickness and resistivity ratio decreased, then so did the transition

temperature, the minimum value of 1.4°K was found for a film 115Å thick.

The decrease in transition temperature with decreasing thickness was attributed to the decrease in the value of the mean free path. Two reasons can explain this phenomenom:

a) Reducing the mean free path produces a cutting off of some low frequency phonons so a modification of the phonon spectrum takes place and consequently a reduction in the value of the electron-phonon coupling is produced and applying Mac Millan equation, a reduction in the transition temperature is found.

b) By reducing the mean free path we affect the sharp density of states N(O) and/or the square of the electronic matrix element $<I^2>$ thus decreasing the parameter λ and through Mac Millan equation a subsequent lowering of Tc takes place.

Empirical correlations have been found between the Tc and the electrical properties of Ta thin films. The agreement between the experimental and empirical values is in most cases within 3%.

When the critical temperature of a film is expressed as a function of electrical properties (ρ_{300}/ρ_{10}, $\rho_{300}-\rho_{10}$, TCR etc.) this takes into account the mean free path effects and includes also all factors such as particle size, impurities, imperfections and lattice contributions.

The presence of a percentage of f.c.c. phase in a b.c.c. sample does not affect the value of the transition temperature either because the Tc of bulk f.c.c. tantalum is very close to b.c.c. tantalum or because the f.c.c. phase is short circuited by the b.c.c. phase which becomes superconductor at a higher temperature than f.c.c. structure.

Critical currents for films immersed directly in liquid helium were measured. It was found that the critical currents were proportional to $(1-T_R^{\ 2}) / (1+T_R^{\ 2})^{\frac{1}{2}}$ as predicted by Glover and Coffey. By

extropolation, the critical currents were estimated at $0^{\circ}K$ and the corresponding critical current densities, according to the theory of Glover and Coffey determined to give a maximum critical current density of 1.4×10^{5} A/cm^{2} for a film 115Å thick and a minimum of 1.09×10^{4} A/cm^{2} for a sample 9200Å thick.

From observation using the ellipsometer the oxide thickness on these tantalum films was determined to be 10Å after six weeks.

The rate of oxidation is a maximum during the first hours and after that it slows down, after five days the oxide formation had dropped to about 0.02Å hour^{-1}.

The optical constants of tantalum have been determined by ellipsometry as $n = 2.28$ and $k=1.89$ at 5487Å wavelength in a good agreement with other workers' values for bulk material. n and k change with wavelength, decreasing with increasing wavelength.

Also a change in n and k is found to correlate with a change in the structure and orientation of the samples.

7.2 Recommendations for future work

There are a number of aspects of the present work which would merit further investigation.

a) As it has been assumed that the production of a mixture of b.c.c. and f.c.c. phases has been due to the presence of some electrostatic phenomenon, it should be of great interest to try to change the deposition parameters from the electrostatic point of view and produce pure thick f.c.c. tantalum films.

b) The use of different material as substrates should help in the search for different tantalum structures and preferred orientations in directions other than the [110] found in this work.

c) In order to test whether the two reasons given above to explain the decrease in Tc with thickness are valid, and whether the two work

simultaneously or not, the following experiment should be carried out : a direct measurement of λ, the electron phonon interaction parameter accompanied by the determination of the phonon distribution of thin films of tantalum.

If there is a variation in the parameter λ without a change in the phonon spectrum of tantalum, then the responsible for the diminution of Tc should be found in the variation of N(O) and $<I^2>$, but if both phonon spectrum and λ change, then it means that both mechanisms work at the same time and that the decrease in Tc should be due to both arguments superimposed.

To measure the phonon spectrum the method used by Leger and Klein[31] for aluminium films could be used.

Klein and Leger[110] have shown that the second derivative of the tunnelling current, d^2I/dV^2, through an aluminium-aluminium junction in the normal state, reflects the phonon density spectrum. Similarly, for tantalum films it should be possible to observe if the low frequency phonons are cut-off from the phonon spectrum.

To directly measure λ, Hopfield[111] has suggested that it could be accomplished by measurement of the infrared (2 to 20μ) optical properties of the metal.

In transition metals the first band to band transitions are generally observed near 2μ, and at frequencies below this one expects a dielectric function

$$\varepsilon = A + \frac{4\pi B}{-\omega^2 + i\omega/\tau} \qquad (7.1)$$

where A, B and τ were constants.

For a material in which this analysis describes the experimental data the parameter λ is given by

$$\lambda = \frac{\hbar}{2\pi\tau}\frac{1}{(KT)} \qquad (7.2)$$

where K is the Boltzmann's constant and T the temperature at which the experiment is carried out.

Equation (7.2) is correct only if the τ observed in optical experiments is due to phonon scattering. If in the optical experiments the lifetime is determined by impurity scattering or surface scattering, the resistivity ρ and B can be used to determine λ from the relation

$$\lambda = B \frac{\hbar}{2\pi K} \cdot \frac{d\rho}{dT} \qquad (7.3)$$

This expression is for the high temperature limit $T > \theta_D$.

This technique requires only clean surfaces for examination and in this respect it is ideally suited to the study of thin films.

d) From section (6.5.4) it might be useful to investigate theoretically whether a definite relation between the electrical properties of thin films and the electron-phonon coupling factor λ exists.

e) More work should be done in the correlation of optical constants and structural properties.

REFERENCES

1. T. Asada and H. Nose : J. Phys. Soc. Japan, 26, 347, (1969)

2. W. L. McMillan : Phys. Rev. 167, 331, (1968)

3. A. Leger and J. Klein : Phys. Letters, 28A, 751, (1969)

4. I. W. Salter : Ph.D. Thesis 1973, Aston University.

5. P. Drude : Ann. Physics, 1, 556, (1900)

6. H. A. Lorentz : Amsterdam Proc. (1904-1905)

7. A. Sommerfield : Z. Physic. 47, 1, (1928)

8. J. J. Thomson : Proc. Cam. Phil. Soc., 11, 120, (1901)

9. K. Fuchs : Proc. Cambridge Phil.Soc., 34, 100, (1938)

10. F. H. Sondheimer : Phys. Rev., 80, 401, (1950)

11. F. H. Sondheimer : Advan. Phys., 1, 1, (1952)

12. A. F. Mayadas : Phys. Rev., 1, 1382, (1970)

13. H. K. Onnes : Commun. Phys. Lab. Univ. Leiden. No.119b, 120b, 122b, 124c, (1911)

14. C. J. Gorter and H. B. G. Casimir : Physica, 1, 305, (1934)

15. F. London and H. London : Physica, 2, 341, (1935)

16. V. L. Ginzburg and L. V. Landau : J.E.P.T. 20, 1064, (1950)

17. A. A. Abrikosov : J.E.T.P. 5, 1174, (1957)

18. A. B. Pippard : Proc. Roy. Soc. A216, 547, (1953)

19. H. Frolich : Phys. Rev., 79, 845, (1950)

20. L. N. Cooper : Phys. Rev., 104, 1189, (1956)

21. J. Bardeen, L. Cooper and J. Schrieffer : Phys. Rev., 108, 1175, (1957)

22. B. T. Matthias : "Progress in Low Temperature Physics". C. J. Gorter Ed. Page 138, N.Y. (1957)

23. V. Ambeghokar and L. Tewordt : Phys. Rev., 134, A805, (1964)

24. D. J. Scalapino, J. Wada and J. C. Swihart : Phys. Rev. Letters., 14, 102, (1965)

25. P. Morel and P. W. Anderson : Phys. Rev., 125, 1263, (1962)

26. V. I. Ginzburg : Phys. Letters, 13, 101, (1964)

27. D. Pines : Phys. Rev., 109, 280, (1958)

28. W. DeSorbo : Phys. Rev., 132, 107, (1963)

29. J. R. Rairden and C. A. Neugebauer : Proc. of IEEE, 52, 10, (1965)

30. F. B. Silsbee : J. Wash. Acad. Sci., 6, 597, (1916)

31. F. London : Proc. Roy. Soc. London, A152, 24, (1935)

32. F. Abelès : Ann. de Physique 3, 504, (1948)

33. O. Heavens : "Optical Properties of Thin Solid Films" (Dover, New York, (1965)

34. R. W. Ditchburn : "Light" (Blackie, London) 1952. p.480.

35. R. W. Ditchburn : J.Opt. Soc. Ann. 45, 743, (1955)

36. P. Rouard : Ann. de Physique, 7, 291, (1937)

37. A. Vasìcek : J. de Physique, 11, 342, (1950)

38. F. L. McCrackin, E. Passacaglia, R. Stromberg and H. L. Steinberg : J. Research Nat. Bar.of Standards, 67A, 363, (1963)

39. M. Burn and E. Wolf : "Principles of Optics", (Pergamon, London) 1970 p.31.

40. J. Holden, L. Holland and L. Laurenson : J. Sci. Instr. 36, 281, (1959)

41. A. B. Winterbottom : Norske Videnskabers Selskab (Trondheim), (1955)

42. R. J. Seward : Ph.D. Thesis, Univ. of Southampton, (1967)

43. K. R. O'Shea : Ph.D. Thesis, Univ. of Aston, (1971)

44. S. Tolansky : "Multiple Beam Interferometry", Clarendon Press, (1949)

45. K. H. Zaininger and A. G. Revesz : R.C.A. Laboratories, March (1964)

46. Kaye and Laby : Book of Physical Constants.

47. L. Young and F. G. R. Zobel : J. Electrochem. Soc. 113, 277 (1966)

48. T. E. Hartman : J. Appl. Phys., 34, 943, (1963)

49. C. A. Neugebauer and M. B. Webb: J. Appl. Phys., 33, 74, (1962)

50. K. L. Chopra : "Thin film phenomena", MacGraw-Hill, New York, (1969)

51. A. I. Bublik and B. I. A. Pines : Doki. Akad. Nark SSSR, 87, 215, (1952)

52. T. E. Hutchinson and K. M. Olsen : J. Appl. Phys., 38, 4933, (1967)

53. E. Miska and M. Gillet : Compt. Rend., B263, (1967)

54. R. F. Adamsky : J.Appl. Phys., 40, 11, (1969)

55. K. L. Chopra, M. R. Randlett and R. H. Duff : Phil. Mag., 261, (1967)

56. M. H. Read and C. Altman : Appl. Phys. Lett., 7. 3. (1965)

57. R. B. Marcus and S. Quigley : Thin Sol. Film, 2, 467, (1968)

58. F. Schrey, R. D. Mathis, R. T. Payne and L. E. Murr: Thin Sol. Film, 5, 29, (1970)

59. R. N. Denbigh and P. N. Marcus: J. Appl. Phys., 37, 12, (1966)

60. P. I. Lainer and V. A. Kholmyanskii: Sov. Phys. Crystall. 12, 6, (1968)

61. D. Gerstenberg and M. Hall : J. Electrochem. Soc., 111, 936, (1964)

62. R. B. Marcus : J. App. Phys., 37, 8, (1966)

63. V. P. Belevskiy and M. V. Belous : Kiev Polytechnic Institute 1971, UDC 669.873

64. W. D. Westwood and F. C. Livermore : Thin Sol. Film, 5, 407, (1970)

65. M. H. Read and D. M. Hensler : Thin Sol. Film, 10, 123, (1972)

66. W. D. Westwood : Thin Sol. Film, 15, 15, (1973)

67. P. N. Baker : Thin Sol. Film, 14, 1, (1972)

68. G. L. Miller : "Tantalum and Niobium" Metallurgy of the Rarer Metals, Butterwoth, London, (1959)

69. L. F. Mattheiss : Phys. Rev., 1, 373, (1970)

70. C. H. Kittel : Introduction to Solid State Physics" T. Wiley & Sons, London, (1971)

71. E. Gebhardt and R. Rothenbacher : J. Metallk, 54, 623, (1963)

72. E. Gebhardt, H. D. Seghezzi and W. Dürrschnobel : J. Metallk., 49. 577, (1958)

73. J. Desserre and J. C. Goulet : C. R. Acad. Sc. Paris., 272, 808, (1971)

74. D. P. Seraphim, N. R. Stemple and D. T. Novick : J. Appl. Phys., 33, 136, (1962)

75. I. J. Budnick : Phys. Rev., 119, 1578, (1959)

76. C. Sulkowski and J. Mazur : Acta Physica Polonica, 29, 107, (1966)

77. J. J. Hauser and H. C. Theuseur : Rev. Mod. Phy., 36 , 80, (1964)

78. E. A. Lynton, B. Serin and M. Zucker : J. Phys. Chem. Sol., 3, 165, (1957)

79. C. A. Neugebauer and R. A. Ekwall : J. Appl. Phys., 35, 547, (1964)

80. M. Strongin, O. F. Kammerer and A. Paskin : Phys. Rev. Letters., 14, 949, (1965)

81. W. Buckel and R. Hilsch : J. Physic., 139, 109, (1954)

82. B. Abeles, R. W. Cohen and W. R. Stowell : Phys. Rev. Letters., 18, 902, (1967)

83. B. Abeles, R. W. Cohen and G. W. Cullen : Phys. Rev. Letters, 17, 632, (1966)

84. A. Rothwarf : Phys. Letters, 30A, 55, (1969)

85. R. C. Theil : Z. Physik, 200, 227, (1967)

86. S. W. Marshall and R. M. Wilenzick : Phys. Rev. Letters, 16, 219, (1966)

87. M. Strongin, O. F. Kammerer, V. E. Crow, R. D. Parks, D. H. Douglas and M. A. Jenson, : Phys. Rev. Letters, 21, 1320, (1968)

88. L. T. L. Shen : Phy. Rev. Letters, 24, 1104, (1970)

89. L. Meyers and W. A. Little : Phy. Rev. Letters, 11, 156, (1963)

90. A. D. B. Woods : Phy. Rev., 136, A781 (1964)

91. F. H. Featherston and I. H. Neighbours,: Phys. Rev., 130, 1324, (1963)

92. J. J. Hanak, J. I. Gittleman, J. P. Pellicane and I Bozowski : Phy. Letters, 30A, , (1969)

93. M. Strongin : Physica, 55, 155, (1971)

94. L. R. Testardi : IEEE Transactions on Magnetics, MAG-11, 197, (1975)

95. C. Varmazis and M. Strongin: Phy. Rev., 10, 1885, (1974)

96. B. B. Goodman : 1BM J. Res. Develop., 6, 63, (1962)

97. L. P. Gorkov : Sov. Phy. JETP, 9, 1364, (1960)

98. S. L. Wipf : Rev. Mod. Phys., , 83, (1964)

99. J. Bardeen : Rev. Mod. Phys., 34, 667 (1962)

100. R. E. Glover and H. T. Coffey : Rev. Mod. Phy., 36, 299, (1964)

101. J. A. Mydosh and H. Meissner : Phys. Rev., 140, A1568, (1965)

102. J. E. Mercereau and T. K. Hunt : Phys. Rev. Letters., 8. 243, (1962)

103. H. London and G. R. Clark : Rev. Mod. Phys., 36, 320, (1964)

104. W. H. Meiklejohn : Rev. Mod. Phys., 36, 302, (1964)

105. M. Prutton : Nature, 193, 565, (1962)

106. D. W. Juenker : J. Opt. Soc. of America, 58, 164, (1968)

107. W. D. Cornish and L. Young : Proc. R. Soc. Lond., A335, 39, (1973)

108. D. A. Vermilyea : Acta Metall., 6, 166, (1958)

109. N. Cabrera and N. F. Mott : Ref. Progr. Phys., 12, 163, (1949)

110. J. Klein and A. Leger : Phys. Letters, 26A, 134, (1968)

111. J. J. Hopfield : Comments on Solid State Physics, 3, 48, (1970)